Testing Protocol, Data Storage, and Recalibration for Pavement-ME Design

Final Report

Michigan Department of Transportation
Research Administration
8885 Ricks Road
Lansing, MI 48909

By

Syed Waqar Haider, M. Emin Kutay, Bora Cetin, Rahul Raj Singh, Hamad Bin Muslim, and Celso Santos (Michigan State University)

Zhanping You, Dongzhao Jin, and Kai Xin (Michigan Technological University)
Will Hansen and Yuguo Zhong (University of Michigan)

Report Number: SPR-1723

Michigan State University
Department of Civil and Environmental Engineering
3546 Engineering Building
East Lansing, MI 48824

September 2023

Technical Report Documentation Page

1. Report No. SPR-1723	**2. Government Accession No.** N/A	**3. Recipient's Catalog No.** N/A
4. Title and Subtitle Testing Protocol, Data Storage, and Recalibration for Pavement-ME Design		**5. Report Date** September 2023 **6. Performing Organization Code** N/A
7. Author(s) Syed Waqar Haider, M. Emin Kutay, Bora Cetin, Rahul Raj Singh, Hamad Bin Muslim, Celso Santos, Zhanping You, Dongzhao Jin, Kai Xin, Will Hansen, and Yuguo Zhong		**8. Performing Org. Report No.** N/A
9. Performing Organization Name and Address Michigan State University Department of Civil and Environmental Engineering 428 S. Shaw Lane, 3546 Engineering Building East Lansing, MI 48824		**10. Work Unit No.** N/A **11. Contract No.** 2020-0235
12. Sponsoring Agency Name and Address Michigan Department of Transportation Research Administration 8885 Ricks Road Lansing MI 48909 P.O. Box 33049 Lansing, Michigan 48909		**13. Type of Report & Period Covered** Final Report, 1/21/2020 – 9/30/2023 **14. Sponsoring Agency Code** N/A
15. Supplementary Notes Conducted in cooperation with the U.S. Department of Transportation, Federal Highway Administration. MDOT research reports are available at www.michigan.gov/mdotresearch.		

16. Abstract

This study focuses on calibrating and validating performance models for pavement in Michigan and provides testing protocols for field and laboratory material testing. The research team selected various new and rehabilitation projects for flexible and rigid pavements to evaluate previous calibration efforts, verify global models in the Pavement-ME, perform local calibration, and provide suitable calibration coefficients for different pavement types. The Report documents the calibration results, input data, future local calibration guidelines, and data needs. The study estimated the resilient moduli of different pavement layers using various field and lab tests. The laboratory-determined median subgrade moduli range between 12 to 17 ksi, while the subbase moduli range between 15 to 25 ksi. FWD data analyses resulted in the highest moduli values, whereas LWD resulted in the lowest ones for all pavement layers. The surface absorptivity data collected showed a difference between old and new HMA and PCC layers. The material characterizations for HMA, PCC, and unbound materials validated the design values used for various pavement layers. Finally, the study includes the protocols for in-situ testing frequency and material sampling quantity and frequency for collecting material library data in the future.

17. Key Words Pavement-ME, local calibration, resampling techniques, pavement analysis, and design		**18. Distribution Statement** No restrictions. This document is available to the public through the Michigan Department of Transportation.	
19. Security Classification Unclassified	**20. Security Classification** Unclassified	**21. No. of Pages** 277	**22. Price** N/A

ACKNOWLEDGMENTS

The authors would like to thank the Michigan Department of Transportation (MDOT) for funding this project, specifically the Research Advisory Panel (RAP) members. During this study, the authors appreciate the continuous interaction with the MDOT pavement group, Justin P. Schenkel, Michael Eacker, and Fawaz Kaseer. Thanks to Ethan Akerly for the material samples and in-situ test data collection on the field projects. Their inputs were invaluable to the researchers and helped improve the quality and results of the Report.

The authors highly appreciate the efforts on the material and in-situ tests performed by Michigan Technological University (MTU) researchers, namely Tiankai Che, Dongdnog Ge, Xiaodong Zhaou, Juan Deng, Josh King, Kwadwo Boateng, and Yin Lei, to achieve the objectives of the study.

TABLE OF CONTENTS

List of Tables

List of Figures

EXECUTIVE SUMMARY

The main objectives of the study are to (a) identify significant Pavement-ME inputs from literature based on design sensitivity, availability, and testing costs, (b) develop a prioritized list (most to least critical) of in-situ (including FWD testing) and laboratory tests to be conducted during or after construction to obtain significant inputs, (c) develop a protocol for materials sampling for laboratory and in-situ testing during or after construction. The protocol would at least include project type, test locations, sampling frequency, and schedule/timing for samples. The scope and amount of in-situ and laboratory testing should be practical and reasonable within the resources available to MDOT, (d) Establish a selection criterion for identifying projects for local calibration, (e) determine the applicability and feasibility of using in-situ FWD testing to estimate layer moduli instead of using modulus testing in the laboratory to improve efficiency and save resources, (f) determine if a tool/database exists for storing construction data (e.g., layer material properties relevant to the Pavement-ME software) and can be updated with the future acquisition of such data, (g) add collected inputs (construction data and material test results) to the database, including data from previous calibration efforts, (h) evaluate the differences in performance predictions of version 2.3 and the latest version of the Pavement-ME software, and (i) compare pavement designs and, if needed, perform local recalibration of the performance models in the version of AASHTOWare Pavement-ME.

The research team identified and selected 163 new and 121 flexible rehabilitation projects. Similarly, the team selected 46 new JPCP and 11 unbonded overlay sections for rigid pavements for local calibration of performance models. The team used several statistical techniques for the calibrations—no sampling, bootstrapping, split sampling, and repeated split sampling. Verification using global models shows that global models could not provide reasonable predictions, and there was a need for local calibration. Local recalibration results show that the performance model predictions improve significantly after calibration for Michigan conditions. The pavement designs using new local models show fatigue and thermal cracking for flexible, while IRI and joint faulting are critical distresses for rigid pavements.

LWD resulted in the lowest moduli values for all pavement layers (base, subbase, and subgrade) among in-situ field tests. The laboratory results show that the median subgrade moduli for all projects are between 12 and 17 ksi. The FWD and the DCP data estimated higher moduli for the subgrade layer for all projects with considerable spatial variability. The median subbase moduli values determined in the laboratory range between 15 to 25 ksi for all projects. The LWD and DCP data display similar trends with median subbase moduli determined from field tests below 10 ksi. FWD data analyses resulted in the highest subbase moduli values, slightly higher than the laboratory-determined median subbase moduli values. The laboratory determined median base moduli range between 30 to 40 ksi. FWD data analyses resulted in the highest moduli values for all the projects. Surface absorptivity data collected on a few projects show that there should be a difference between old and new HMA and PCC layers. The results of material characterizations for HMA, PCC, and unbound materials validate the design values used for various pavement layers. Protocols for in-situ testing frequency and material sampling quantity and frequency are developed for collecting material library data in the future.

CHAPTER 1 - INTRODUCTION

1.1 PROBLEM STATEMENT

The Pavement-ME (mechanistic-empirical) analysis and design procedure has been implemented in Michigan for designing new and reconstruct pavements. Several studies were performed in the recent past to characterize climate, traffic, material properties, and calibration of the performance models to address the local conditions, materials, and construction practices in the Pavement-ME procedure. While all the material properties and calibration of performance models were addressed to improve the approach's local applicability and accuracy, there were still some data gaps, specifically for material characterization and pavement construction. Examples of past data gaps that were improved include the clustered traffic data, HMA mix, and binder properties. Gaps in data need to be estimated (corresponds to Level 3 for Pavement-ME input levels), which may not be accurate for the location; therefore, having the actual values for new projects is likely to improve mechanistic-empirical (ME) calibration accuracy. Also, a limited number of rigid pavement sections were available for previous MDOT calibration (conducted in 2014 and 2017), so adding more data from new sections would improve ME performance model prediction.

Furthermore, MDOT does not have criteria for selecting and a method for storing relevant data for calibration, material sampling, and testing for ME inputs for future calibration projects. Thus, there is a need to have a consistent procedure to include new pavement sections in the performance model calibration and obtain actual as-constructed material properties for ME inputs. Such procedures will enhance the accuracy and adequacy of the performance models for future pavement designs.

Additionally, with updated Michigan ME data (climate and performance data), MDOT would benefit from a recalibration of AASHTOWare Pavement-ME Design to improve design prediction accuracy. Based on the above discussion, the following three main goals are accomplished in this study:

1. A framework was developed to identify and include new pavement projects in the Pavement-ME database. The framework addresses (a) collecting initial IRI (smoothness) data, (b) characterizing the in-situ material properties of the pavement sections by non-destructive and destructive sampling and testing, (c) establishing climate, traffic and pavement cross-section inputs, and (d) documenting the construction-related issues (if any). Establishing the framework resulted in a database to store all the needed Pavement-ME inputs. It is envisioned that as these sections get older and sufficient performance data becomes available, those can be part of future calibration efforts to improve performance models' accuracy.
2. Once the framework is established, the input data for the pavement sections used in the previous local calibration efforts are stored in the database. The input data for additional pavement sections identified in this study were also appended to the database. Further, the performance data from the existing (i.e., already in the

calibration dataset) sections were updated to improve the local calibrations of the performance models.

3. The Pavement-ME performance models were calibrated for Version 2.6. The updated pavement sections and performance data were used for calibration. The team used updated Pavement-ME inputs for traffic, HMA mix and binder properties, and climatic data files. The team also evaluated the effect of calibration on pavement design.

1.2 BACKGROUND AND SIGNIFICANCE OF WORK

In 2004, mechanistic empirical-based pavement analysis and design methods were implemented in the National Cooperative Highway Research Program 1-37 (*1*). The method modified the empirical pavement design procedure of the American Association of State Highway and Transportation Officials (*2*). The Mechanistic-Empirical Pavement Design Guide (MEPDG) provides highway agencies with a practical tool for designing new and rehabilitated pavements. The analyses in ME principles use primary pavement responses (stresses, strains, and deflections) and incremental damage over time to predict surface distress through transfer functions. The reliability of performance prediction models depends on the accuracy of the transfer functions, which is achieved through calibration and subsequent validation with observed pavement condition data. A satisfactory correlation between measured and predicted performance indicators increases the viability, acceptance, and usage of the MEPDG procedures of pavement analysis and design procedures. Calibration is a mathematical procedure to reduce the difference between predicted and measured distress values. Cross-validation refers to a process that evaluates the performance of mathematical models to independent or global datasets (i.e., data that are not used for model development). The default transfer functions in the MEPDG were calibrated nationally using the Long-Term Pavement Performance (LTPP) and other experimental test sections data such as MnRoad. However, roadway design, construction, maintenance, rehabilitation policies, and local weather vary across the US. Therefore, NCHRP 1-40B provides the guidelines for local calibration (within a state or region) for transfer functions in flexible and rigid pavements (*3*). The local calibration process adjusts the Pavement-ME transfer functions for construction practices, material, traffic, climate, and pavement performance within a state or region.

State Highway Agencies (SHAs) have identified the practical challenges in implementing the Pavement-ME analysis and design process. These challenges include:

(a) Identifying the most significant input variables,
(b) Establishing data requirements and developing historical roadway conditions and management database for continuous calibration of the performance models and
(c) Calibrating the pavement performance prediction model considering the local traffic, climate, and material properties.

This study recognizes significant inputs and their corresponding levels for Pavement-ME use. It also provides guidelines for missing/incomplete inputs and their best estimates. Moreover,

recalibration of Pavement-ME v2.6 performance models using additional data provides MDOT officials higher confidence in using the MEPDG design approach.

1.3 RESEARCH OBJECTIVES

The following are the specific objectives of the study:

1. Identify significant Pavement-ME inputs from literature based on design sensitivity, availability, and testing costs,
2. Develop a prioritized list (most to least critical) of in-situ (including FWD testing) and laboratory tests to be conducted during or after construction to obtain significant inputs,
3. Develop a protocol for materials sampling for laboratory and in-situ testing during or after construction. The protocol would at least include project type, test locations, sampling frequency, and schedule/timing for samples. The scope and amount of in-situ and laboratory testing should be practical and reasonable within the resources available to MDOT,
4. Establish a test matrix and selection criterion for identifying projects to be investigated in this study. The criteria should meet the time and resource constraints for the study,
5. Determine the applicability and feasibility of using in-situ FWD testing to estimate layer moduli instead of using modulus testing in the laboratory to improve efficiency and save resources,
6. Determine if a tool/database exists for storing construction data (e.g., layer material properties relevant to the Pavement-ME software) and can be updated with the future acquisition of such data. The database tool should address the following needs:

    a. Ability to extract/export data for ME design purposes. Moreover, the storage of performance data from the Pavement Management System (PMS) is preferred. It would be beneficial if it could view individual project data or all data of one type (e.g., rutting, cracking, material input items), and
    b. Evaluate the ARA ME calibration and Prep-ME tools as a potential solution. Develop a customized database tool with RAP (Research Advisory Panel) approval if no tool/database currently exists that meets these requirements, if approved by the RAP.

7. Add collected inputs (construction data and material test results) to the database, including data from previous calibration efforts,
8. Evaluate the differences in performance predictions of version 2.3 and the latest version of the Pavement-ME software and
9. Compare pavement designs and, if needed, perform local recalibration of the performance models in the version of AASHTOWare Pavement-ME with RAP approval.

1.4 RESEARCH PLAN

The research was conducted in ten (10) tasks, briefly discussed below, to accomplish the above objectives.

1.4.1 Task 1: Review of Literature

The team reviewed several studies related to the local calibration of the Pavement-ME performance models. The review's objective was to identify any gaps in construction, materials, and performance data (and the sensitivity of the Pavement-ME to these data) for the previously selected projects. Moreover, the team also reviewed local calibration efforts by different states, which have been summarized in this report.

1.4.2 Task 2: Develop a Prioritized Inputs List and Relevant Testing Protocols

Based on the sensitivity of the materials input in affecting pavement performance, a prioritized list of inputs/information necessary for calibration of reconstruct and rehab designs was developed in this task. Also, the testing protocols for materials testing at Levels 1 and 2, including lab and field testing along with appropriate sampling needs, were chosen.

1.4.3 Task 3: Develop a Test Matrix and Set of Criteria for ME-based Testing

Some of the inputs have already been obtained via laboratory testing in previous MDOT projects [e.g., HMA $|E^*|$ and D(t)] *(4)*. However, the mixes tested were determined by the availability of construction projects during the research project. During this research project, in consultation with RAP, the construction projects were identified to add data from new mixes to the DynaMOD database. Also, some critical inputs, such as the AC Surface Shortwave Absorptivity (1-Albedo), have never been measured in Michigan, and constant value is always assumed. The ASTM E1918 was used, along with a dual-pyranometer, to measure AC Surface Shortwave Absorptivity. Furthermore, HMA air voids and effective binder volume are also quite sensitive inputs. Historical JMF data was analyzed to determine clusters (i.e., regional patterns if any) of these variables that can be used by MDOT.

For the PCC materials, there are various material properties related to ME inputs, including E, $f_c^{'}$, modulus of rupture (*MOR)*, coefficient of thermal expansion (*CTE)*, unit weight, and Poisson's ratio. The team measured all these properties for the selected projects. Since *MOR* and *CTE* inputs significantly impact the predicted JPCP performance, these were measured in the laboratory for the projects chosen for verification purposes.

There is also a need to characterize sensitive inputs of unbound layer properties, such as base and subgrade resilient modulus (MR), which are both currently assumed to be within a specific limited range. A database of these parameters is also needed. Other relatively sensitive inputs such as HMA, base, and subgrade Poisson's ratio can also be included in the testing program to establish a limited database (instead of assuming constant values from the literature). All base/subbase and subgrade materials were also subjected to index tests,

including sieve and hydrometer tests, Atterberg limit tests, specific gravity (Gs), and absorption tests.

Crushed waste concrete [recycled concrete aggregate (RCA)] and crushed asphalt concrete [reclaimed asphalt pavement (RAP)] are considered alternative materials to be used in roadway base layer construction (*5*). Variability in the characteristics of these materials is very high and highly source-dependent. If available, RCA and RAP used in the selected projects were characterized during this study.

While laboratory characterization of these pavement foundation materials is crucial for the Pavement-ME analysis, the laboratory process may take a long time and require more resources. The correlation of lab properties to non-destructive field measurements/testing would reduce necessary resources and save time. The proposed field measurements include density and moisture (nuclear gauge density), lightweight deflectometer (LWD), dynamic cone penetrometer (DCP), and falling weight deflectometer (FWD) tests. Correlations were established between the laboratory measurements (MR in particular) and stiffness (elastic modulus) obtained from LWD and FWD and the California Bearing Ratio (CBR) collected from DCP for unbound materials. Environmental impacts (e.g., freeze-thaw and elevated temperature) were considered during site selection since soil temperature and moisture significantly impact the behavior of base/subbase materials and subgrade soils. Environmental impacts would be more critical for evaluating the performance of recycled aggregates (RCA and RAP).

The test matrices for critical inputs were prepared to cover a wide range of materials used in local construction. The MDOT's DynaMOD database (i.e., HMA $|E^*|$, asphalt binder $|G^*|$ and creep compliance D(t)) and other data collected in Michigan were thoroughly reviewed, gaps were identified, and recommendations for further testing were made. Construction projects in the Summers of 2020 and 2021 were evaluated for potential additional HMA/WMA, PCC, base, subbase, and subgrade material collection and testing.

Based on Tasks 1 to 3, the team developed test matrices for different material types for project selection to obtain materials for laboratory and field testing. After this task, the team recommended the final number of projects and the quantity of testing to be conducted in this research study. In summary, by the end of tasks 1 to 3, the following information is available to MDOT:

(1) Recommended new projects for characterizing ME inputs for this study (construction projects from the 5-year future program)
(2) The ME inputs for material characterization at different levels were identified for new projects constructed between the years 2020 and 2021 (best input levels)
(3) List of tests and sampling needs for destructive/non-destructive tests for new projects constructed between 2020 and 2021 and preliminary protocols for future projects (finalized in Task 10).

1.4.4 Task 4: Conduct Laboratory Testing and Collect/Analyze FWD Data

This task involved laboratory testing on the (HMA, PCC, and unbound) materials collected from the construction sites. Also, the research team worked with MDOT while collecting FWD data to back-calculate the layer properties, such as MR for unbound layers and the equivalent elastic modulus of the HMA layer. It should be noted that the HMA $|E^*|$ master curve was also backcalculated. The analysis requires (i) the FWD equipment to be able to store the time history of the deflection data, (ii) temperature with depth is measured, and (iii) temperature differential from top to bottom is more than 5°C. The techniques presented in the literature can be used to back-calculate the HMA $|E^*|$ *(6, 7).* As part of this project, the feasibility of FWD testing to obtain $|E^*|$ master curve was also explored.

The UM team has extensive experience evaluating frost durability resistance, a significant problem in recent JPCP projects. Therefore, the team tested the selected field samples for durability to establish a materials database explaining non-load-related long-term pavement performance. Such testing results were used to explain the poor and good performance of selected pavement sections. Also, available data for joint deflection and time history from MDOT's FWD (if available) was used to evaluate the impact of unbound and stabilized base types on pavement performance to establish threshold deflections for loss of load transfer and dowel-bar looseness and impact on pavement performance (i.e., development of joint faulting). Reduced joint deflections are crucial in delaying the onset of dowel-bar looseness and faulting in jointed concrete pavements constructed on a stabilized base (ATB/CTB) or unbound OGDC.

LWD tests conducted on the newly constructed subgrade and base layers, along with the compaction data (dry unit weight and moisture content), were used to obtain moduli and their variability. Samples were also collected to determine the index properties of both subgrade and base layer aggregates. Besides, DCP tests conducted after each layer's compaction process was used to obtain field CBR. This study also proposed to conduct FWD on base layers right after compaction is completed.

Finally, laboratory/field correction factors for different unbound materials were recommended based on the work performed in this task. Also, this task identifies inputs that can be efficiently and accurately obtained by conducting FWD testing.

1.4.5 Task 5: Evaluate Databases for Storing Construction and Performance Data

The team evaluated the calibration assistance tool (CAT), an existing Prep-ME tool, and other existing tool/database(s) as the storage location for calibration data. Potential platforms for the database include MS Excel, MS Access, and Power BI. The team also evaluated the existing DYNAMOD tool to include laboratory test data for the HMA mix and binder, unbound layer, and PCC properties.

1.4.6 Task 6: Review of Project Data for Calibration

The main objectives of this task include:

(a) review the list of projects included in the last full calibration,
(b) add PMS data for the years that have passed since then,
(c) review MDOT lists of projects built since the last full calibration,
(d) suggest projects to be added to the calibration dataset,
(e) review project records to obtain information for ME inputs and
(f) add the data collected as part of this research to the appropriate database (including PMS data).

In order to locally calibrate the performance prediction models, in-service pavement sections were selected, which represent Michigan pavement design, construction practices, and performance. These pavement sections represent all current pavement types and rehabilitation types that are constructed by MDOT. The process for identifying and selecting pavement sections includes:

- Determine the minimum number of pavement sections based on the statistical requirements,
- Identify all available in-service pavement projects constructed between 2007 and 2019 (projects and performance data before 2007 have already been incorporated in the previous calibration effort and are being used in the current calibration),
- Extract all pavement distresses from the MDOT databases for all identified projects,
- Evaluate the measured performance for all the identified projects, and
- Establish a refined list of the potential projects that exhibit multiple distresses with sufficient magnitude.

The team identified additional candidate projects during this study and added those to the existing database. Moreover, the materials and traffic-related inputs were revised from the previous calibration effort (*8, 9*) based on material testing results and new traffic data used during this study.

1.4.7 Task 7: Evaluate the Local Calibration of Performance Models

In this task, the team evaluated changes (if any) in all the performance models in software Version 2.3 and Version 2.6 of the Pavement-ME. The impact of the modifications in the performance models on the performance predictions based on the local and global coefficients was identified. A representative sample of the pavement sections used in Michigan's last local calibration and identified in this study was re-analyzed using both software versions and performance predictions were compared.

1.4.8 Task 8: Recalibrate Performance Models

In this task, the team conducted recalibration of the new rigid, new flexible, unbonded rigid, and rehabilitated flexible coefficients utilizing the methodologies from the previous recalibration efforts. The results from Task 7 warranted local recalibration of the performance models; therefore, the models were recalibrated using no sampling, split sampling, and bootstrapping approaches. Recommended changes to the Michigan calibration coefficients were provided to MDOT upon completing this task. Further, the research team developed simple Excel sheets (where possible) to recalibrate the rigid and flexible pavement

performance models. These Excel files will be given to MDOT for the future in-house recalibration of the models. The Excel files can be used to verify calibration results outside the Pavement-ME software.

1.4.9 Task 9: Evaluate the Impact of Recalibration on Pavement Design

The impact of the model recalibrations on pavement designs was quantified using recalibration results from Task 8. A set of pavement sections were analyzed with the previous and new calibration coefficients from Task 8, and comparisons were documented on the PCC slab and HMA layer thicknesses (i.e., AASHTO 93, versions 2.3 and 2.6). Recommendations are made to modify Michigan calibration coefficients based on such comparisons.

1.4.10 Task 10: Final Report and Technology Transfer

The final report contains all work performed during the study—test results of laboratory testing, database development for materials, traffic, performance data, design features, recommended sampling and testing protocols for future MDOT projects, the methodology for recalibration of performance models, and recommended new model coefficients. Also, a technology transfer workshop will be developed and presented to MDOT engineers. The workshop will include (a) an introduction to the Pavement-ME analysis and design for pavements, (b) material characterization of as-constructed materials using FWD deflections, DCP, and LWD testing, (c) the need and process of updating materials and performance data for calibration dataset, and (d) the orientation of the existing or developed database tool to update input variables. Additionally, quarterly reports and presentations have been submitted before the quarterly meetings with MDOT.

1.5 OUTLINE OF REPORT

This report contains seven (7) chapters. Chapter 1 outlines the problem statement, research objectives, and details of various tasks. Chapter 2 documents the literature review from previous studies on material characterization and local calibration efforts for the performance models in the Pavement-ME and implementation issues. Chapter 3 discusses the input and performance data used for calibration efforts. This includes data collection efforts, a summary of the performance, and input data for the selected pavement sections in Michigan for model calibrations. Chapter 4 details the local calibration methods and procedures used in this study. Chapter 5 presents the local calibration results for the various performance prediction models. Chapter 6 documents the material characterization, in-situ testing results, data collection, sampling protocols for new projects, and correlations between in-situ and lab properties. Chapter 7 includes the conclusions and detailed recommendations. Appendix A contains input data for all the pavement sections used in the local calibration of the performance models, while all the local calibration results are presented in Appendix B.

CHAPTER 2 - LITERATURE REVIEW

2.1 INTRODUCTION

The AASHTOWare design software is a tool for designing new and rehabilitated pavements with flexible, rigid, and composite structures. It is based on the mechanistic-empirical (ME) analysis approach, which is supported by the AASHTO's Mechanistic-Empirical Pavement Design Guide (MEPDG). The MEPDG was developed under the National Cooperative Highway Research Program (NCHRP) 1-37A project in 2004 (*1*). The software predicts different types of pavement distress, including top-down and bottom-up fatigue cracking, rutting, thermal cracking, and the international roughness index (IRI) in flexible pavements. The mechanistic part of this approach calculates the cumulative damages over time based on the pavement responses to traffic and environmental loads. The estimated damage is transferred to pavement distresses through the existing empirical functions. These empirical functions were calibrated and validated using the data collected from the Long-Term Pavement Performance (LTPP) pavement sections across the nation, as reported by Li et al. (2011) (*2*).

The use of Pavement-ME models in pavement engineering has increased over the past few years. However, accurate calibration of these models is critical for reliable pavement performance predictions. Several researchers have tried calibrating the Pavement-ME models since implementing MEPDG (*3-5*). These efforts have become more robust since the advancements of computational techniques. Haider et al. (2018) used resampling methods (bootstrapping and repeated sampling) to calibrate transverse cracking and the International Roughness Index (IRI) in Michigan *(6)*. These techniques are beneficial in accommodating the variability caused by model predictions. Tabesh and Sakhaeifar (2021) calibrated the bottom-up, top-down, rutting, transverse cracking, and IRI models for Oklahoma, separately for the east and west regions *(7)*. This study used a narrow-down iterative approach to minimize the standard error by changing the transfer function coefficient in Microsoft Excel Solver.

The Pavement-ME has been implemented or is in the process of implementation by several agencies throughout the world. The performance models need calibration for their complete applicability to the local conditions. Dong et al. (2020) calibrated the joint faulting model for the pavements in Ontario using three different optimization approaches: (1) one at a time; (2) generalized reduced gradient (GRG) in MS Excel Solver; and (3) levenberg-marquardt algorithm (LMA) fitting *(8)*. Shakhan et al. (2021) conducted a study to develop a methodology for using the Pavement-ME for the local conditions in Turkey (*9*). Bustos et al. (2011) calibrated the transfer functions for pavements in Argentina using 9 JPCP sections, mainly from the central part of Argentina(*10*). All these studies significantly improved the performance predictions compared to the global model.

2.2 LOCAL CALIBRATION PROCESS

As mentioned, the Pavement-ME uses performance prediction models that are nationally calibrated based on pavement material properties, structure, climate, truck loading conditions, and data from the Long-term Pavement Performance (LTPP) program *(11)*.

However, these models may not accurately predict pavement performance if the input properties and data used for calibration do not reflect the state's unique conditions. Therefore, it is recommended that each State Highway Agency (SHA) evaluates how well the nationally calibrated models predict field performance. If the predictions are unsatisfactory, local calibration of the Pavement-ME models is recommended to improve the pavement performance predictions that reflect the state's specific field conditions and design practices. The local calibration process confirms that the prediction models can accurately predict pavement distress and smoothness and determines the standard error associated with the prediction equations. This section summarizes the local calibration process per the local calibration guide, 2010 *(12)* and MEPDG, 2015 *(13)*.

Step 1: *Selection of input levels*

The hierarchical input level must be selected before local calibration. This depends on the availability of inputs in the local database and the agency's laboratory and field-testing capabilities. The selection of input levels is a critical step as it impacts the standard error of prediction.

Step 2: *Develop an experimental plan and sampling strategy*

The agency needs to develop a statistically sound and practical experimental plan and sampling template for this step. The sampling strategy should consider the local construction, design, and rehabilitation practices. The design matrix should include a wide range of traffic, materials, and climatic inputs.

Step 3: *Assess the adequate sample size for each distress*

A reasonable number of sections should be selected for calibration. The minimum sample size for any distress can be estimated using Equation (2-1).

$$n = \left(\frac{Z_{\alpha/2} \times \sigma}{e_t}\right)^2 \quad (2\text{-}1)$$

where,
$Z_{\alpha/2}$ = z-value from a standard normal distribution
n = Minimum number of pavement sections
σ = Performance threshold
e_t = Tolerable bias = $Z_{\alpha/2} \times SEE$
SEE = Standard error of the estimate

Step 4: *Selection of pavement sections*

This step involves selecting the pavement sections to populate the experimental matrix developed in step 2. Selection should include local construction practices, sections with and without overlay, pavements with non-conventional materials, and replicates. A minimum of three measured distress data should be available over ten years to incorporate any time-dependent effects. In case of inadequacy of sections, LTPP sections can be added to enhance the database.

Step 5: *Get Pavement-ME inputs and measured distress data*

The Pavement-ME inputs and the measured distress data must be extracted from the local agency database based on the hierarchical input level determined in step 1. The performance data must be converted to the Pavement-ME compatible units if the agency measurements are different. The average maximum distress from the selected sections should exceed 50% of the threshold design criteria to incorporate considerable distress in the calibration process. Any outliers in the performance data should be reviewed, considering the maintenance activities or changes in agency policies. Further field investigation can be conducted to resolve any discrepancies.

Step 6: *Conduct field and forensic investigation*

This step aims to collect any missing data and investigate any discrepancies in the input data available in the local database. The testing protocol to be followed should be in accordance with the agency's practices. At the end of this step, the agency should ensure that a reasonable number of samples remain in the experimental matrix.

Step 7: *Validation of global model coefficients to local conditions*

For this step, the global coefficients are used to predict each performance measure for all sections included in the experimental matrix. A reliability of 50% should be used for this step. The predicted values are compared with the measured ones to calculate the bias and SEE. A plot of predicted versus measured values is created for each distress to visualize the accuracy of predictions to a line of equality (LOE). For a good fit, the points should lie along the LOE. The measured distress $y_{Measured}$ and predicted distress $x_{Predicted}$ can be modeled in the form of a linear model as shown in Equation (2-2) where m is the slope, and b_o is the intercept.

$$y_{\text{Measured}} = b_o + m \times x_{\text{Predicted}} \tag{2-2}$$

Three hypothesis tests are conducted to evaluate the reasonableness of the global model. If any of these hypotheses fail, the models are recalibrated for local conditions:

- There is no systematic bias between the measured and predicted distress (Equation 2-3). This can be tested using a paired *t*-test.

$$H_0: \sum(y_{\text{Measured}} - x_{\text{Predicted}}) = 0 \tag{2-3}$$

- The slope parameter m is 1, and the intercept parameter b_o is zero (Equations 2-4 and 2-5).

$$H_0: m = 1.0 \tag{2-4}$$
$$H_o: b_o = 0 \tag{2-5}$$

Step 8: *Eliminate the local bias for Pavement-ME models*

This step should eliminate the local bias by systematically changing the model coefficients. The approach should be based on the overall bias, SEE between the predicted and measured values, and the causes associated with them. The calibration coefficients should be incorporated into the calibration process if they depend on material property, site factor, or design features. Table 2-1 summarizes the calibration coefficients affecting the bias and standard error.

Table 2-1 Calibration coefficients eliminating standard error and bias (*14*)

Pavement Type	Distress	Eliminate Bias	Reduce Standard Error
Asphalt	Total rut depth	$k_{1r}, \beta_{1r}, \beta_{s1}$	$k_{2r}, k_{3r}, \beta_{2r}, \beta_{3r}$
	Fatigue bottom-up cracking	k_1, C_2	k_2, k_3, C_1
	Fatigue top-down cracking	k_1, C_2	k_2, k_3, C_1
	Thermal cracking	β_{f3}, k_{f3}	β_{f3}, k_{f3}
	IRI	C_4	C_2, C_3, C_4
JPCP	Faulting	C_1	C_1
	Transverse cracking	C_1, C_4	C_2, C_5
	IRI - JPCP	J_4	J_1

Step 9: *Estimate the standard error of the estimate*

After the bias has been eliminated, the SEE is computed between the measured and predicted distress. This SEE must be compared with the global SEE. Table 2-2 shows the standard value for global SEE for different models.

Table 2-2 Recommended standard error values

Pavement type	Performance prediction model	S_e
Flexible	Fatigue cracking (%)	5
	Thermal cracking (ft/mile) Thermal reflection cracking	650
	Rutting (inches)	0.2
	IRI (in/mile)	65
Rigid	Transverse cracking (%)	15
	Joint faulting (inches)	0.07
	IRI (in/mile)	65

If the SEE is lower than recommended, the calibration coefficients can be accepted and used for design. The hypothesis tests given in step 7 must be validated before accepting the coefficients. If the SEE exceeds the global value, the agency can still accept the coefficients or move to step 10 to eliminate the standard error.

Step 10: *Eliminate standard error of estimate*

If the standard error of the estimate calculated in step 9 is higher than the recommended global value, it should be eliminated in the local calibration process. The standard error should be estimated for each category of the experimental matrix to identify the effects of any input parameter on the overall standard error. The coefficients resulting in the minimum standard error can be used for design purposes.

Step 11: *Assessment of the calibration process*

After the above ten steps have been performed to establish the local calibration coefficients, they should be examined for reasonableness within each category of the experimental matrix and at different reliability levels.

2.3 LOCAL CALIBRATION EFFORTS AND CHALLENGES

Several SHAs have locally calibrated the Pavement-ME models to adopt ME design practices. As previously outlined, the process involves matching the predictions with the measured value by optimizing the transfer function coefficients. This process is very tedious and poses the following challenges:

- Project selection: identify the available sections with performance data
- Pavement-ME inputs: the data might not be available with the required information and assumptions.
- Calculate performance data: measured data might not be available in the database for the Pavement-ME compatible units. Necessary assumptions must be made for conversion.
- Local calibration techniques: identify mathematical tools/processes for local calibration

The local calibration process and calibration coefficients for several states have been outlined in the previous calibration effort for Michigan *(15)*. These states include:

- Arkansas
- Colorado
- FHWA
- Minnesota
- Missouri
- Montana
- New Mexico
- North Carolina
- Ohio
- Oklahoma
- Oregon
- South Carolina
- Texas
- Utah
- Washington

Some states have recalibrated their performance models, and some new states have been added. The following sections summarize the calibration efforts for flexible and rigid pavements.

2.3.1 Local Calibration Efforts for Flexible Pavements

Oklahoma (7): Tabesh and Sakhaeifar (2021) conducted a study to calibrate the Pavement-ME models in Oklahoma. A total of 65 flexible pavement sections (53 new LTPP sections and, 9 LTPP sections from the previous study in Oklahoma, and 3 LTPP sections from Texas and Kansas) were considered in this study. The inputs were obtained from the LTPP database and previous calibration studies. Moreover, for any missing information, typical level 3 recommended values were used. The Pavement-ME V2.3 was used to predict pavement performance, where each section was considered a new construction project up to any significant rehabilitation/reconstruction. The calibration coefficients were divided based on whether they reduced bias or standard error. Coefficients corresponding to eliminate bias were optimized outside of the Pavement-ME using the Generalized Reduced Gradient (GRG) nonlinear method in Microsoft Excel Solver. For coefficients that reduce the standard error, an iterative approach was followed where the software was run each time to reduce the standard error systematically. Overall, local calibration resulted in lower standard error and bias than the global mode. IRI and rutting models correlated better with top-down, bottom-up, and thermal cracking models. This study did not calibrate the standard deviation equations for different prediction models.

Missouri (16): Glover et al. (2020) conducted a study funded by the Missouri Department of Transportation (MoDOT) to calibrate the Pavement-ME models in Missouri. This study included new and rehabilitated sections from MoDOT's Pavement Management System (PMS) database and LTPP. AC over AC and JPCP sections were considered rehabilitated sections. Inputs to the Pavement-ME were collected from the LTPP database, MoDOT PMS database, laboratory and field tests, and previous studies *(17)*. PMED V2.5.5 was used to calibrate the performance models. Local calibration significantly improved the prediction for all models, although the top-down cracking model was not calibrated in this effort, and global coefficients are recommended. Reliability prediction models were not calibrated, and the global models were accepted.

Michigan (15): Calibration for new flexible and rehabilitated pavements for Michigan was conducted in a research study by Haider et al. (2014). A total of 129 reconstructed flexible sections and 40 rehabilitated sections were selected for this project. The Pavement-ME inputs were obtained from the Michigan Department of Transportation (MDOT) Pavement Management System (PMS) database, construction records, and previous studies conducted in Michigan. Models were calibrated outside the Pavement-ME using no sampling and bootstrapping resampling techniques. For validation of these models, traditional split sampling and repeated split sampling were used, with 70% of the sections used for calibration and the remaining 30% for validation. Bootstrapping and repeated split sampling provide a distribution of calibration coefficients and error terms instead of single-point estimates. Standard deviation equations for all performance models were calibrated to incorporate reliability using local performance and prediction data.

Georgia (16): Quintus et al. (2015) conducted the calibration of the Pavement-ME models for Georgia. Forty flexible sections (22 LTPP + 18 non-LTPP) were selected for this study, including new flexible pavements and HMA overlays. Non-LTPP sections were added due to the insufficient number of LTPP sections, insufficient measured distress, and the inability of

LTPP sections to truly represent the construction practices in Georgia. PMED inputs were extracted from the LTPP database, as-built plans and construction records, and field and laboratory investigations. Measured distress data for the non-LTPP sections were collected from Georgia's Department of Transportation (GDOT) PACES and CPACES database. Rut depth was found to be overpredicted using global calibration coefficients and was recalibrated to obtain local calibration coefficients. The coefficients K1 and K3 were calibrated separately for neat and polymer-modified binder, whereas K2 was kept at global value. Finally, a value of K1 = -2.45 (for neat), -2.55 (for polymer-modified), and K3=0.30 (for neat and polymer-modified mixes) was adopted. Bottom-up fatigue cracking was found to be underpredicting using the global model. The top-down fatigue cracking model was not calibrated in this study because of the argument on the usability of the crack initiation mechanism, and no field investigations were conducted to confirm crack initiation at the surface. For IRI, global calibration coefficients were found applicable and were recommended for use.

Tennessee (17): The Tennessee Department of Transportation (TDOT) conducted a study to calibrate the transfer functions in the Pavement-ME models for Tennessee. The performance and traffic data were obtained from the TDOT PMS database. Annual average daily truck traffic (AADTT) is not recorded in the PMS database, which is a required input to PMED. The Average Annual daily traffic (AADT) was multiplied by the percent truck traffic available in the PMS database to obtain AADTT. A total of 76 sections (PMS + LTPP) were used for calibrating models in the Pavement-ME version 2.1. Total rutting was overpredicted, and fatigue cracking was underpredicted using the national model coefficients. The models were calibrated outside the Pavement-ME software using Microsoft Excel Solver and MATLAB curve fitting functions. The jackknifing resampling method was used for the calibration and validation of models. This provides the standard deviation and confidence limits for calibration coefficients, leading to more reliable estimations. Rutting, bottom-up, and top-down cracking models were calibrated locally, whereas, for the IRI model, global model coefficients were recommended. A separate set of calibration coefficients was recommended for rutting based on terrain. Reliability equations for standard error were not calibrated in this study. Moreover, the authors find the reliability model in MEPDG questionable. Apart from the calibration effort, a questionnaire was also generated and sent to different DOTs in the US and Canadian transportation administration agencies to analyze the current design practices and feedback on the MEPDG design process. Results revealed that most of the states in the US and Canadian provinces use AASHTO 1993 to design both flexible and rigid pavements. Also, bottom-up cracking was the most challenging model for calibration, followed by longitudinal and thermal cracking. Moreover, most states were not completely satisfied with the Pavement-ME software due to the multiple inputs and interpretations required for design.

Iowa (18): The Pavement-ME models in Iowa were calibrated using V1.1. The inputs were collected from the Iowa DOT Pavement Management Information System (PMIS), laboratory testing, and previous relevant studies in Iowa. Thirty-five (35) flexible sections were selected from the available database. Of these, 25 sections (237 data points) were used for calibration and 10 sections for validation (90 data points). The study used the default values for any missing inputs considering the sensitivity of the information. Before

calibrating the models, a sensitivity analysis was conducted to estimate the effect of each coefficient on the predicted performance. Rutting and fatigue cracking models were calibrated by trial runs in the Pavement-ME, whereas the IRI model was calibrated using optimization in MS Excel Solver. The normalized sensitivity index calculated was used as a reference to estimate the contribution of bias from each coefficient and the approximations to local coefficient values. Top-down cracking was underpredicted using national model coefficients. Rutting and top-down cracking models were calibrated, whereas, for bottom-up cracking and IRI, the nationally calibrated models performed well and were accepted. Reliability equations were not calibrated for this study.

Wyoming (19): Bhattacharya et al. (2015) calibrated the Pavement-ME models in Wyoming using V2.2. Initially, the calibration effort was planned to include only LTPP sections in Wyoming. However, due to the limited number of such sections, the study also included LTPP sections from nearby states with similar design practices. A total of 86 new flexible pavements (77 LTPP + 9 non-LTPP) were selected. The Pavement-ME inputs were taken from the WYDOT's construction files, LTPP database, and field investigation by the University of Wyoming. Any outlier in the measured data was removed. Since global models over-predicted Rut depth and bottom-up fatigue cracking, those were recalibrated. For both of these models, the global standard equation was recommended. For rutting model, coefficient K1 (WYDOT value = -2.45) and K3 (WYDOT value = 0.30) were calibrated while K2, β1r, β2r, β3r were kept to the global value. The top-down cracking model was not calibrated in this effort due to discrepancies in the model. For IRI, the global model was found reasonable and recommended for use.

Kansas (20): Sun et al. (2015) conducted a research study to calibrate the Pavement-ME models in Kansas. A total of 28 new flexible sections were selected from the KDOT PMS database, and V1.3 was used. The material properties, traffic data, and climate data were obtained from the KDOT, and MEPDG recommended level 3 values were used if data were unavailable. The measured performance data was extracted from the KDOT PMS database. No field or forensic investigation was conducted for this study, as the available data was considered sufficient. The sections were divided into two parts based on the resilient modulus of the subgrade (equal to 2700 psi and greater than 4000 psi). The magnitude of measured bottom-up cracking was almost zero; hence, the global model was accepted. Top-down cracking was underpredicted, and the global model coefficients overpredicted rutting and IRI. This study did not calibrate the standard deviation used for reliability.

The following section presents the formulation of transfer functions for flexible pavement models and the local calibration coefficients for different states.

2.3.1.1. Fatigue cracking (bottom-up)

Bottom-up cracking is a load-related distress caused by the repeated axle load. These cracks initiate at the bottom of the asphalt concrete (AC) layer and propagate to the surface. The total cumulative damage *DI* can be estimated by summing the cumulative damage that can be computed using Miner's law *(21)*, as shown in Equation (2-6).

$$DI = \sum(\Delta DI)_{j,m,l,p,T} = \sum\left(\frac{n}{N_{f-HMA}}\right)_{j,m,l,p,T} \quad (2\text{-}6)$$

where,

n = number of actual axle load applications within a specific time period
j = axle load-interval
m = axle type (single, tandem, tridem, quad)
l = truck type classified in the MEPDG
p = month
T = median temperature for five temperature quintiles used in MEPDG
$N_{f\text{-}HMA}$ = the allowable number of axle load applications, which can be computed using Equation (2-7).

$$N_{f-HMA} = C \times k_1 \times C_H \times \beta_{f1}(\varepsilon_t)^{-k_2\beta_{f2}}(E_{HMA})^{-k_3\beta_{f3}} \quad (2\text{-}7)$$

where,

ε_t = tensile strain at critical AC locations
E_{HMA} = dynamic modulus (E^*) of the Hot mix asphalt (HMA), psi
$k1$, $k2$, $k3$ = laboratory regression coefficients, and β_{f1}, β_{f2}, β_{f3} = local or field calibration constants
C = Adjustment factor (laboratory to the field) as shown in Equation (2-8) and Equation (2-9).

$$C = 10^M \quad (2\text{-}8)$$

$$M = 4.84\left(\frac{V_{be}}{V_a + V_{be}} - 0.69\right) \quad (2\text{-}9)$$

where,

V_{be} = effective binder content by volume, percent
V_a = In-situ air voids in the HMA mixture (%)
C_H = thickness correction factor for bottom-up cracking as shown in Equation (2-10).

$$C_H = \frac{1}{0.000398 + \frac{0.003602}{1 + e^{(11.02 - 3.49H_{HMA})}}} \quad (2\text{-}10)$$

where,

H_{HMA} = AC layer thickness

Once the cumulative damage is calculated, the bottom-up fatigue cracking (%) can be estimated using the transfer function given in Equation (2-11)

$$FC_{\text{Bottom}} = \left(\frac{1}{60}\right)\left(\frac{C_4}{1 + e^{C_1C_1^* + C_2C_2^*\log(DI_{\text{Bottom}} \cdot 100)}}\right) \quad (2\text{-}11)$$

where,

FC_{Bottom} = Bottom-up fatigue cracking (in the percentage of area)
DI_{Bottom} = cumulative damage at the bottom of the AC layer
C_1, C_2, C_4 = Transfer function coefficients where C2 is a function of thickness for HMA thickness between 5 and 12 inches
C_1^* and C_2^* can be determined using Equation (2-12) and Equation (2-13).

$$C_1^* = -2C_2^* \quad (2\text{-}12)$$

$$C_2^* = -2.40874 - 39.748(1 + H_{HMA})^{-2.856} \quad (2\text{-}13)$$

Table 2-3 summarizes the local calibration coefficients among several states.

Table 2-3 Local calibration coefficients for bottom-up cracking

States	C_1	C_2	C_4	Standard deviation
Oklahoma (East region)	3.26	-	6000	-
Oklahoma (West region)	4.12	-	6000	-
Missouri	-0.31	hac<5: 1.367 5<hac<12: 0.867+0.1*h_{ac} Hac>12: 2.067	6000	-
Michigan	0.67	0.56	6000	$0.01 + \frac{32.913}{1 + e^{1.3972 - 0.5976 \times \log(D)}}$
Georgia	2.2	2.2	6000	$1.0 + \frac{10}{(1 + \text{Exp}(7.5 - 6.5 * \log 10(DI_{\text{Bottom}} + 0.0001)}$
Tennessee	1.023	0.045	6000	-
Iowa	-	-	-	-
Wyoming	0.4951	1.469	6000	-
Kansas	-	-	-	-
Arkansas	0.688	0.294	6000	-
New Mexico	0.625	0.25	6000	-
Washington	1.071	1	6000	-
Colorado	0.07	2.35	6000	-
Pavement-ME v2.6	1.31	hac<5: 2.1585 5<hac<12: (0.867+0.2583*h_{ac})*1 Hac>12: 3.9666	6000	$1.13 + \frac{13}{(1 + \text{Exp}(7.57 - 15.5 * \log 10(DI_{\text{Bottom}} + 0.0001)}$

2.3.1.2. Fatigue cracking (top-down)

Top-down or longitudinal cracking is a load-related distress due to repeated axle load. It appears in the form of cracks parallel to the wheel path and starts at the surface of the AC layer.

Old model: The damage calculation for top-down cracking is the same as bottom-up cracking for the old model except for the thickness correction factor and the transfer function, as shown in Equation (2-14) and Equation (2-15).

$$C_H = \frac{1}{0.01 + \frac{12.00}{1 + e^{(15.676 - 2.8186 H_{\text{HMA}})}}} \quad (2\text{-}14)$$

$$FC_{\text{Top}} = 10.56 \left(\frac{C_3}{1 + e^{C_1 - C_2 Log(DI_{\text{Top}})}} \right) \quad (2\text{-}15)$$

where,

FC_{Top} = Top-down fatigue cracking (in ft/mile)
DI_{Top} = cumulative damage at the top of the AC layer
C_1, C_2, C_3 = Transfer function coefficients

New model: The new top-down cracking model is based on fracture mechanics concepts *(22)*. It is expressed in percentage rather than ft./mile. The model involves crack initiation and propagation [based on Paris' law (*23*)]. Crack initiation is defined as a crack length of 7.5mm

(0.3 inches). Equation (2-16) shows the time to crack initiation formulated using regression over longitudinal and alligator cracking data from the LTPP database.

$$t_0 = \frac{\mathrm{K}_{L1}}{1 + e^{\mathrm{K}_{L2}\times 100\times(\mathrm{a}_0/2\mathrm{A}_0)+\mathrm{K}_{L3}\times\mathrm{HT}+\mathrm{K}_{L4}\times LT+K_{L5}\times\log_{10}\ \mathrm{AADTT}}} \quad (2\text{-}16)$$

where,

t_0 = Time to crack initiation, days
H_T = Annual number of days above 32ºC
L_T = Annual number of days below 0ºC
AADTT = Annual average daily truck traffic (initial year)
$a_0/2A_0$ = Energy parameter
K_{L1}, K_{L2}, K_{L3}, K_{L4}, K_{L5}= Calibration coefficients for time to crack initiation

The top-down cracking is expressed in percentage using the transfer function, as shown in Equation (2-17).

$$L(t) = L_{MAX}e^{-\left(\frac{C_1\rho}{t-C_3t_0}\right)^{C_2\beta}} \quad (2\text{-}17)$$

where,

$L(t)$ = Top-down cracking expressed as total lane area (%)
L_{MAX} = Maximum area of top-down cracking (%) – a value of 58% is assumed
t = Analysis month in days
ρ = Scale parameter for the top-down cracking curve as shown in Equation (2-18).

$$\rho = \alpha_1 + \alpha_2 \times \text{ Month} \quad (2\text{-}18)$$

β = Shape parameter for the top-down cracking curve as shown in Equation (2-19).

$$\beta = 0.7319 \times (\log_{10}\ \text{Month}\ )^{-1.2801} \quad (2\text{-}19)$$

where,

α_1 and α_2 are functions of the climatic zone (wet freeze, wet non-freeze, dry freeze, dry non-freeze)

Table 2-4 summarizes the local calibration coefficient of the top-down cracking model. These coefficients have been calibrated using the top-down cracking model.

Table 2-4 Local calibration coefficients for top-down cracking

States	C_1	C_2	C_3	Standard deviation
Oklahoma (East region)	6.6	4.5	723	-
Oklahoma (West region)	6.1	4.23	723	-
Michigan	2.97	1.2	1000	$300 + \frac{3000}{1 + e^{1.8-0.61\times\log\,(D_{si}+0.0001)}}$
Tennessee	6.44	0.27	204.54	-
Iowa	0.82	1.18	1000	-
Kansas	4.5	-	36000	-
Arkansas	3.016	0.216	1000	-
New Mexico	3	0.3	1000	-
Washington	6.42	3.596	1000	-
Pavement-ME	7	3.5	1000	-

2.3.1.3. Transverse (thermal) cracking model

Thermal cracking is associated with the contraction of the HMA material due to surface temperature fluctuations. The temperature variations affect the volume changes of the material. As a consequence, stresses develop due to the continual contraction of the materials and the restrained conditions, which causes thermal cracks. Typically, thermal cracking in flexible pavements occurs due to the temperature drop experienced by the pavement in cold conditions. A thermal crack will initiate when the tensile stresses in the HMA layers become equal to or greater than the material's tensile strength. The initial cracks propagate through the HMA layer with more thermal cycles. The amount of crack propagation induced by a given thermal cooling cycle is predicted using the Paris law of crack propagation. Experimental results indicate that reasonable estimates of *A* and *n* can be obtained from the indirect tensile creep-compliance and tensile strength of the HMA per Equations (2-20 and 2-21).

$$\Delta C = A(\Delta K)^n \tag{2-20}$$

where,

ΔC = Change in the crack depth due to a cooling cycle
ΔK = Change in the stress intensity factor due to a cooling cycle
A, n = Fracture parameters for the HMA mixture

$$A = k_t \beta_t 10^{[4.389 - 2.52 Log(E_{HMA} \sigma_m \eta)]} \tag{2-21}$$

where,

η = $\eta = 0.8\left[1 + \frac{1}{m}\right]$
k_t = Regression coefficient determined through field calibration
E_{HMA} = HMA indirect tensile modulus, psi
σ_m = Mixture tensile strength, psi
m = The m-value derived from the indirect tensile creep compliance curve measured in the laboratory
β_t = Local or mixture calibration factor

The stress intensity factor, *K*, has been incorporated in the Pavement-ME through a simplified equation developed from theoretical finite element studies using the model shown in Equation (2-22).

$$K = \sigma_{tip}\left(0.45 + 1.99(C_o)^{0.56}\right) \tag{2-22}$$

where,

σ_{tip} = Far-field stress from pavement response model at a depth of crack tip, psi
C_o = Current crack length, feet

Equation (2-23) shows the transfer function for transverse cracking in the Pavement-ME.

$$TC = \beta_{t1} N(z)\left[\frac{1}{\sigma_d} Log\left(\frac{C_d}{H_{HMA}}\right)\right] \tag{2-23}$$

where,

TC	=	Observed amount of thermal cracking, ft/500ft
β_{t1}	=	Regression coefficient determined through global calibration (400)
$N[z]$	=	Standard normal distribution evaluated at [z]
σ_d	=	Standard deviation of the log of the depth of cracks in the pavement (0.769), in
C_d	=	Crack depth, in;
H_{HMA}	=	Thickness of HMA layers, in

Table 2-5 summarizes the modified local calibration coefficients for the various States.

Table 2-5 Local calibration coefficients for the thermal cracking model

Calibration coefficient	Level 1 K	Level 2 K	Level 3 K
Missouri	0.61	-	-
Montana	-	-	0.25
Colorado	6.3	0.5	6.3
Michigan	0.75	-	-
Oklahoma	East: $3 \times 10^{-7} \times MAAT^{4.0319} - 54$ west: $3 \times 10^{-7} \times MAAT^{4.0319} - 23$	-	-
Pavement-ME	$3 \times 10^{-7} \times MAAT^{4.0319}$	$3 \times 10^{-7} \times MAAT^{4.0319}$	$3 \times 10^{-7} \times MAAT^{4.0319}$

2.3.1.4. Rutting model

Due to axle loads, rutting is the total accumulated plastic strain in different pavement layers (AC, base/sub-base, and subgrade). It is calculated by summing up the plastic strains at the mid-depth of individual layers accumulated for each time increment. Equation (2-24) shows the permanent plastic strain for the AC layer.

$$\Delta_{p(HMA)} = \varepsilon_{p(HMA)} h_{HMA} = \beta_{1r} k_z \varepsilon_{r(HMA)} 10^{k_{1r}} T^{k_{2r}\beta_{2r}} N^{k_{3r}\beta_{3r}} \quad (2\text{-}24)$$

where,

$\Delta_{p(HMA)}$ = permanent plastic deformation in the AC layer
$\varepsilon_{p(HMA)}$ = accumulated permanent or plastic axial strain in the AC layer/sublayer
$\varepsilon_{r(HMA)}$ = resilient or elastic strain calculated by the structural response model at the mid-depth of each AC sublayer
$h_{(HMA)}$ = thickness of the AC layer/sublayer
N = number of axle load repetitions
T =Pavement temperature
k_z = depth confinement factor
k_{1r}, k_{2r}, k_{3r} = global field calibration parameters
β_{1r}, β_{2r}, β_{3r}, = local or mixture field calibration constants

The permanent plastic strain can be expressed for the unbound layers, as shown in Equation (2-25).

$$\Delta_{p(soil)} = \beta_{s1} k_{s1} \varepsilon_v h_{soil} \left(\frac{\varepsilon_o}{\varepsilon_r}\right) e^{-\left(\frac{\rho}{n}\right)^{\beta}} \quad (2\text{-}25)$$

where,

$\Delta_{p(Soil)}$ = permanent plastic deformation for the unbound layer/sublayer
ε_o = intercept determined from laboratory repeated load permanent deformation tests
n = number of axle load applications
ε_r = resilient strain imposed in laboratory tests to obtain material properties ε_o, β, and ρ
ε_v = average vertical resilient or elastic strain in the layer/sublayer and calculated by the structural response model
h_{soil} = unbound layer thickness

k_{s1} = global calibration coefficients (different for granular and fine-grained material)
β_{s1} = local calibration constant for rutting in the unbound layers (base or subgrade)

The total rutting is calculated based on Equation (2-26) below:

$$\text{Rut depth}_{Total} = \Delta_{HMA} + \Delta_{Base/subbase} + \Delta_{Subgrade} \quad (2\text{-}26)$$

Table 2-6 presents the local calibration coefficients for different states.

Table 2-6 Local calibration coefficients for the rutting model

States	β_{1r}	β_{2r}	β_{3r}	β_{gb}	β_{sg}	Standard deviation
Oklahoma (East region)	0.79	0.53	1.48	0.15	1.29	-
Oklahoma (West region)	0.21	0.74	1.03	0.23	1.03	-
Missouri	0.899	-	-	1.0798	0.9779	-
Michigan	0.9453	1.3	0.7	0.0985	0.0367	HMA: $0.1126*RUT^{0.2352}$ BASE: $0.1145*RUT^{0.3907}$ SG: $3.6118*RUT^{1.0951}$
Georgia	-	-	-	0.50	0.30	HMA: $0.20*RUT^{0.55}+0.001$
Tennessee (Plain area)	0.111	-	-	0.196	0.722	-
Tennessee (Mountain area)	0.177	-	-	1.034	0.159	-
Iowa	-	1.15	-	0.001	0.001	-
Wyoming	-	-	-	0.4	0.4	-
Kansas	0.9	-	-	-	0.3251	-
Arkansas	1.2	1	0.8	1	0.5	-
New Mexico	1.1	1.1	0.8	0.8	1.2	-
North Carolina	13.1	0.4	1.4	0.303	1.102	-
Ohio	0.51	-	-	0.32	0.33	-
Texas	2.39	-	0.856	-	0.5	-
Washington	1.05	1.109	1.1	-	0	-
Colorado	1.34	1	1	0.4	0.84	-
Pavement-ME v2.6	0.4	0.52	1.36	1	1	HMA: $0.24*RUT^{0.8026}+0.001$ BASE: $0.1477*RUT^{0.6711}+0.001$ SG: $0.1235*RUT^{0.5012}+0.001$

2.3.1.5. IRI model (flexible pavements)

IRI is a measure of ride quality provided by a pavement surface and affects the vehicle operation cost, safety, and comfort of the driver. The IRI model is based on findings from multiple studies showing that IRI at any age is a function of the initial construction ride quality and the development of different distresses over time that impact the ride quality. IRI can be formulated using the initial IRI and distresses (fatigue cracking, transverse cracking, and rutting), as shown in Equation (2-27).

$$IRI = IRI_o + C1(RD) + C2(FC_{\text{Total}}) + C3(TC) + C4(SF) \quad (2\text{-}27)$$

where,

IRI_o = initial IRI at construction
FC_{Total} = percent area of fatigue cracking (bottom-up), fatigue cracking (top-down), and reflection cracking in the wheel path
TC = length of transverse cracking (including the reflection of transverse cracks in existing AC pavements)
RD = average rut depth
C1, C2, C3, C4 = Calibration coefficients
SF = site factor, which can be expressed as shown in Equation (2-28) to Equation (2-30).

$$SF = (\text{Frost} + \text{Swell}) \times Age^{1.5} \quad (2\text{-}28)$$

$$\text{Frost} = \text{Ln}[(\text{Rain} + 1) \times (FI + 1) \times P_4] \quad (2\text{-}29)$$

$$\text{Swell} = \text{Ln}[(\text{Rain} + 1) \times (PI + 1) \times P_{200}] \quad (2\text{-}30)$$

where,
SF = Site factor
Age = Pavement age (years)
FI = Freezing index
PI = Subgrade soil plasticity index
Rain = Mean annual rainfall
P_4 = Percent subgrade material passing No. 4 sieve
P_{200} = Percent subgrade material passing No. 200 sieve.

Table 2-7 presents the adjusted calibration coefficients in different states. Table 28 summarizes the distress thresholds used in various states.

Table 2-7 Local calibration coefficients for the IRI model

States	C1	C2	C3	C4
Oklahoma (East region)	5.23	0.127	0.013	0.0128
Oklahoma (West region)	6.46	0.187	0.0098	0.023
Missouri	58.9	0.3	0.0072	0.0129
Michigan	50.3720	0.4102	0.0066	0.0068
Kansas	95	0.04	0.001	-
New Mexico	0.015	-	-	-
Ohio	0.066	1.37	0.01	17.6
Colorado	0.019	0.3	0.02	35
Pavement-ME v2.6	40	0.4	0.008	0.015

Table 2-8 Summary of design thresholds for flexible pavements

States	Bottom-up cracking (%)	Top-down cracking (ft/mile)	Total rutting	Thermal cracking	IRI
Oklahoma	20	-	0.4	630	169
Missouri	10	-	0.5	2000	172
Michigan	20	-	0.5	1000	172
Colorado	10	2000	0.55	1500	160
Arizona	20	-	0.4	630	169
Kansas	20	-	0.4	630	169

2.3.2 Local Calibration Efforts for Rigid Pavements

Idaho (24): Bayoumy et al. (2019) calibrated the performance models for JPCP sections in Idaho. Transverse cracking, joint faulting, and IRI models were calibrated using V2.5.3. Forty (40) JPCP pavement sections were selected across Idaho, and the performance data along with the Pavement-ME inputs were obtained from construction records, material testing records, and the Idaho Transportation Department (ITD) Transportation Asset Management System (TAMS) database. Missing data was taken from the Idaho PMED user guide (*25*). The models were calibrated by systematically changing the coefficients and running the Pavement-ME for each trial. A traditional split sampling approach was adopted for validation, with 80% of the sections for calibration and 20% for validation. Recalibration results show a good correlation between predicted and measured distress for faulting and IRI models. The transverse cracking model was recalibrated with additional data due to poor correlation. Standard deviation equations were not recalibrated in this calibration study.

Missouri (26): Glover et al. calibrated the Pavement-ME models for new JPCP and unbonded overlay over JPCP for Missouri. A total of 44 sections (35 new JPCP and 9 unbonded overlays over JPCP) were used for this study. Due to insufficient performance data for these sections, a non-regression classification analysis approach was used to assess the need for local calibration. The authors recommend using the national calibration coefficients for new JPCP and unbonded overlay over JPCP sections until a local calibration is performed. Standard deviation equations were not recalibrated in this calibration study.

Michigan (15): Haider et al. conducted a study to calibrate the Pavement-ME models for new JPCP and unbonded overlay over JPCP pavements in Michigan. A total of 29 reconstructed JPCP sections and 16 unbonded overlays over JPCP sections were selected for this project. The Pavement-ME inputs were taken from the Michigan Department of Transportation (MDOT) Pavement Management System (PMS) database, construction records, and previous studies conducted in Michigan. For transverse cracking and IRI models, the calibration was performed outside the Pavement ME using no sampling and bootstrapping resampling technique. For validation of these models, traditional split sampling and repeated split sampling were used, with 70% of the sections used for calibration and the remaining 30% for validation. For the joint faulting model, the Pavement-ME was run every time by changing the coefficient (Only C1 was optimized by keeping other coefficients fixed to the global value). This study gives a new approach to using resampling techniques to obtain distributions of model coefficients and error terms. Reliability equations for each performance model were calibrated using the MEPDG approach for the Michigan performance data.

Georgia (16): Quintus et al. (2015) calibrated the Pavement-ME performance models for the state of Georgia. A total of 20 sections (8 LTPP+12 non-LTPP) were used for this calibration. Non-LTPP sections were added due to the insufficient number of LTPP sections, insufficient measured distress, and the inability of LTPP sections to represent the construction practices in Georgia truly. The PMED inputs were extracted from the LTPP database, as-built plans and construction records, and field and laboratory investigations. Measured distress data for the non-LTPP sections were collected from Georgia's Department of Transportation (GDOT) PACES and CPACES database. Global coefficients were

finalized for the transverse cracking model after verification using LTPP and non-LTPP sections. Moreover, future calibration was recommended using more sections and performance data. The joint faulting and IRI models were recalibrated for the local conditions. The global standard deviation equation was accepted for transverse cracking to incorporate reliability in the design. In contrast, the standard deviation equation was modified for joint faulting to match the prediction data.

Iowa (18): The local calibration effort for the Pavement-ME models in Iowa was conducted using V1.1. The inputs were collected from the Iowa DOT Pavement Management Information System (PMIS), material testing records, and previous relevant studies in Iowa. 35 JPCP sections were selected from the available database. Of these, 25 sections (248 data points) were used for calibration and 10 sections for validation (101 data points). For any missing inputs, the default values were taken considering the sensitivity of the information. Faulting was underpredicted, and transverse cracking and IRI were overpredicted using the national coefficients. Before calibrating the models, a sensitivity analysis was conducted to estimate the effect of each coefficient on the predicted performance. The normalized sensitivity index calculated was used as a reference to assess the contribution of bias from each coefficient and the approximations to local coefficient values. Multiple runs calibrated faulting and fatigue cracking in Pavement ME, whereas transverse cracking and IRI were calibrated using MS Excel Solver. Predictions for all models were significantly improved after calibration. Standard error equations were not calibrated for this study.

Wyoming (19): Bhattacharya et al. (2015) conducted a research study for the Wyoming Department of Transportation (WYDOT) to calibrate the Pavement-ME models for local conditions in Wyoming. V2.2 was used for this calibration effort. Initially, the calibration effort was planned to include only LTPP sections in Wyoming, but due to the limited number of such sections, LTPP sections from nearby states with similar design practices were added. A total of 26 LTPP JPCP sections (1 from Wyoming + 25 from adjacent states) were selected for this study. The Pavement-ME inputs were taken from the WYDOT's construction files, LTPP database, and field investigation by the University of Wyoming. Any outliers in the measured data were removed. The verification using the global model coefficient showed that the transverse cracking model predictions were appropriate. Therefore, the global coefficient and standard deviation equation were recommended. The possible reason for this good fit can be the limited number of sections and most of the sections showing low values for transverse cracking. IRI predictions using the global model also showed no significant bias, and the global coefficients were accepted. Faulting was overpredicted using the global model, and the model coefficients and the standard deviation equation were calibrated for the local conditions.

Kansas (20): The Kansas Department of Transportation (KDOT) funded a research study to calibrate the Pavement-ME models for Kansas. A total of 32 new JPCP sections were selected from the KDOT PMS database, and V1.3 was used for this study. The material properties, traffic data, and climate data were taken from the KDOT and MEPDG recommended values and were considered level 3 inputs. No field or forensic investigation was conducted for this study, as the available data was considered sufficient. The measured performance data was taken from the KDOT PMS database. Faulting was overpredicted, and

IRI was slightly underpredicted using global coefficients. The transverse cracking model was not calibrated in this study. The calibration coefficients were also compared with other states *(14)* and were found within a reasonable range.

Louisiana (27): Wu et al. (2014) calibrated the Pavement-ME models in Louisiana using V1.3. 19 JPCP projects selected for this study have two bases: PCC over HMA and PCC over the unbound base. The joint faulting was underpredicted, whereas transverse cracking was overpredicted using the global model coefficients. Based on the available literature at the time of the project, only the most sensitive coefficients were calibrated. *C1* was calibrated for transverse cracking and *C6* for the faulting model. After calibrating the transverse cracking and joint faulting model, the IRI model was found to be reasonable, and global coefficients were accepted. The effect on design thicknesses was also compared, and the results showed that the Pavement-ME designs had thinner PCC thicknesses (about 2 cm or 7%) compared to the AASHTO 1993 method *(28)*.

The following is a summary of transfer functions for Pavement-ME models applicable to rigid pavements and a review of local calibration coefficients for various states.

2.3.2.1. Transverse cracking model

Transverse slab cracking in the Pavement-ME is calculated as the percentage of slabs cracked, including all severity levels. The mechanism involves independently predicting the bottom-up and top-down cracking and utilizing a probabilistic relationship to combine both, eliminating the possibility of both co-occurring. The fatigue damage for both bottom-up and top-down is defined using Miner's law as given in Equation (2-31):

$$DI_F = \sum \frac{n_{i,j,k,l,m,n,o}}{N_{i,j,k,l,m,n,o}} \tag{2-31}$$

where,

DI_F = total fatigue damage (bottom-up or top-down)

$n_{i,j,k,l,m,n,o}$ = actual load applications applied at age *i*, month *j*, axle type *k*, load level *l*, the equivalent temperature difference between top and bottom PCC surfaces *m*, traffic offset path *n*, and hourly truck traffic fraction *o*

$N_{i,j,k,l,m,n,o}$ = allowable number of load applications applied at age *i*, month *j*, axle type *k*, load level *l*, the equivalent temperature difference between top and bottom PCC surfaces *m*, traffic offset path *n*, and hourly truck traffic fraction *o*

The allowable number of load applications is a function of PCC strength and applied stress and is calculated based on Equation (2-32):

$$\log\left(N_{i,j,k,l,m,n,o}\right) = C_1 \cdot \left(\frac{MR_i}{\sigma_{i,j,k,l,m,n,o}}\right)^{C_2} \tag{2-32}$$

where,

MR_i = Modulus of rupture of the PCC slab at the age *i*

$\sigma_{i,j,k,l,m,n}$ = applied stress at the age *i*, month *j*, axle type *k*, load level *l*, the equivalent temperature difference between top and bottom PCC surface *m*, traffic offset path *n*, and hourly truck traffic fraction *o*

C_1, C_2 = fatigue life calibration coefficients

The fraction of slabs cracked is predicted using Equation (2-33) for both bottom-up and top-down cracking:

$$CRK = \frac{1}{1 + C_4(DI_F)^{C_5}} \quad (2\text{-}33)$$

where,
CRK = predicted fraction of bottom-up or top-down cracking
Once the bottom -up and top-down cracking is estimated, the percentage of slabs cracked is calculated using Equation (2-34).

$$TCRACK = \left(CRK_{\text{Bottom-up}} + CRK_{\text{Top-down}} - CRK_{\text{Bottom-up}} \cdot CRK_{\text{Top-down}}\right) \cdot 100 \quad (2\text{-}34)$$

where,
TCRACK = total transverse cracking (percentage of slabs cracked with all severities)
$CRK_{Bottom\text{-}up}$ = predicted fraction of bottom-up transverse cracking
$CRK_{Top\text{-}down}$ = predicted fraction of top-down transverse cracking

Table 2-9 summarizes the transverse cracking model local calibration coefficients in different states.

Table 2-9 Local calibration coefficients for the rigid transverse cracking model

States	C1	C2	C4	C5	Standard deviation
Idaho	2.366	1.22	0.52	-2.17	Global
Michigan	-	-	0.23	-1.80	$1.34*CRK^{0.6593}$
Missouri	-	-	-	-	-
Georgia	-	-	-	-	-
Iowa	2.17	1.32	1.08	-1.81	-
Wyoming	-	-	-	-	-
Kansas	-	-	-	-	-
Louisiana	2.6	-	-	-	-
Washington	-	-	0.139	-2.115	-
Ohio	-	-	1	-1.98	-
Colorado	-	-	1	-1.98	-
Minnesota	-	-	0.9	-2.61	-
Pavement-ME v2.6	2	1.22	0.52	-2.17	$3.5522*CRK^{0.3415}+0.75$

2.3.2.2. Joint faulting model

The transverse joint faulting is calculated monthly in the Pavement-ME using the material properties, climatic conditions, present faulting level, pavement design properties, and axle loads applied. Total faulting is the sum of faulting increments from previous months and is predicted using Equations (2-35) to (2-38) below.

$$\text{Fault}_m = \sum_{i=1}^{m} \Delta\text{Fault}_i \quad (2\text{-}35)$$

$$\Delta\ \text{Fault}_i = C_{34} \times (\ \text{FAULTMAX}_{i-1} - \ \text{Fault}_{i-1})^2 \times\ \text{DE}_i \quad (2\text{-}36)$$

$$FAULTMAX_i = FAULTMAX_0 + C_7 \times \sum_{j=1}^{m} DE_j \times \log\left(1 + C_5 \times 5.0^{EROD}\right)^{C_6} \quad (2\text{-}37)$$

$$\text{FAULTMAX } X_0 = C_{12} \times \delta_{\text{curling}} \times \left[\log\left(1 + C_5 \times 5.0^{\text{EROD}}\right) \times \log\left(\frac{P_{200} \times \text{WetDays}}{P_s}\right)\right]^{C_6} \quad (2\text{-}38)$$

where,

$Fault_m$ = mean joint faulting at the end of month m
$\Delta Fault_i$ = incremental change (monthly) in mean transverse joint faulting during month i
$FAULTMAXi$ = maximum mean transverse joint faulting for month i
$FAULTMAX_0$ = initial maximum mean transverse joint faulting
$EROD$ = erodibility factor for base/subbase
DE_i = differential deformation energy of subgrade deformation accumulated during month i.
$\delta_{curling}$ = maximum mean monthly slab corner upward deflection PCC due to temperature curling and moisture warping., P_S = overburden pressure on subgrade, P_{200} = percent subgrade soil material passing No. 200 sieve
$WetDays$ = average annual number of wet days (greater than 0.1 in rainfall)
$C1,2,3,4,5,6,7,12,34$ = calibration coefficients

C_{12} and C_{34} are defined by Equation (2-39) and Equation (2-40):

$$C_{12} = C_1 + C_2 \times FR^{0.25} \quad (2\text{-}39)$$
$$C_{34} = C_3 + C_4 \times FR^{0.25} \quad (2\text{-}40)$$

FR = base freezing index defined as the percentage of time (in hours) the top base temperature is below freezing (32 °F) temperature to the total number of hours in design life

Damage in a doweled joint for the current month is estimated using Equation (2-41).

$$\Delta DOWDAM_{tot} = \sum_{j=1}^{N} C_8 \times F_j \frac{n_j}{10^6 df_c^*} \quad (2\text{-}41)$$

where,

$\Delta DOWDAM_{tot}$ = cumulative dowel damage for the current month
n_j = number of axle load applications for the current increment and load group j for the current month
N = number of load categories
fc^* = estimated PCC compressive stress
d = dowel diameter
C_8 = calibration constant
F_j = effective dowel shear force induced by axle loading of load category j

The faulting model local calibration results for several states are summarized in Table 2-10.

Table 2-10 Local calibration coefficients for the faulting model

States	C1	C2	C3	C4	C5	C6	C7	C8	Standard deviation
Idaho	0.516	-	-	-	-	-	-	-	-
Michigan	0.4	-	-	-	-	-	-	-	$0.0442*FAULT^{0.2698}$
Missouri	-	-	-	-	-	-	-	-	-
Georgia	0.595	1.636	0.00217	0.00444	-	0.47	7.3	-	$0.07162*FAULT^{0.368}+0.00806$
Iowa	2.0427	1.8384	0.00438	0.00177	-	0.8	-	-	-
Wyoming	0.5104	0.00838	0.00147	0.08345	5999	0.504	5.9293	-	$0.0831*FAULT^{0.3426}+0.00521$
Kansas	-	-	0.00164	-	-	0.15	0.01	-	-
Louisiana	-	-	-	-	-	1.2	-	-	-
Washington	0.934	0.6	0.001725	0.004	250	0.4	0.65	400	-
Pavement-ME v2.6	0.595	1.636	0.00217	0.00444	250	0.47	7.3	400	$0.07162*FAULT^{0.368}+0.00806$

2.3.2.3. IRI model (rigid pavements)

IRI in the Pavement-ME is a linear relationship between the IRI at construction and change in other distresses (transverse cracking, joint faulting, and joint spalling) over time. IRI, as a linear relationship of these factors, can be expressed by Equation (2-42).

$$IRI = IRI_I + C1 \times CRK + C2 \times SPALL + C3 \times TFAULT + C4 \times SF \quad (2\text{-}42)$$

where,

IRI = Predicted IRI
IRI$_I$ = Initial IRI at the time of construction
CRK = Percent slabs with transverse cracking (all severities).
SPALL = Percentage of joints with spalling (medium and high severities).
TFAULT = Total joint faulting cumulated per mi
C$_1$, *C$_2$*, *C$_3$*, *C$_4$* = Calibration coefficients
SF = Site factor, which can be calculated as shown in Equation (2-43)

$$SF = AGE(1 + 0.5556 \times FI)(1 + P_{200}) \times 10^{-6} \quad (2\text{-}43)$$

where,

AGE = Pavement age
FI = Freezing index, °F-days.
P200 = Percent subgrade material passing No. 200 sieve.
The joint faulting and transverse cracking for IRI calculation is obtained using the models described previously. The joint spalling is calculated as shown in Equation (2-44)

$$SPALL = \left[\frac{AGE}{AGE + 0.01}\right]\left[\frac{100}{1 + 1.005(-12 \times AGE + SCF)}\right] \quad (2\text{-}44)$$

where,

SPALL = percentage joints spalled (medium- and high-severities)
AGE = pavement age since construction
SCF = scaling factor based on site-, design-, and climate-related variables, which is estimated as given in Equation (2-45)

$$SCF = -1400 + 350 \times ACPCC \times (0.5 + PREFORM) + 3.4f_c'^{0.4} - 0.2(\text{FTcycles} \times AGE) + 43h_{PCC} - 536WC_{PCC} \quad (2\text{-}45)$$

where,

ACPCC = PCC air content
AGE = time since construction
PREFORM = 1 if preformed sealant is present; 0 if not
f'$_c$ = PCC compressive strength
FTcycles = average annual number of freeze-thaw cycles
h$_{PCC}$ = PCC slab thickness; *WC$_{PCC}$* = PCC water/cement ratio

The IRI local calibration coefficients for various states are summarized in Table 2-11. Table 2-12 shows threshold values used for different distresses in various states.

Table 2-11 Local calibration coefficients for rigid IRI model

States	C1	C2	C3	C4
Idaho	0.845	0.4417	1.4929	28.24
Michigan	1.198	3.570	1.4929	25.24
Missouri	-	-	-	-
Georgia	1.05	0.5417	1.85	33.8
Iowa	0.04	0.04	0.07	1.17
Wyoming	-	-	-	-
Kansas	-	-	9.38	70
Louisiana	-	-	-	-
Ohio	0.82	3.7	1.711	-
Colorado	0.82	0.442	1.493	-
Pavement-ME v2.6	0.8203	0.4417	1.4929	25.24

Table 2-12 Summary of design thresholds for rigid pavements

States	Transverse cracking (%)	Joint faulting (in)	IRI (in/mile)
Colorado	7	0.12	160
Idaho	10	0.15	169
Arizona	10	0.15	169
Kansas	10	0.15	169
Michigan	15	0.125	172

2.3.3 Challenges and Lessons Learned

A survey of SHAs was conducted recently to document the implementation status and challenges (*14*). The survey was sent to all the SHA's to identify their current design practices and plan for implementing the ME-based design. The questionnaire focused on the practices, policies, and procedures successfully used by the various SHA's. The challenges related to the implementation of the Pavement-ME are of particular interest. The challenges relate to the design software's complexity, availability of the needed input data, defining the most appropriate hierarchical input levels, and local calibration. Most SHAs are concerned with the software complexity, the training necessary for the ME-based design practices, and the operation and functionality of the software. The availability of the required input data is a significant concern. Most SHAs indicated that pavement condition data, existing pavement structure information, and traffic data are readily available. Very few SHA's indicated that material-related data were readily available. Collecting and testing the missing information requires a significant effort by the SHAs. Selecting Level 1 inputs also requires considerable effort by the agencies. The survey indicated that only site-specific vehicle classification and average annual daily truck traffic (AADTT) are likely available for most SHAs. Based on the lack of available data for Level 1 inputs, regional averages or the Pavement-ME default values are used for pavement designs.

The survey respondents provided several challenges and lessons learned during the implementation process. As expected, one of the most common challenges reported was the lack of readily available traffic and materials data and the considerable effort required to obtain the needed data. In addition, SHAs indicated that contacting the respective office or division in an agency (e.g., construction, materials, traffic, or planning) early on in the

implementation process is helpful. This proactive awareness and coordination among different offices will ensure everyone understands what data are needed and why. Further, this communication will help prepare the respective staff to conduct field sampling and testing if the required data are unavailable. The survey results describe the following challenges in implementing the ME-based designs:

- District offices are resistant to change from empirical-based designs to ME-based designs. The main reason is a higher comfort level with the inputs and resulting outputs (i.e., layer thickness) with the AASHTO 1993 Guide. Therefore, shifting to using design inputs and predicting distresses in the Pavement-ME, contrary to obtaining layer thickness as the final result, has been challenging to accept.
- Variations and changes in the pavement condition data collection in different highway agencies have resulted in inconsistency with condition measurement. These discrepancies among agencies have lowered their ability to obtain reliable pavement condition data for calibration.
- Another hurdle identified is the lack of resources for in-house local calibration and staff training.
- While the Pavement-ME is too complex for most practicing engineers, adopting the procedure may improve through training to increase the engineer's confidence in the long-term benefits of the design procedure.
- The procedure is evolving, and several variations and improvements have been made in the last couple of years (various software versions). Therefore, a potential for more work remains (i.e., recalibration of performance models) as a result of newer versions and modifications to the software.

The survey results also presented the following lessons learned in the implementation process:

- Establish realistic timelines for the calibration and validation process
- Allow sufficient time for obtaining materials and traffic data.
- Ensure the data related to the existing pavement layer, materials properties, and traffic is readily available.
- If necessary, develop a plan for collecting the needed data; this can require an expensive field sampling and testing effort.
- Develop agency-based design inputs to avoid default or other inputs to minimize design variability.
- Provide training to agency staff in ME design fundamentals, MEPDG procedures, and the Pavement-ME software.

2.4 IMPLEMENTATION EFFORTS IN MICHIGAN

To support the Pavement-ME implementation process in Michigan, the pavement researchers at Michigan State University (MSU) and other institutions have been working with MDOT to explore the various attributes of the design and analysis software. As a result of these efforts over the last 15 years, the following reports have been published:

- Evaluation of the 1-37A Design Process for New and Rehabilitated JPCP and HMA Pavements (Report No. RC-1516) (*29*)
- Quantifying Coefficient of Thermal Expansion Values of Typical Hydraulic Cement Concrete Paving Mixtures (Report No. RC-1503) (*30*)Pavement Subgrade MR Design Values for Michigan's Seasonal Changes (Report No. RC-1531) (*31*)
- Backcalculation of Unbound Granular Layer Moduli (Report No. RC-1548) (*32*)
- Preparation for Implementation of the Mechanistic-Empirical Pavement Design Guide in Michigan - Part 1: HMA Mixture Characterization (Report No. RC-1593) (*33*)
- Preparation for Implementation of the Mechanistic-Empirical Pavement Design Guide in Michigan - Part 2: Rehabilitation Evaluation (Report No. RC-1594) (*34*)
- Preparation for implementation of the mechanistic-empirical pavement design guide in Michigan, part 3: local calibration and validation of the pavement-ME performance models (Report No.: RC-1595) *(15)*
- Improvement of Michigan climatic files in Pavement-ME design (Report No.: RC-1626) (*35*)
- Characterization of Traffic for the New M-E Pavement Design Guide in Michigan (Report No. RC-1537) (*36, 37*)

The results from these studies are considered throughout the local calibration process in this report. Brief findings from these works are summarized below.

2.4.1 MDOT Sensitivity Study

The MSU research team conducted a study entitled "Evaluation of the 1-37A Design Process for New and Rehabilitated JPCP and HMA pavements" *(30)*. The main objectives of the study were to:

a. Evaluate the Pavement-ME pavement design procedures for Michigan conditions.
b. Verify the relationship between predicted and observed pavement performance for selected pavement sections in Michigan. and
c. Determine if local calibration is necessary.

The report outlined the performance models for JPCP and HMA pavements. Two types of sensitivity analyses were performed: a preliminary one-variable-at-a-time (OAT) and a detailed analysis consisting of a full factorial design. Both analyses were conducted to reflect MDOT pavement construction, materials, and design practices. For both new rigid and flexible pavement designs, the methodology contained the following steps:

1. Determine the input variables available in the Pavement-ME and the range of values that MDOT uses in pavement design.
2. Determine the practical range for each input variable based on MDOT practice and Long Term Pavement Performance (LTPP) data.
3. Select a base case and perform the OAT.
4. Use OAT results to design the detailed sensitivity analysis.
5. Determine statistically significant input variables and two-way interactions
6. Determine the practical significance of statistically significant variables

7. Draw conclusions from the results

Tables 2-13 and 2-14 show the impact of input variables on different pavement performance measures for rigid and flexible pavements, respectively.

Table 2-13 Impact of input variables on rigid pavement performance

Design/material variable	Impact on distress/smoothness		
	Transverse joint faulting	Transverse cracking	IRI
PCC thickness	High	High	High
PCC modulus of rupture	None	High	Low
PCC coefficient of thermal expansion	High	High	High
Joint spacing	Moderate	High	Moderate
Joint load transfer efficiency	High	None	High
PCC slab width	Low	Moderate	Low
Shoulder type	Low	Moderate	Low
Permanent curl/warp	High	High	High
Base type	Moderate	Moderate	Low
Climate	Moderate	Moderate	Moderate
Subgrade type/modulus	Low	Low	Low
Truck composition	Moderate	Moderate	Moderate
Truck volume	High	High	High
Initial IRI	NA	NA	High

Table 2-14 Impact of input variables on flexible pavement performance

Fatigue cracking	Longitudinal cracking	Transverse cracking	Rutting	IRI
HMA thickness HMA effective binder content HMA air voids Base material type Subbase material type	HMA thickness HMA air voids HMA effective binder content Base material Subbase material Subgrade material	HMA binder grade HMA thickness HMA effective binder content HMA air voids HMA aggregate gradation	HMA thickness Subgrade material Subgrade modulus HMA effective binder content HMA air voids Base material Subbase material Base thickness Subbase thickness	HMA thickness HMA aggregate gradation HMA effective binder content HMA air voids Base material type Subbase thickness Subbase material type Subgrade material type

Note: The input variables are listed in order of importance.

2.4.2 Pavement Rehabilitation Evaluation in Michigan

The study was performed to determine the sensitive inputs for the pavement rehabilitation options (*34*). Three different sensitivity analyses were completed for each rehabilitation option. The rankings of important inputs for each rehabilitation option are summarized below (Tables 2-15 to 2-18):

Table 2-15 List of significant inputs — HMA over HMA

Input variables	Ranking (NSI)
Overlay air voids	1 (6)
Existing thickness	2 (5)
Overlay thickness	3 (4)
Existing pavement condition rating	4 (4)
Overlay effective binder	5 (2)
Subgrade modulus	6 (2)
Subbase modulus	7 (1)

Note: NSI = Normalized sensitivity index

Table 2-16 List of significant inputs — Composite pavement

Inputs	Ranking (NSI)
Overlay air voids	1 (9)
Overlay thickness	2 (2)
Existing PCC thickness	3 (1)

Table 2-17 List of significant inputs — Rubblized PCC pavement

Inputs	Ranking (NSI)
Overlay air voids	1 (6)
Overlay effective binder	2 (2)
Overlay thickness	3 (1)

Table 2-18 List of significant inputs — Unbonded PCC overlay

Design inputs	Ranking (NSI)
Overlay PCC thickness	1 (23)
Overlay PCC coefficient of thermal expansion (CTE)	2 (12)
Overlay PCC modulus of rupture (MOR)	3 (8)
Overlay joint spacing	4 (5)
Existing PCC elastic modulus	6 (1)
Climate	7 (1)

2.4.3 HMA Mixture Characterization in Michigan

As part of a more extensive MDOT study, "Preparation for Implementation of the Mechanistic-Empirical pavement Design Guide in Michigan" (*33*), laboratory testing was preformed to determine HMA mixture properties for typical mixtures used in Michigan. The Level 1 HMA inputs require laboratory tests to characterize a pavement in the Pavement-ME software. The most critical properties obtained from this study include the following:

- Dynamic modulus (E^*)
- Binder G^*
- Creep compliance and,
- Indirect tensile strength (IDT)

The study determined Level 1 HMA mixture and binder characterizations as inputs in the Pavement-ME. Additionally, the study used artificial neural networks (ANN) to better predict dynamic moduli from asphalt volumetrics. The research team also reviewed the current HMA test data as part of the MDOT testing program and compared it to the necessary data by the Pavement-ME. Standalone software, called DYNAMOD, was developed to serve as a database to obtain the required HMA properties in a form compatible with the Pavement-ME software.

2.4.4 Local Calibration and Validation of Pavement-ME Models

The primary aim of this study *(15)* was to calibrate and validate the mechanistic-empirical pavement design guide (Pavement-ME) performance models to Michigan's conditions and to evaluate the data needs for the implementation of Pavement-ME. Local calibration of the performance models in Pavement-ME was challenging due to the limited data available. A total of 108 and 20 reconstructed flexible and rigid pavement candidate projects, respectively, were selected. Also, 33 flexible and 8 rigid rehabilitated projects were selected for local calibration. The selection process was based on various factors, including pavement type, age, geographical location, and the number of data collection cycles. The selected pavement sections met specific requirements, such as adequate sections for each performance model, a wide range of traffic, climate, design, material characterization inputs, and reasonable observed condition data over time.

Nationally calibrated performance models were evaluated using the data from the selected pavement sections, and it found that the global models in Pavement-ME were inadequate in predicting pavement performance for Michigan's conditions. Hence, local calibration of the models was crucial. Local calibrations were performed for all performance prediction models for flexible and rigid pavements using multiple datasets (reconstruct, rehabilitation, and a combination of both) and robust statistical techniques (such as repeated split sampling and bootstrapping). The results of local calibration and validation of various models indicated that locally calibrated models significantly improved the performance predictions for Michigan's conditions. The report documents the local calibration coefficients for all performance models and recommends the most appropriate calibration coefficients for each of the performance models in Michigan, along with future guidelines and data needs.

2.4.5 Traffic Inputs in Michigan

The research team has extensively worked on the traffic characterization for the Pavement-ME in Michigan (*36, 37*). The following traffic characteristics were investigated:

1. Monthly distribution factors
2. Hourly distribution factors
3. Truck traffic classifications
4. Axle groups per vehicle
5. Axle load distributions for different axle configurations

The data were collected from 44 Weigh-in-motion (WIM) sites distributed throughout the entire state of Michigan. The data were used to develop Level 1 (site-specific) traffic inputs for the WIM locations. Cluster analysis was conducted to group sites with similar characteristics for developing Level 2 (regional) inputs. Statewide (Level 3) averages were

also determined. The inputs and their recommended input levels are summarized in Table 2-19.

Table 2-19 Conclusions and recommendations for traffic input levels

Traffic Characteristic	Impact on pavement performance		Suggested input levels (when level I data not available)	
	Rigid pavement	Flexible pavement	Rigid pavement	Flexible pavement
TTC	Significant	Moderate	Level II	
HDF	Significant	Negligible	Level II	Level III[1]
MDF	Negligible		Level III (State average)	
AGPV	Negligible		Level III (State average)	
Single ALS	Negligible		Level III (State average)	
Tandem ALS	Significant	Moderate	Level II (State average)	
Tridem ALS	Negligible	Negligible	Level III (State average)	
Quad ALS	Negligible	Moderate	Level III (State average)	

[1] Level III inputs were available for flexible pavements in the MEPDG version 1.1 and are no longer available as input in the Pavement-ME

2.4.6 Unbound Material Inputs in Michigan

Two studies to characterize unbound material in Michigan were carried out in the last few years (*31, 32*). The first study outlined the importance of the roadbed soil's resilient modulus (MR) and how it affects pavement systems. The study focused on developing reliable methods to determine the MR of the roadbed soil for inputs in the Pavement-ME. The study divided the state of Michigan into fifteen clusters based on similar soil characteristics. Laboratory tests were performed to determine moisture content, grain size distribution, and Atterberg limits. Furthermore, another aspect of the study was to determine the differences between lab-tested MR values and back-calculated MR. The analysis concluded that the values between laboratory MR and back-calculated MR are almost equal if the stress boundaries used in the laboratory matched those of the FWD tests. Table 2-20 summarizes the recommended MR values for design based on different roadbed types in Michigan. The study suggests that the design recommended value should be used for design.

Table 2-20 Average roadbed soil MR values

Roadbed Type		Average MR			
USCS	AASHTO	Laboratory determined (psi)	Back-calculated (psi)	Design value (psi)	Recommended design MR value (psi)
SM	A-2-4, A-4	17,028	24,764	5,290	5,200
SP1	A-1-a, A-3	28,942	27,739	7,100	7,000
SP2	A-1-b, A-3	25,685	25,113	6,500	6,500
SP-SM	A-1-b,A-2-4, A-3	21,147	20,400	7,000	7,000
SC-SM	A-2-4, A-4	23,258	20,314	5,100	5,000
SC	A-2-6, A-6,A-7-6	18,756	21,647	4,430	4,400
CL	A-4, A-6, A-7-6	37,225	15,176	4,430	4,400
ML	A-4	24,578	15,976	4,430	4,400
SC/CL/ML	A-2-6, A-4, A-6, A-7-6	26,853	17,600	4,430	4,400

The second study focused on the backcalculation of MR for the unbound base and subbase materials and made the following recommendations *(32)*:

1. In the design of flexible pavement sections using design Levels 2 or 3 of the Pavement-ME, the materials beneath the HMA surface layer should consist of the following two layers:
   a. Layer 1 - An aggregate base whose modulus value is 33,000 psi
   b. Layer 2 - A sand subbase whose modulus is 20,000 psi
2. In the design of rigid pavement sections using design Levels 2 or 3 of the Pavement-ME, the materials beneath the PCC slab could be either:
   a. An aggregate base layer whose modulus value is 33,000 psi supported by a sand subbase with a modulus value of 20,000 psi
   b. A granular layer made up of aggregate and sand mix whose composite modulus value is 25,000 psi
3. For the design of flexible or rigid pavement sections using design Level 1 of the Pavement-ME, it is recommended that:
   - For an existing pavement structure where the PCC slabs or the HMA surface will be replaced, FWD tests will be conducted every 500 feet along the project. The deflection data will be used to backcalculate the moduli of the aggregate base and sand subbase or the granular layer. The modulus values to be used in the design should correspond to the 33rd percentile of all values. The 33rd percentile value is the same as the average value minus half the standard deviation value.
   - For a total reconstruction or for a new pavement section, the modulus values of the aggregate base and the sand subbase or the granular layer could be estimated as twice the average laboratory-determined modulus value.
4. Additional FWD tests and backcalculation analyses should be conducted when information regarding the types of aggregate bases under rigid and flexible pavements becomes known, and no previous FWD tests were conducted.
5. MDOT should keep all information regarding the various pavement layers. The information should include the HMA and the PCC mix design parameters, the type, source, gradation, aggregate angularity, subbase material type, and source. The above information should be kept in easily searchable electronic files.

2.4.7 Coefficient of Thermal Expansion

The CTE input values were obtained from the MDOT study that determined the CTE for various aggregates available across Michigan (*30*). It was decided later that the CTE values for concrete in Michigan are either 4.5 or 5.8 in/in/°F×$10^{-6,}$ depending on the location of the pavement section. For University and Metro regions, a CTE value of 5.8 in/in/°F×10^{-6} while for other regions, a value of 4.5 in/in/°F×10^{-6} should be used.

2.4.8 Improved Climatic Files for Michigan

Climatic inputs are crucial in the Mechanistic-Empirical design of flexible and rigid pavements. This study aimed to improve the climatic files in Michigan for PMED by conducting quality and quantity checks of the existing files to identify potential missing and erroneous data *(35)*. Michigan had 24 climatic files embedded in Pavement-ME, but several limitations had been identified. Firstly, five of the climatic files had a month of missing data, which needed to be appropriately filled. Secondly, the geographical distribution of the 24 weather stations was not uniform, with some regions poorly represented, and it was desirable

to add new weather stations to fill the gap regions. Thirdly, the existing climatic files have not been updated since 2006, and there was a need for the data length to be extended to represent the long-term climatic conditions better. Procedures for filling in the missing and correcting the erroneous data have also been proposed.

The sensitivity of the Pavement-ME design performance to weather station variation in Michigan, the five individual climatic variables, and the depth to the groundwater table were investigated for two traffic levels (heavy and medium) and two pavement types (flexible and rigid). Typical traffic load spectra, pavement structures, and materials in Michigan were incorporated into the sensitivity analysis. Additional weather data from Automated Surface Observation Systems (ASOS) and Michigan Road Weather Information System (RWIS) were investigated as potential sources to fill the gap regions and extend the existing climatic files. Quantity and quality checks on both data sources were conducted to evaluate their feasibility for use in PMED. It was found that the ASOS data and the existing climatic data are from the same historical data records, and 15 additional weather stations were added using the ASOS data to fill the gap regions. Additionally, all existing climatic files were extended from Feb. 2006 to Dec. 2014.

Finally, preliminary investigations were carried out to establish climatic zones for Michigan based on pavement surface temperatures and distress predictions, resulting in the establishment of 15 climate zones. The improvements made to the climatic files in Michigan for Pavement-ME will lead to more accurate predictions and better pavement designs.

2.5 SIGNIFICANT INPUT VARIABLES IN THE PAVEMENT-ME DESIGN

The identification of significant inputs is crucial for local calibration efforts. Such information addresses feasible and economic concerns since data collection for calibration or design requires considerable laboratory and field testing for material characterization. Such actions are labor-intensive and require resources that may become economically challenging. An input variable is significant when its variation causes substantial variations in pavement performance prediction. Therefore, the identification of influential inputs can provide guidelines in terms of data collection needs. When an input variable is highly sensitive to pavement performance prediction, agencies will be more inclined to collect higher-quality data attributes (i.e., Level 1). On the other hand, if an input variable does not show much sensitivity in performance prediction, agencies can adopt estimated values (i.e., Level 3).

2.5.1 Sensitivity Analysis Efforts

State Highway Agencies often struggle to identify the Pavement-ME's most critical data collection needs. An implementation protocol was developed for the Pavement-ME by reviewing two decades of research on the Pavement-ME. Particular emphasis was given to Weigh-in-Motion (WIM) data collection efforts for traffic input parameters and HMA dynamic modulus parameter (E^*), and coefficient of thermal expansion for Portland Concrete Cement (PCC) parameters for flexible and rigid pavement input parameters *(38)*.

2.5.1.1. Flexible Pavements

The Idaho Transportation Department conducted an extensive sensitivity analysis of rigid and flexible pavement design inputs and ranked them based on the variations observed for

each accumulated pavement distress *(25)*. Alligator fatigue cracking, rutting, transverse cracking, and IRI were considered performance measures.

Alligator fatigue cracking—HMA thickness, in-situ air void, effective binder content, existing HMA condition, bonding with base, base modulus, and truck volume are very influential. Other inputs such as contact area, pressure, mixture gradation, HMA binder grade, subgrade modulus, climate, truck axle load distribution, truck speed, and wander have moderate effects. The base thickness and groundwater table have a small impact on fatigue cracking.

Surface rutting—Tire pressure, HMA gradation, truck volume, and speed were found to have a significant effect. On the other hand, HMA thickness, in-situ air voids, binder grade, effective binder content, base and subgrade moduli, climate, axle load distribution, and wander moderately impact surface rutting. The bonding with the base and groundwater table was found to have small effects on surface rutting.

Transverse cracking—HMA tensile strength, binder grade, and groundwater table have a significant impact. While HMA coefficients of thermal contraction, HMA air void in situ, and effective binder content have moderate effects, HMA thickness was found to have a small impact on transverse cracking.

Surface roughness—HMA binder grade and initial IRI have a substantial effect. HMA thickness, tire load, contact area, and pressure, HMA air voids in situ have a moderate impact on surface roughness. The effective binder content and climate have minor effects on IRI. Table 2-21 summarizes the sensitive results for flexible pavements from the Idaho study.

A detailed sensitivity for pavement performance predicted by the MEPDG was performed under the NCHRP 1-47 study (*34*, *39*). A normalized sensitivity index (NSI) was used to estimate the percentage change in predicted performance from the design limit due to a specified percentage change in the design input. Based on the NSI values, four types of sensitive parameters were defined—hypersensitive (NSI > 5), very sensitive (1< NSI < 5), sensitive (0.1 < NSI < 1), and non-sensitive (NSI < 0.1). Longitudinal cracking, alligator cracking, thermal cracking, AC rut depth, total rut depth, and IRI were considered performance measures for flexible pavements. Table 2-22 summarizes sensitivity analysis results for flexible pavements.

Table 2-21 Summary of sensitive input parameters for flexible pavements - Idaho

Distress type	Impacts of input parameters on performance prediction		
	Large	Moderate	Small
Alligator fatigue cracking	• HMA thickness • HMA air void in situ • Effective HMA binder content • Existing HMA condition • Bonding with base • Base modulus • Truck volume	• Tire load • Contact area and pressure • Mixture gradation • HMA binder grade • Subgrade modulus • Climate • ALS • Truck speed • Wheel wander	• Base thickness • Groundwater table
Rutting	• ALS • Contact area and pressure • Mixture gradation • Truck volume • Truck speed	• HMA thickness • HMA air voids in situ • HMA binder grade, • Effective HMA binder content • base modulus • subgrade modulus • climate • ALS • Wheel wander	• Bonding with base • Groundwater table
Transverse cracking	• HMA tensile strength, HMA binder grade • Groundwater table	• HMA air void in situ • Effective HMA binder content	• HMA thickness
IRI	• HMA binder grade and • Initial IRI	• HMA thickness, • ALS • Contact area and pressure • HMA air voids in-situ	• Effective HMA binder content • Climate

Table 2-22 Summary of sensitive input parameters for flexible pavements *(39, 40)*

Distress type	The sensitivity of input parameters on performance prediction		
	Hypersensitive (NSI > 5)	Very sensitive (1 < NSI < 5)	Sensitive (0.1 < NSI <1)
Longitudinal Cracking	• HMA E^* alpha, delta • HMA thickness	• Base resilient modulus • Surface shortwave absorptivity • HMA air voids • HMA Poisson's ratio • Truck volume • HMA effective binder content • Subgrade resilient modulus • Base thickness • Subgrade % passing #200 • Truck speed	• HMA unit weight • Base Poisson ratio • HMA heat capacity • Subgrade liquid limit • Binder low-temperature PG • HMA thermal conductivity • Binder high-temperature PG • Subgrade Poisson's ratio • Groundwater depth • Subgrade plasticity index
Alligator Cracking	• HMA E^* alpha, delta • HMA thickness	• Base resilient modulus • Surface shortwave absorptivity • HMA air voids • HMA Poisson's ratio • Truck volume • HMA effective binder content • Subgrade resilient modulus • Base thickness	• Subgrade % passing #200 • Truck speed • HMA unit weight • Base Poisson's ratio • HMA heat capacity • Subgrade liquid limit • Binder low-temperature PG • HMA thermal conductivity • Binder high-temperature PG • Subgrade Poisson's ratio • Groundwater depth • Subgrade plasticity index
Thermal Cracking		• HMA E^* delta, • HMA air voids, • HMA creep compliance	• HMA E^* • HMA thickness • Base resilient modulus • HMA Poisson's ratio • HMA air voids • Truck volume • HMA effective binder content • Subgrade resilient modulus • Base thickness • Surface shortwave absorptivity • Subgrade % passing #200 • Truck speed • HMA unit weight • Base Poisson's ratio • HMA heat capacity • Subgrade liquid limit • Binder low-temperature PG • HMA thermal conductivity • Binder high-temperature PG • Subgrade Poisson's ratio • Groundwater depth • Subgrade plasticity index

Table 2-22 Summary of sensitive input parameters for flexible pavements (continued…)

AC Rut Depth	HMA *E**alpha and delta	• HMA thickness, • Surface shortwave absorptivity, • HMA Poisson's ratio, • HMA air voids, • truck volume	• HMA effective binder content • Subgrade resilient modulus • Base thickness and MR • HMA air voids • Subgrade percent passing #200 • Truck speed • HMA unit weight • Base Poisson's ratio • HMA heat capacity • Subgrade LL and PI • Binder low-temperature PG • HMA thermal conductivity • Binder high-temperature PG • Subgrade Poisson's ratio • Groundwater depth
Total Rut Depth	HMA *E**alpha and delta	• HMA thickness, • surface shortwave absorptivity, • HMA Poisson's ratio, • HMA air voids	• HMA unit weight • Base Poisson's ratio • HMA heat capacity • Subgrade LL, PI, and MR • Binder low-temperature PG • HMA thermal conductivity • Binder high-temperature PG • Subgrade Poisson's ratio • Groundwater depth • HMA air voids • Truck volume • HMA effective binder content • Base thickness and MR • Subgrade percent passing #200 • Operational speed
IRI		• HMA *E**alpha, delta • HMA thickness	• Base resilient modulus • Surface shortwave absorptivity • HMA air voids • HMA Poisson's ratio • Truck volume • HMA effective binder content • Base thickness • Subgrade percent passing #200 • Truck speed • HMA unit weight • base Poisson's ratio • HMA heat capacity • subgrade LL, PL, and MR • binder low-temperature PG • HMA thermal conductivity • binder high-temperature PG • Subgrade Poisson's ratio, • Groundwater depth

A climatic inputs parameter sensitivity investigation was conducted in Michigan, considering traffic, pavement structural inputs, material properties, and six climatic locations (*41*). Each of the climatic inputs was evaluated to estimate its sensitivity for pavement performance prediction. The temperature was identified as the most sensitive climatic input parameter, followed by wind speed and percent sunshine. Precipitation and relative humidity did not cause significant variation in pavement performance predictions. Interactions among the

climatic input revealed that higher temperature and percent sunshine generated higher rutting and IRI predictions and lower fatigue cracking. Increased wind speed or precipitation generated lower rutting and IRI predictions and increased fatigue cracking predictions.

The sensitivity of traffic levels and material-related inputs were evaluated through simulation techniques with Latin Hypercube Sampling (LHS) and the multiple regression analysis in Minnesota (*42*). Two-way traffic volume level, dual tire spacing, and operational vehicle speed were identified as the most significant among other traffic parameters.

Rutting—the most sensitive material properties were found to be HMA air void and HMA Poisson's ratio.

Cracking—the most sensitive input parameters were found to be HMA air void, HMA Poisson's ratio, and effective binder content.

In West Virginia, Latin hypercube sampling, standardized regression coefficients, and Gaussian stochastic processes were employed to identify the relative importance of the Pavement-ME input parameters (*43-45*). Such computer experiments analyzed typical flexible pavement structures used in West Virginia, and sensitivity for material and traffic inputs were tested with a one-at-a-time approach. Standardized regression coefficients were used to identify the most sensitive inputs. Surface roughness, rutting, and cracking were considered performance measures.

Surface roughness—the most sensitive traffic parameters were found to be two-way traffic, and dual tire spacing, and the most sensitive material parameter was found to be HMA air void.

Rutting—the most sensitive traffic parameters were found to be two-way traffic and dual tire spacing, and the most sensitive material parameters were found to be subgrade modulus and HMA air voids.

Cracking—the most sensitive traffic parameters were found to be two-way traffic, and dual tire spacing, and the most sensitive material parameters were found to be HMA air voids and effective binder content.

Table 2-23 summarizes the results of the sensitivity analyses in Michigan, Minnesota, and West Virginia.

Table 2-23 Summary of sensitivity analysis findings in different states

Location	Sensitive data inputs
Michigan	Climate — temperature, wind speed, and percent sunshine
Minnesota	Traffic — two-way traffic, dual tire spacing, operational speed Materials — HMA air void, Poisson's ratio, effective binder content
West Virginia	Traffic — two-way traffic and dual tire spacing Materials — HMA air void, effective binder content, subgrade MR

In another simulation study, 100 pavement design sections were generated with Monte Carlo sampling and analyzed to identify the sensitive parameters in the MEPDG (*46*). The variations in the prediction of performance measures (i.e., longitudinal cracking, HMA and total rutting, and IRI) due to the changes in parameters— nominal maximum aggregate size, climatic location, HMA thickness, AADTT, subgrade strength, truck traffic category, construction season, and binder grade, were investigated with Pearson's and Spearman's correlation coefficients. A negative correlation coefficient means an increase in that input parameter decreases the output response and vice versa. A positive correlation coefficient means that an increase in that input parameter increases the output response and vice versa. The absolute values from these coefficients were used to develop a relative rank of importance of the individual parameters. AADTT, HMA thickness, and subgrade MR were identified as the significant input parameters, and the remainder of the parameters were shown to have a limited impact on performance predictions.

2.5.1.2. Rigid Pavements

Idaho Transportation Department conducted an extensive sensitivity analysis on rigid pavement design inputs and ranked them based on the variations observed for each pavement distress *(25)*. Transverse joint faulting, transverse cracking, and IRI were considered performance measures.

Transverse joint faulting—PCC CTE, joint LTE, edge support, permanent curl and warp, base type, and truck volume were found to be very significant inputs. On the other hand, PCC thickness, joint spacing, zero stress temperature, climate, and truck lateral offset were found to have moderate effects. PCC unit weight, subgrade modulus, groundwater table, and truck axle load distribution were found to have minor effects on transverse joint faulting.

Transverse cracking—PCC thickness, MOR and E_c, CTE, existing PCC condition, joint spacing, edge support, permanent curl and warp, friction between base and slab, truck axle load distribution, truck volume, and truck lateral offset were found to have significant effects. On the other hand, PCC unit weight, base type, climate, subgrade modulus, and truck wander were found to have moderate effects. Groundwater table, truck speed, and tire pressure had a negligible impact on transverse cracking.

Surface roughness—PCC thickness, CTE, joint LTE, permanent curl and warp, truck volume, and initial IRI were found to have significant effects. On the other hand, MOR, E_c, joint spacing, edge support, friction between base and slab, climate, and truck lateral offset were found to have moderate effects. Existing PCC conditions, unit weight, zero stress temperature, subgrade modulus, base type, groundwater table, truck axle load distribution, and truck wander had a negligible impact on surface roughness. Table 2-24 shows the summary of the results of the sensitivity study.

Table 2-24 Summary of sensitive input parameters for rigid pavements - Idaho

Modes of Distress	Impacts of Input Parameters in Performance Prediction		
	Large	Moderate	Small
Transverse Joint Faulting	• PCC CTE • Joint LTE • Edge support • Permanent curl & warp • Base type • Truck volume	• PCC thickness • Joint spacing • Zero stress temperature • Climate • Lateral offset	• PCC unit weight • Subgrade modulus • Groundwater table • ALS
Transverse Cracking	• PCC thickness, • MOR, E_c • CTE • Existing PCC condition • Joint spacing • Edge support • Permanent curl • Friction between base and slab • ALS • Truck volume • Lateral offset	• PCC unit weight • Base type • Climate • Subgrade MR • Truck wander	• Groundwater table • Truck speed • Tire pressure
IRI	• PCC thickness, • CTE • Joint LTE, • Permanent curl • Truck volume • Initial IRI	• MOR, E_c • Joint spacing • Edge support • Friction between base and slab, • Climate • Truck lateral offset	• Existing PCC condition • PCC unit weight • Zero stress temperature • Subgrade MR • Base type • Groundwater table • ALS • Truck wander

The NCHRP 1-47 project also conducted the sensitivity of inputs for rigid pavements. Faulting, transverse cracking, and IRI were considered performance measures. Table 2-25 summarizes the sensitive inputs for different performance measures (*47*, *48*).

Table 2-25 Summary of sensitive input parameters for rigid pavements (*47*, *48*)

Distress type	The sensitivity of input parameters on performance prediction		
	Hypersensitive (NSI > 5)	Very sensitive (1< NSI < 5)	Sensitive (0.1 < NSI < 1)
Faulting	• Slab width	• design lane width • PCC unit weight • PCC CTE	• Subgrade MR, dowel diameter • PCC Poisson's ratio, Traffic volume, PCC cement content • Base MR & thickness • Groundwater table depth, edge support • LTE, MOR, PCC thickness • Erodibility index • MOR, E_c • Surface shortwave absorptivity • Joint spacing, PCC water-to-cement ratio, PCC thermal conductivity, construction month

Table 2-25 Summary of sensitive input parameters for rigid pavements (continued…)

Distress type	The sensitivity of input parameters on performance prediction		
	Hypersensitive (NSI > 5)	Very sensitive (1< NSI < 5)	Sensitive (0.1 < NSI < 1)
Transverse Cracking	• Slab width	• MOR • PCC thickness • Design lane width • PCC unit weight • CTE, MOR, E_c • Surface shortwave absorptivity • Joint spacing • PCC water to cement ratio • PCC thermal conductivity	• Subgrade resilient modulus • Dowel diameter • PCC Poisson's ratio • Traffic volume • PCC cement content • Base MR • Groundwater depth • Base thickness • Edge support, LTE • Erodibility index • Construction month
IRI	• Slab width	• PCC unit weight, PCC CTE	• Subgrade MR, • Dowel diameter • PCC Poisson's ratio • Traffic volume • PCC cement content • Base MR • Groundwater depth • Base thickness • MOR, E_c • Surface shortwave absorptivity • Joint spacing • PCC water-to-cement ratio • PCC thermal conductivity • Construction month

A study in Arkansas considered 29 out of over 100 inputs in the MEPDG, and the significance of these parameters on faulting, cracking, and IRI predictions was evaluated *(49)*. The results show that 17 of the 29 variables in the study were found insensitive.

Faulting—curl warp effective temperature difference, joint spacing, dowel diameter, edge support, PCC thickness, unit weight, and CTE were found to be sensitive.

Cracking—curl warp effective temperature difference, joint spacing, edge support, surface shortwave absorptivity, PCC layer thickness, unit weight, Poisson's ratio, CTE, thermal conductivity, MOR, and f_c' were reported as sensitive inputs.

Smoothness—curl warp effective temperature difference, joint spacing, dowel diameter, edge support, PCC layer thickness, unit weight, CTE, MOR, and f_c' were reported as influential inputs.

A sensitivity analysis was also conducted in Michigan (*50*). About 23 most significant inputs were identified for rigid pavements. The study used a one-at-a-time sensitive analysis approach for a range of parameters, and based on local experience and engineering

judgments, 6 out of these 23 parameters were investigated with a factorial design. PCC thickness, joint spacing, and edge support were found to have significant effects on JPCP-predicted performance. The coefficient of thermal expansion, modulus of rupture, base type, and subgrade were found to impact considerably JPCP predicted performance among material-related parameters.

2.6 RECOMMENDED PRACTICES IN DIFFERENT STATES

SHAs typically generate Level 1 hierarchical inputs for the Pavement-ME based on local data availabilities, practical considerations, and testing capabilities. For Levels 2 and 3 hierarchical inputs, SHAs follow 3-step procedures to develop a localized database with default values, as shown in Figure 2-1. Table 2-26 documents the recommended data collection practices of different SHAs for hierarchical input levels for the Pavement-ME (*51-56*).

Figure 2-1 Recommended practices for local default values in the Pavement-ME

Table 2-26 Recommended data collection practices of different SHAs

Input levels	Recommended data sources				
	Idaho	Colorado	Virginia	Arizona	South Carolina
Level 1	Lab tests & field experiments	Lab tests & field experiments	Lab tests & field experiments	Lab tests & field experiments	Lab tests & field experiments
Level 2	Local defaults	Local defaults	Local defaults	Local defaults	Local defaults/Pavement-ME defaults
Level 3	Pavement-ME default values	Local and Pavement-ME defaults	Pavement-ME defaults	Local and Pavement-ME defaults	Local and Pavement-ME defaults

Similar practices are recommended by other SHAs listed below.

- Iowa *(57)*
- Mississippi (*58*)
- Missouri *(59)*
- Nevada *(60)*
- North Carolina *(5)*
- Ohio *(61)*
- Oregon *(62)*
- Tennessee *(63)*
- Utah *(64)*
- Washington *(65)*
- Wyoming *(19, 66)*

Table 2-27 shows the recommended data attributes of different SHAs for hierarchical input levels in the Pavement-ME. Table 2-28 presents typical data attributes of interest by different SHAs for localized database development for the Pavement-ME.

Table 2-27 Recommended input levels of different SHAs in the Pavement-ME

Agency	Hierarchical input levels		
	Level 1	Level 2	Level 3
Idaho	HMA materials: *E**, *G**, Job Mix Formula Unbound materials: MR (if possible) Traffic: WIM data PCC materials: Slump, air content, unit weight, concrete temperature, , , μ, splitting tensile strength, MOR, CTE, ultimate drying shrinkage	Unbound material properties: Base, subbase, and subgrade	Volumetric properties of HMA materials
Virginia	Traffic: AADTT, vehicle class distribution and growth rate Climate: Station and groundwater table depth HMA Material: Thickness PCC Materials: Thickness Design: Shoulder type, steel (%), bar diameter, steel depth, base/slab friction coefficient, joint spacing, sealant type, doweled joints, widened slab, tied shoulders, erodibility index (EI), PCC-base contact friction Stabilized base: Thickness Base: Thickness Subgrade Materials: Thickness, gradation and other engineering properties, resilient modulus	Traffic: Vehicle class distribution and growth rate HMA Materials: Unit weight, effective binder content, air void, dynamic modulus, asphalt binder, creep compliance, indirect tensile PCC Materials: Unit weight, CTE, cement type, cementitious material content, water-cement ratio, aggregate type, strength, and modulus Stabilized base: Resilient modulus Base: Resilient modulus, gradation, and other engineering properties Subgrade materials: Resilient modulus, gradation, and other engineering properties	Traffic: Traffic capacity, axle configuration, lateral wander, wheelbase, monthly and hourly factors, single, tandem, tridem, and quad-axle distribution HMA Materials: Poisson's ratio, *E**, reference temperature, thermal conductivity, thermal contraction, Surface shortwave absorptivity, endurance limit applied, endurance limit (micro strain), layer interface, Poisson's ratio, PCC Materials: Poisson's ratio, thermal conductivity, heat capacity, zero stress, ultimate shrinkage, reversible shrinkage, time to develop 50% ultimate shrinkage, curing method, surface shortwave absorptivity, permanent curl/warp, crack spacing Stabilized base: Unit weight, Poisson's ratio, thermal conductivity, heat capacity Base: Poisson's ratio, coefficient of lateral earth pressure Subgrade Materials: Poisson's ratio, coefficient of lateral earth pressure, resilient modulus, gradation, and other engineering properties

Table 2-27 Recommended input levels of different SHAs in the Pavement-ME (continued…)

Arizona	PCC Material: PCC thickness, PCC CTE, Design: joint spacing, edge support, Unbound Materials: Base modulus and thickness, subgrade modulus, climate HMA Material: HMA thickness, creep compliance	Traffic: Truck axle load distribution, Truck volume, PCC Material: PCC modulus of rupture and elasticity HMA material: HMA coefficient of thermal contraction, dynamic modulus, Base: Base modulus	Traffic: Truck wander, lateral offset, tire pressure, Traffic speed, Tire load, the contact area Design: Lane to PCC shoulder long-term load transfer efficiency, permanent curl/warp HMA Materials: HMA air void in situ, effective binder content, tensile strength, GWT
South Carolina	Traffic: AADTT, vehicle class distribution, lane, and directional truck distribution, Climate: Climate stations PCC Material: PCC coefficient of thermal expansion, modulus of rupture, elastic modulus, compressive strength, unit weight Unbound Materials: Stabilized base resilient modulus, modulus of rupture, unit weight, Base and subgrade resilient modulus, gradation, liquid limit, plasticity index, dry unit weight HMA Material: HMA dynamic modulus, unit weight, binder grade, air void, effective binder content, Stabilized base resilient modulus, modulus of rupture, unit weight	Traffic: Axle load distribution Unbound Materials: Base and subgrade hydraulic conductivity, specific gravity, optimum moisture content, soil water relation, Base: Stabilized base thermal conductivity, heat capacity PCC Material: PCC thermal conductivity, heat capacity HMA Material: HMA Creep compliance, indirect tensile strength, fatigue endurance limit, thermal conductivity, heat capacity, thermal contraction	Traffic: Axle configuration, tire spacing, tire pressure, hourly and monthly traffic distribution, truck wander Unbound Materials: Base and subgrade Poisson's ratio, coefficient of lateral earth pressure, Base: Stabilized base Poisson's ratio PCC Material: PCC cement type, aggregate type, cementitious material content, water-cement ratio, ultimate shrinkage, reversible shrinkage HMA Material: HMA Poisson's ratio

Table 2-28 Recommended data attributes for database development for the Pavement-ME

Agency	Recommended data attributes for database development
Colorado	Base and subgrade resilient modulus, gradation, Atterberg limits, maximum dry density, optimum moisture content, specific gravity, saturated hydraulic conductivity HMA *E**, asphalt binder properties, tensile strength at 14 F, creep compliance, *G**, phase angle, penetration test, ring and ball softening point test, absolute viscosity, kinematic viscosity, specific gravity, Brookfield viscosity PCC elastic modulus, flexural strength, compressive strength, unit weight, Poisson's ratio, coefficient of thermal expansion
Mississippi	PCC flexural strength, modulus of elasticity, Poisson's ratio, CTE, unit weight, cementitious materials content, w/c ratio, cement type, and curing type
Nevada	Subgrade soil classification, Atterberg limit, gradation, unconfined compression, resilient modulus testing, moisture density relationship, R test

2.6.1 Flexible Pavements

Based on local experiences, data availability, and practical considerations, the Arizona Department of Transportation recommended hierarchical ranking for the input parameters *(51)*.

- Level 1 inputs—HMA thickness, creep compliance, base thickness, subgrade modulus, and climate were recommended as the most critical input parameters.
- Level 2 inputs—HMA coefficient of thermal contraction, dynamic modulus, base modulus, truck volume, and axle load configuration were recommended as moderate important input parameters.
- Level 3 inputs—HMA in situ air void, effective binder content, tensile strength, GWT, truck wander, speed, and tire pressure were recommended as less important input parameters.

South Carolina Department of Transportation recommended a similar ranking of input parameters based on local factors *(52)*.

- Level 1 inputs—AADTT, vehicle class distribution, lane, and directional truck distribution; climate; base and subgrade resilient modulus, gradation, liquid limit, plasticity index, dry unit weight; HMA dynamic modulus, unit weight, binder grade, air void, effective binder content; stabilized base resilient modulus, modulus of rupture, unit weight were recommended as the most critical input parameters.
- Level 2 inputs—Axle load distribution; base and subgrade hydraulic conductivity, specific gravity, optimum moisture content, soil water relation, stabilized base thermal conductivity, heat capacity; HMA creep compliance, indirect tensile strength, fatigue endurance limit, thermal conductivity, heat capacity, thermal contraction were recommended as moderate important input parameters.
- Level 3 inputs—Axle configuration, tire spacing, tire pressure, hourly and monthly traffic distribution, truck wander; base and subgrade Poisson's ratio, coefficient of lateral earth pressure; stabilized base Poisson's ratio; HMA Poisson's ratio were recommended as less essential input parameters.

Idaho Transportation Department recommended a similar ranking based on local factors *(56)*.

- Level 1 inputs—HMA properties E^*, G^*, weigh-in-motion traffic data and base, subbase, and subgrade resilient modulus (if possible) values are recommended as level 1 inputs.
- Level 2 inputs—in the absence of resilient modulus test results, Idaho Transportation Department prediction models are used for Level 2 inputs for resilient modulus properties.
- Level 3 inputs—volumetric properties of HMA materials are considered as level 3 inputs.

Virginia Department of Transportation recommended a similar ranking based on local factors *(54)*.

- Level 1 inputs—AADTT, Vehicle class distribution, growth rate, climate, groundwater table depth, HMA thickness, stabilized base thickness, base thickness, subgrade materials thickness, gradation, and other engineering properties, resilient modulus.
- Level 2 inputs—Vehicle class distribution and growth rate; HMA unit weight, effective binder content, air void, dynamic modulus, asphalt binder, creep compliance, indirect tensile; Stabilized base resilient modulus; base resilient modulus, gradation, and other engineering properties; subgrade resilient modulus, gradation, and other engineering properties.
- Level 3 inputs—Traffic capacity, axle configuration, lateral wander, wheelbase, monthly and hourly factors, single, tandem, tridem, and quad-axle distribution; HMA Poisson's ratio, *E**, reference temperature, thermal conductivity, thermal contraction, Surface shortwave absorptivity, Endurance limit applied, Endurance limit (microstrain), Layer Interface, Poisson's ratio; stabilized base unit weight, Poisson's ratio, thermal conductivity, heat capacity; base Poisson's ratio, coefficient of lateral earth pressure; subgrade material Poisson's ratio, coefficient of lateral earth pressure, resilient modulus, gradation, and other engineering properties.

The Colorado Department of Transportation recommends that input variables are classified based on project importance level, where project priority is selected based on Table 2-29 (*53*). Table 2-30 presents a summary of recommended practices from different states.

Table 2-29 Pavement-ME input hierarchical levels in Colorado based on project importance

Input hierarchical level	Description
Level 1	Very critical: high-volume interstates, urban freeways, and expressways
Level 1 or 2	Critical: principal arterials, rural interstates, heavy haul (i.e., mining, logging routes)
Level 2 or 3	Somewhat critical: minor arterial and collectors
Level 3	Not critical: local roads

Table 2-30 Recommended levels of inputs for flexible pavement design

Input level	Data attributes
Level 1	• HMA thickness, creep compliance, base thickness, subgrade modulus, climate, AADTT, vehicle class distribution, lane, and directional truck distribution, base and subgrade resilient modulus, gradation, liquid limit, plasticity index, dry unit weight, HMA dynamic modulus, unit weight, binder grade, air void, effective binder content, Stabilized base resilient modulus, modulus of rupture, unit weight.
Level 2	• HMA coefficient of thermal contraction, axle load configuration, axle load distribution, base and subgrade hydraulic conductivity, specific gravity, optimum moisture content, soil water relation, stabilized base thermal conductivity, heat capacity, HMA creep compliance, indirect tensile strength, fatigue endurance limit, thermal conductivity, heat capacity, thermal contraction.
Level 3	• GWT, Traffic speed, tire pressure, tire spacing, hourly and monthly traffic distribution, truck wander, Base and subgrade Poisson's ratio, coefficient of lateral earth pressure, Stabilized base Poisson's ratio, HMA Poisson's ratio.

2.6.2 Rigid Pavements

The Arizona Department of Transportation recommended hierarchical ranking for the input parameters based on local experiences, data availability, and practical considerations *(51)*.

- Level 1 inputs—PCC thickness, CTE, joint spacing, edge support, base modulus, subgrade modulus, and climate were recommended as the most critical input variables.
- Level 2 inputs—Truck axle load distribution, truck volume, PCC modulus of rupture, and elasticity were recommended as moderate essential input variables.
- Level 3 inputs—Truck wander, lateral offset, tire pressure, lane to PCC shoulder long-term load transfer efficiency, and permanent curl/warp were recommended as the least important input variables.

South Carolina Department of Transportation recommended a similar ranking of input parameters based on local factors *(52)*.

- Level 1 inputs—AADTT, vehicle class distribution, lane, and directional truck distribution; climate; PCC coefficient of thermal expansion, modulus of rupture, elastic modulus, compressive strength, unit weight; stabilized base resilient modulus, modulus of rupture, unit weight; base and subgrade resilient modulus, gradation, liquid limit, plasticity index, dry unit weight were recommended as most important input variables.
- Level 2 inputs—Axle load distribution; base and subgrade hydraulic conductivity, specific gravity, optimum moisture content, soil water relation; stabilized base thermal conductivity, heat capacity; PCC thermal conductivity, and heat capacity were recommended as moderate essential input variables.
- Level 3 inputs—Axle configuration, tire spacing, tire pressure, hourly and monthly traffic distribution, truck wander; base and subgrade Poisson's ratio, coefficient of lateral earth pressure; stabilized base Poisson's ratio, PCC cement type, aggregate type, cementitious material content, water-cement ratio, ultimate shrinkage, reversible shrinkage were recommended as least essential input variables.

Idaho Transportation Department recommended a similar ranking based on local factors (*24*).

- Level 1 inputs—PCC tests such as slump, air content, unit weight, concrete temperature, f'_c, E_c, poisson's ratio, splitting tensile strength, MOR, CTE, ultimate drying shrinkage, weigh-in-motion traffic data and base, subbase, and subgrade resilient modulus (if possible) values are recommended as Level 1 inputs.
- Level 2 inputs—Without resilient modulus test results, Idaho Transportation Department prediction models are used for Level 2 inputs for resilient modulus properties.

Virginia Department of Transportation recommended a similar ranking based on local factors *(54)*.

- Level 1 inputs—AADTT, vehicle class distribution, and growth rate; climate station and groundwater table depth; PCC thickness; shoulder type, steel (%), bar diameter, steel depth, base/slab friction coefficient, PCC joint spacing, sealant type, doweled joints, widened slab, tied shoulders, erodibility index (EI), PCC-base contact friction; stabilized base thickness; base thickness; subgrade thickness, gradation, and other engineering properties, and resilient modulus.
- Level 2 inputs—Vehicle class distribution and growth rate; PCC unit weight, CTE, cement type, cementitious material content, water-cement ratio, aggregate type, strength, and modulus; stabilized base resilient modulus; base resilient modulus, gradation, and other engineering properties; subgrade materials resilient modulus, gradation, and other engineering properties.
- Level 3 inputs—Traffic capacity, axle configuration, lateral wander, wheelbase, monthly and hourly factors, single, tandem, tridem, and quad-axle distribution; PCC Poisson's ratio, thermal conductivity, heat capacity, zero stress, ultimate shrinkage, reversible shrinkage, time to develop 50% ultimate shrinkage, curing method, surface shortwave absorptivity, permanent curl/warp, crack spacing; stabilized base: unit weight, Poisson's ratio, thermal conductivity, heat capacity; base Poisson's ratio, coefficient of lateral earth pressure; subgrade materials Poisson's ratio, coefficient of lateral earth pressure, resilient modulus, gradation, and other engineering properties.

Table 2-31 presents a summary of recommended practices from different states.

Table 2-31 Recommended levels of inputs for rigid pavement design in Pavement-ME

Input level	Data attributes
Level 1	• PCC thickness, PCC CTE, joint spacing, edge support, base modulus, subgrade modulus, climate, AADTT, vehicle class distribution, lane and directional truck distribution, climate, PCC coefficient of thermal expansion, modulus of rupture, elastic modulus, compressive strength, unit weight, Stabilized base resilient modulus, modulus of rupture, unit weight, Base and subgrade resilient modulus, gradation, liquid limit, plasticity index, dry unit weight
Level 2	• Truck axle load distribution, Truck volume, PCC modulus of rupture and elasticity, Axle load distribution, Base and subgrade hydraulic conductivity, specific gravity, optimum moisture content, soil water relation, Stabilized base thermal conductivity, heat capacity, PCC thermal conductivity, heat capacity
Level 3	• Truck wander, lateral offset, tire pressure, Lane to PCC shoulder long-term load transfer efficiency, permanent curl/warp, Axle configuration, tire spacing, tire pressure, hourly and monthly traffic distribution, truck wander, Base and subgrade Poisson's ratio, coefficient of lateral earth pressure, Stabilized base Poisson's ratio, PCC cement type, aggregate type, cementitious material content, water-cement ratio, ultimate shrinkage, reversible shrinkage

2.6.3 Recommended Inputs for Materials

Typical design values for subgrade MR, PCC, and HMA materials properties of different states are compared with Michigan design values in Tables 2-32 to 2-34 *(15, 56, 57)*.

Table 2-32 Recommended design values for subgrade MR

AASHTO Soil Classification	Recommended Design Resilient Modulus (psi)			
	Colorado		Virginia	Michigan
	Flexible	Rigid		
A-1-a	19700	14900	-	7000
A-1-b	16500	14900	-	6500
A-2-4	15200	13800	-	5200-7000
A-2-5	15200	13800	-	-
A-2-6	15200	13800	-	4400
A-2-7	15200	13800	-	-
A-3	15000	13000	-	6500-7000
A-4	14400	18200	8000	4400-5200
A-5	14000	11000	8500	-
A-6	17400	12900	13500	4400
A-7-5	13000	10000	13000	-
A-7-6	12800	12000	14000	4400

Table 2-33 Recommended design values for PCC properties

Concrete Properties	Colorado	Virginia	Michigan
CTE (in/in)/F*10^{-6}	4.72-4.89	5.5	5 for University and Metro regions; 4.4 for all other regions
w/c ratio	0.36-0.44	0.45	0.42
Unit weight (pcf)	138.6-140.8	150	145

Table 2-34 Recommended design values for HMA materials

HMA Properties	Colorado	Virginia	Michigan
Air voids (%)	4.7-13	5.3-6.7	4.8-7.3
Effective binder content (%)	0.3-14.4	9.8-12.1	9.7-14
Unit weight (pcf)	-	149.6-151.4	145.2-151.6

CHAPTER 3 - RECALIBRATION DATA

3.1 INTRODUCTION

This chapter discusses the inputs and performance data used for the local calibration process. A crucial step in local calibration involves choosing enough pavement sections that accurately represent the prevailing conditions in the area. The next step is to gather the necessary data for each of the selected pavement sections, including information on the pavement performance, maintenance history, and various Pavement-ME inputs (material, traffic, and climate) that directly influence performance predictions for each project. The predictions are then compared to the actual performance of the constructed pavement sections. A pavement section refers to a specific stretch of road corresponding to a construction project, which may include up to two sections (such as different directions on a divided highway) with similar data inputs but varying measured pavement performance, traffic, and initial IRI. The accuracy of the predicted pavement performance in the Pavement-ME software depends on the information used to describe the in-service pavement. Thus, several inputs are essential for analyzing a particular pavement in the design software, particularly those with significant impacts on the expected performance. This chapter outlines the process for selecting pavement sections for local calibration and the steps in obtaining the required information for each pavement section.

The previous local calibration effort used 108 flexible and 20 JPCP pavement projects and performance data from 1991 to 2011 *(1)*. Therefore, the research team first focused on identifying and reviewing all these projects in the MDOT database to determine the additional distress data availability. In this process, the team evaluated time-series trends of all distress types. Also, these trends were explained, considering any significant maintenance activities over time. The information about maintenance activities over time will help to model a section in the Pavement-ME, i.e., whether an existing project should be considered a reconstruct or rehabilitated overlay project. The Pavement-ME inputs for these sections were also reviewed to obtain more current or higher input levels.

Another objective was identifying and selecting new potential candidate projects to be added to the local calibration dataset. For this task, all available sections (flexible and rigid) after 2011 were reviewed from the MDOT databases for their performance and data availability. It's worth noting that a "project" refers to a specific job number in the construction records, while a "section" refers to multiple directions in a divided highway within a project. Hence, the number of sections is always greater than or equal to the number of projects. The project selection process, Pavement-ME inputs, and performance data have been summarized in this chapter. The following topics are discussed:

1. Readily available observed condition data
2. Project selection criteria
3. Pavement cross-section information
4. Traffic inputs
5. Construction materials inputs
6. Climate inputs

3.2 MDOT PMS DATA

MDOT's Pavement Management System (PMS) and other available construction data sources were reviewed to identify the available input levels, units of measured performance data, and best possible estimates. The team evaluated the PMS and other sources to extract the following data:

a. Performance data were evaluated for their measurement process and units and converted to the Pavement-ME compatible units (wherever required). Necessary assumptions were made for these conversions.
b. The construction records, plans, job-mix formula (JMF), and other sources were used to identify the pavement cross-sections and material properties during construction. Any unavailable data was acquired from MDOT, or MDOT provided test results for the best possible estimates.
c. Traffic data were collected from the construction records and MDOT Transportation Data Management System (TDMS). Level 2 data were used for traffic data based on road type, number of lanes, and percentage of vehicle class 9 traffic.
d. For Asphalt concrete (AC) mix and binder properties, DYNAMOD software was used, which is based on laboratory tests for Michigan mixes. For base, subbase, and subgrade properties, the most common construction materials in Michigan were used.
e. For climatic data, the updated NARR files for Michigan have been used *(2)*.

3.2.1 Pavement Condition Measures Compatibilities

MDOT provided the PMS data from 1992 to 2019 (sensor data from 1998 to 2019). Biannually, MDOT obtains performance data on their pavement network by utilizing distress and laser-based measurements (sensors) for a 0.1-mile section. The information gathered on pavement distress in MDOT's PMS is categorized by distinct principle distress (PD) codes, where each PD code corresponds to a specific distress type. The research team extracted pavement performance data for the selected projects and converted them to Pavement-ME compatible units (where needed). In addition, the research team held several meetings with MDOT to discuss the concerns regarding the measured project length unit conversion. MDOT personnel explained the distress calls made for the 2012 – 2017 data were only at the sampled locations (about 29.41% of any 0.1-mile segment of each control section). Therefore, it was suggested to consider a 0.2941 division factor to expand distress quantities out to any total mileage of interest for those years of measured PMS data.

3.2.1.1. Selected distresses

The MDOT PMS and sensor database were carefully analyzed, and relevant data were extracted to obtain the required distress information. The current distress Manual of MDOT PMS was referred to determine all the principle distress (PD) codes corresponding to the predicted distresses in the Pavement-ME. The earlier versions of the PMS manual were also reviewed to ensure accurate data was extracted for all the years. The necessary steps for PMS data extraction include:

1. Identify the PDs that correspond to the Pavement-ME predicted distresses

2. Extract PDs, and sensor data for each project
3. Convert (if necessary) MDOT PDs to the units compatible with the Pavement-ME
4. Summarize time-series data for each project and each distress type

The identified and extracted pavement distresses, and conditions for flexible and rigid pavements are summarized in Tables 3-1 and 3-2. This section also presents a detailed discussion of the conversion process for both flexible and rigid pavements.

Table 3-1 Flexible pavement distress measurement by MDOT

Flexible pavement distress	MDOT principle distresses (PDs)	MDOT units	Pavement-ME units	Conversion needed?
IRI	Directly measured	in/mile	in/mile	No
Top-down cracking	204, 205, **724, 725**, 501	miles	% area	Yes
Bottom-up cracking	234, 235, **220, 221, 730, 731**, 501	miles	% area	Yes
Thermal cracking	**101,** 103, 104, 114, **701, 703, 704,** 110, 501	No. of occurrences	ft/mile	Yes
Rutting	Directly measured	in	in	No
Reflective cracking	No specific PD	None	% area	N/A

Note: Bold numbers represent older PDs that are not currently in use; PD code 501 = No distress

Table 3-2 Rigid pavement distress measurement by MDOT

Rigid pavement distresses	MDOT principle distresses	MDOT units	Pavement-ME units	Conversion needed?
IRI	Directly measured	in/mile	in/mile	No
Faulting	Directly measured	in	in	Yes
Transverse cracking	112, 113, 501	No. of occurrences	% slabs cracked	Yes

Note: PD code 501 = No distress

3.2.1.2. Pavement distress unit conversion for HMA designs

It should be noted that the team only considered the distress types predicted by the Pavement-ME for the local calibration. The corresponding MDOT PDs were determined and compared with distress types predicted by the Pavement-ME to verify if any conversions were necessary. MDOT measures pavement distresses related to HMA pavements are listed in Table 3-1. PD code 501 corresponds to no distress condition and has been used in all distresses except rutting and IRI. The conversion process (if necessary) for all distress types is as follows:

IRI: The IRI measurements in the MDOT sensor database are compatible with those in the Pavement-ME. Therefore, no conversion or adjustments were needed, and data could be used directly.

Top-down cracking: Top-down cracking is load-related longitudinal cracking in the wheel path. The PDs 204, 205, 724, and 725 were assumed to correspond to the top-down cracking in the MDOT PMS database because those may not have developed an interconnected pattern that indicates alligator cracking. Those cracks may show an early stage of fatigue cracking, which could also be bottom-up. Since it is difficult to estimate such cracking based on the PMS data, these cracks were first converted to % area crack and then categorized into bottom-up or top-down cracking based on the thicknesses. The PDs are recorded in miles and need conversion to % area. Data from the wheel paths were summed into one value and divided by the total project length, as shown in Equation (3-1). The lane width was assumed to be 12 ft. The typical wheel path width of 3 feet was assumed as recommended by the LTPP distress identification manual *(3).*

$$\%\, AC_{top-down} = \frac{\text{Length of cracking (miles)} \times \text{width of wheelpaths (feet)}}{\text{Length of section (miles)} \times \text{Lane width (feet)}} \times 100 \qquad (3\text{-}1)$$

Literature shows that the AC thickness determines whether the crack initiates from the bottom or the top. Therefore, top-down cracking can be a primary distress based on AC layer thickness. The calculated top-down cracking using Equation (3-1) is assigned as either bottom-up or top-down based on the total AC layer thickness. If the thickness is greater than a certain threshold, the cracking is considered top-down cracking; otherwise, it is categorized as bottom-up cracking. These thicknesses were obtained by a mechanistic approach using Mechanistic Empirical Asphalt Pavement Analysis (MEAPA) software. MEAPA was run for different surface types using typical MDOT design inputs, and damage was calculated for the first 12 months for a single axle load of 9000 lb. Threshold thicknesses were determined where the tensile strain at the top of the AC layer is higher than at the bottom. Table 3-3 presents the minimum threshold thicknesses for top-down cracking for each fix type.

Table 3-3 Minimum thicknesses for top-down cracking

Fix type	Threshold thickness (in)
HMA overlay on rubblized concrete	6
HMA overlay on existing composite or concrete pavement	6
HMA overlay on crushed and shaped HMA	4
HMA overlay on existing HMA pavement	6
New or reconstruct	5

Bottom-up cracking: Bottom-up cracking is defined as alligator cracking in the wheel path. The PDs 234, 235, 220, 221, 730, and 731 match this requirement in the MDOT PMS database. The PDs have units of miles; however, to make those compatible with the Pavement-ME alligator cracking units, conversion to the percent of the total area is needed. This can be achieved by using the following Equation (3-2):

$$\%AC_{bottom-up} = \frac{\text{Length of cracking (miles)} \times \text{width of wheelpaths (feet)}}{\text{Length of section (miles)} \times \text{Lane width (feet)}} \times 100 \qquad (3\text{-}2)$$

The width of each wheel path and lane were assumed to be 3 feet and 12 feet, respectively. The typical wheel path width of 3 feet is recommended by the LTPP distress identification manual *(3)*.

Thermal cracking: Thermal cracking corresponds to transverse cracking in flexible pavements. The transverse cracking is recorded as the number of occurrences, but the Pavement-ME predicts thermal cracking in feet/mile. To convert transverse cracking into feet/mile, the number of occurrences was multiplied by 3 feet for PDs 114 and 701 because these PDs are defined as "tears" (short cracks) that are less than half the lane width. For all other PDs, the number of occurrences was multiplied by the lane width (12 ft). All transverse crack lengths were summed and divided by the project length to get feet/mile, as shown in Equation (3-3).

$$TC = \frac{\sum \text{No. of Occurrences} \times \text{Lane Width (ft)}}{\text{Section Length (miles)}} \quad (3\text{-}3)$$

Thermal cracking predictions in the Pavement-ME are restricted to a maximum value of 2112 ft/mile due to a minimum crack spacing limit of 30 feet. This means Pavement-ME predictions at 50% reliability cannot exceed 2112 ft/mile. Due to this limitation and ARA recommendations, the research team decided to have a 2112 ft/mile cutoff where any measured data for a section above 2112 ft/mile was not used for calibration.

Rutting: This is the total amount of surface rutting all the pavement layers and unbound sub-layers contribute. The average rutting (left & right wheel paths) was determined for the entire project length. No conversion was necessary. It is assumed that the measured rutting corresponds to the total surface rutting predicted by the Pavement-ME.

Reflective cracking: MDOT does not have any specific PDs for reflective cracking. Therefore, separating thermal and reflective cracks at the surface is challenging. Thus, the total measured transverse cracking was considered a combination of thermal and reflective cracking, and both models were calibrated.

3.2.1.3. Pavement distress unit conversion for JPCP designs

For JPCP sections, transverse cracking requires unit conversion. For all other distresses, MDOT records them in the Pavement-ME compatible units. Table 3-2 summarizes the distresses related to JPCP overlays, and the conversion process is discussed below:

IRI: The IRI in the MDOT sensor database does not need any conversion; the values were used directly.

Faulting: In the Pavement-ME, faulting is predicted as average per joint. MDOT's sensor data records the number of faults (FaultNum), average faulting (avgFault), and the maximum faulting (FaultMax) for every 0.1-mile segment. The faulting values had some inconsistencies. For the years between 2000 and 2011, faulting values are maximum fault callouts only (not average values). For 2012 and after, both average and maximum fault

values are available. A correlation was developed between the maximum and average faulting values using data from 2013 to 2017 to resolve this issue. After discussing with MDOT, the team used these correlations to estimate the average faulting from 2000 to 2011. Table 3-4 shows the regression equations between average and maximum faulting using the data from 2013 to 2017. These equations are based on the number of faults. It is important to note that ideally, the number of faults cannot be greater than the number of joints, but the number of faults in the database has records where they are more than the number of joints. These pseudo-fault values might come from cracking, spalling, bridge segments, etc. Therefore, the maximum number of fault counts was restricted to 36, and the average faulting to 0.4 inches to address this issue. Accordingly, any 0.1-mile section above these restricted faulting values was omitted from the calibration data.

Table 3-4 Correlation equations based on the number of faults

FaultNum		Equation (y is avgFault, x is FaultMax)	R-squared (2013-2017data)
From	To		
0	1	y=x	1
2	4	y = 0.3438x + 0.03	0.7189
5	40	y = 0.2132x + 0.0377	0.6074
41	ALL	y = 0.0936x + 0.0777	0.2476

The average joint faulting is calculated based on the number of faulting in a 0.1-mile section. It is assumed that if the number of faults is less or equal to the number of joints, faulting occurs at the joints only. In that case, the faulting unit conversion equation is as shown in Equation (3-4). If, for any 0.1-mile section, the number of faults is greater than the number of joints, that section is removed (cut) from the calibration data, as previously mentioned.

$$Fault = \frac{\text{FAULnum} \times \text{FAULi}}{\text{N}_{\text{joints}}} \tag{3-4}$$

where,

FAULnum = number of faults in a 0.1 mile

FAULi =(FAULT_(Avg_Right) + FAULT_(Avg_Left))/2 = Average faulting in a 0.1 mile (inches)

N_{joints} is the number of joints in 0.1-mile (528 ft) segments, i.e., N_{joints}=528/Joint Spacing.

Transverse cracking: The transverse cracking distress is predicted as % slabs cracked in the Pavement-ME. However, MDOT measures transverse cracking as the number of transverse cracks. PDs 112 and 113 correspond to transverse cracking. The estimated transverse cracking needs conversion to percent slabs cracked using Equation (3-5).

$$\%\ \text{Slabs Cracked} = \frac{\sum PD_{112,113}}{\left(\frac{\text{Section Length (miles)} \times 5280\ ft}{\text{Joint Spacing (ft)}}\right)} \times 100 \tag{3-5}$$

3.2.2 Condition Database for Local Calibration

To efficiently analyze the condition of selected Pavement Distresses (PDs), customized databases were created, which included distress and sensor data for multiple years. These databases were compiled using Microsoft Access and allowed for easy extraction of relevant data for projects of any length. The PMS condition data from 1992 to 2019 and sensor data from 1998 to 2019 were included in these databases. MATLAB codes were used to extract performance data for a section of the given length. For divided highways, which can have an increasing and decreasing direction to indicate north/south or east/west bounds, both directions were included in the time-series data and considered separate sections. In contrast, distress data was collected in one direction for undivided highways.

3.3 PROJECT SELECTION CRITERIA

For local calibration, selecting in-service pavement sections that represent Michigan's pavement design, currently used materials, construction practices, and performance is essential. These selected pavement sections should encompass all the current pavement types and rehabilitation techniques employed by the MDOT. The research team established a set of project selection criteria to identify and choose these representative pavement sections. This approach ensured that the selected pavement sections met the required standards and could accurately represent Michigan's pavement network. The process for identifying and selecting pavement sections consists of the following steps:

1. Determine the minimum number of pavement sections required for calibration based on the statistical requirements.
2. Identify all available in-service pavement projects.
3. Extract all pavement distresses (pavement condition data) from the customized database for all identified projects in Step 2.
4. Evaluate the measured performance for all the identified projects.
5. Identify projects with adequate data, age, trend, and the Pavement-ME inputs available to develop a refined list.

3.3.1 Identify the Minimum Number of Required Pavement Sections

The MEPDG local calibration guide provides a method to evaluate the minimum number of required sections for each distress type. The minimum number of sections was calculated using Equation (3-6), and the results are summarized in Table 3-5 for each condition measure. The total number of projects available in Table 3-5 are combined projects from the previous calibration study and newly selected projects from the current calibration effort.

$$n = \left(\frac{Z_{\alpha/2} \times \sigma}{e_t}\right)^2 \quad (3\text{-}6)$$

where;

$Z_{\alpha/2}$ = The z-value from a standard normal distribution
n = Minimum number of pavement sections
σ = Performance threshold
e_t = Tolerable bias $Z_{\alpha/2} \times SEE$
SEE = Standard error of the estimate

Table 3-5 Minimum number of sections for local calibration

Performance Model	Nationally calibrated SEE	Z_{90}	Threshold	*N* (required number of sections)	Number of sections used	Total number of projects available
Flexible Pavements						
Fatigue, bottom-up (%)	5.01	1.64	20%	16	184	163[2] 121[3]
Fatigue, top-down (ft/mile or %)	583		2000 or 20%	12	275	
Thermal cracking (ft/mile)[1]	-		1000	-	275	
Rutting (in)	0.107		0.5	22	360	
IRI (in/mile)	18.9		172	83	309	
Rigid Pavements						
Transverse cracking (%)	4.52	1.64	15	11	64	46[2] 11[3]
Joint faulting (in)	0.033		0.125	14	107	
IRI (in/mile)	22		172	61	65	

Note: Fatigue top-down has been updated in the recent Pavement-ME V2.6. It is expressed in ft/mile for the old model and in % for the updated model.

N= minimum number of samples required for a 90% confidence level

1. No *SEE*, threshold, or *N* was reported for thermal cracking in the literature
2. A total of 163 and 46 projects were identified for new reconstructed flexible and rigid pavements, respectively, based on the construction date and PMS data availability
3. Rehabilitation projects selected

3.3.2 Available In-Service Pavement Projects

The team identified the common pavement types in Michigan. These include:

1. HMA reconstruct
2. HMA over crush & shaped existing HMA
3. HMA over existing HMA
4. HMA over rubblized PCC
5. HMA over existing PCC (composite)
6. JPCP reconstruct, and
7. Unbonded concrete overlay

It is important to note that HMA over crushed & shaped existing HMA and HMA over rubblized existing PCC projects were analyzed as a new reconstructed pavement. Sections were selected for the local calibration based on performance trends and to accommodate wide ranges of different inputs, including layer thicknesses, traffic, region, etc. The selection process has been outlined in the succeeding sections.

3.3.3 Initial Projects Selection

MDOT provided a comprehensive database consisting of all the projects constructed in Michigan. Initially, all existing projects (140 flexible and 28 JPCP) used in previous calibration efforts were reviewed, and additional performance data were extracted where possible. The team also identified additional projects that can be potential candidates for the

current local calibration effort. The PMS data extraction was completed for all required distress types in a compatible format with the Pavement-ME software. The team then looked at the time series for each pavement section's performance measures to finalize the preliminary list of new potential candidate projects.

To ensure a robust and appropriate set of data, the criteria used to identify additional performance data and the selection of new potential pavement projects include:

- The pavement section must have at least three measured data points over time. There are some exceptions to this criterion. Bottom-up cracking has relatively fewer data points; some sections with even two points have been included, considering further data points will be collected in the future. The same process was followed for transverse cracking in rigid sections. As previously noted and explained, joint faulting and thermal cracking have been cut at specific values, so these data points are omitted from the calibration database.
- At least one of the distresses should have an increasing trend. Any section with decreasing and no or flat trends over time was excluded from the list.
- The team also looked at previous maintenance history for all pavement sections to explain any decrease or flat trend observed in the time series plot. If there were any major rehabilitation or reconstruction activities, the measured data from the year traffic opened initially to the very last year until the major repair took place are considered.
- The last recorded point should have a Distress Index (DI) of at least 5 for a section. DI is calculated by taking a weighted average of different distress types. DI was observed and limited to ensure sufficient distress for calibration and to capture adequate pavement performance trends.

Figures 3-1 through 3-4 illustrate example distress progressions for the flexible pavement of different construction types. The top-down cracking for the initial project selection was evaluated in feet/mile and later converted to a percentage. Figure 3-5 shows an example of a flexible pavement section that was omitted in the new dataset. Similarly, Figures 3-6 and 3-7 present a few examples of the selected and omitted rigid pavement sections. The vertical dashed red line is the last reported construction, whereas the dotted blue line in the DI plot indicates reported maintenance activities. For example, Figure 3-4 shows the vertical dotted blue line in the DI plot that shows a cold mill and resurface (CM&R) treatment was applied in 2012. In the same figure, the effect of this rehabilitation event can be noticed with a drop in measured distress in individual distress plots. Therefore, in this particular case, pavement section performance can be considered from 2001 to 2011. It should be noted that generally, minor maintenance [e.g., crack treatment (CT) or joint sealing (JS)] does not affect the time series trend since these minor maintenances represent non-structural fixes. It is also to be noted that time series plots for rutting show a consistent drop in the 2012-2013 collection years, regardless of whether any maintenance is reported or not. This is likely due to changes in the data collection process or vendor differences.

Based on the criteria mentioned above, a total of 468 flexible sections and 114 rigid sections were initially selected. The performance of the selected pavement sections was compared

with all sections available in the MDOT database (2081 flexible sections and 442 rigid sections) to verify if the chosen sections represent the overall pavements in Michigan. Sections with at least three available data points are considered. Each section was categorized as good, fair, or poor performing based on the performance trend lines modified to reflect Michigan conditions *(1)*. These trend lines are available only for bottom-up cracking, total rutting, and IRI for flexible sections, and transverse cracking and IRI for rigid sections. The performance categories depend on the measured performance trend relative to the reference lines. If the measured performance is below the good performance line, it is categorized as a good performing section, between the good and poor line, as fair, and above the poor performance line, as the poor performing section. The performance category was decided based on a previous calibration study *(1)*. When the performance trend passes through more than one category zone, the zone with the maximum points is considered the performance category for that section. Also, the low-performance category is selected in case of an equal number of points for two different categories. Figures 3-8 and 3-9 show example sections for good, fair, and poor categories for IRI performance for flexible and rigid sections, respectively. A similar method was followed for categorizing sections based on all other distresses. Figures 3-10 and 3-11 show the distribution of good fair, and poor sections for flexible and rigid sections based on different distress criteria. Figures 3-10 and 3-11 show that the selected sections satisfactorily represent MDOT all sections for both flexible and rigid pavements.

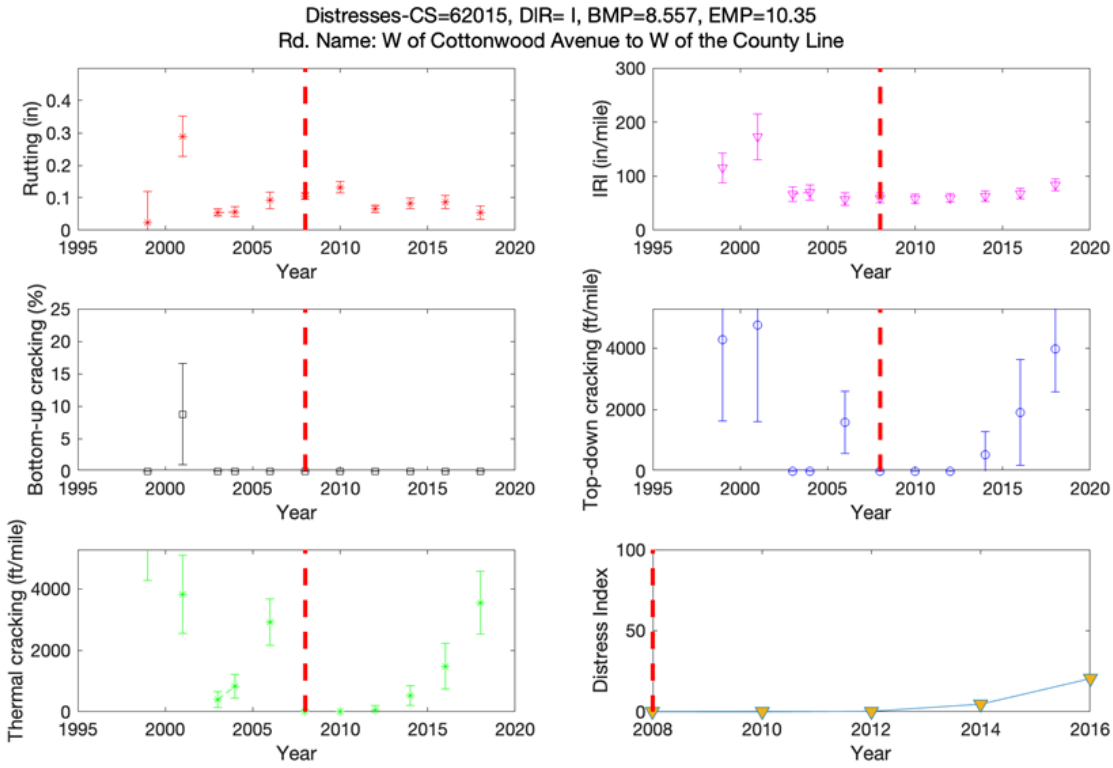

Figure 3-1 Example of selected section for crushed & shaped flexible pavement

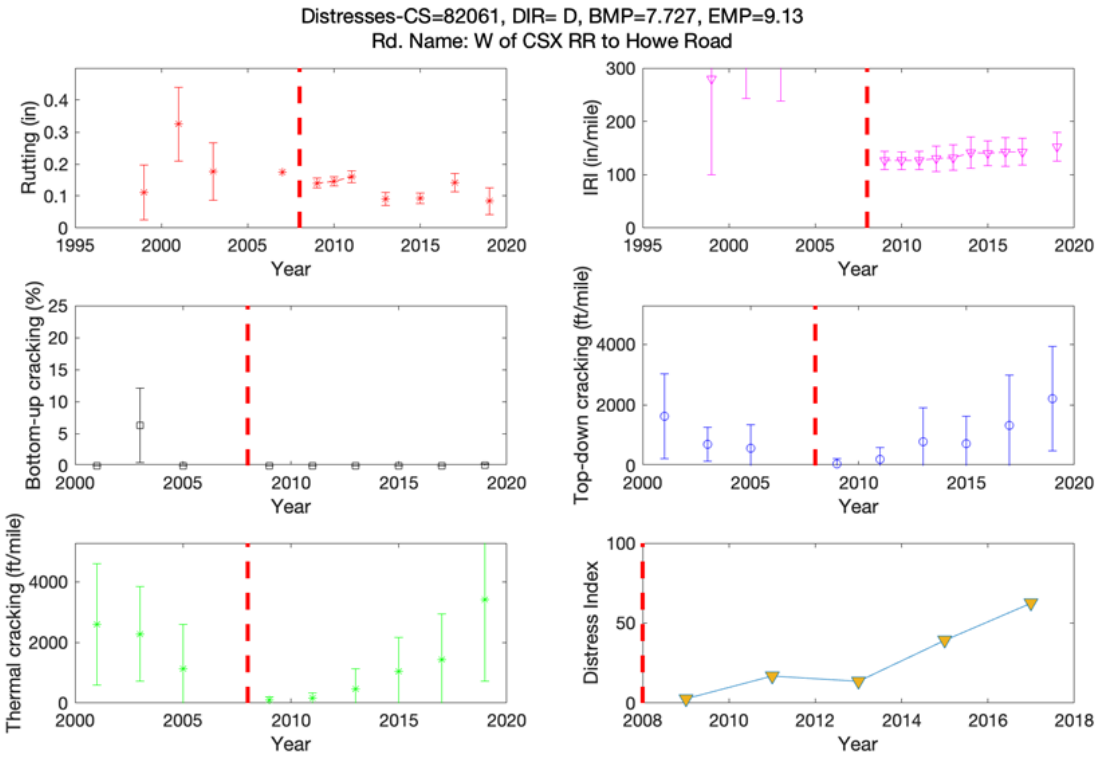

Figure 3-2 Example of selected section for new/reconstructed flexible pavement

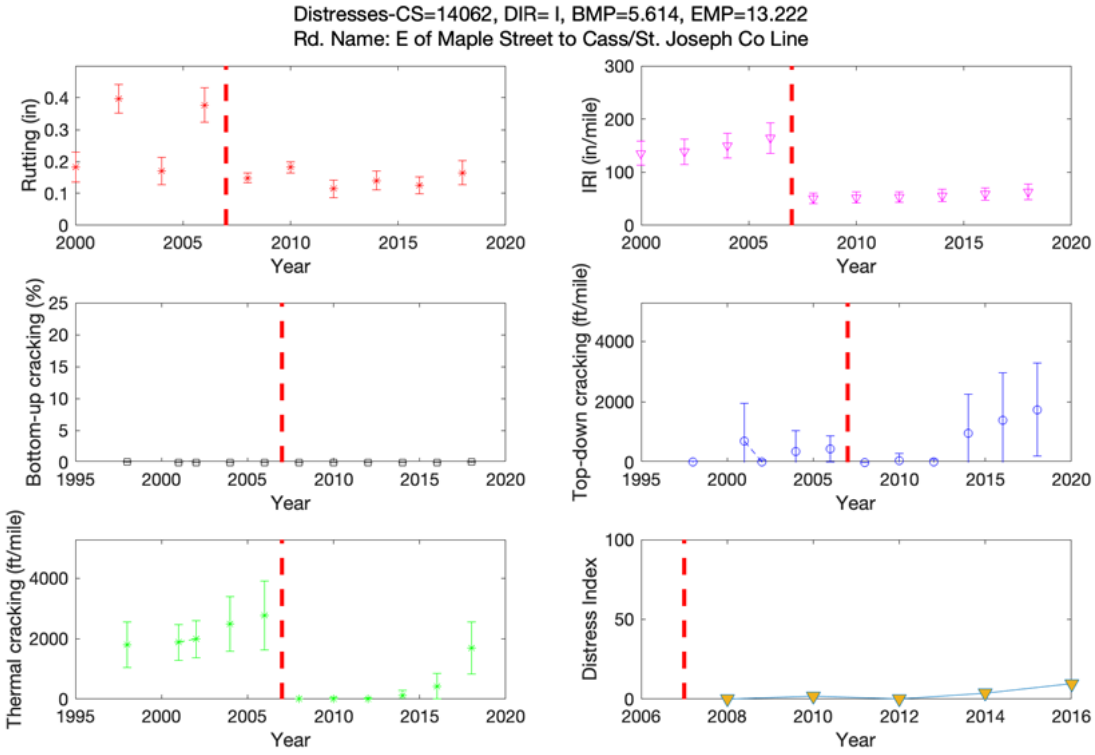

Figure 3-3 Example of selected section for bituminous overlay on rubblized concrete pavement

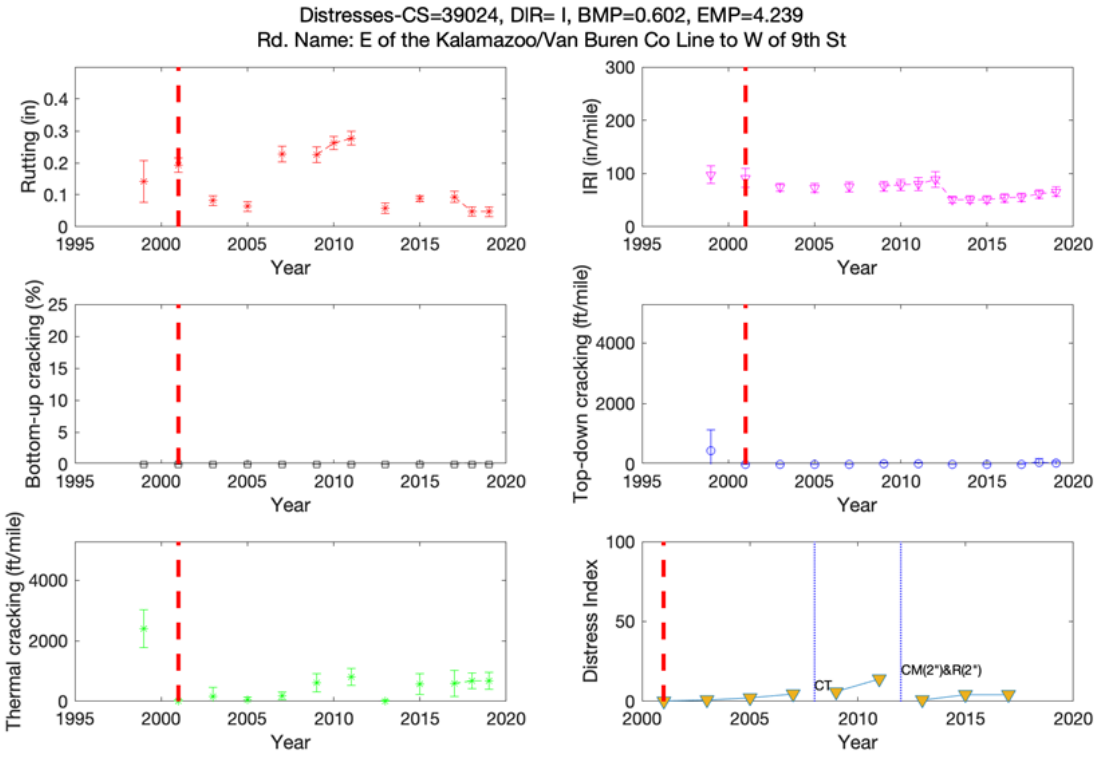

Figure 3-4 Example of selected section for multicourse bituminous overlay flexible pavement

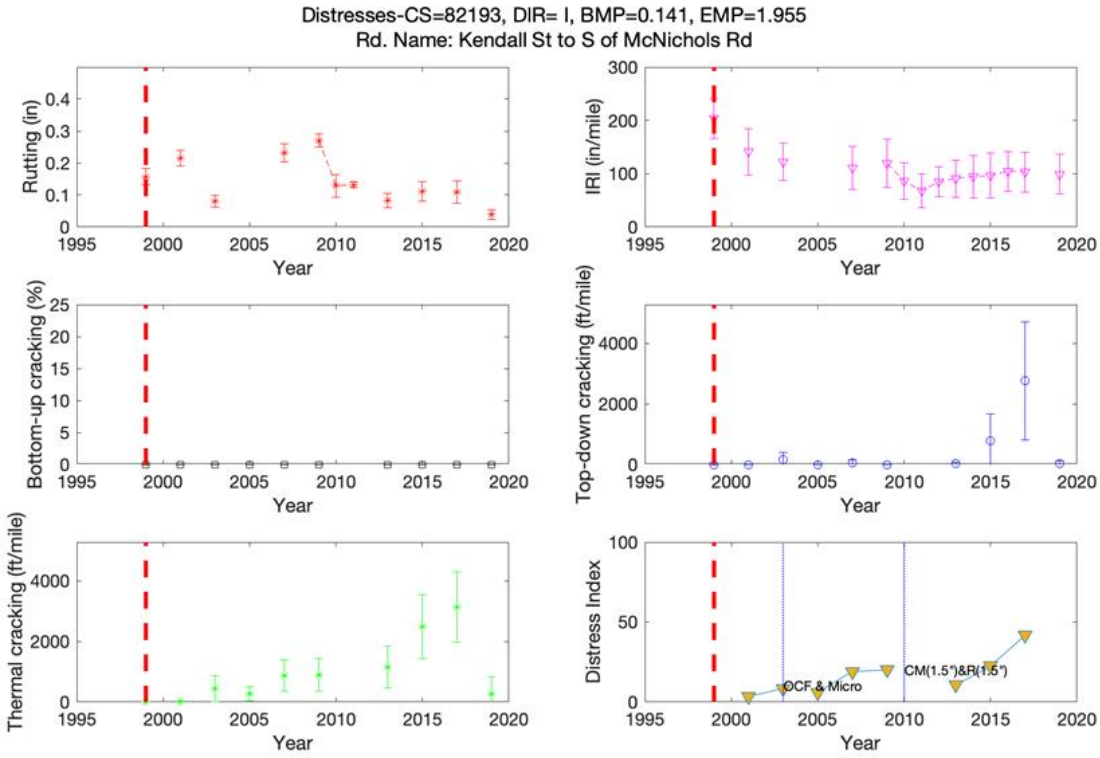

Figure 3-5 Example of an omitted flexible section

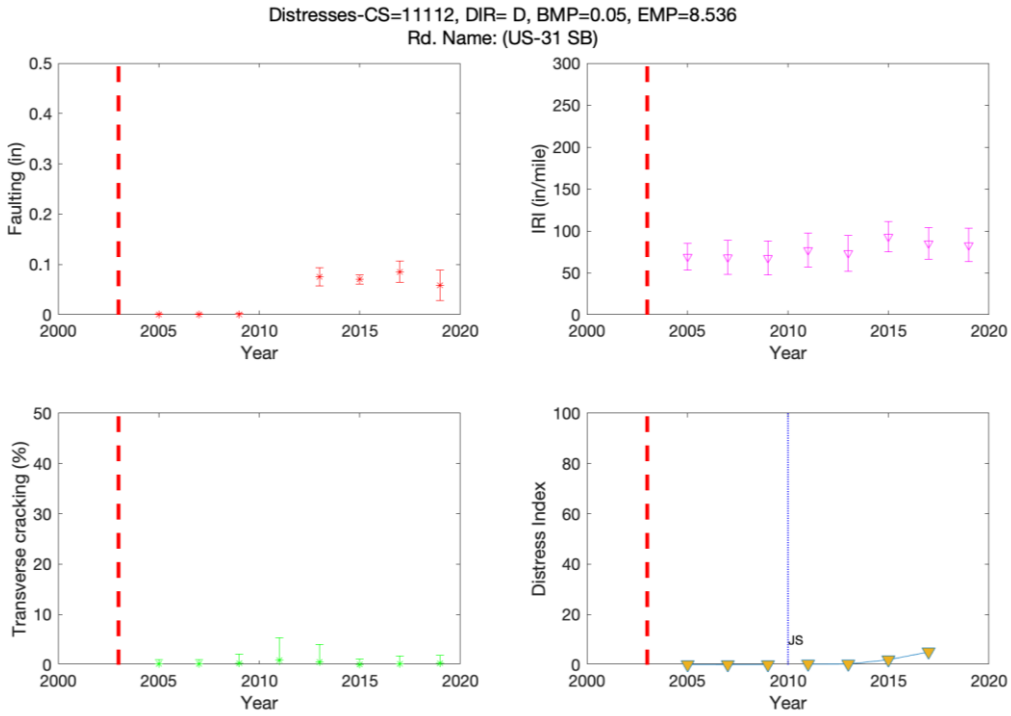

Figure 3-6 Example of a selected rigid section

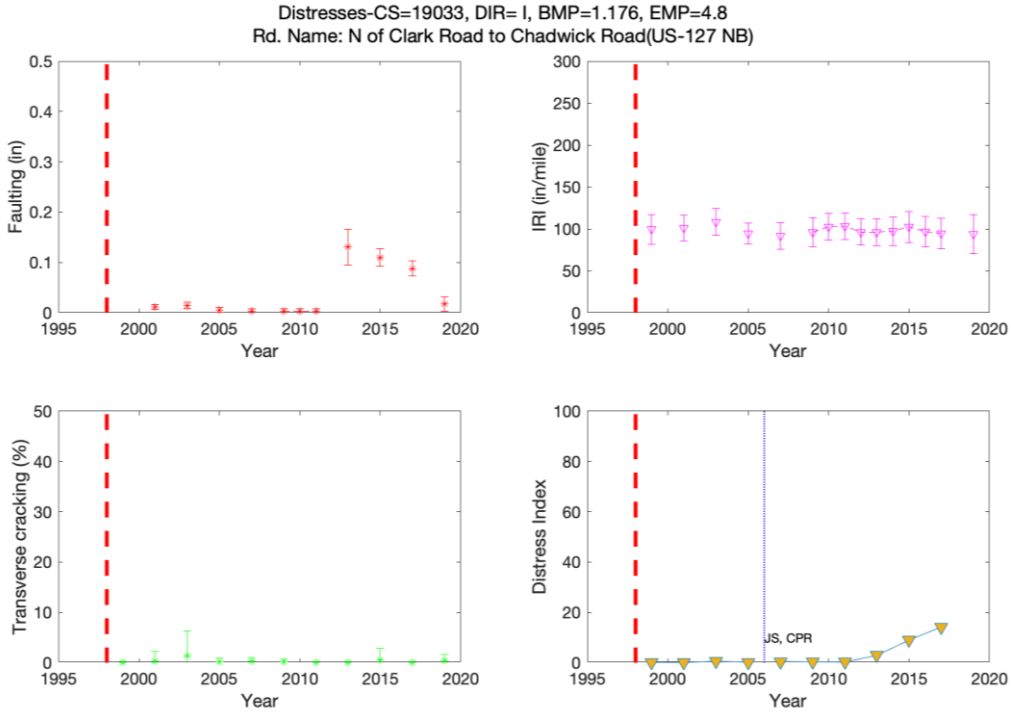

Figure 3-7 Example of an omitted rigid section

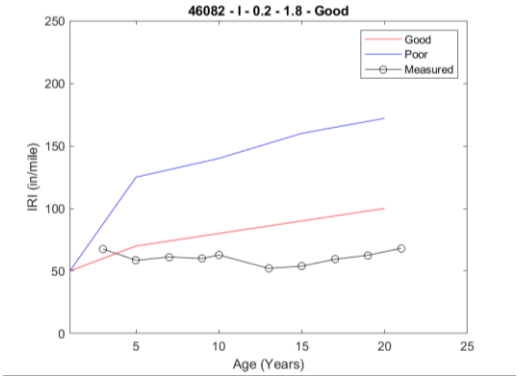

(a) Good section

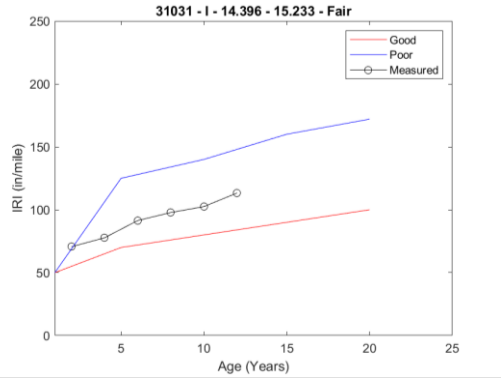

(b) Fair section

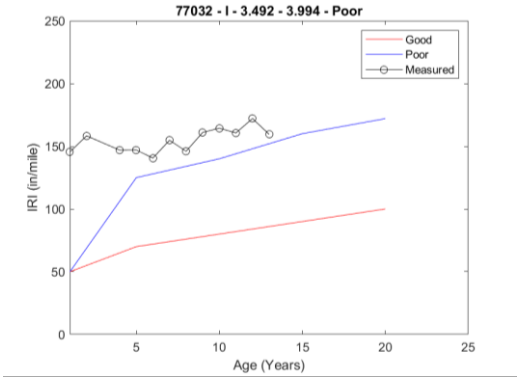

(c) Poor section

Figure 3-8 Categorization of flexible sections based on performance trends

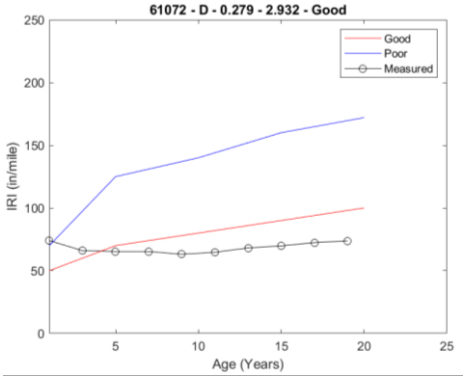

(a) Good performing section

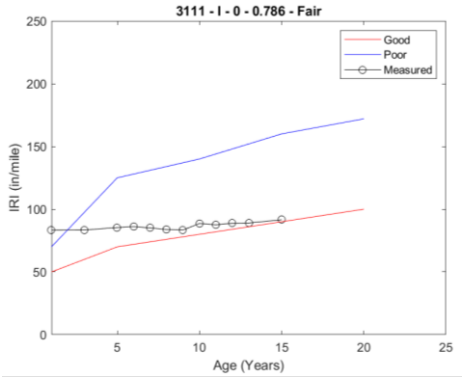

(b) Fair performing section

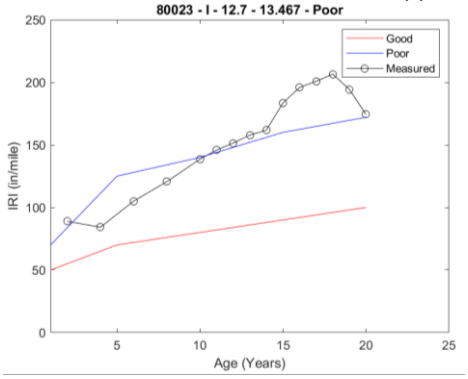

(c) Poor performing section

Figure 3-9 Categorization of rigid sections based on performance trends

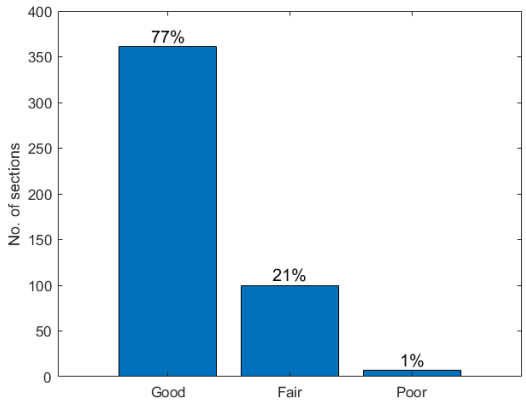

(a) Bottom-up cracking (selected sections)

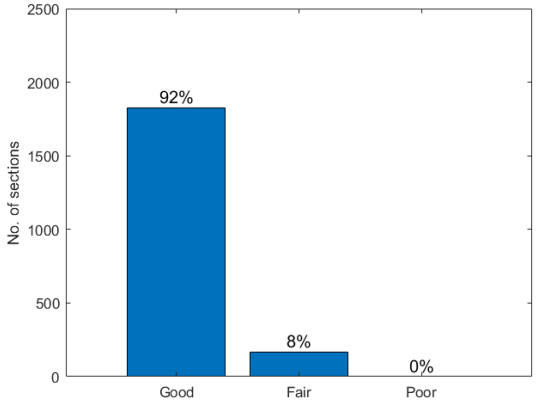

(b) Bottom-up cracking (All MDOT sections)

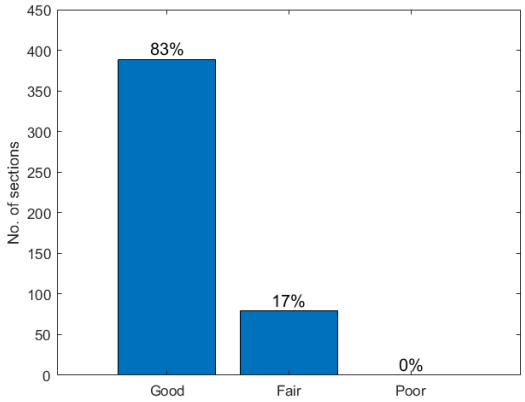

(c) Total rutting (selected sections)

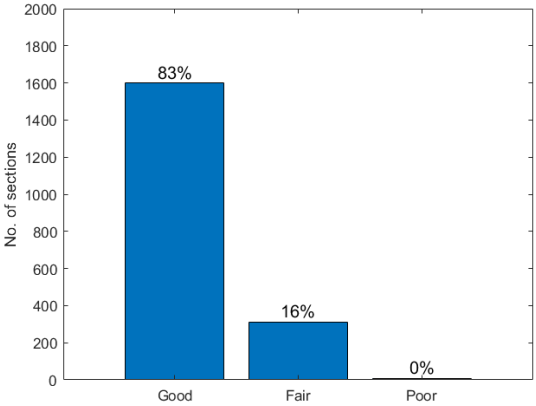

(d) Total rutting (All MDOT sections)

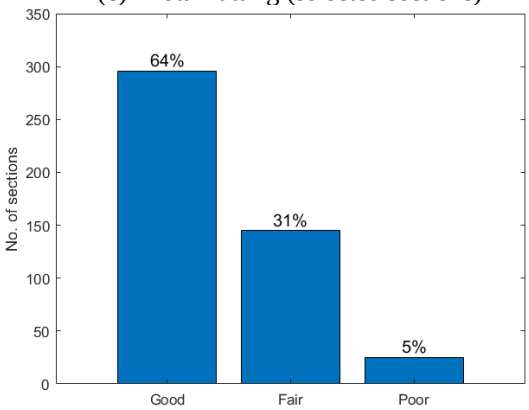

(e) IRI (selected sections)

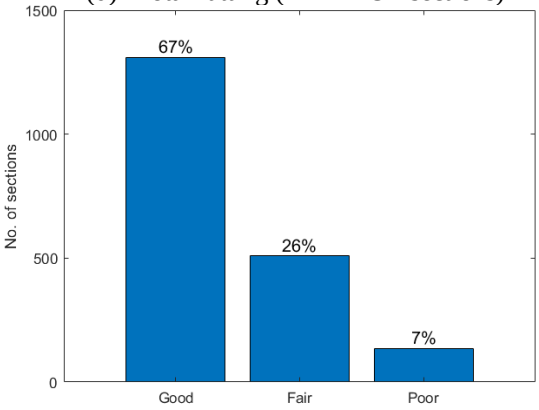

(f) IRI (All MDOT sections)

Figure 3-10 Comparison of selected flexible sections with all MDOT sections

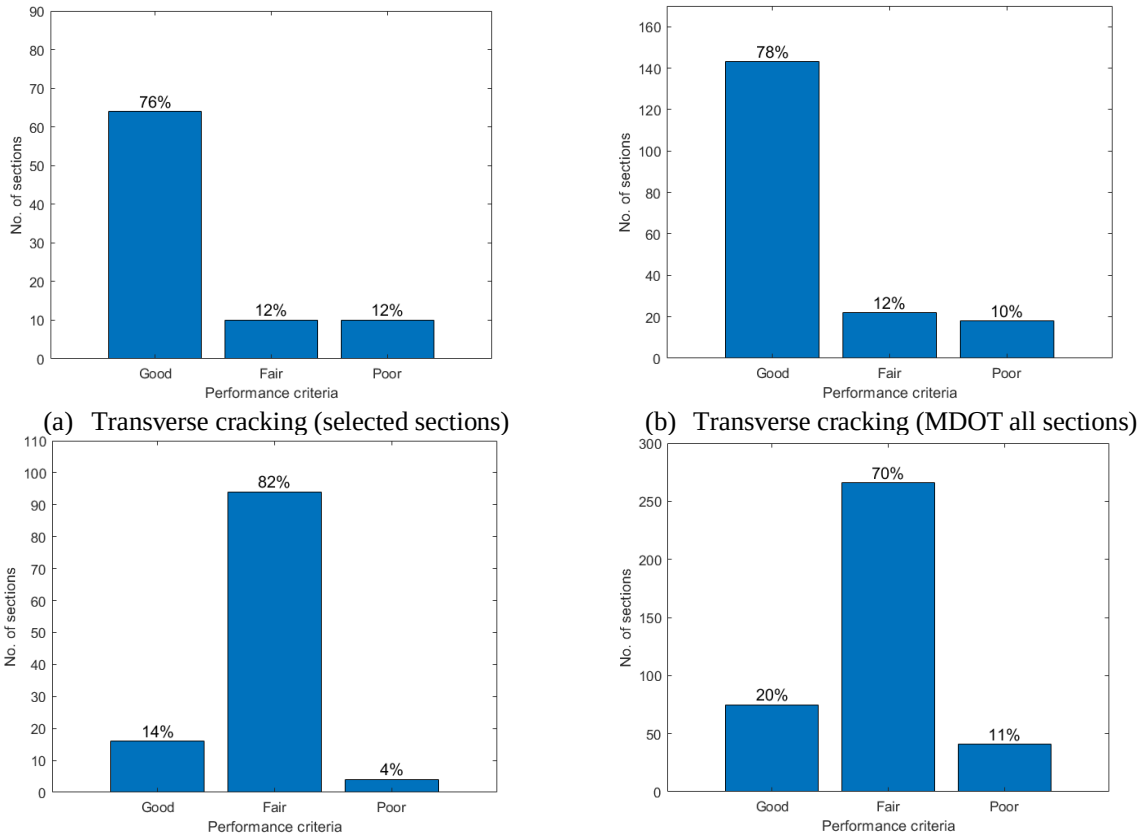

(a) Transverse cracking (selected sections)

(b) Transverse cracking (MDOT all sections)

(c) IRI (selected sections)

(d) IRI (MDOT all sections)

Figure 3-11 Comparison of selected rigid sections with all MDOT sections

3.3.4 Summary of the Selected Projects

The initially selected projects were further refined based on performance, availability of inputs, and initial IRI. The performance data for these initially selected sections is the average for the entire section length. This data is calculated by averaging the performance for every 0.1-mile segment in the project length. Data for every 0.1 mile has been reviewed to estimate performance data extent and reasonableness. Figures 3-12 to 3-16 show performance data for every 0.1-mile segment with age for all flexible sections. Figures 3-17 to 3-19 show the same for all rigid sections.

As previously noted, cutoff values of 2112 ft/mile and 0.4 inches were adopted for thermal cracking and joint faulting, respectively. These values were selected based on the raw (0.1-mile segment) data, limitations of the Pavement-ME models, and consensus with MDOT. Moreover, sections with Superpave mixes are only used to calibrate the thermal cracking model to have consistent Level 1 input in the Pavement-ME.

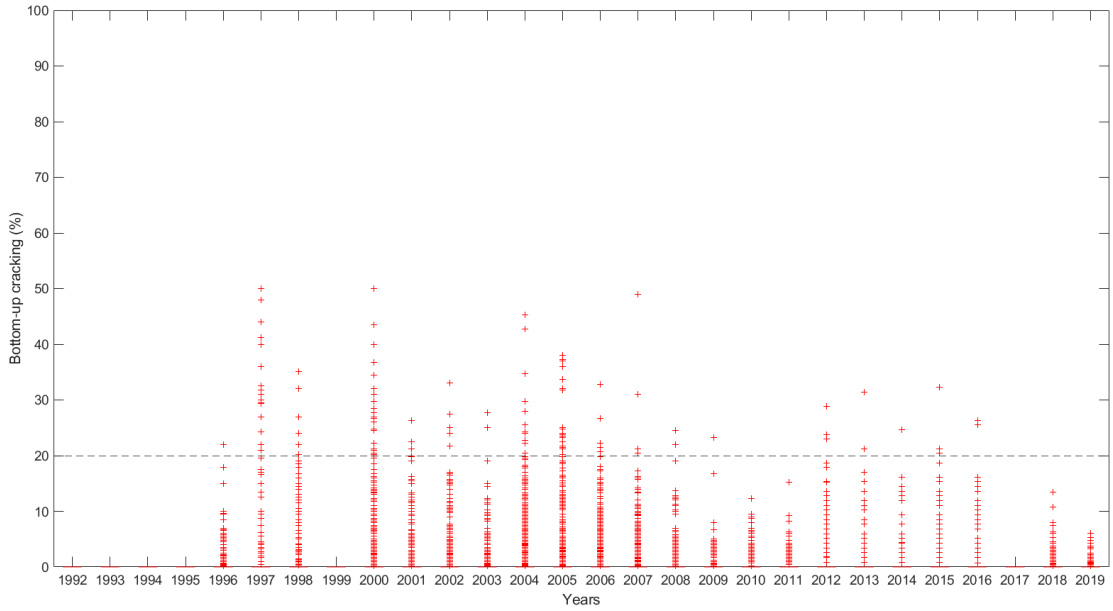

Figure 3-12 Bottom-up cracking at every 0.1-mile segment for flexible sections

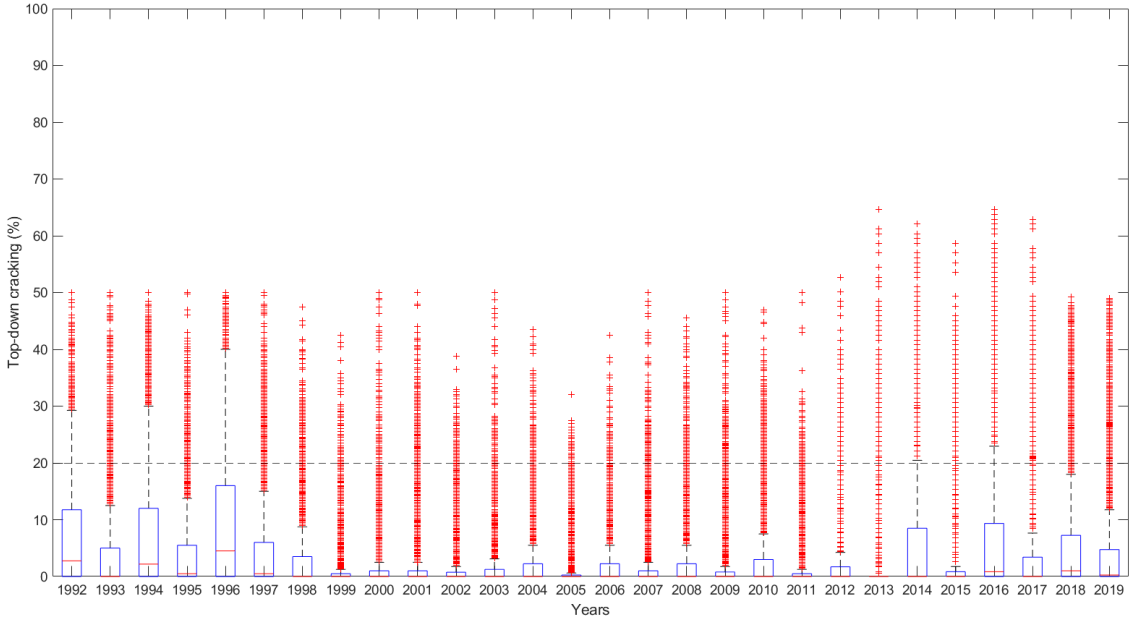

Figure 3-13 Top-down cracking at every 0.1-mile segment for flexible sections

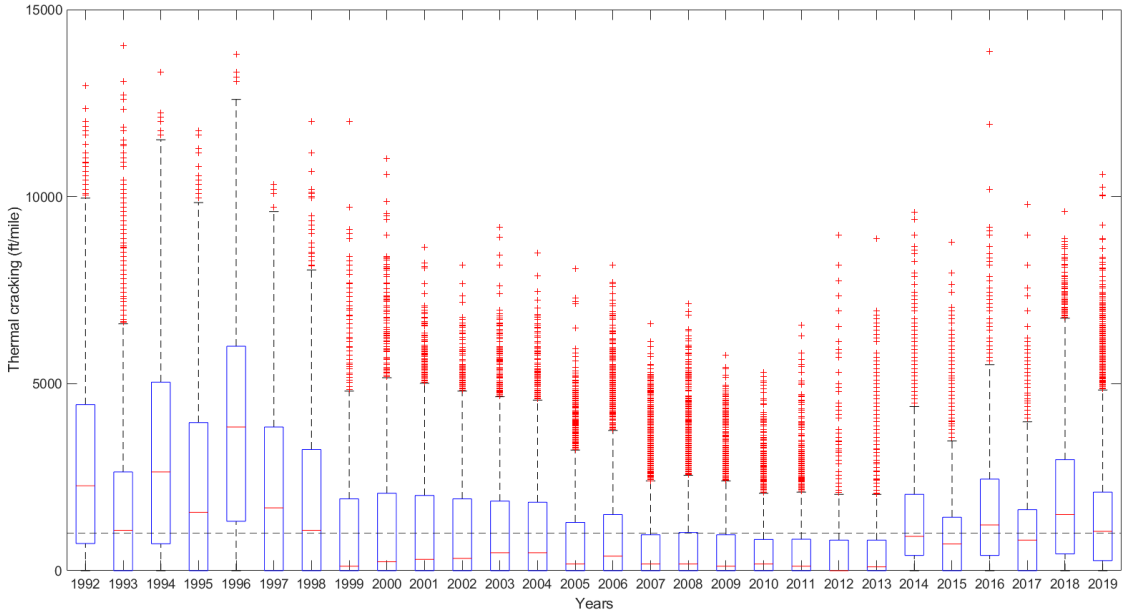

Figure 3-14 Thermal cracking at every 0.1-mile segment for flexible sections

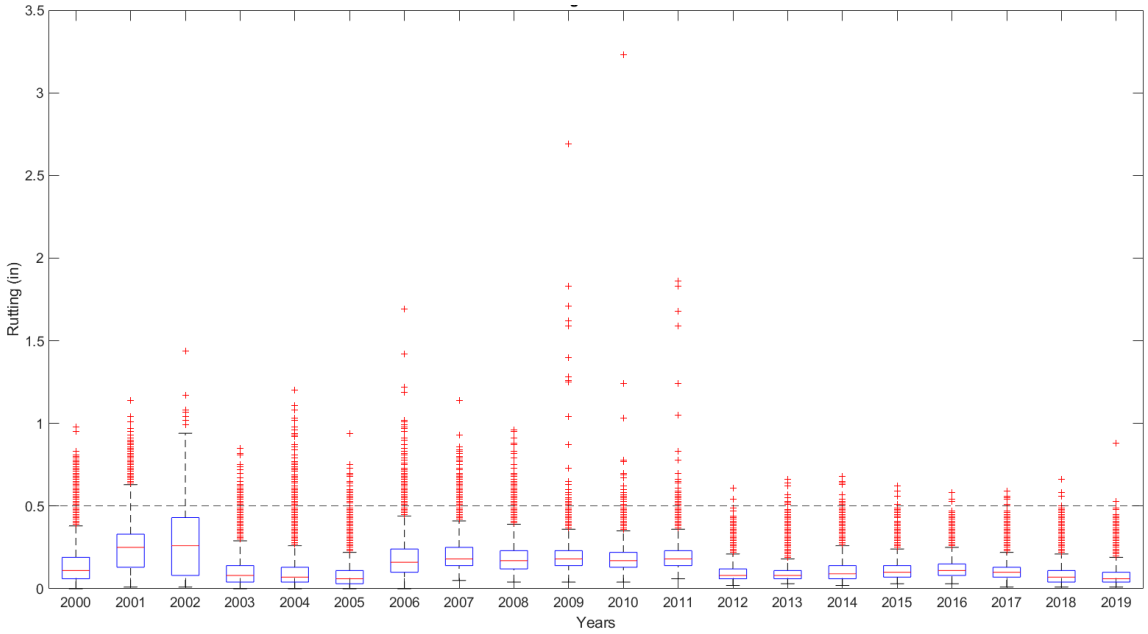

Figure 3-15 Rutting at every 0.1-mile segment for flexible sections

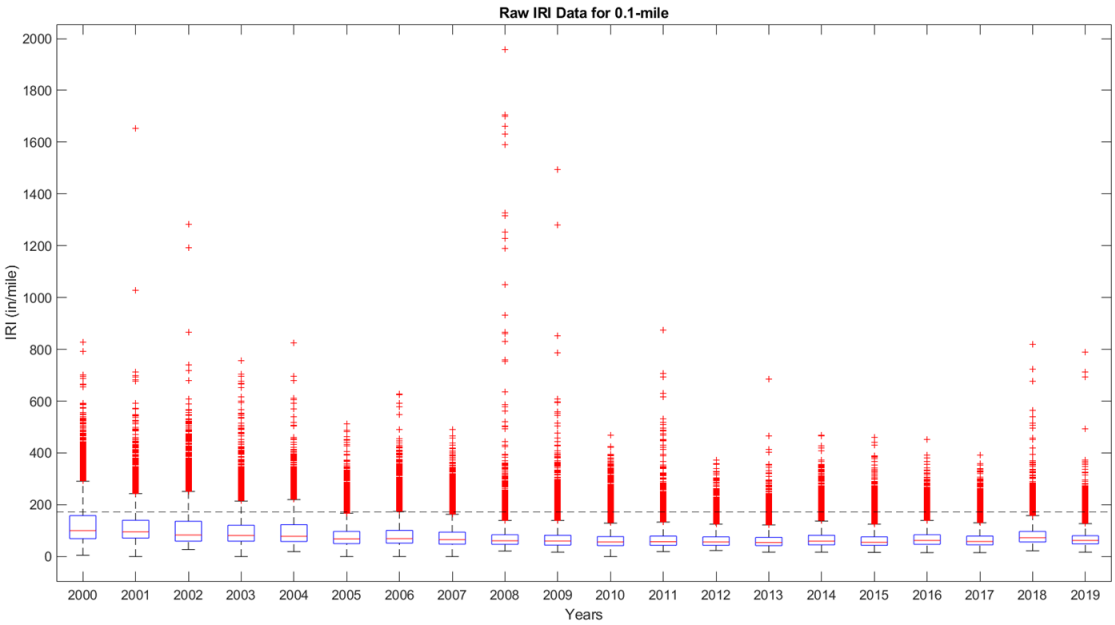

Figure 3-16 IRI at every 0.1-mile segment for flexible sections

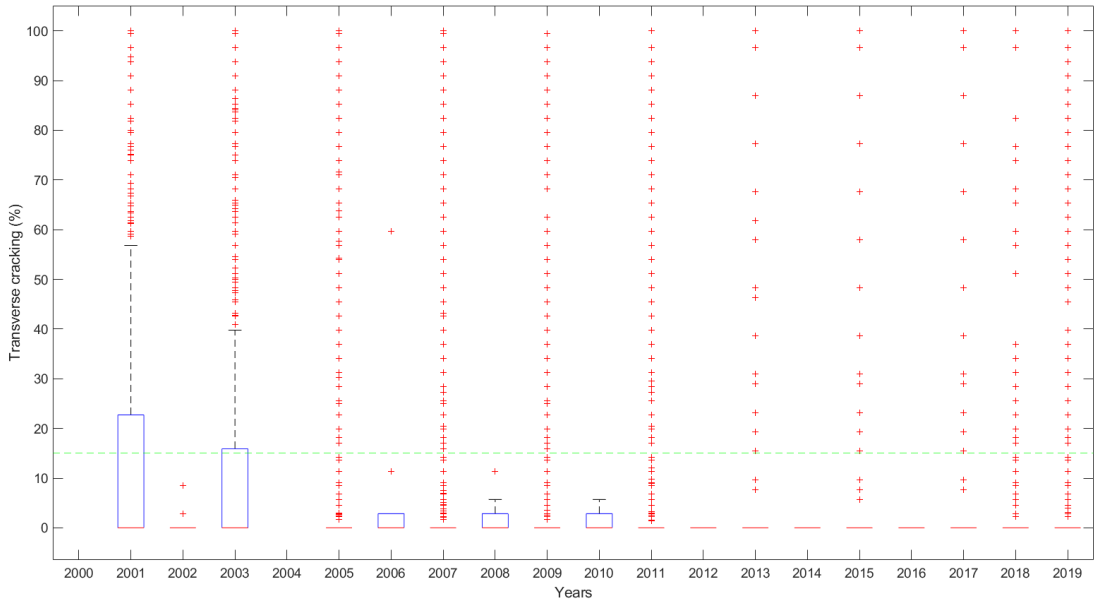

Figure 3-17 Transverse cracking at every 0.1-mile segment for rigid sections

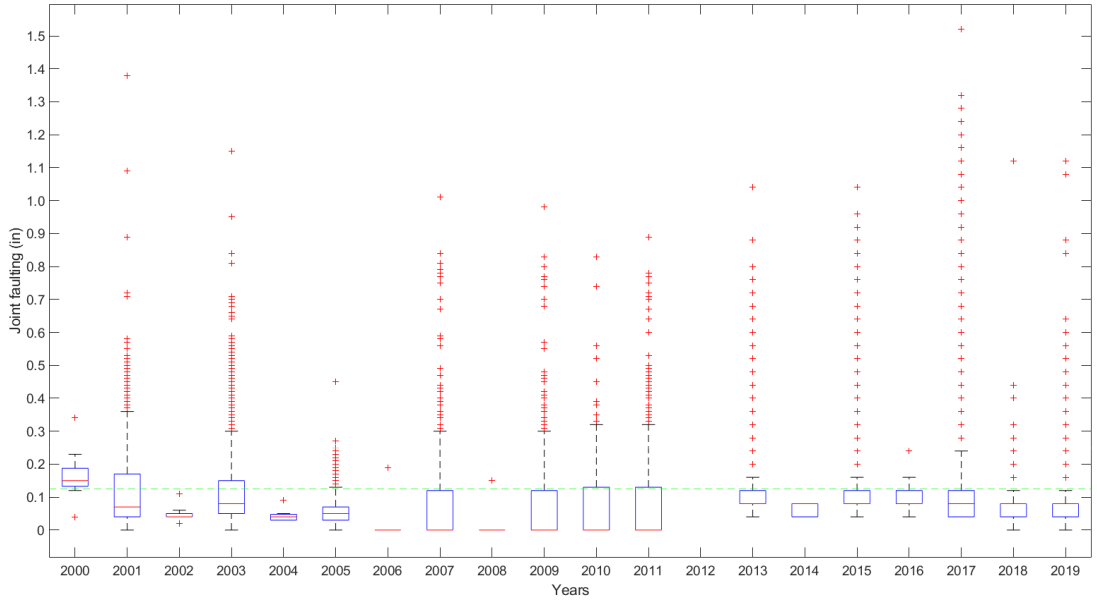

Figure 3-18 Joint faulting at every 0.1-mile segment for rigid sections

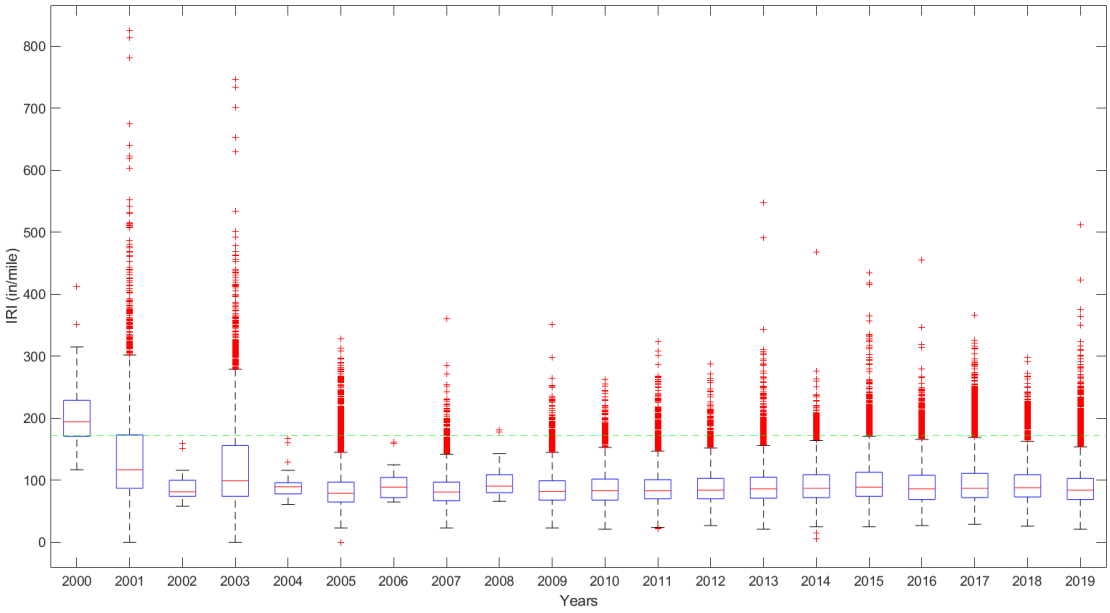

Figure 3-19 IRI at every 0.1-mile segment for rigid sections

Figures 3-20 to 3-23 show the geographical location of the finally selected projects. Tables 3-6 and 3-7 summarize the reconstruction and rehabilitation projects as per region. Tables 3-8 and 3-9 outline the selected projects based on the design matrix (of traffic, thickness, and age) for reconstruction and rehabilitation projects.

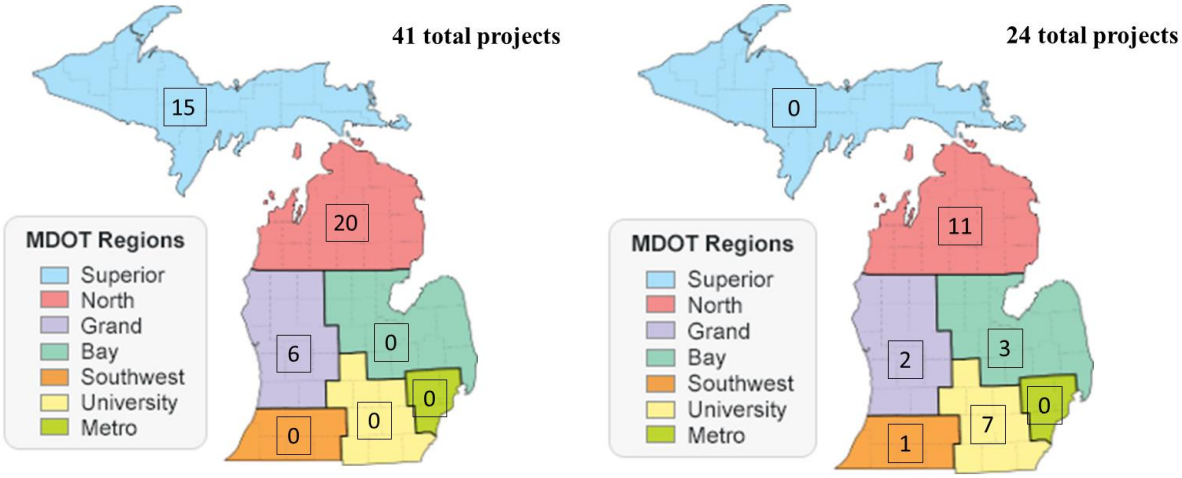

(a) Crush and shape (b) Rubblized

Figure 3-20 Geographical location of selected crush and shape and rubblize projects

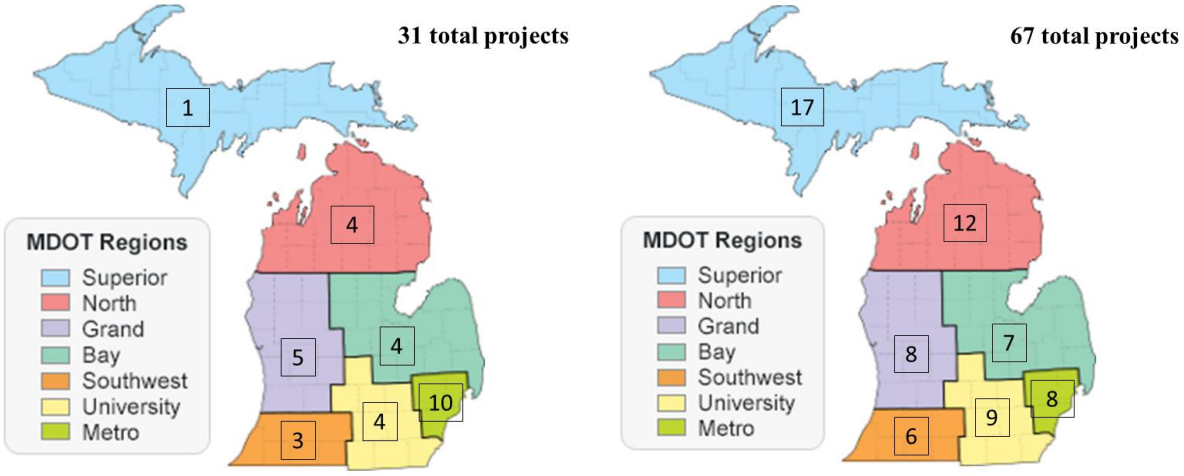

(a) Freeway (b) Non-freeway

Figure 3-21 Geographical location of selected HMA reconstruct projects

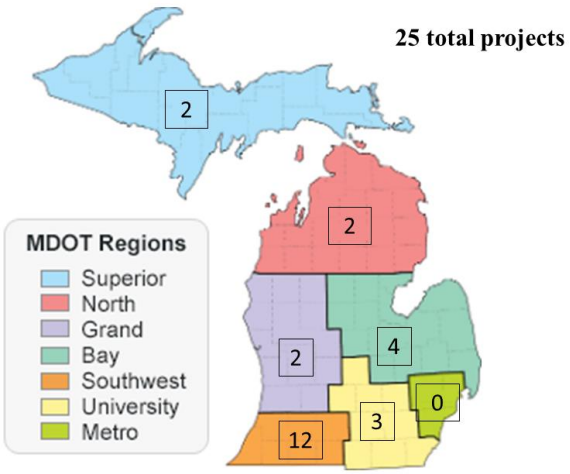

(a) HMA over HMA

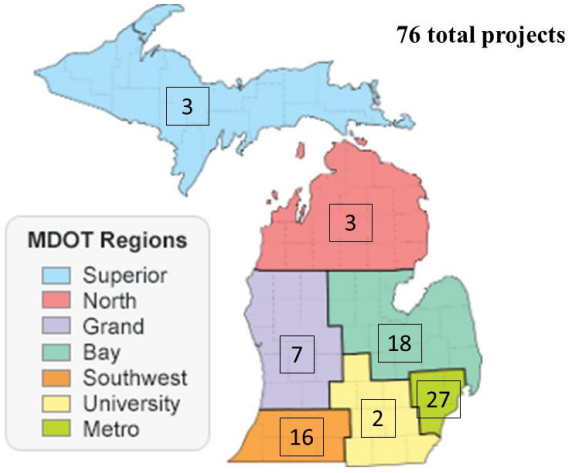

(b) Composite

Figure 3-22 Geographical location of selected HMA overlay projects

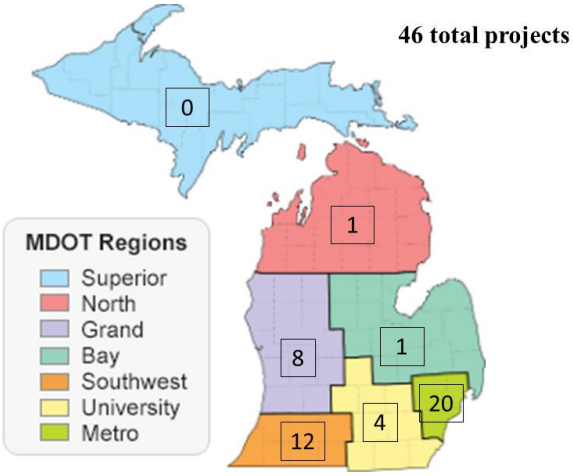

(a) New JPCP

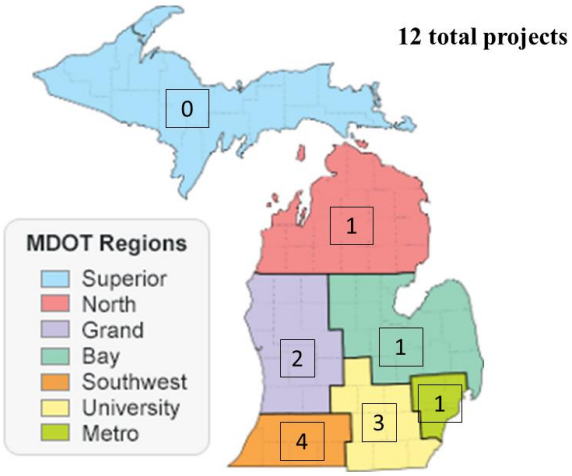

(b) Unbonded overlay

Figure 3-23 Geographical location of selected rigid pavement projects

Table 3-6 Number of new construction projects by pavement type & region

Pavement type	MDOT region	Number of projects
Crush and Shape	Grand	6
	North	20
	Superior	15
HMA over rubblized PCC	Bay	3
	Grand	2
	North	11
	Southwest	1
	University	7
HMA Reconstruct Freeway	Bay	4
	Grand	5
	Metro	10
	North	4
	Southwest	3
	Superior	1
	University	4
HMA Reconstruct Non-freeway	Bay	7
	Grand	8
	Metro	8
	North	12
	Southwest	6
	Superior	17
	University	9
JPCP Reconstruct	Bay	1
	Grand	8
	Metro	20
	North	1
	Southwest	12
	University	4
Total		209

Table 3-7 Number of rehabilitation projects by MDOT region

Pavement type	MDOT region	Number of projects
Composite overlay	Bay	18
	Grand	7
	Metro	27
	North	3
	Southwest	16
	Superior	3
	University	22
HMA over HMA overlay	Bay	4
	Grand	2
	North	2
	Southwest	12
	Superior	2
	University	3
Unbonded overlay	Bay	1
	Grand	2
	Metro	1
	North	1
	Southwest	4
	University	3
Total		133

Table 3-8 Selection matrix displaying selected sections (rehabilitation)

Rehabilitation type	Traffic level*	Overlay thickness level*	Age (years)			Total
			<10	10 to 20	>20	
Composite overlay	1	1		1		140
		2	5	66	1	
	2	2	2	18	7	
	3	2	10	29	1	
HMA over HMA	1	1			3	36
		2	3	16	7	
	2	2		1	4	
	3	2			2	
Unbonded overlay	2	2		1		28
		3		4		
	3	3		21	2	
Total			20	157	27	204

*Levels	1	2	3
Traffic (AADTT)	<1000	1000-3000	>3000
Overlay thickness (in)	<3	3-6	>6

Table 3-9 Selection matrix displaying selected sections (reconstruct)

Road type	Traffic level*	Thickness level*	Age Level			Total
			<10	10-15	>15	
Crush and Shape	1	1			3	3
		2	11	8	20	39
		3				
	2	1				
		2		7	11	18
		3				
	3	1				
		2				
		3				
HMA over rubblized PCC	1	1				
		2		4	16	20
		3		2	4	6
	2	1				
		2		9	3	12
		3				
	3	1				
		2			7	7
		3			4	4
HMA Reconstruct Freeway	1	1				
		2	2	4	8	14
		3		2	8	10
	2	1				
		2			1	1
		3	1	3	11	15
	3	1				
		2			2	2
		3		5	8	13

Table 3-9 Selection matrix displaying selected sections (continued…)

HMA Reconstruct Non-freeway	1	1			1	1
		2	3	25	12	40
		3			9	9
	2	1				
		2	1	22	43	66
		3	1	1		2
	3	1				
		2		2	2	4
		3		2		2
JPCP Reconstruct	1	1				
		2				
		3		1	3	4
	2	1				
		2				
		3		2	9	11
	3	1				
		2				
		3		31	39	70
Total			19	130	224	373

*Levels	1	2	3
Traffic (AADTT)	<1000	1000-3000	>3000
Thickness (in)	<3	3-7	>7

3.4 SELECTED SECTION PERFORMANCE DATA SUMMARY

The team extracted the measured condition for each project and made the necessary conversions to ensure compatibility with the Pavement-ME predicted performance, as discussed in Section 3.2.

The team conducted a detailed review to evaluate the level of distress in all pavement sections identified for local calibration. The calibration process entails comparing each chosen project's predicted and measured performance. To have a robust local calibration, the levels of distress must fall within a reasonable range (i.e., above and below threshold limits for each type of distress). Therefore, the distress levels for all projects were compiled and analyzed to determine their respective ranges. This section summarizes the observed performance for the selected rehabilitation and reconstruction pavement sections. Efforts were undertaken to gather sufficient information to achieve a precise and dependable local calibration of the performance models. Due to changes in construction practices and/or data availability, most sections are less than 20 years old, so it is expected that most sections do not have poor performance or exceed performance thresholds. Furthermore, these represent the average values of the Pavement-ME prediction using 50% reliability. When designing, a higher reliability factor is applied to account for project variability (including climate, traffic, material, and construction), which will increase the resulting distress values. Therefore, while designs will correlate with the calibration sections, it should not be anticipated that pavement designs will exactly match the sections used in calibration because of the increased reliability factor.

a. A total of 132 rehabilitation projects were considered in the local calibration. Of these selected projects, 121 are flexible rehabilitation sections, while 11 are JPCP unbonded

overlays. The 121 HMA and 11 PCC unbonded overlay projects (which comprise 176 HMA and 28 PCC unbonded overlay sections) were analyzed to test the calibration procedures for different distresses in flexible and rigid pavements, respectively.

- *HMA overlay performance data*: The time series and age distribution for the HMA rehabilitation projects are shown in Figures 3-24 to 3-28. The following observations can be made from the results:

  - Bottom-up fatigue cracking: Most sections exhibit low bottom-up cracking, with only a few reaching the threshold of 20%, ranging between 5 to 20 years. It should be noted that the Pavement-ME does not predict bottom-up cracking for composite sections; therefore, only the top-down cracking model was calibrated for composite sections.
  - Longitudinal/top-down fatigue cracking: Top-down cracking is observed more frequently than bottom-up cracking. The age at maximum distress ranged from 5 to 20 years.
  - Rutting: Most sections did not exhibit significant rutting, with no section reaching the threshold of 0.5 inches. The age distribution ranged from 3 to 19 years. Figure 3-32 shows the distribution of categories (good, fair, and poor) for these sections. As shown, all of these sections fall under good and fair categories for rutting.
  - Transverse (thermal) cracking: The thermal cracking for the rehabilitation projects observed significant cracking with two sections nearing 5000 feet/mile. The age at which the maximum thermal cracking occurred ranged from 6 to 20 years. Sections with Superpave (PG) binder have been used for thermal cracking calibration. It should be noted that some of the thermal cracks could be reflective cracks. MDOT PMS does not distinguish between reflective or transverse (thermal) cracks.
  - IRI: The IRI time series is usually flat, with only 2 sections exceeding the 172 in/mile threshold. The age at maximum IRI ranged from 7 to 20 years. It is worth noting that only sections with an initial IRI less than or equal to 82 in/mile were selected for calibration of the IRI model. Almost all sections fall under good or fair categories, as shown in Figure 3-32.

- *Unbonded overlay performance data*: Figures 3-29 to 3-31 show the magnitude and age distribution for the JPCP rehabilitation projects. The following observations can be made:

  - Transverse cracking: Fairly low values are observed for transverse cracking, with none of the projects exceeding the distress threshold of 15% of slabs cracked. The maximum transverse cracking observed is 4%. The age distribution ranges from 6 to 19 years. All of these sections fall in the good category, as shown in Figure 3-32.
  - Transverse joint faulting: One section exceeds the joint faulting threshold of 0.125 inches with a maximum value of 0.14 inches. The age distribution ranges from 11 to 19 years. These observed values for joint faulting have been cut off at 0.4 inches. Any values (for a 0.1-mile segment) above 0.4 inches have been removed.

- IRI: A maximum IRI of 144 in/mile was observed for the unbonded overlay sections. None of the sections exceeded the IRI threshold of 172 in/mile. The age at maximum IRI ranges from 13 to 19 years. It is worth noting that the initial IRI was limited to 82 in/mile. Only sections with less than or equal to 82 in/mile were selected to calibrate the IRI model. Most of these sections are in the fair category, as shown in Figure 3-32

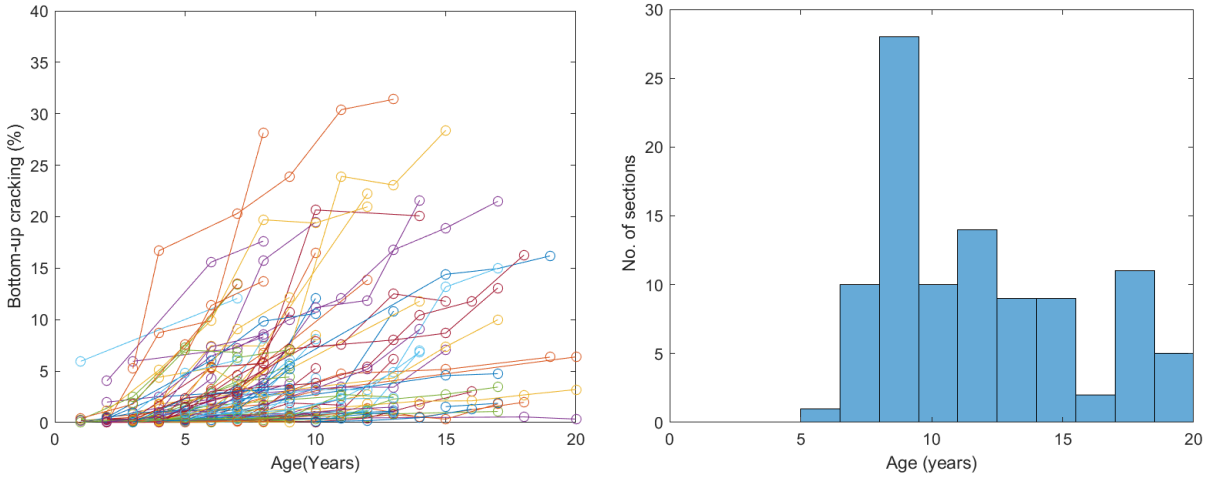

(a) Time series (b) Age distribution

Figure 3-24 Selected HMA rehabilitation sections — Bottom-up cracking

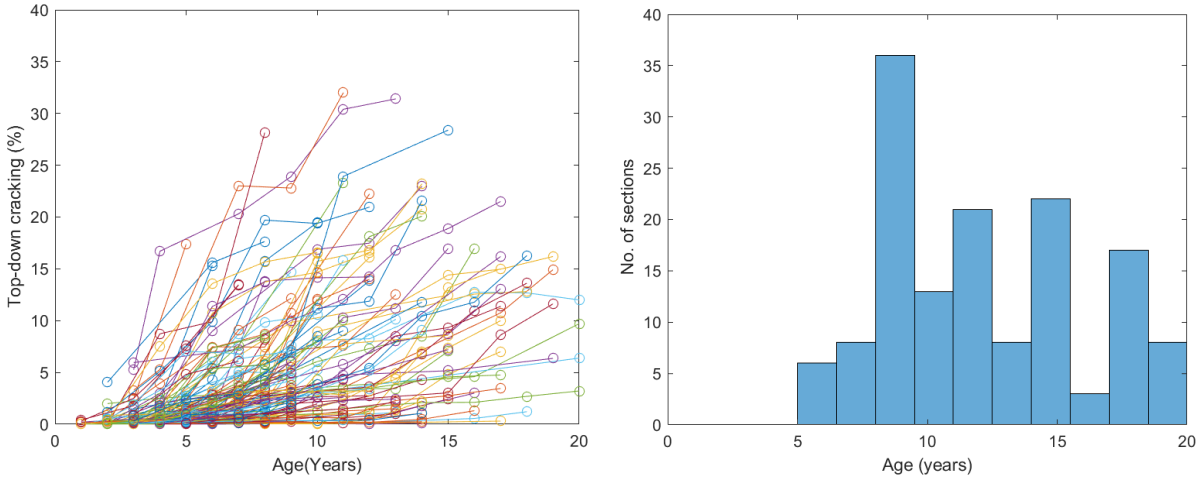

(a) Time series (b) Age distribution

Figure 3-25 Selected HMA rehabilitation sections — Top-down cracking

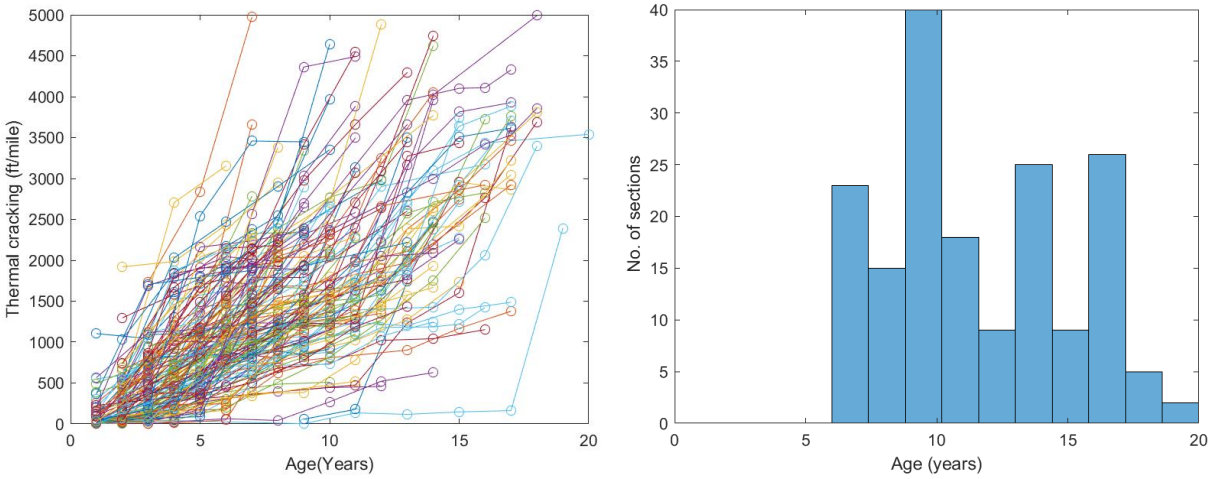

(a) Time series (b) Age distribution

Figure 3-26 Selected HMA rehabilitation sections — Transverse (thermal) cracking

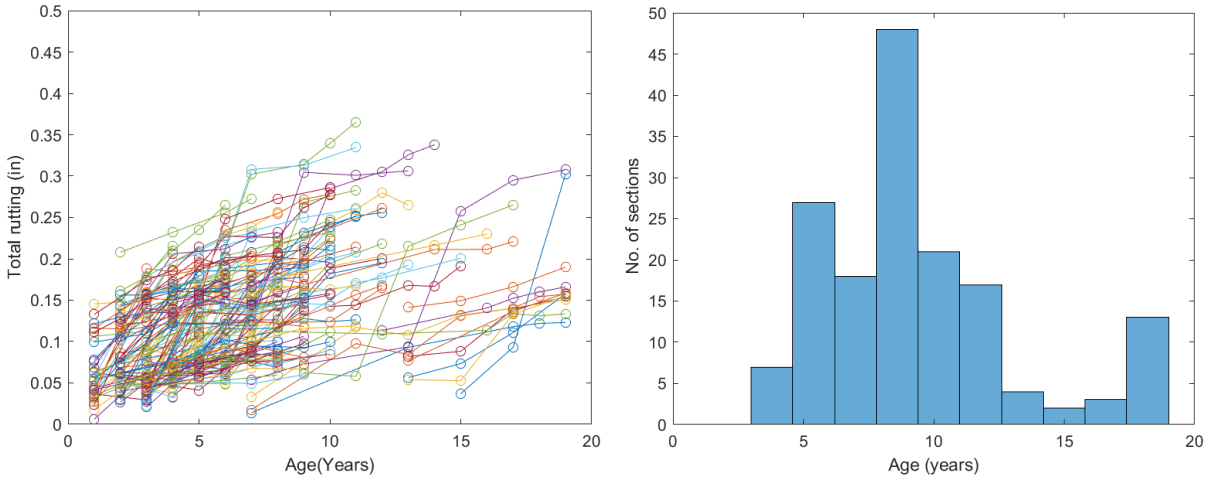

(a) Time series (b) Age distribution

Figure 3-27 Selected HMA rehabilitation sections — Total rutting

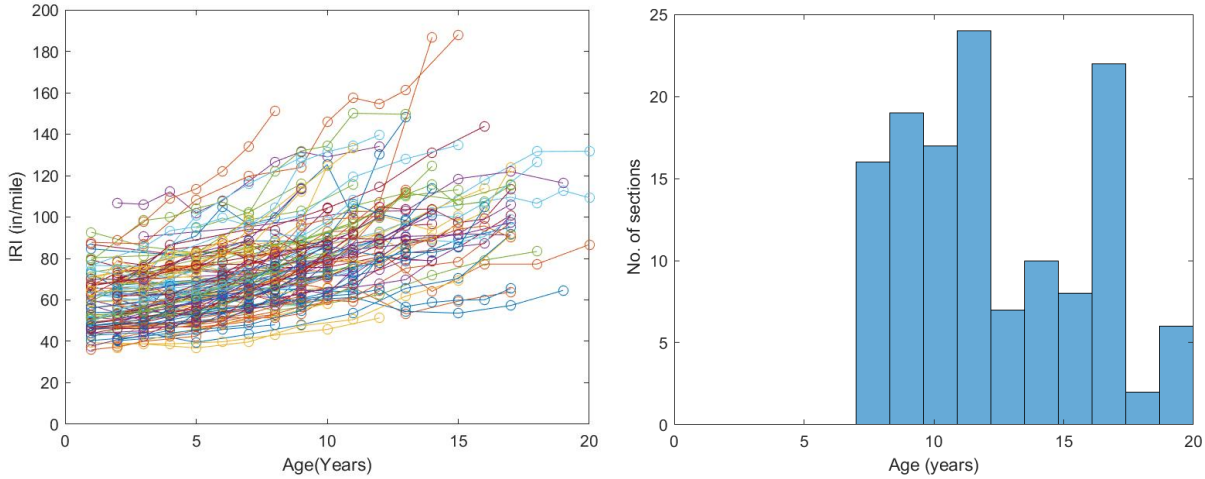

(a) Time series (b) Age distribution

Figure 3-28 Selected HMA rehabilitation sections — IRI

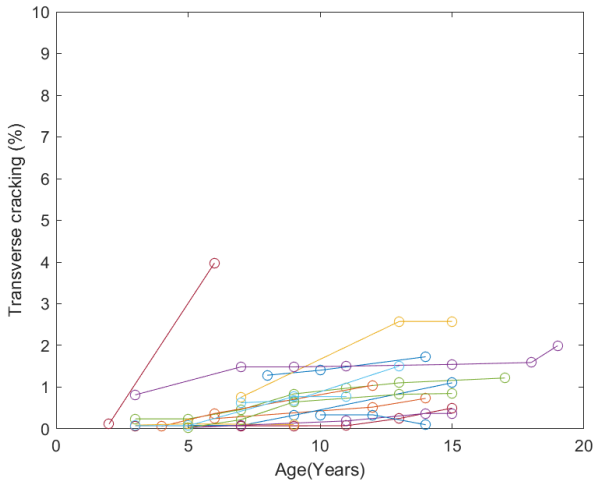

(a) Time series

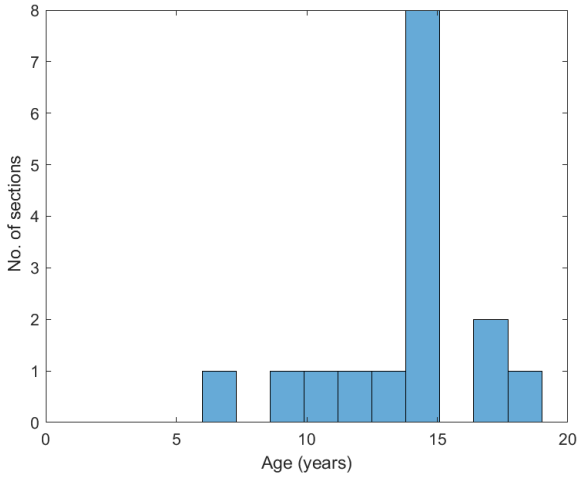

(b) Age distribution

Figure 3-29 Selected JPCP rehabilitation sections — Transverse cracking

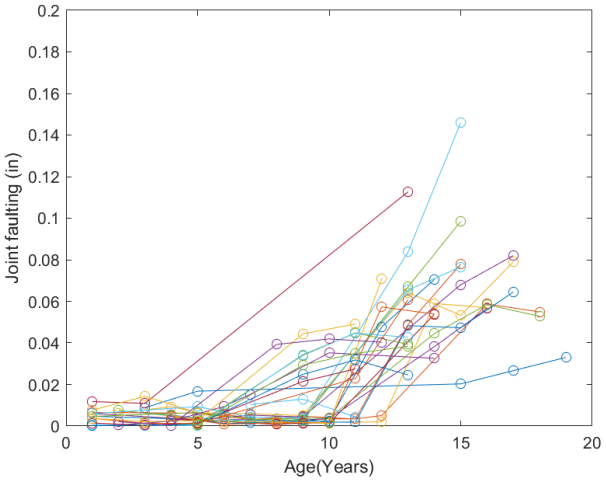

(a) Time series

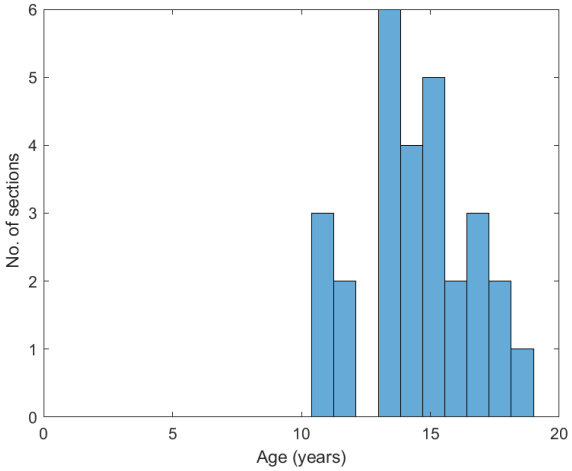

(b) Age distribution

Figure 3-30 Selected JPCP rehabilitation sections — Joint faulting

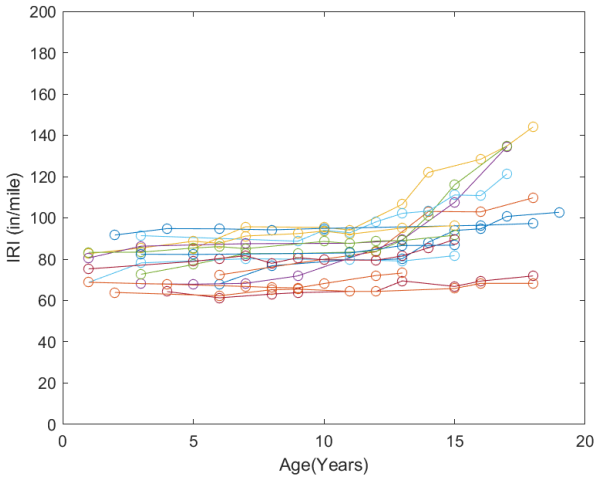

(a) Time series

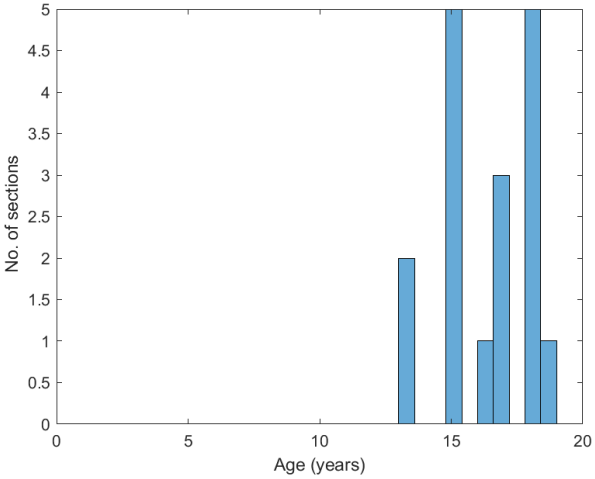

(b) Age distribution

Figure 3-31 Selected JPCP rehabilitation sections — IRI

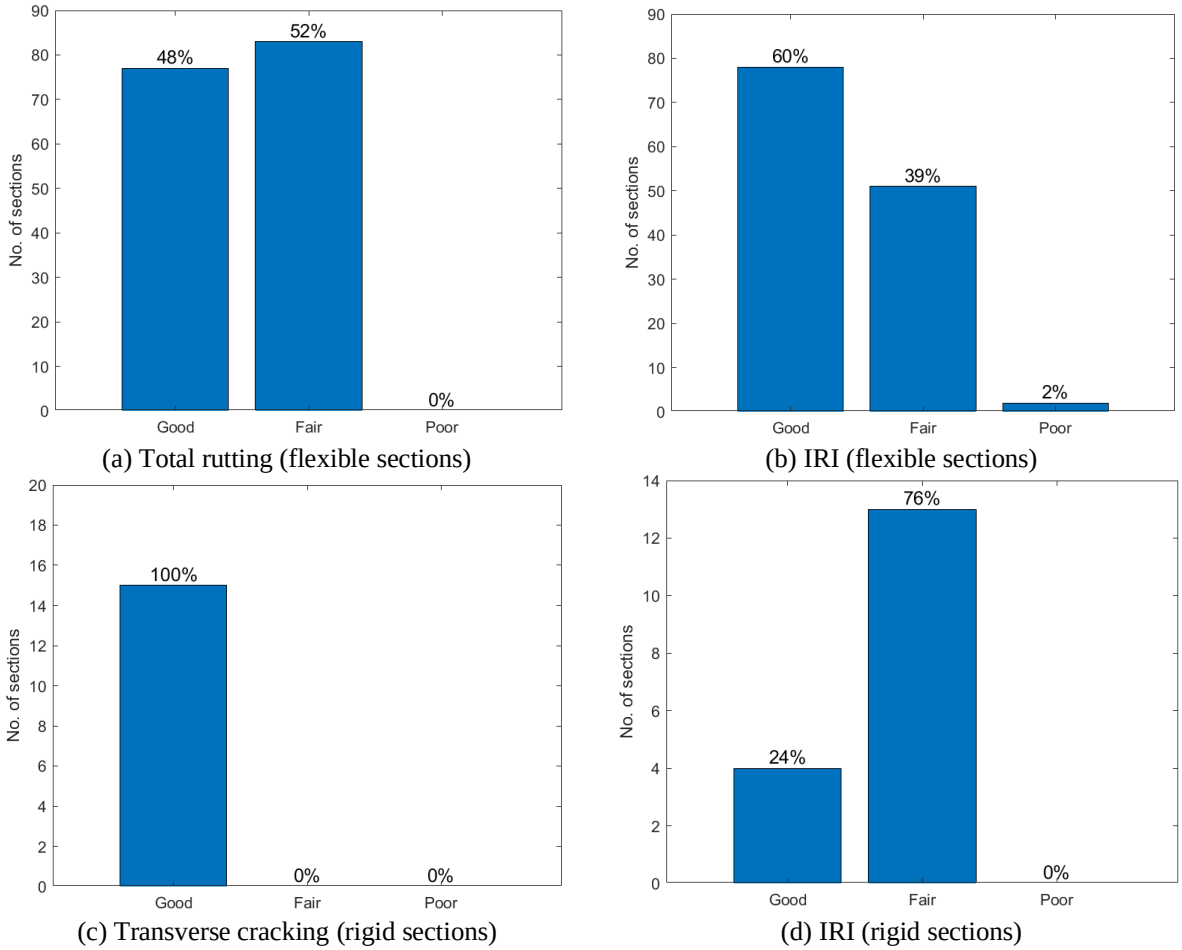

(a) Total rutting (flexible sections)

(b) IRI (flexible sections)

(c) Transverse cracking (rigid sections)

(d) IRI (rigid sections)

Figure 3-32 Category distribution for rehabilitation sections

b. The research team selected 163 HMA and 46 JPCP reconstruct pavement projects in Michigan.

   - *Flexible reconstruct performance data*: The magnitude and age distribution for the HMA reconstruct sections (also includes crush and shape and HMA over rubblized PCC) are shown in Figures 3-33 to 3-37. The following observations were made:

     - Bottom-up cracking: Bottom-up cracking magnitudes are usually low for most sections, with only a seven crossing the threshold of 20% with a maximum of almost 40%. The maximum age ranges from 4 to 20 years. Almost all of these sections fall in the good category, as shown in Figure 3-41.
     - Longitudinal/top-down cracking: Top-down cracking is observed more frequently than bottom-up cracking. More sections have observed top-down cracking compared to bottom-up cracking. The age at maximum distress ranged from 5 to 20 years.
     - Thermal cracking: Higher thermal cracking values are observed, ranging up to 4000 ft/mile. The design threshold used by MDOT is 1000 ft/mile. The age at

which the maximum thermal cracking is observed ranges from 5 to 19 years. Sections with performance grade (PG) binders have been used for thermal cracking calibration.

- Rutting: Selected sections do not exhibit significant rutting. All sections were below the threshold of 0.5 inches. The age distribution ranged from 3 to 19 years. Two third of the sections are in the fair performance category, as shown in Figure 3-41.
- IRI: The IRI time series is usually flat, with no sections exceeding the 172 in/mile threshold. The maximum observed IRI is 168.5 in/mile. The age at maximum IRI ranged from 5 to 20 years. It is worth noting that a cutoff value of the initial IRI less than or equal to 77 in/mile is selected for calibration of the IRI model. 74% of sections are in good, followed by 25% of sections in fair category. Only 1% of sections showed poor performance.

- *Rigid reconstruct performance data*: The magnitude and age distribution for the JPCP rehabilitation projects are shown in Figures 3-38 to 3-41. The following observations can be made from the figures:

  - Transverse cracking: A maximum transverse cracking value of 85% is observed, with 5 sections crossing the distress threshold of 15% slabs cracked. The age distribution ranges from 4 to 20 years. About 72% of these sections fall under the fair performance category.
  - Transverse joint faulting: A total of 10 sections exceeds the joint faulting threshold of 0.125 inches with a maximum value of 0.17 inches. The age distribution ranges from 8 to 20 years. These observed values for joint faulting have been cut off at 0.4 inches, where a 0.1-mile segment is above 0.4 inches.
  - IRI: A maximum IRI of 167 in/mile was observed. The age at maximum IRI ranges from 5 to 20 years. It is worth noting that a cutoff value for the initial IRI less than or equal to 82 in/mile is used to calibrate the IRI model. All sections fall under good and fair categories, with none exhibiting poor performance.

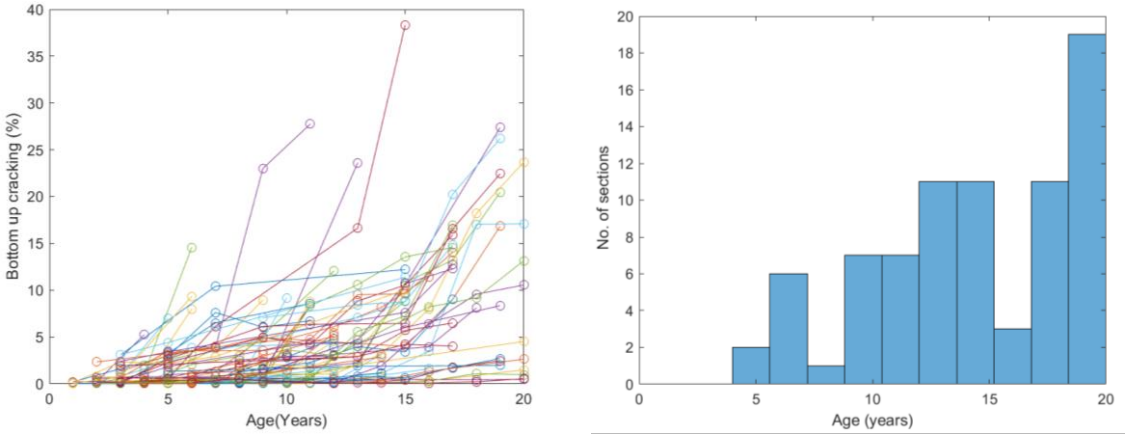

(a) Time series (b) Age distribution

Figure 3-33 Selected HMA reconstruct sections — Bottom-up cracking

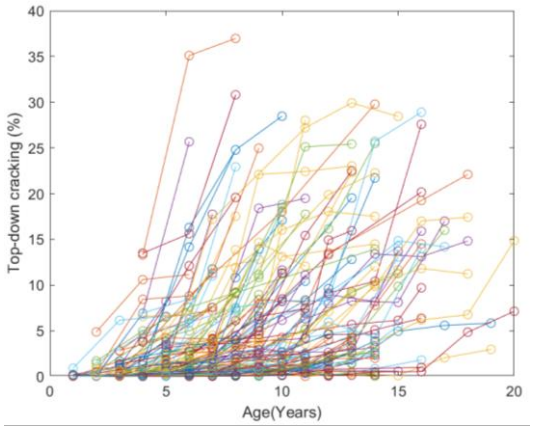

(a) Time series

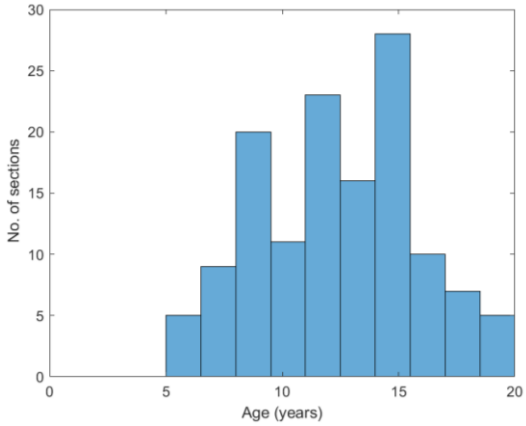

(b) Age distribution

Figure 3-34 Selected HMA reconstruct sections — Top-down cracking

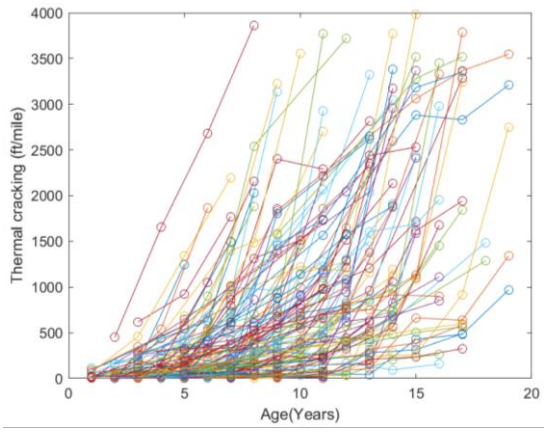

(a) Time series

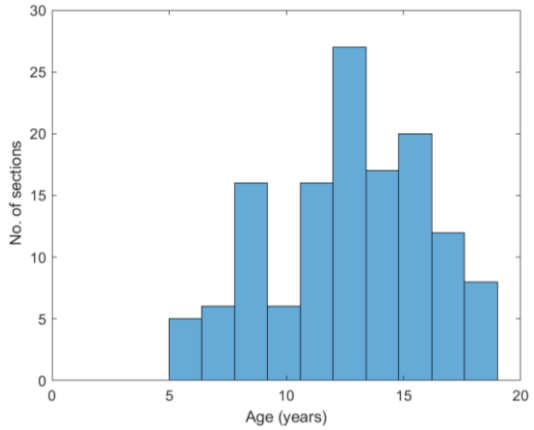

(b) Age distribution

Figure 3-35 Selected HMA reconstruct sections — Transverse (thermal) cracking

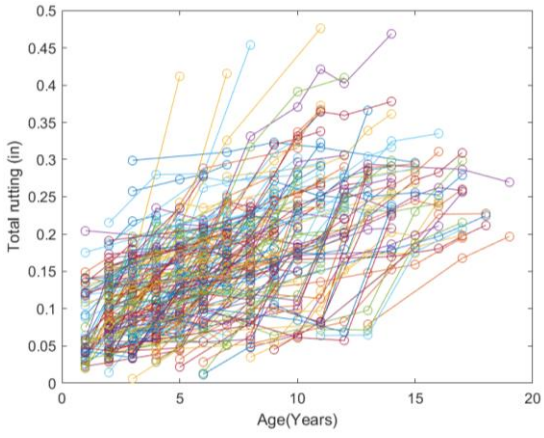

(a) Time series

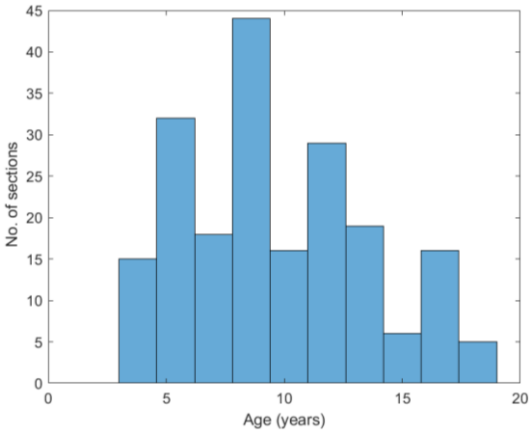

(b) Age distribution

Figure 3-36 Selected HMA reconstruct sections — Total rutting

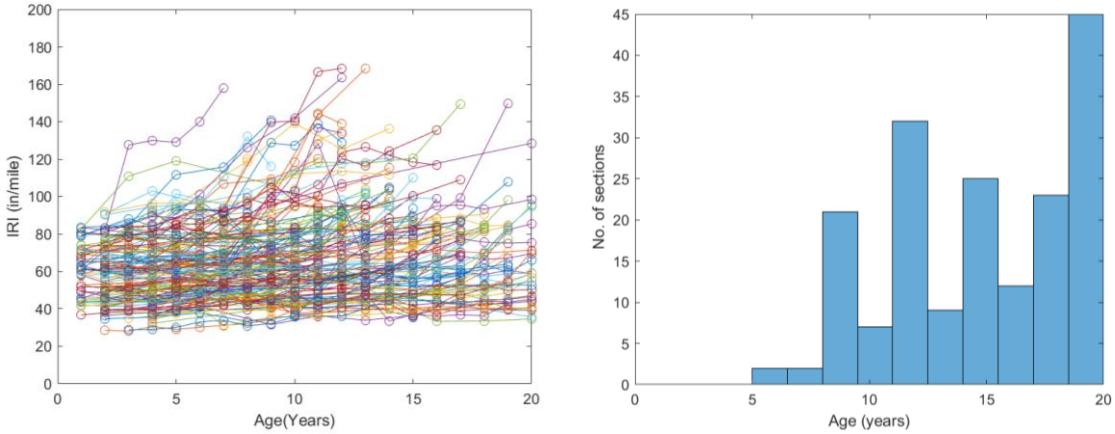

(a) Time series (b) Age distribution

Figure 3-37 Selected HMA reconstruct sections — IRI

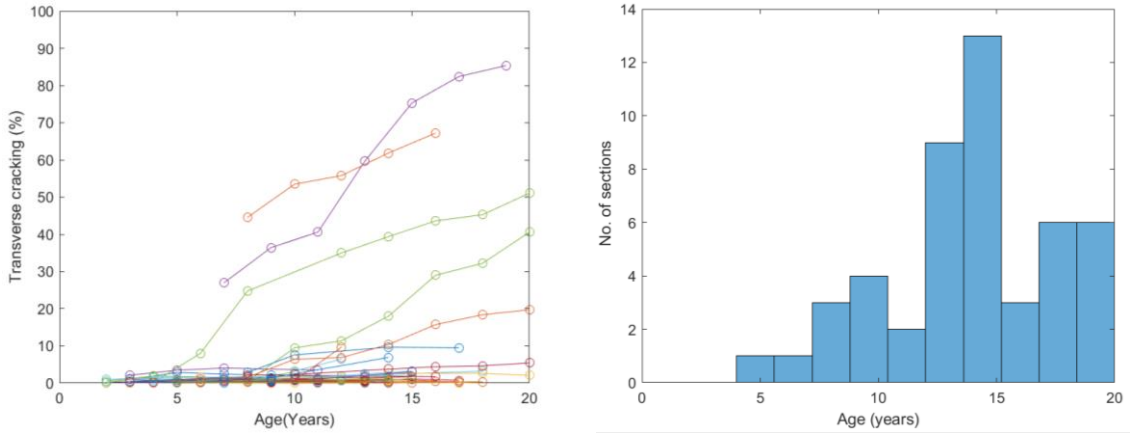

(a) Time series (b) Age distribution

Figure 3-38 Selected JPCP reconstruct sections — Transverse cracking

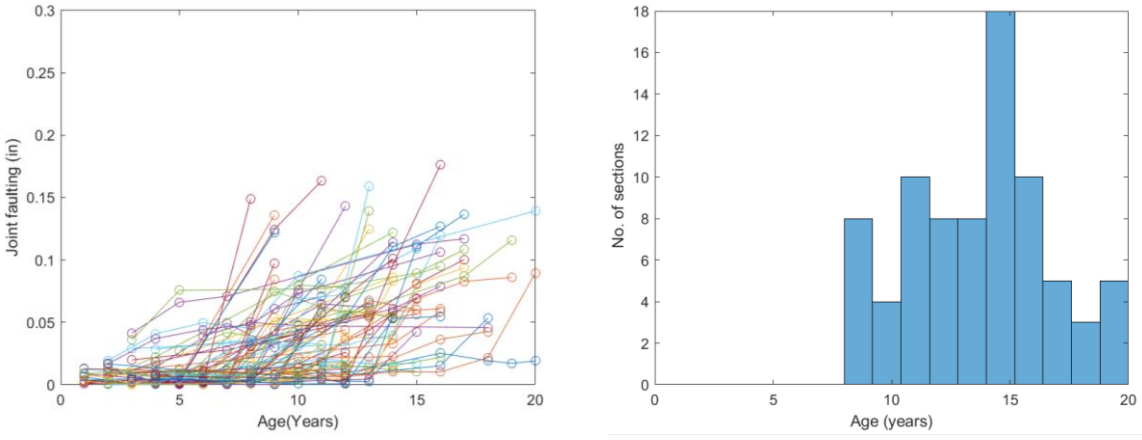

(a) Time series (b) Age distribution

Figure 3-39 Selected JPCP reconstruct sections — Joint faulting

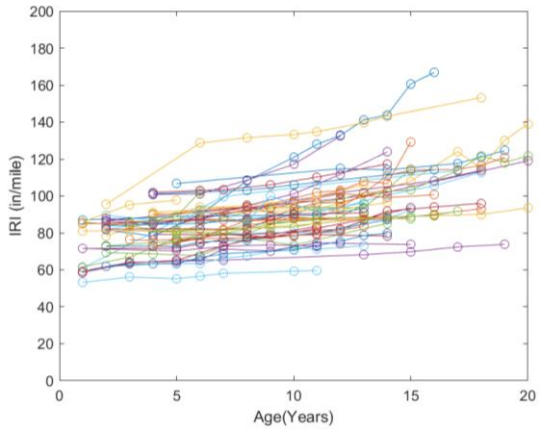

(a) Time series

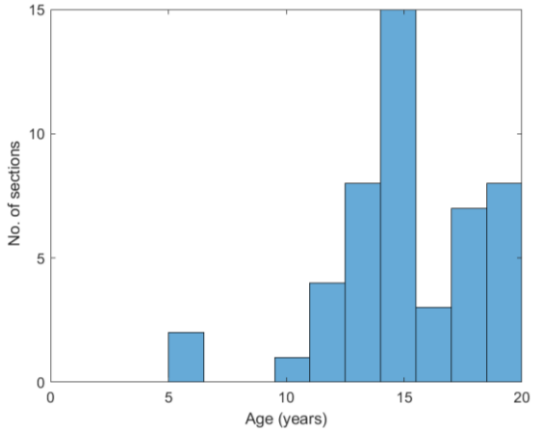

(b) Age distribution

Figure 3-40 Selected JPCP rehabilitation sections — IRI

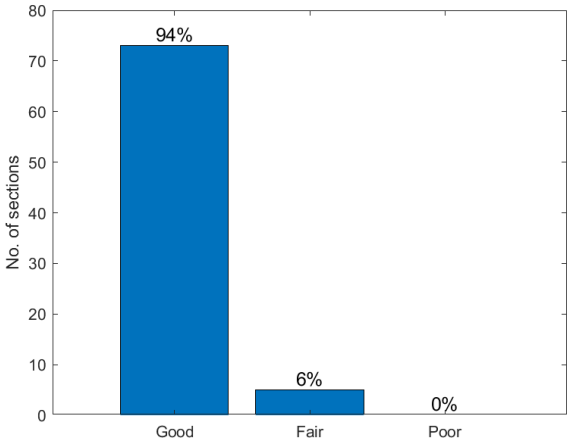

(a) Bottom-up cracking (flexible sections)

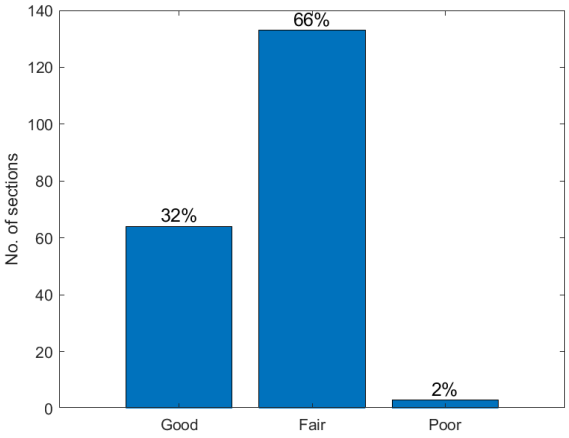

(b) Total rutting (flexible sections)

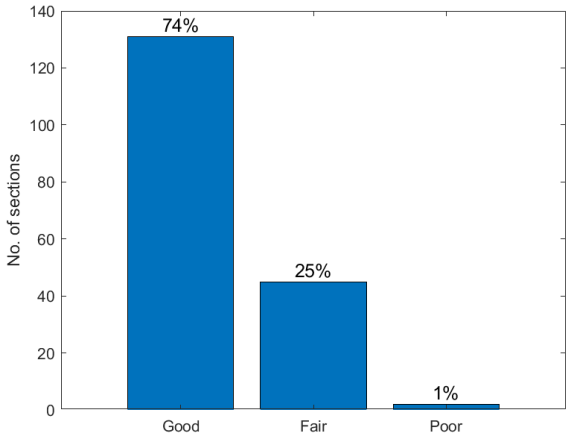

(c) IRI (flexible sections)

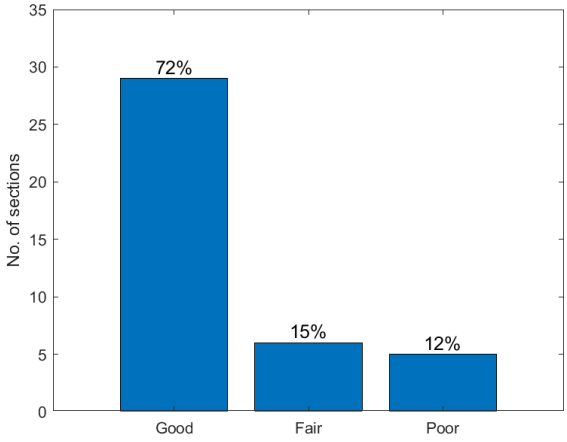

(d) Transverse cracking (rigid sections)

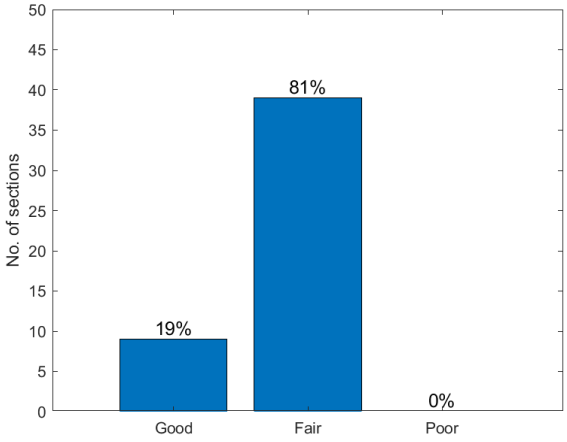

(e) IRI (rigid sections)

Figure 3-41 Category distribution for reconstruct sections

3.5 INPUT DATA EXTENT

Accurate pavement cross-sectional, traffic, climate, and material input data are essential for adequately characterizing as-constructed pavements since the information directly affects performance prediction accuracy in the Pavement-ME software. Due to the large number of inputs required to properly characterize a pavement in the Pavement-ME, input data collection can be time-consuming. Moreover, many of the critical input parameters have three levels of inputs within the hierarchical structure of the Pavement-ME. The process of collecting as-constructed input data, including the source of the data, how to address missing data, and the selection of input values, is thoroughly discussed in this section. The team used the best available input level for the selected pavement sections.

3.5.1 Pavement Cross-Section and Layer Inputs

The pavement cross-sectional information is necessary to characterize the layer thicknesses of the various layers. The cross-sectional information is obtained from the construction records. Typically, in the case of HMA pavements, the drawings provided the asphalt application rate of the HMA layers (dividing the application rate by 110), which was used to determine the HMA lift thicknesses in inches. For the sections used in the previous

calibration effort *(1)*, the team used the Pavement-ME inputs data sheet to extract design inputs. For the newly selected sections, the drawings (construction plans) were provided by MDOT. The thickness, mix type, traffic, and unbound layer information were included in these drawings. For HMA over HMA overlays and composite overlays, the thickness information related to the existing (underlying) pavement layer was not available for all sections. In that case, the most commonly used thicknesses were used as inputs to Pavement-ME. A summary of the design thicknesses for flexible and rigid reconstruct and rehabilitation selected pavement projects is shown in Tables 3-10 through 3-13.

Table 3-10 Average HMA reconstruct thicknesses

Pavement types	HMA top course thickness (in.)	HMA leveling course thickness (in.)	HMA base course thickness (in.)	Base thickness (in.)	Subbase thickness (in.)
Crush and Shape	1.6	1.9	2.0	7.5	20.5
Freeway	1.6	2.1	4.5	7.1	16.8
Non-freeway	1.5	2.1	3.2	6.6	16.4
Rubblized	1.6	2.0	3.0	3.8	11.1
Statewide Average	1.6	2.0	3.1	5.7	15.0

Table 3-11 Average HMA rehabilitation project thicknesses

Pavement types	Overlay thickness (in.)	Existing pavement thickness (in.)	Base thickness (in.)	Subbase thickness (in.)
Composite	3.6	8.9	5.0	12.4
HMA over HMA	3.5	4.3	6.9	16.0
Statewide Average	3.5	5.2	6.5	15.3

Table 3-12 JPCP reconstruct thickness ranges

Pavement type	Average PCC thickness (in.)	Average base thickness (in.)	Average subbase thickness (in.)
JPCP	11.4	6.9	12.1

Table 3-13 Unbonded PCC overlay thickness ranges

Pavement type	Average PCC thickness (in.)	Average existing PCC thickness (in.)	Average base thickness (in.)	Average subbase thickness (in.)	Average asphalt interlayer thickness (in.)
Unbonded overlay	6.9	9.1	3.7	12.2	1.0

3.5.2 Traffic Inputs

The traffic data is a critical input to the Pavement-ME. Level 2 traffic data was used for all sections. MDOT provided a spreadsheet with traffic distribution tables which was used to extract Pavement-ME inputs for traffic. These tables include:

- Vehicle class distribution
- Hourly distribution (only for rigid sections)
- Monthly adjustment factor

- Number of axles per truck
- Single axle load spectra
- Tandem axle load spectra
- Tridem axle load spectra
- Quad axle load spectra

The inputs (with input categories) required to obtain these tables are summarized in Table 3-14.

Table 3-14 Traffic inputs

Inputs	Categories
Percentage of vehicle class 9	• Less than 45 • 45 to 70 • Above 70
Region type	• Rural • Urban
COHS type	• National • Regional • Statewide
Number of lanes	• 2 • 3 • 4+

The number of lanes was identified from the plans. Wherever the number of lanes was unavailable, they were visually estimated utilizing Google Maps coordinates. The COHS (Corridors of Highest Significance) type was estimated using each project's PR number and beginning and ending milepost. The percentage of class 9 vehicles was estimated for each section using the MDOT Transportation Data Management System (TDMS) website from the following URL: https://mdot.public.ms2soft.com/tcds/tsearch.asp?loc=mdot. For sections where the traffic data was unavailable at the exact location, nearby locations in the same section were used. The range and average two-way AADTT values for all reconstruct and rehabilitation projects are summarized in Table 3-15 and 3-16, respectively.

Table 3-15 Ranges of AADTT for all reconstruct projects

Road Type	Min AADTT	Max AADTT	Average AADTT
Crush and Shape	60	1986	669
Rubblized	173	3707	1502
HMA Reconstruct Freeway	313	6745	2076
HMA Reconstruct Non-freeway	63	1600	431
JPCP Reconstruct	150	18297	7141
Statewide Average	134	6502	2381

Table 3-16 Ranges of AADTT for all rehabilitation projects

Pavement Type	Minimum AADTT	Maximum AADTT	Average AADTT
Composite	113	20876	2715
HMA over HMA	61	3780	722
Unbonded overlay	1458	6100	4473
Statewide average	262	7115	1588

3.5.3 As-constructed Material Inputs

The as-constructed material inputs were obtained from the construction records, JMFs, and other test records. Ideally, these inputs are to be recorded at the time of construction. These inputs range between project-specific and statewide average values. The details of material properties for each pavement structural layer are discussed in this section.

3.5.3.1. HMA layer inputs

All inputs were collected at the highest available hierarchy level; however, the needed data were not available for all pavement sections. In that case, the data was collected using other correlations/sources. Data collection for each HMA layer input is as follows:

- Dynamic modulus (E^*): E^* was obtained from the DYNAMOD software developed in a previous study *(4)*. E^* for the Superpave mixes was directly obtained from the database. For older mixes (marshal mixes), the volumetric, binder, and gradation information was used to predict the E^* using DYNAMOD's Artificial Neural Networks (ANNs). E^* was obtained at Level 1.
- Binder (G^*): G^* was also obtained from the DYNAMOD database using the region and binder information. G^* was obtained at Level 1.
- Creep compliance (D(t)): D(t) was obtained from the DYNAMOD database. D(t) was obtained at Level 1 for Performance grade (PG) sections and Level 3 for other sections.
- Indirect tensile strength (IDT): IDT was obtained from the DYNAMOD database at Level 2 for Performance grade (PG) sections and Level 3 for other sections.
- AC layer thickness: These were obtained from construction records. Usually, the application rate in lbs/yards^2 is available, which can be utilized to obtain the layer thickness, as previously mentioned.
- Air voids and binder content: As constructed, air voids and binder content were obtained from construction records. Table 3-17 summarizes the average as-constructed air voids for different pavement types. Historical test records were utilized for unavailable data to obtain an average value based on mix type, as shown in Table 3-19.
- Aggregate gradation: Gradation was obtained from JMFs. Tables 3-18 summarize the average gradation for the top, leveling, and base layers, respectively, for different pavement types. For unavailable data, historical test records were utilized to obtain an average value based on mix type, as shown in Table 3-19.

It is important to note that Level 1 G^* and Level 2 IDT data were used for the calibration of the thermal cracking model.

Table 3-17 As-constructed percent air voids for HMA layers

HMA layer	Road Type	Average as-constructed air voids
Top course	Crush and Shape	6.1
	Rubblized	6.8
	HMA Reconstruct Freeway	6.6
	HMA Reconstruct Non-freeway	6.8
	HMA over HMA	6.2
	Composite	6.1
Leveling course	Crush and Shape	6.2
	Rubblized	6.4
	HMA Reconstruct Freeway	6.7
	HMA Reconstruct Non-freeway	6.7
	HMA over HMA	6.2
Base course	Crush and Shape	5.8
	Rubblized	5.8
	HMA Reconstruct Freeway	6.4
	HMA Reconstruct Non-freeway	6.8

Table 3-18 HMA layer average aggregate gradation

HMA layer	Road type	Effective AC binder content	Percent passing sieve size			
			3/4	3/8	#4	#200
Top course	Crush and Shape	11.5	100.0	89.7	68.4	5.2
	Rubblized	11.9	99.4	89.8	67.3	5.9
	HMA Reconstruct Freeway	11.2	100.0	92.4	67.4	5.2
	HMA Reconstruct Non-freeway	11.1	100.0	94.6	71.4	5.3
	HMA over HMA	12.3	100.0	93.4	72.2	5.6
	Composite	12.5	100.0	94.4	72.1	5.6
Leveling course	Crush and Shape	10.6	100.0	81.8	61.1	5.0
	Rubblized	11.2	100.0	87.0	67.8	5.2
	HMA Reconstruct Freeway	10.1	99.8	81.3	63.3	4.8
	HMA Reconstruct Non-freeway	10.2	100.0	82.6	73.4	4.8
	HMA over HMA	11.3	100.0	84.9	64.0	5.2
Base course	Crush and Shape	10.8	99.6	77.9	60.3	4.6
	Rubblized	10.6	99.3	78.9	59.9	4.8
	HMA Reconstruct Freeway	9.4	95.8	72.9	51.6	4.9
	HMA Reconstruct Non-freeway	9.6	98.9	76.6	57.5	4.9

Table 3-19 MDOT recommended values volumetrics and gradation

Mix type	Air voids (%)	Effective binder content (%)	% Passing 3/4" Sieve	% Passing 3/8" Sieve	% Passing # 4Sieve	% Passing #200 Sieve
3E1	5.8	10.8	99.85	80.44	62.94	4.40
4E1	6.1	11.5	100.00	87.24	70.43	5.11
5E1	6	12.6	100.00	97.14	78.23	5.63
2E3	4.8	9.7	92.65	68.70	53.95	4.40
3E3	5.8	10.8	99.63	77.88	60.33	4.56
4E3	6.1	11.5	100.00	86.91	68.66	4.92
5E3	6	12.6	100.00	97.86	79.81	5.49
2E10	4.8	9.7	94.55	73.50	59.70	4.50
3E10	5.8	10.8	99.78	80.27	62.78	4.84
4E10	6.1	11.5	100.00	87.65	70.06	5.26
5E10	6	12.6	100.00	98.30	81.27	5.67
2E30	4.8	9.7	99.00	71.80	60.60	4.20
3E30	5.8	10.8	99.95	79.20	59.82	4.40
4E30	6.1	11.5	100.00	88.63	66.90	4.33
5E30	6	12.6	100.00	99.00	81.24	5.68

3.5.3.2. PCC material inputs

The Pavement-ME transverse cracking prediction model is very sensitive to concrete strength (compressive or flexural). The team obtained the PCC material-related inputs from material testing results. If these results were unavailable, typical MDOT values were used.

PCC strength:
MDOT collected the concrete core compressive strength (f'c) test data. These tests represent the concrete compressive strength close to the construction time for the selected pavement sections. These test values were used directly for each corresponding project. If compressive strength is unavailable, an average value of 5239 psi was used. This value was obtained from the sections with available values. The transverse cracking model in the Pavement-ME directly uses the modulus of rupture (MOR) to estimate the damage. The MOR values were estimated based on the ACI correlation between MOR and f'_c (used in the Pavement-ME), as shown by Equation (3-7). Figure 3-42 shows the f'_c and estimated MOR distributions. It should be noted that these cores' specific testing age was unavailable; however, all cores were tested after or at least 28 days. The Pavement-ME internally calculates the relationship between f'_c and MOR.

$$MOR = 9.5 \times \sqrt{f_c'} \quad (3\text{-}7)$$

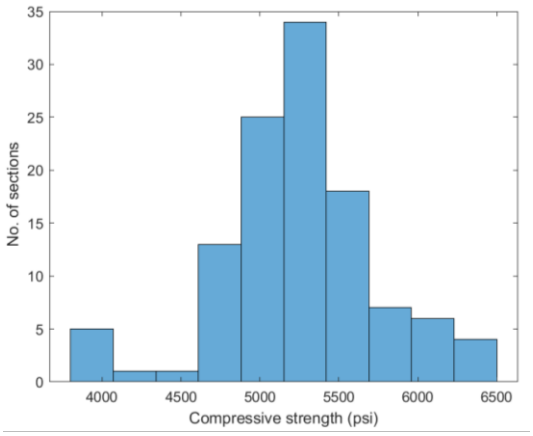

(a) Compressive strength (f'_c)

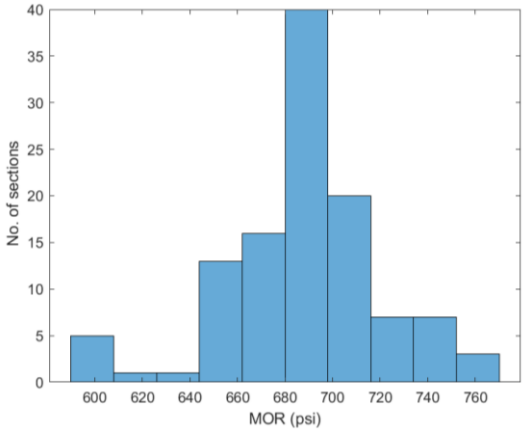

(b) Modulus of rupture (MOR)

Figure 3-42 Distribution of concrete strength properties

Coefficient of thermal expansion:

The CTE input values were obtained from the MDOT recommended values *(5)*. A value of 4.4 in/in/°F×10^{-6} was used for Bay, Grand, North, Southwest, and Superior regions, whereas 5.0 in/in/°F×10^{-6} was used for Metro and University regions.

3.5.3.3. Aggregate base/subbase and subgrade input values

The aggregate base/subbase and subgrade input values were obtained from the following sources:

- Backcalculation of unbound granular layer moduli *(6)*
- Pavement subgrade MR design values for Michigan's seasonal changes *(7)*

The resilient modulus (MR) values for the base and subbase material were selected based on the results from previous MDOT studies*(6, 7)*. The typical backcalculated values for base and subbase MR is 33,000 psi and 20,000 psi, respectively. It is worth noting that crushed and shaped and rubblized sections have been modeled as new flexible pavements. The existing layer has been modeled as a dense aggregate base with an MR of 125,000 psi for crush and shape and 70,000 for rubblized sections. These values were assumed for all projects since in-situ MR values were not available. For base/subbase layers, the software default to "Modify input values by temperature/moisture" was selected. The subgrade material type and resilient modulus were selected based on the Subgrade MR study *(6, 7)*. The study outlined the location of specific soil types and their MR values across the entire State. Annual representative values for subgrade MR were used in Pavement-ME. The recommended design MR value corresponding to the soil type is shown in Table 3-20.

Table 3-20 Average roadbed soil MR values

Roadbed Type		Average MR		
USCS	AASHTO	Laboratory-determined (psi)	Back-calculated (psi)	Recommended design MR value (psi)
SM	A-2-4, A-4	17,028	24,764	5,200
SP1	A-1-a, A-3	28,942	27,739	7,000
SP2	A-1-b, A-3	25,685	25,113	6,500
SP-SM	A-1-b,A-2-4, A-3	21,147	20,400	7,000
SC-SM	A-2-4, A-4	23,258	20,314	5,000
SC	A-2-6, A-6,A-7-6	18,756	21,647	4,400
CL	A-4, A-6, A-7-6	37,225	15,176	4,400
ML	A-4	24,578	15,976	4,400
SC/CL/ML	A-2-6, A-4, A-6, A-7-6	26,853	17,600	4,400

3.5.4 Climatic Inputs

The Enhanced Integrated Climatic Model (EICM) in Pavement-ME requires hourly climatic data. This data includes air temperature, precipitation, relative humidity, percent sunshine, and wind speed. A statistical comparison between Modern-Era Retrospective Analysis for Research and Applications (MERRA) and North American Regional Reanalysis (NARR) data was performed to identify the most suitable climatic data for calibration. Both MERRA and NARR data files used include climatic information for different periods. For that purpose, a common temporal overlap of 13 years was identified for which continuous hourly data is available for all climatic files from September 2000 to September 2013. The MERRA stations falling in the lake region were removed from the database. Moreover, for each NARR station, the four closest MERRA stations were identified, and the weighted average (proportional to the distance) for all four stations based on their distances was used for comparison. A total of 29 NARR stations and the four closest corresponding MERRA stations to each have been compared. Table 3-21 shows the SEE, bias, and correlation coefficient (R) between MERRA and NARR for hourly, daily, and monthly data *(8)*.

MDOT has been using default Pavement-ME climate data along with ground-based climate automated surface observation systems (ASOS) data. This data was reviewed for errors/anomalies and was improved in MDOT's previous study *(2)*. The following observations were made based on the comparison and previous study *(2, 8)*:

- MERRA and NARR climatic data are comparable for air temperature followed by humidity and wind speed. Percent sunshine showed a low correlation, and precipitation data is significantly different (i.e., a very low correlation) among all climatic inputs.
- The predicted pavement performance using MERRA-2 and NARR climatic data showed good agreement except for thermal cracking in flexible pavement and transverse cracking in rigid pavements. These differences are expected mainly because of sunshine data.

- MERRA has anomalies in humidity data. Several humidity values were erroneously higher than 100.
- MERRA appeared to be incorrectly estimating precipitation. Specifically, the number of wet days was extremely high such that the data review showed wet event days in the data on actual dry days. The ground-based stations are more closely aligned with actual wet event days. Furthermore, it was unclear why the percent sunshine was significantly different.

Table 3-21 Descriptive statistics for MERRA and NARR data comparison

Climatic input	Descriptive statistics	Hourly			Daily			Monthly		
		SEE	Bias	R	SEE	Bias	R	SEE	Bias	R
Humidity	Mean	12.784	4.437	0.764	9.582	4.437	0.705	7.387	4.437	0.538
	Std. Dev.	0.726	2.230	0.035	1.014	2.230	0.055	1.283	2.230	0.145
	COV	5.68%	50.27%	4.60%	10.58%	50.27%	7.86%	17.37%	50.27%	26.96%
Precipitation	Mean	0.049	0.002	0.062	0.009	0.002	0.610	0.002	0.002	0.678
	Std. Dev.	0.005	0.000	0.022	0.001	0.000	0.045	0.000	0.000	0.059
	COV	10.85%	15.22%	34.59%	7.90%	15.22%	7.33%	11.21%	15.22%	8.73%
Sunshine	Mean	44.614	-1.457	0.411	29.317	-1.457	0.570	11.847	-1.457	0.821
	Std. Dev.	3.908	6.809	0.071	2.777	6.809	0.079	1.788	6.809	0.033
	COV	8.76%	-467.39%	17.27%	9.47%	-467.39%	13.84%	15.09%	-467.39%	4.04%
Temperature	Mean	3.924	-0.771	0.982	2.710	-0.771	0.992	1.837	-0.771	0.997
	Std. Dev.	0.548	0.766	0.006	0.436	0.766	0.003	0.428	0.766	0.002
	COV	13.98%	-99.43%	0.58%	16.08%	-99.43%	0.31%	23.32%	-99.43%	0.20%
Wind speed	Mean	3.318	-0.165	0.752	2.031	-0.165	0.863	1.470	-0.165	0.848
	Std. Dev.	0.946	1.700	0.100	1.097	1.700	0.105	1.145	1.700	0.145
	COV	28.52%	-1029.25%	13.25%	54.00%	-1029.25%	12.16%	77.92%	-1029.25%	17.10%

Note: $SSE = \sqrt{\frac{\sum (MERRA - NARR)^2}{n-2}}$; $Bias = \frac{\sum (MERRA - NARR)}{n}$

In the previous study, additional weather stations were added to improve the climate coverage using ASOS and the Michigan Road Weather Information System (RWIS) as potential data sources *(2)*. Moreover, additional years of climatic data were added from February 2006 to December 2014 to enhance the data. Since the predicted performance did not show significant differences and the NARR data was improved for Michigan climate, the improved MDOT NARR climatic files were used for climatic inputs for both flexible and rigid pavements. The files were downloaded as *.hcd files, which can be read directly in Pavement-ME. The closest weather station to each selected project was used. For rigid sections, these files were directly used (since these are default files in the Pavement-ME), and for flexible sections, custom stations were formed using these files. Table 3-22 summarizes the climatic files used for calibration.

Table 3-22 Michigan climate station information

HCD filename	City/Location	Climate identifier	Latitude	Longitude
4847	Adrian	Adrian Lenawee County Arpt	41.868	-84.079
94849	Alpena	Alpena Co Rgnl Airport	45.072	-83.581
94889	Ann Arbor	Ann Arbor Municipal Arpt	42.224	-83.74
14815	Battle Creek	W K Kellogg Airport	42.308	-85.251
94871	Benton Harbor	Sw Michigan Regional Arpt	42.129	-86.422
14822	Detroit	Detroit City Airport	42.409	-83.01
94847	Detroit	Detroit Metro Wayne Co Apt	42.215	-83.349
14853	Detroit	Willow Run Airport	42.237	-83.526
14826	Flint	Bishop International Arpt	42.967	-83.749
4854	Gaylord	Otsego County Airport	45.013	-84.701
94860	Grand Rapids	Gerald R Ford Intl Airport	42.882	-85.523
14858	Hancock	Houghton County Memo Arpt	47.169	-88.506
4839	Holland	Tulip City Airport	42.746	-86.097
94814	Houghton Lake	Roscommon County Airport	44.368	-84.691
94893	Iron Mountain/Kingsford	Ford Airport	45.818	-88.114
14833	Jackson	Jakson Co-Rynolds Fld Arpt	42.26	-84.459
94815	Kalamazoo	Klmazo/Btl Creek Intl Arpt	42.235	-85.552
14836	Lansing	Capital City Airport	42.78	-84.579
14840	Muskegon	Muskegon County Airport	43.171	-86.237
14841	Pellston	Pton Rgl Ap Of Emmet Co Ap	45.571	-84.796
94817	Pontiac	Oakland Co. Intnl Airport	42.665	-83.418
14845	Saginaw	Mbs International Airport	43.533	-84.08
14847	Sault Ste Marie	Su Ste Mre Muni/Sasn Fl Ap	46.467	-84.367
14850	Traverse City	Cherry Capital Airport	44.741	-85.583
AMN	Alma	Gratiot Community Airport	43.322	-84.688
BAX	Bad Axe	Huron County Memorial Airport	43.78	-82.985
CFS	Caro	Tuscola Area Airport	43.459	-83.445
ERY	Newberry	Luce County Airport	46.311	-85.4572
ESC	Escanaba	Delta County Airport	45.723	-87.094
FKS	Frankfort	Frankfort Dow Memorial Field Airport	44.625	-86.201
IRS	Sturgis	Kirsch Municipal Airport	41.813	-85.439
ISQ	Manistique	Schoolcraft County Airport	45.975	-86.172
IWD	Ironwood	Gogebic Iron County Airport	46.527	-90.131
LDM	Ludington	Mason County Airport	43.962	-86.408
MOP	Mount Pleasant	Mount Pleasant Municipal Airport	43.622	-84.737
OSC	Oscoda	Oscoda Wurtsmith Airport	44.452	-83.394
PHN	Port Huron	Saint Clair County Intnl Airport	42.911	-82.529
RQB	Big Rapids	Roben Hood Airport	43.723	-85.504
SAW	Gwinn	Sawyer International Airport	46.354	-87.39

3.6 ESTIMATION OF INITIAL IRI

Initial IRI is an essential input for IRI prediction and pavement design. Initial IRI is the IRI value just after construction. Measured IRI at zero year can be used as initial IRI, but it poses the following challenges:

- The exact date of construction and IRI measurement at zero year is unknown (the exact year is known, but not the day and month). Therefore, the recorded IRI for the same year may be before or after construction.
- The IRI for the construction year is not available for all sections.

The following five approaches were used to estimate initial IRI:

- Selecting the IRI at year zero (if available)
- Linear backcasting IRI based on the measured data for the first ten years
- Linear backcasting IRI based on the measured information for all available years
- Reducing the first measured IRI (after construction) by 5 inches per mile/year up to a zero year
- Reducing the first measured IRI (after construction) by 5 inches per mile /year if greater than 100; by 4 inches per mile /year if between 70 and 100; by 3 inches per mile /year if less than 70 up to a zero year

Based on the above five approaches, the number of sections available and initial IRI caps were selected for the initial IRI for each pavement type. A cap on the initial IRI means that sections with an initial IRI greater than the cap were not included for IRI calibration. The initial IRI cap values were selected as per MDOT construction standards and potential tenth mile variability. A cap of 82 in/mile was selected for rigid sections. A cap of 77 in/mile was selected for new or reconstruct, crush and shape, and bituminous overlay on rubblized concrete for flexible sections, whereas a cap of 82 in/mile was selected for multicourse bituminous and composite overlays. The details of the initial IRI estimation can be found in Appendix-A.

3.7 JOINT SPALLING IN RIGID PAVEMENTS

Joint spalling is the rupture of concrete slabs near the edge of joints. It may result from excessive compressive stresses due to high traffic, infiltration of incompressible materials, infiltrated water under freezing and thawing cycles, etc. Spalling is used in Pavement-ME for the calculation of IRI. The Pavement-ME uses an empirical model to calculate spalling for joints with medium and high severities. According to the MDOT PMS-associated distress (AD) matrix, four possible options were identified to quantify medium and high severity levels for measured joint spalling. The team analyzed joint spalling data with the following goals:

- To estimate the most suitable AD matrix to categorize measured spalling.
- To analyze the applicability of measured spalling (using the most suitable AD matrix) for IRI model calibration.

The most suitable AD matrix was selected based on the contribution of each AD matrix cell on the spalling and the callouts of each cell in the PMS database. Table 3-23 shows the recommended AD matrix for spalling calculation per those highlighted in yellow or orange. The yellow cells are the medium severity, and the orange cells are high severity spalling.

Table 3-23 Recommended matrix for spalling calculation

ASSOCIATED DISTRESS MATRIX (AD1,AD2): AD_{12} 0001 x 0011					
TRANSVERSE LENGTH Across Lane (AD1)	**MAX WIDTH (Perpendicular to Transverse Joint) (AD2)**				
	No Distress	**>0 - 1 ft.**	**>1 - 3 ft.**	**>3 - 6 ft.**	**>6 - 8 ft.**
No Distress	*(1,1)*	*xxxxx*	*xxxxx*	*xxxxx*	*xxxxx*
>0 - 1 ft.	*xxxxx*	(2,2)	(2,3)	(2,4)	(2,5)
>1 - 3 ft.	*xxxxx*	(3,2)	(3,3)	(3,4)	(3,5)
>3 - 6 ft.	*xxxxx*	(4,2)	(4,3)	(4,4)	(4,5)
>6 - 12 ft.	*xxxxx*	(5,2)	(5,3)	(5,4)	(5,5)
Note that cells marked with xxxxx are not applicable.					

Measured and predicted spalling (from Pavement-ME) were used to calibrate the IRI model. However, no significant differences were found in the model coefficients. Moreover, measured spalling cannot be incorporated into the IRI model within Pavement-ME. Therefore, the calibration based on measured spalling was not used for local calibration. The detailed analysis results for spalling are shown in Appendix-A.

3.8 SUMMARY

The steps to data collection, project selection, and obtaining the Pavement-ME inputs have been outlined in this chapter. Details about each input, source, and possible estimates in case of unavailable data have also been discussed. The number of projects for each performance type and pavement type has also been summarized. Table 3-24 summarizes the inputs and corresponding levels for traffic, climate, and material characterization data used for the local calibration.

Table 3-24 Summary of input levels and data source

Input			Pavement-ME input level	Data source level	Input source
Traffic	Vehicle class distribution		1	2	MDOT specified traffic per cluster data
	Hourly distribution		1	2	
	Monthly adjustment factor		1	2	
	Number of axles per truck		1	2	
	Single, tandem, tridem, and quad axle load distribution		1	2	
	AADTT		1	1	From design drawings
	Vehicle class 9 percentage		1	1	MDOT TDMS website
Cross-section layers (new and existing)	HMA thickness		1	1	Project-specific HMA thicknesses based on design drawings
	PCC thickness		1	1	Project-specific PCC thicknesses based on design drawings
	Base thickness		1	1	Project specific base thicknesses based on design drawings
	Subbase thickness		1	1	Project-specific subbase thicknesses based on design drawings
Layer materials	HMA	Mix properties	1	Mix of 2 and 3	MDOT HMA mixture characterization study (DYNAMOD database)
		HMA mixture aggregate gradation	1	1 or 3	Project-specific mixture gradation data obtained from data collection or average statewide values
		Binder properties	1	3	MDOT HMA mixture characterization study (DYNAMOD database)
	PCC	Strength (f'_c, MOR)	3	1 or 3	Project specific testing values or average statewide value
		CTE	1	2	MDOT recommended values
	Base/ subbase	MR	3	3	Recommendations from MDOT unbound material study
	Subgrade	MR	3	3	Soil-specific MR values per MDOT subgrade soil study
		Soil properties	Mix of all levels	3	Location-based soil type per MDOT subgrade soil study
Climate			1	1	Closest available climate station

Note:
Data source Level 1 is project-specific data
Data source Level 2 inputs are based on regional averages in Michigan
Data source Level 3 inputs are based on statewide averages in Michigan

CHAPTER 4 - LOCAL CALIBRATION PROCEDURES

4.1 INTRODUCTION

The MEPDG was developed under the NCHRP project 1-37A *(1)* to overcome the limitations of the AASHTO 1993 method *(2)*. It is an advanced pavement design tool for new and rehabilitated pavements. MEPDG incorporates material properties, traffic, and climate to estimate the incremental damage using mechanical responses of the pavement. The cumulative damage is empirically used to predict the field distresses using transfer functions. The transfer functions used in Pavement-ME have been calibrated using the Long-term Pavement Performance (LTPP) pavement sections at the national level *(3)*. Although the nationally calibrated models provide a fair performance prediction for the entire US road network, these may not represent the construction practices, materials, and climatic conditions of a particular state/region. Therefore, nationally calibrated models may underpredict or overpredict the pavement performance in specific state/region. Recalibration of these models has been recommended for local conditions in the local calibration guide *(4)*. Several studies have been conducted to locally recalibrate the transfer function coefficients for new and reconstructed rigid pavement sections. The critical performance distress in the Pavement-ME includes transverse cracking (percentage of slabs cracked), transverse joint faulting (inches), and international roughness index (IRI in inches/mile) for rigid pavements. For flexible pavements, the critical distress include bottom-up cracking (percentage), top-down cracking (percentage), rutting (inches), thermal (transverse) cracking (feet/mile), reflective cracking (feet/mile), and IRI (inches/mile). This chapter briefly highlights the calibration methods, approaches for each model, and the concept of reliability.

4.2 CALIBRATION APPROACHES

Local calibration of the Pavement-ME models aims to optimize the model coefficients to minimize bias and standard error. The aim is achieved by matching the predicted and measured distress. Bias in the predictions signifies if there is a systematic over- or under-prediction, whereas standard error shows the scatter and variability. Figure 4-1 shows a representation of bias and standard error. Genetic Algorithm (GA) has been used to optimize transfer function coefficients using MATLAB program. GA is an evolutionary optimization technique that can converge towards a global minimum solution even with local minima. GA involves the following operations:

- Initialization: GA generates solutions by randomly selecting a subset inside the allowed search space called the population.
- Selection: The generated solutions are selected based on the value of the objective function.
- Generation of offspring: New solutions are created using the selected solutions or populations (offspring) based on mainly two processes: mutation and crossover.
- Termination: This process continues till the termination criteria for the given population or the number of generations is reached.

The empirical transfer functions can be of two types: (a) model that directly calculates the magnitude of surface distress, and (b) model that calculates the cumulative damage index rather than actual distress magnitude. Based on the model, two different calibration approaches have been followed (as shown in Table 4-1):

Approach 1: For specific models (e.g., fatigue cracking, rutting, transverse cracking, and IRI), damage is directly obtained from Pavement-ME outputs. The transfer functions predict distress from the damage and have been calibrated using the MATLAB program outside the Pavement-ME. Different resampling techniques have been used to calibrate these functions.

Approach 2: The Calibration Assistance Tool (CAT) is used to calibrate the models (e.g., thermal cracking and joint faulting) where the damage is not obtained from Pavement-ME outputs. These models predict distress by calculating cumulative damage over time.

Table 4-1 summarizes the transfer functions and the approaches used to calibrate flexible and rigid pavements.

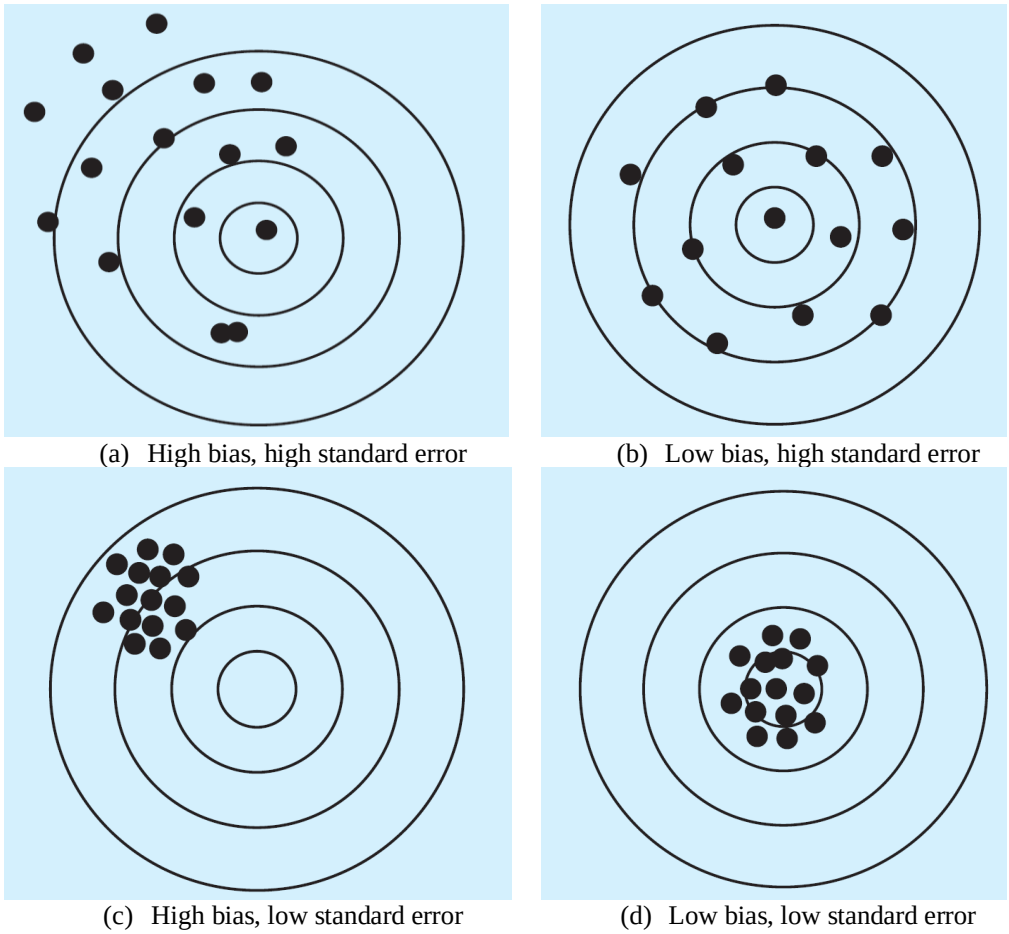

Figure 4-1 **Schematic representation of bias and standard error** ***(5)***

Table 4-1 Model transfer functions and calibration approaches

Pavement type	Performance prediction model		Approach I	Approach II	Model transfer functions
Flexible pavements	Fatigue cracking – bottom up		✓		$FC_{Bottom} = \left(\frac{1}{60}\right)\left(\frac{6000}{1+e^{C_1C_1^*+C_2C_2^*Log(DI_{Bottom}\bullet 100)}}\right)$
	Fatigue cracking – top down		✓		$t_0 = \frac{K_{L1}}{1+e^{K_{L2}\times 100\times(a_0/2A_0)+K_{L3}\times HT+K_{L4}\times LT+K_{L5}\times log_{10}\ AADTT}}$ $L(t) = L_{MAX}e^{-\left(\frac{C_1\rho}{t-C_3t_0}\right)^{C_2\beta}}$
	Rutting	HMA	✓	✓	$\Delta_{p(HMA)} = \varepsilon_{p(HMA)}h_{HMA} = \beta_{1r}k_z\varepsilon_{r(HMA)}10^{k_{1r}}n^{k_{2r}\beta_{2r}}T^{k_{3r}\beta_{3r}}$
		Base/subgrade	✓		$\Delta_{p(soil)} = \beta_{s1}k_{s1}\varepsilon_v h_{soil}\left(\frac{\varepsilon_o}{\varepsilon_r}\right)e^{-\left(\frac{\rho}{n}\right)^{\beta}}$
	Thermal cracking			✓	$A = 10^{k_t\beta_t(4.389-2.52Log(E_{HMA}\sigma_m\eta))}$
	IRI		✓		$IRI = IRI_o + C_1(RD) + C_2(FC_{Total}) + C_3(TC) + C_4(SF)$
Rigid pavements	Transverse cracking		✓		$CRK_{BU/TD} = \frac{100}{1+C_4(DI_F)^{C_5}}$ $TCRACK = (CRK_{Bottom-up} + CRK_{Top-down} - CRK_{Bottom-up}\cdot CRK_{Top-down})\cdot 100\%$
	Transverse joint faulting			✓	$Fault_m = \sum_{i=1}^{m}\Delta Fault_i$ $\Delta Fault_i = C_{34}\times(FAULTMAX_{i-1} - Fault_{i-1})^2\times DE_i$ $FAULTMAX_i = FAULTMAX_0 + C_7\times\sum_{j=1}^{m}DE_j\times Log(1+C_5\times 5.0^{EROD})^{C_6}$ $FAULTMAX_0 = C_{12}\times\delta_{curling}\times\left[Log(1+C_5\times 5.0^{EROD})\times Log(\frac{P_{200}\times WetDays}{p_s})\right]^{C_6}$ $C_{12} = C_1 + C_2\times FR^{0.25}$ $C_{34} = C_3 + C_4\times FR^{0.25}$
	IRI		✓		$IRI = IRI_I + C_1\times CRK + C_2\times SPALL + C_3\times TFAULT + C_4\times SF$

*Red font indicates calibration coefficients

4.3 CALIBRATION TECHNIQUES

This section discusses the various resampling techniques, optimization methods, and their advantages and limitations. Resampling techniques include (a) repeated split sampling, (b) bootstrapping, and (c) jackknifing. The optimization methods include (a) least squares and (b) maximum likelihood estimate (MLE). Both these methods have been used with resampling techniques to improve calibration results. These techniques and methods have been used within the approaches mentioned previously (Approach I and II) and are briefly discussed below.

4.3.1 Traditional Technique

The NCHRP Project 1-40B and local calibration guide provide recommended practices for local calibration of the Pavement-ME performance models. The traditional approach includes no resampling and is based on a random split into the calibration and validation subsets. The calibration-validation process depends on the number of selected sections, and as previously noted, two different calibration approaches (Approach I and II) may be needed depending on the distress predicted through the transfer function. Data collected from in-service pavements are used to establish calibration coefficients that minimize the overall standard error of the estimate between the predicted and measured distress. The validation process demonstrates that the calibrated model can produce accurate predictions for independent sections not used in the calibration. An efficient validation is determined by the bias in the predicted values and standard error of the estimate. Statistical hypothesis tests are used to determine if a significant difference exists between the calibrated model and the model validation.

4.3.2 Bootstrapping

Bootstrap resampling is a statistical technique widely used in many research fields, including statistics, economics, finance, and computer science. This method allows researchers to estimate a statistic's sampling distribution and construct confidence intervals for a population parameter, even when the underlying population distribution is unknown. The basic idea of bootstrap resampling is to draw many bootstrap samples from the original sample with replacement. Each bootstrap sample is a resampling of the original data with the same sample size but may contain some duplicate observations. The bootstrapped resampling can be performed using different methods: (a) resampling randomly or (b) resampling based on the residuals. The type of resampling approach for bootstrapping depends on the amount and type of data. The statistic of interest is calculated for each bootstrap sample, and the statistic distribution is estimated using the bootstrap sample statistics. The general steps involved in the bootstrap resampling method are as follows:

1. Draw a random sample of size *n* with a replacement from the original data set.
2. Calculate the statistic of interest for the sample. For calibration, this can be the estimation of calibration coefficients.
3. Repeat steps 1 and 2 for a number (B) of times to obtain B bootstrap samples. The team used 1000 bootstrap resamples for calibration.
4. Calculate the statistic's standard error and confidence interval using the bootstrap samples.

In practice, the number of bootstrap samples B is often large, such as 1,000 or 10,000, to ensure accurate estimates of the standard error and confidence interval. The standard error of a statistic estimated using bootstrap resampling can be calculated using Equation (4-1):

$$\mathrm{SE} = \sqrt{\frac{1}{B-1}\sum(\theta_b - \theta^*)^2} \tag{4-1}$$

where;
SE = estimated standard error of the statistic
B = number of bootstrap samples
θ_b = value of the statistic for the b_{th} bootstrap sample
θ^* = mean of the B bootstrap sample values.

The confidence interval for the statistic can be calculated using the percentile method, which involves ranking the B bootstrap sample values and taking the 2.5th and 97.5th percentiles as the lower and upper bounds of the confidence interval, as shown in Equation (4-2).

$$\mathrm{CI} = (\theta^* - \theta_{\frac{\alpha}{2}}, \theta^* + \theta_{\frac{\alpha}{2}}) \tag{4-2}$$

where;
CI = bootstrap confidence interval
θ^* = mean of the B bootstrap sample values
$\theta_{\frac{\alpha}{2}}$ = $\frac{\alpha}{2}$th percentile of the bootstrap sample values

Bootstrap resampling has several advantages over other statistical methods. First, it does not require population distribution or sample size assumptions. This is particularly useful when the sample size is small or the population distribution is unknown or not normally distributed. Second, it allows researchers to estimate the variability of a statistic and construct confidence intervals without resorting to complex mathematical formulas or asymptotic approximations. Third, it can be easily implemented using standard statistical software packages like R, Python, or SAS.

However, bootstrap resampling also has some limitations and potential pitfalls. First, it can be computationally intensive, especially when the number of bootstrap samples or the original sample size is large. Second, the bootstrap samples may not accurately reflect the true population distribution, especially if the original sample is biased or contains outliers. Third, the results may be sensitive to the choice of the statistic and the resampling method.

4.3.3 Jackknifing

Jackknifing is a statistical method used to estimate a statistic's bias and variance and make inferences about population parameters based on a sample of data. This method is similar to bootstrap resampling. Instead of creating multiple bootstrap samples, jackknifing involves leaving out one observation at a time from the original data set and calculating the statistic for each subsample. The basic idea of jackknifing is to divide the original data set into n subsamples, each of size *n*-1, by systematically leaving out one observation at a time. The general steps involved in the jackknife method are as follows:

- Divide the original data set into *n* subsamples, each of size *n*-1, by systematically leaving out one observation at a time.
- Calculate the statistic of interest for each subsample.
- Calculate the bias of the statistic as the average difference between the statistic calculated on the full data set and the statistic calculated on each subsample.
- Calculate the variance of the statistic as the sum of the squared differences between the statistic calculated on each subsample and the mean of the subsample statistics, divided by *n*-1.
- Calculate the statistic's standard error and confidence interval using the bias and variance estimates.

In practice, jackknifing is often used to estimate the standard error of a statistic, which can be used to construct confidence intervals or to test hypotheses about population parameters. Jackknifing has several advantages over other statistical methods. First, it is simple to understand and implement, requiring only basic statistical software. Second, it is generally less computationally intensive than bootstrap resampling, as it involves only n calculations instead of B calculations. Third, it can be used to estimate the bias and variance of a statistic separately, providing valuable information about the accuracy and precision of the estimate.

However, jackknifing also has some limitations and potential pitfalls. It assumes that each observation in the sample is independent and identically distributed, which may not be true in practice. Also, it may be less robust than bootstrap resampling to outliers or non-normal distributions. Moreover, it may be less accurate than bootstrap resampling when the sample size is small or the population distribution is unknown.

4.3.4 Maximum Likelihood Estimation (MLE)

MLE is a powerful statistical technique used for parameter estimation in various fields, including biology, physics, economics, and engineering. MLE is an optimization method that has been combined with resampling techniques for improved results. In the traditional calibration approach, the error term is assumed to be normally distributed. This might not be the case for all distress types. MLE seeks to estimate the parameters of a probability distribution that best describes the observed data based on the likelihood function. The likelihood function measures the probability of observing the data given a particular set of model parameters. MLE finds the set of model parameters that maximize the likelihood function, resulting in the most likely estimates of the parameters. Consider a dataset X = {x1, x2, ..., xn} that is assumed to be generated by a probability distribution with parameters θ. The likelihood function L(θ|X) is defined as the joint probability density function of the observed data, given the model parameters as shown in Equation (4-3).

$$L(\theta|X) = P(X|\theta) = P(x1, x2, \ldots, xn|\theta) \tag{4-3}$$

where; *P* denotes the probability density function, and the likelihood function measures the probability of observing the data *X* given the model parameters θ. The goal of MLE is to find the set of model parameters θ that maximize the likelihood function. In practice, it is often

easier to work with the log-likelihood function, which is the natural logarithm of the likelihood function. The log-likelihood function is given by Equation (4-4):

$$l(\theta|X) = \log L(\theta|X) = \log P(X|\theta) = \log \prod P(xi|\theta) = \sum \log P(xi|\theta) \quad (4\text{-}4)$$

where;
Π = product operator
Σ = summation operator

Taking the logarithm of the likelihood function simplifies the computation of the derivative, which is required for optimization. The optimization problem can be solved by finding the values of θ that maximize the log-likelihood function. This can be done using numerical optimization algorithms, such as gradient descent, Newton's method, or quasi-Newton methods. These algorithms require the derivative of the log-likelihood function for the model parameters.

Numerical optimization algorithms iteratively update the values of the model parameters based on the score function to maximize the log-likelihood function. The optimization process continues until the algorithm converges to a maximum of the log-likelihood function. The MLEs obtained from the optimization process represent the most likely estimates of the model parameters that can explain the observed data. These estimates can be used for parameter inference, hypothesis testing, and model selection.

One of the main advantages of MLE is that it provides a robust and rigorous approach to parameter estimation. The MLEs are derived from a well-defined likelihood function based on the data's underlying probability distribution. This ensures that the estimates are statistically valid and can be interpreted meaningfully. Another advantage of MLE is that it is a computationally efficient optimization method. The likelihood function can often be evaluated using standard probability distributions, and the optimization problem can be solved using numerical optimization algorithms that are widely available. This makes MLE a practical and scalable method for parameter estimation, even in high-dimensional and complex models. MLE is particularly useful when the model is complex and contains multiple parameters that are difficult to estimate using other methods. For example, in machine learning, MLE is used to estimate the parameters of probabilistic models, such as hidden Markov models and Bayesian networks. MLE was used for calibration, and the results have been summarized in Appendix A.

4.3.5 Summary of Resampling Techniques

Traditional no-sampling or split sampling technique provides a convenient approach to selecting pavement sections from the calibration database. Though these techniques are easy to implement and can be used for any Pavement-ME model, they might impose some limitations. Resampling techniques have several advantages over traditional approaches. Since these are non-parametric techniques, the model parameters can be estimated without making assumptions about the data distribution. The distribution of the model coefficients and error parameters can be estimated instead of the point estimate. This can give a better estimation of parameters within desired confidence intervals. Since a new sample is created

every time, the outliers or sections controlling the calibration process can be identified. Though these resampling techniques have several advantages over traditional approaches, there are also certain limitations. Bootstrapping cannot be used for small datasets or when the independence assumption is unmet. Jackknifing cannot be used for skewed data and is more conservative, i.e., it provides slightly higher estimated standard errors. Resampling techniques also require higher computing power and time and can be used only for those performance models where the damage and other inputs are available from Pavement-ME. Table 4-2 summarizes the advantages and limitations of all calibration techniques.

Table 4-2 Summary of calibration techniques

Technique	Advantages	Limitations
No sampling	• Computationally efficient • Applicable even for small sample size	• Provides point estimates • It may not be suitable for non-normally distributed data
Split sampling	• Computationally efficient • Provides validation	• Provides point estimates • It may not be suitable for non-normally distributed data
Bootstrapping	• Provides confidence intervals • Identifies outliers • Distribution assumption is not required	• Computationally time-consuming • It cannot be used for smaller sample size • It may not be suitable for non-normally distributed data
Repeated split sampling	• Provides confidence intervals • Provides validation • Identifies outliers • Distribution assumption is not required	• Computationally time-consuming • It cannot be used for smaller sample size • It may not be suitable for non-normally distributed data
Jackknifing	• Identifies outliers • Distribution assumption is not required	• Computationally time-consuming • It cannot be used for skewed data
MLE	• Suitable for non-normally distributed data • Identifies outliers • Can be used with resampling techniques and for validation	• Distribution assumption is required • Computationally time-consuming and requires prior knowledge of the concept of maximum likelihood

4.4 PROCEDURE FOR CALIBRATION OF PERFORMANCE MODELS

The details for input data, performance data, and project selection have already been discussed in Chapter 3. Once the data is extracted, it can be used to run the Pavement-ME files (.dgpx files) and generate outputs (structural responses). The process for local calibration is summarized below:

1. Run Pavement-ME (using global model coefficients)and extract critical responses and predicted distresses.
2. Compare the predicted distress with measured distress.
3. Based on the results from step 2, test the accuracy of the global models and the need for local calibration.
4. If predictions using global models are satisfactory, local calibration is not required, and global models can be accepted. If the global model has significant bias and standard error, local calibration is required.
5. Check your calibration results by validating them on an independent set of sections not used for calibration.
6. Estimate the reliability equations based on the calibrated model predictions and measured distress.

4.4.1 Testing the Accuracy of the Global Calibration Coefficients

Before locally calibrating the Pavement-ME models, it is vital to determine the need for calibration. This includes testing the accuracy of the global model predictions at a reliability of 50%, which is the mean expected prediction. Once the predictions from the global model are obtained, they are compared with measured values for calculating bias and standard error. A plot of predicted versus measured values is created for each distress to visualize the accuracy of predictions to a line of equality (LOE). Testing the global model also includes hypothesis testing. For a good fit, the points should lie along the LOE. The measured distress $y_{Measured}$ and predicted distress $x_{Predicted}$ can be modeled in the form of a linear model as shown in Equation (4-5), where m is the slope, and b_o is the intercept.

$$y_{\text{Measured}} = b_o + m \times x_{\text{Predicted}} \tag{4-5}$$

Three hypothesis tests are conducted to evaluate the reasonableness of the global model. If any of these hypotheses fail, the models are recalibrated for local conditions:

- There is no systematic bias between the measured and predicted distress (Equation (4-6)). This can be tested using a paired t-test.

$$H_0: \sum(y_{\text{Measured}} - x_{\text{Predicted}}) = 0 \tag{4-6}$$

- The slope parameter m is 1 (Equation (4-7)).

$$H_0: m = 1.0 \tag{4-7}$$

- The intercept parameter b_o is zero (Equation (4-8)).

$$H_o: b_o = 0 \tag{4-8}$$

4.4.2 Local Calibration Coefficient Refinements

This section outlines the calibration approach used for each Pavement-ME model. Moreover, different calibration techniques used and subsets of selected sections have also been discussed.

4.4.2.1. Data subpopulations

The Pavement-ME models have been calibrated using different subsets of sections for both rigid and flexible pavements. The goal was to verify if a single set of coefficients for all pavement types would suffice or if an individual calibration is required for different pavement types. Three different options have been considered:

Option 1: Reconstruct sections only
Option 2: Reconstruct and rehabilitation sections
Option 3: Rehabilitation sections only

4.4.2.2. Sampling techniques

The following techniques have been used to calibrate the Pavement-ME models for the above subsets. All these methods have been used for models calibrated and validated using Approach I. Approach II was used for models which cannot be calibrated outside of Pavement-ME using MATLAB codes. Therefore, for models calibrated using Approach II, only no sampling and traditional split sampling have been used in the CAT tool.

- No sampling (include all data)
- Traditional split and repeated split sampling
- Bootstrapping

The entire dataset (all available data points) is considered in no sampling. Bootstrapping has been used by considering 1,000 bootstrap resamples with replacement. For calibration-validation, a split of 70%-30% has been used where 70% of the data goes to the calibration set, whereas 30% goes to the validation set. In traditional split sampling, calibration-validation is performed once, whereas repeated split sampling has been repeated 1000 times by randomly picking different data sets each time.

4.5 FLEXIBLE PAVEMENT MODEL COEFFICIENTS

The design distress in the Pavement-ME includes bottom-up cracking, top-down cracking, rutting, thermal (transverse) cracking, reflective cracking, and IRI. The calibration of each model and the specific coefficients calibrated has been discussed in the next section.

4.5.1 Fatigue Cracking Model (bottom-up)

The fatigue cracking (bottom-up) model was calibrated by optimizing the C_1 and C_2 coefficients (see Table 4-1). In Pavement-ME v2.6, coefficient C_1 is a single value, whereas coefficient C_2 has three different values depending on the total HMA thickness. Table 4-3 shows the global values for C_1 and C_2.

Table 4-3 Global values for bottom-up cracking model coefficients

Calibration coefficient	Global values
C_1	1.31
C_2	H_{ac} < 5 in. : 2.1585
	5 in. <= H_{ac} <=12 in.: (0.867 + 0.2583 × H_{ac}) ×1
	H_{ac} > 12 in.: 3.9666

H_{ac}: Total HMA thickness in inches

Notably, no sections were selected for the bottom-up calibration with a total HMA thickness of more than 12 inches. The coefficient C_2 was calibrated separately for the thickness ranges less than 5 inches and 5 to 12 inches, respectively. For a thickness range of 5 to 12 inches, only the multiplying factor 1 (marked in bold here: (0.867 + 0.2583 × H_{ac}) ×**1**) was calibrated while other values (0.867 and 0.2583) were kept at global values. For a thickness range of more than 12 inches, the same function ((0.867 + 0.2583 × H_{ac}) ×1) was used with a single value. The H_{ac} was kept at 12 inches, and the multiplying factor 1 was kept at the same value for the 5 to 12-inch thickness range. The crack initiation time is affected by C_1, whereas the slope of the bottom-up cracking curve is affected by C_2. The effects of C_1 and C_2 on the predicted bottom-up cracking are shown in Figure 4-2. It is difficult to determine whether a crack has initiated from the top or bottom of the pavement. Consequently, the calibration was performed using two different approaches (a) combined measured bottom-up and top-down cracking and (b) bottom-up cracking only.

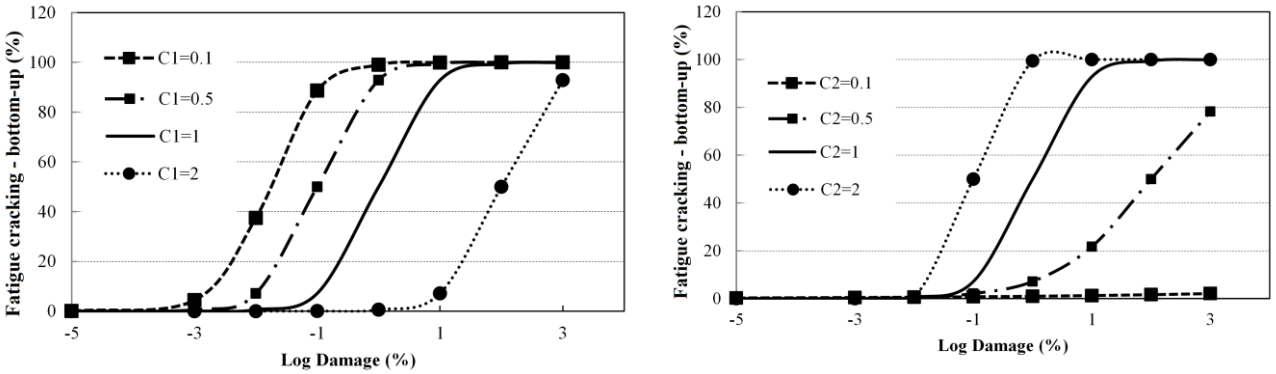

(a) Effect of C_1 (b) Effect of C_2

Figure 4-2 Effect of calibration coefficients on fatigue cracking (bottom-up) cracking

4.5.2 Fatigue Cracking Model (top-down)

The top-down cracking model has been modified in the Pavement-ME v2.6. The model consists of a crack initiation function that calculates the time to crack initiation and a crack propagation function that calculates the percent lane area cracked. This makes it a total of 8 coefficients combined from both functions. Since the actual crack initiation time is not known, it was not possible to calibrate the crack initiation model separately. So, a single function was used by substituting the crack initiation function with the crack propagation function. Initially, an attempt was made to change all 8 coefficients simultaneously. This approach had some challenges:

- The model has some mathematical limitations. High values for C_3 gives mathematical error while using it in Pavement-ME.
- There is no current literature available for the top-down cracking model calibration. Therefore, estimating the range for each coefficient to be used in optimization was difficult.
- The model has many coefficients with coefficient values ranging from 0.011 to 64271618. This makes the optimization challenging to converge.

Four coefficients from the crack initiation function (*kL2, kL3, kL4, kL5)* and two coefficients from the crack propagation function (C_1, C_2) have been calibrated, based on the understanding and limitations of the model as mentioned above.

4.5.3 Rutting Model

Due to axle loads, rutting is the total accumulated plastic strain in different pavement layers (HMA, base/sub-base, and subgrade). It is calculated by summing up the plastic strains at the mid-depth of individual layers accumulated for each time increment. In the Pavement-ME, rutting is predicted separately for the different layers (HMA, base, and subgrade). The total rutting is the sum of rutting from all layers. The AC rutting model has three coefficients (β_{1r}, β_{2r}, β_{3r}). β_{1r} is a direct multiplier and can be calibrated using optimization outside the Pavement-ME. In this model, β_{2r} and β_{3r} are power to the pavement temperature and the number of axle load repetitions. Calibration of β_{2r} and β_{3r} cannot be done outside of the Pavement-ME and requires running the Pavemet-ME multiple times or optimizing these in the CAT tool. Initially, β_{2r} and β_{3r} values from the previous calibration effort were used, and β_{1r} was calibrated *(5)*. This calibration approach provided reasonable results; therefore, β_{2r} and β_{3r} from the previous calibration were accepted, and only β_{1r} was calibrated. Figure 4-3 shows the impact of the β_{2r} and β_{3r} calibration coefficients on the predicted HMA rutting. Legends in Figure 4-3 indicate β_{2r} and β_{3r} combination such that only one is changed at a time.

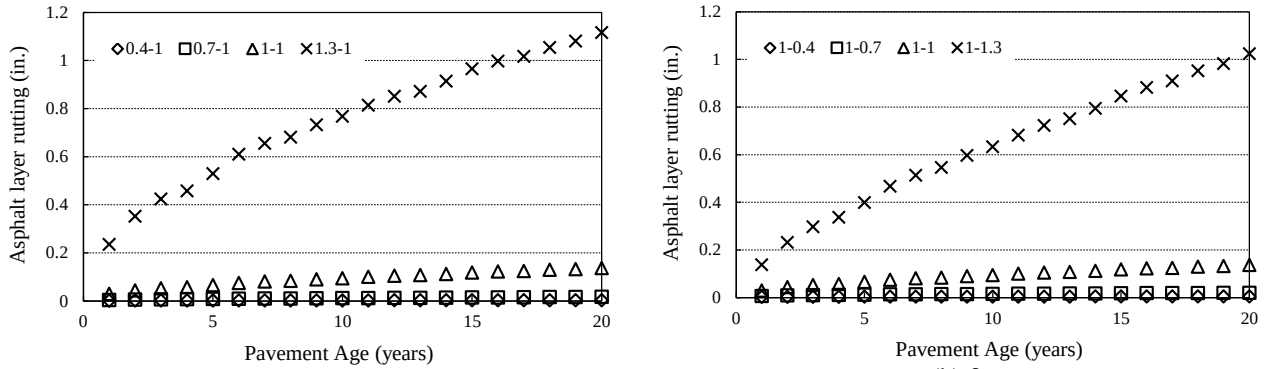

Figure 4-3 Effect of β_{2r} and β_{2r} on HMA rutting

The unbound layers (base and subgrade) rutting model have one calibration coefficient each (β_{s1}). Since β_{s1} is a direct multiplier, it can be calibrated using optimization outside the Pavement-ME without running the software or CAT tool. Since both base and subgrade have the same model and calibration coefficient, the base calibration coefficient is referred to as

$\beta_{s1,}$ and the subgrade coefficient is referred to as β_{sg1} to avoid confusion. The rutting model in the Pavement-ME was calibrated using the following two methods:

1. *Method 1: Individual layer rutting calibrations* — For this approach, the measured rutting from individual layers was matched against the predictions from the Pavement-ME (β_{1r}, $\beta_{s1,}$ and β_{sg1} were calibrated separately). The total measured rutting was multiplied by the percent contribution from each layer to obtain measured rutting for the individual layer. The percentage contribution was estimated using transverse pavement profile analysis, as shown in Figure 4-4. The width and depth of the measured rut channel were used to determine the seat of rutting and rutting in individual layers. AC layer rutting contributes more than 70% to all pavement types [based on transverse profile analysis (*6*)]. The standard error equations for rutting in the Pavement-ME are separate for individual layers. This method evaluated the standard error equations for rutting in each layer.
2. *Method 2: Total surface rutting calibration* — The total measured rutting was calibrated against the sum of individual predicted rutting (i.e., β_{1r}, $\beta_{s1,}$ and β_{sg1} were calibrated simultaneously).

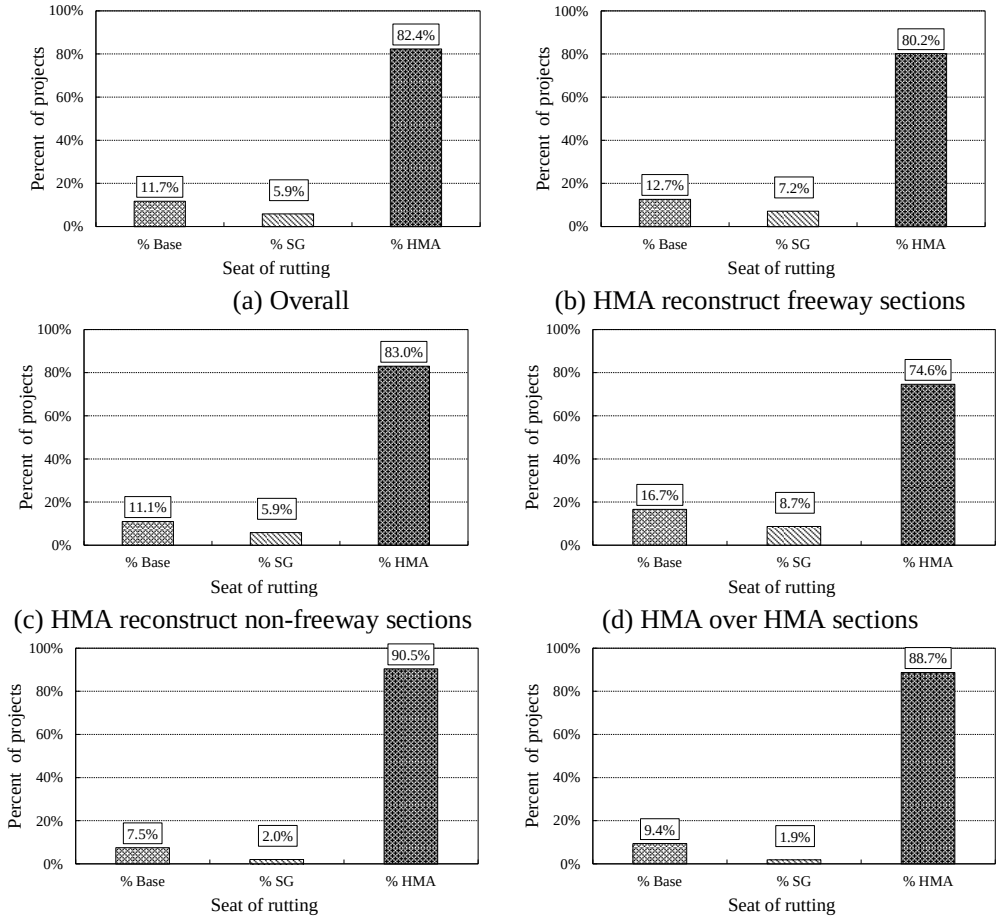

Figure 4-4 Transverse profile analysis results

4.5.4 Thermal Cracking Model

The thermal cracking model in the Pavement-ME has three different levels for the calibration coefficient. These levels are based on the level of HMA input. Level 1 *G** and Level 2 IDT have been used to calibrate the thermal cracking model. This corresponds to Level 1 thermal cracking calibration coefficients. Both *G** and IDT values were obtained from the DYNAMOD software database. In the DYNAMOD database, *G** and IDT values are available only for sections with Performance grade (PG) binder type. Therefore, sections with PG binder type (Superpave mixes) have been used to calibrate the thermal cracking model. In the Pavement-ME v2.6, the calibration coefficient k_t is originally a mean annual air temperature (MAAT) function, whereas, in v2.3, it was a single representative value. For the reconstruction sections, two different approaches were used:

- Using the CAT tool, an initial attempt was made to calibrate k_t (using the original equation as a function of MATT).
- A second attempt was made to calibrate k_t by running the Pavement-ME multiple times with different k_t values. This time, single values for k_t were used, which were not a function of MAAT.

k_t as a function of MAAT resulted in contradictory results when comparing Michigan temperature extremes, where thermal cracking at cold temperatures was either reduced or equal to thermal cracking at warm temperatures. Moreover, ARA recommends the use of a single k_t value if this is more suitable for the agency and its local conditions. Based on these results, finally, k_t value based on the second approach was recommended. It is important to note that for this calibration, the average thermal cracking for a section was cut at 2112 ft/mile. For overlays, MDOT does not differentiate between thermal cracking and reflective cracking. Hence, thermal and reflective cracking coefficients were calibrated for overlays using the CAT tool. The CAT tool has a limitation on the run time and the total combinations of coefficients that can be calibrated simultaneously. Therefore, the thermal cracking coefficient k_t was set to the calibrated value obtained from the reconstruct sections. Keeping k_t constant, the other four coefficients for reflective cracking were calibrated. This approach was followed for HMA over HMA and composite overlays.

4.5.5 IRI Model for Flexible Pavements

IRI is a linear function of initial IRI, rut depth, total fatigue cracking, transverse cracking, and site factor, as shown in Equation (4-9). The initial IRI was obtained from linear backcasting based on the time series trend for each section. The fatigue cracking, rutting, and transverse cracking models were calibrated before calibrating the IRI model. Since all inputs to the IRI model could be obtained, it was calibrated outside of Pavement-ME without directly using it or using the CAT tool. IRI has a closed-form solution and does not require a standard error equation in the Pavement-ME. The standard error for IRI is calculated using the standard error of its components.

$$\mathrm{IRI} = \mathrm{IRI_o} + \mathrm{C1(RD)} + \mathrm{C2(FC_{Total})} + \mathrm{C3(TC)} + \mathrm{C4(SF)} \quad (4\text{-}9)$$

Where;
IRI_o = Initial IRI after construction, in/mi.

SF = Site factor
FC_{Total} = Area of fatigue cracking (combined bottom-up, top-down, and reflection cracking in the wheel path), percent of total lane area.
TC = Length of transverse cracking (including the reflection of transverse cracks in existing HMA pavements), ft/mi.
RD = Average rut depth, in.

4.6 RIGID PAVEMENT MODEL COEFFICIENTS

The design distresses in the Pavement-ME include transverse cracking (percentage of slabs cracked), transverse joint faulting (inches), and international roughness index (IRI) for rigid pavements. The impact of calibration coefficients on the predicted performance specific to each model is discussed in this section.

4.6.1 Transverse Cracking Model

The coefficients C_4 and C_5 (shown in Table 4-1) were optimized to calibrate the transverse cracking model. These coefficients were calibrated outside the Pavement-ME and without the CAT tool. C_4 affects the crack initiation time, and C_5 affects the slope of the transverse cracking curve. The effect of C_4 and C_5 on the slope and magnitude of the transverse cracking predictions is shown in Figure 4-5.

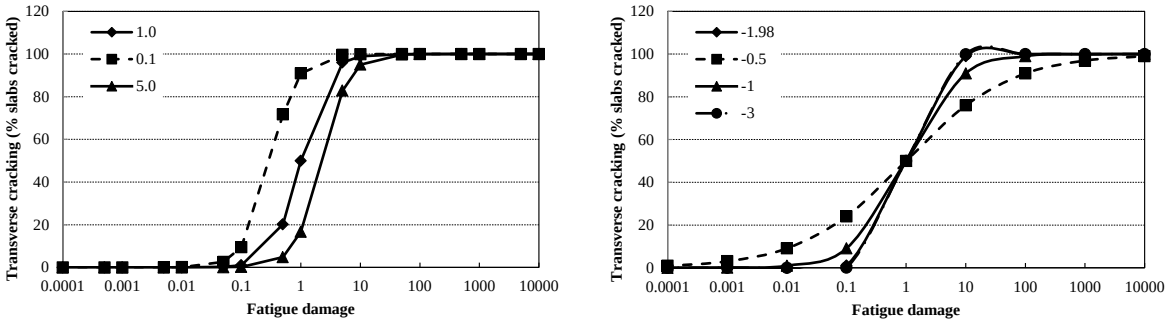

(a) C_4 (b) C_5

Figure 4-5 Effect of transverse cracking model calibration coefficients

4.6.2 Transverse Joint Faulting Model

The joint faulting model in the Pavement-ME consists of a total of eight coefficients. Joint faulting could not be predicted using the available inputs outside the Pavement-ME; therefore, it was calibrated using the CAT tool. CAT tool has a limitation on the run time and the total combinations of coefficients that can be calibrated simultaneously. Therefore, it was essential to identify the most sensitive coefficients. Several research studies *(7, 8)* show that out of the seven calibration coefficients for the faulting model, C_6 is the most sensitive. C_1 is the next sensitive coefficient, followed by C_2. Using this sequence of sensitivity of the different coefficients, C_1 and C_6 were calibrated together. The calibrated coefficients from C_1 and C_6 were then kept fixed, and C_2 was calibrated. In this sequence, the three most sensitive coefficients were calibrated. As previously noted and explained in Chapter 3, the joint faulting (for every 0.1-mile segment) was cut at 0.4 inches for calibration.

4.6.3 IRI Model for Rigid Pavements

IRI in rigid pavements is a linear function of initial IRI, transverse cracking, joint spalling, joint faulting, and site factor, as shown in Equation (4-10). The initial IRI was obtained from linear backcalculation based on the time series trend for each section. The transverse cracking, and joint faulting models were calibrated before calibrating the IRI model. Since all inputs to the IRI model could be obtained, it was calibrated outside Pavement-ME without directly using it or using the CAT tool. IRI has a closed-form solution and does not require a standard error equation in Pavement-ME. The standard error for IRI is calculated using the standard error of its components.

$$\mathrm{IRI} = \mathrm{IRI_I} + \mathrm{C1} \times \mathrm{CRK} + \mathrm{C2} \times \mathrm{SPALL} + \mathrm{C3} \times \mathrm{TFAULT} + \mathrm{C4} \times \mathrm{SF} \quad (4\text{-}10)$$

where,
IRI = Predicted IRI
IRI_I = Initial IRI at the time of construction
CRK = Percent slabs with transverse cracking (all severities).
SPALL = Percentage of joints with spalling (medium and high severities).
TFAULT = Total joint faulting cumulated per mi
C_1, C_2, C_3, C_4 = Calibration coefficients
SF = Site factor

4.7 DESIGN RELIABILITY

The Pavement-ME estimates the performance of a pavement using mechanistic models and transfer functions. Although these estimates are rational for pavement design purposes, the actual field measurements may show variability. This variability may come from the uncertainties in estimating the future traffic, material, and construction variability, measurement error, uncertainties due to the use of level 2 and 3 inputs, and errors associated with the model predictions. To incorporate all these variabilities, Pavement-ME uses a reliability-based design. Reliability for any prediction can be defined as the probability of getting a prediction lower than the threshold prediction over the design life, as shown in Equation (4-11).

$$\mathrm{Reliability} = \mathrm{P}[\text{distress at the end of design life} < \text{Critical distress}] \quad (4\text{-}11)$$

If 100 sections have been designed at 90% reliability, on average, ten of them may fail before the end of design life. Design reliability levels may vary by distress type and IRI or may remain constant for each. It is recommended, however, that the same reliability be used for all performance indicators *(9)*. Except for IRI, reliability for all other models is estimated using a relationship between the standard deviation of measured distress as the dependent variable and mean predicted distress as the independent variable. The basic assumption implies that the error in predicting the distress is normally distributed on the upper side of the prediction (not on the lower side or near zero values). Figure 4-6 shows an example of IRI prediction at 50% reliability (mean prediction), prediction at any desired reliability *R*, and are associated with the probability of failure. For 90 percent design reliability, the dashed curve at reliability *R* should not cross the IRI at the threshold criteria throughout the design analysis

period. Failing to do so may lead to a failure at the required reliability and indicates that a design modification (such as a pavement thickness increase) should be applied.

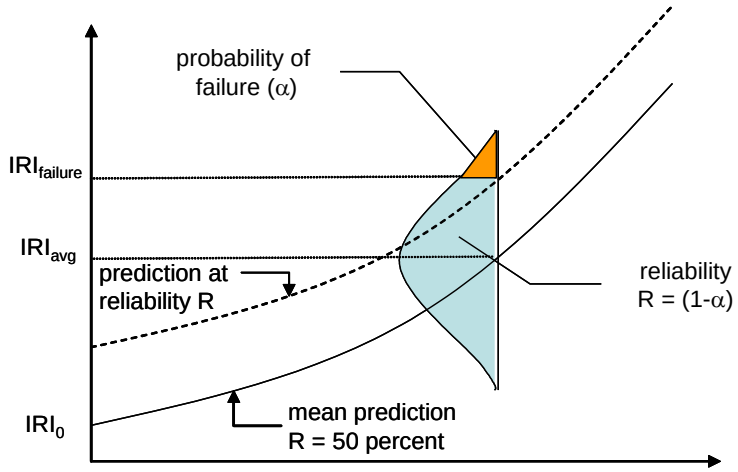

Figure 4-6 Design Reliability Concept for Smoothness (IRI)

Reliability is added to the mean prediction to incorporate any input or performance data variability. It is expressed as a function of the predicted performance and derived using the predicted and measured performance data. A step-by-step approach to estimating the reliability of transverse cracking for rigid pavements is shown below as an example. A similar approach is used for the reliability of all other models except IRI in the Pavement-ME.

Step 1: All predicted and measured data points are grouped by creating bins on the predicted cracking. The number of data points in each group should be equivalent to reduce bias in the results.

Step 2: The average and standard deviation of measured and predicted cracking are computed for each group. The grouping is performed after finalizing the calibration coefficients (global or local) to obtain the predicted performance. Table 4-4 shows the number of data points, bin ranges, and descriptive statistics.

Table 4-4 Summary statistics for reliability analysis for transverse cracking in rigid pavements (example)

Cracking range (%)	No. of data points	Average Measured Cracking	Average Predicted Cracking	Standard dev. of Measured Cracking	Standard dev. of Predicted Cracking
0-0.5	46	0.84	0.54	0.86	0.29
0.5-2	31	1.41	1.35	1.51	0.25
2-5	44	3.53	3.13	3.76	0.72
5-10	29	1.45	12.18	8.93	1.58
10-50	12	15.06	26.52	14.96	1.22

Step 3: A relationship is determined between the standard deviation of the measured cracking on the y-axis and the average predicted cracking on the x-axis. Figure 4-7 shows the fit model to the grouped data in steps 1 and 2. Equation (4-12) shows the relationship between the standard deviation of the measured cracking and the average predicted cracking (when using the no sampling technique).

$$s_{e(CRK)} = 1.3627(CRK)^{0.7473} \tag{4-12}$$

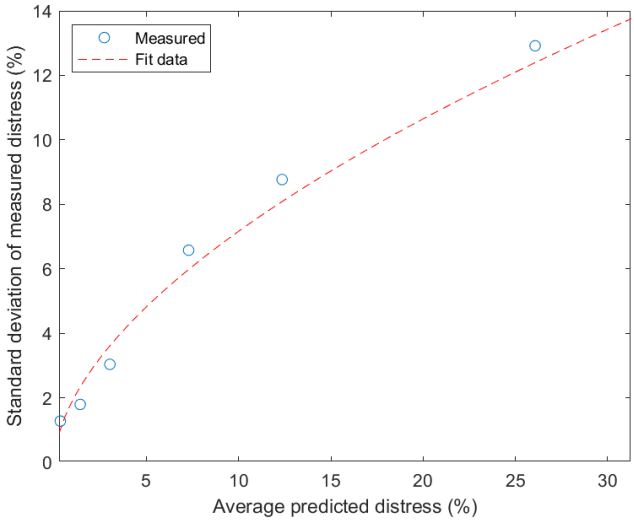

Figure 4-7 Fitting curve for the reliability of transverse cracking in rigid pavements (example)

Step 4: Since the error term is assumed to be normally distributed, the predicted cracking can be adjusted to the desired reliability level using Equation (4-13)

$$C_r = C_{50} + S_e \times Z_{a/2} \tag{4-13}$$

where,
C_r= Predicted cracking at reliability r (%)
C_{50} = Predicted cracking at 50% reliability
S_e = Standard deviation of cracking which can be estimated using Equation (4-12)
$Z_{a/2}$ = Standardized normal deviate (mean = 0; standard deviation = 1) at reliability r

Step 5: For the final step, the reasonableness of the model should be verified based on the actual measured data before using the reliability equation for design.

The reliability model for IRI is different from that of other models. Since a closed-form solution and the variances of different components of IRI are known, the reliability model for IRI is based on the variance analysis of its components. The basic assumption implies that the error in predicting IRI is roughly normally distributed. The total error includes input, repeatability, pure, and model errors. Overall, the IRI prediction error can be estimated by Equation (4-14) and Equation (4-15).

$$\mathrm{IRI_{pe}} = \mathrm{IRI_{meas}} - \mathrm{IRI_{pred}} \quad (4\text{-}14)$$

$$\mathrm{Var}(\mathrm{IRI_{pe}}) = \mathrm{Var}(\mathrm{IRI_{meas}}) + \mathrm{Var}(\mathrm{IRI_{pred}}) - 2R \times \sqrt{\mathrm{Var}(\mathrm{IRI_{meas}}) \times \mathrm{Var}(\mathrm{IRI_{pred}})} \quad (4\text{-}15)$$

where,
$Var(IRI_{pe})$ = Variance in prediction error for IRI (estimated from calibration results)
$Var(IRI_{meas})$ = Variance in measured IRI (estimated from field measurement)
$Var(IRI_{pred})$ = Variance in predicted IRI
R = Correlation coefficient between predicted and actual IRI

The variance in predicted IRI is the sum of the variance in inputs (cracking, spalling, faulting, and initial IRI) and the variance in model + pure error, as shown in Equation (4-16).

$$\mathrm{Var}(\mathrm{IRI_{pred}}) = \mathrm{Var}(\mathrm{IRI_{INPUTS}}) + \mathrm{Var}(\mathrm{model + pure\ error}) \quad (4\text{-}16)$$

The variance in inputs for the IRI model is shown in Equation (4-17).

$$\mathrm{Var}(\mathrm{IRI_{INPUTS}}) = \mathrm{Var_{IRIi}} + \mathrm{C1^2} \times \mathrm{Var_{CRK}} + \mathrm{C2^2} \times \mathrm{Var_{Spall}} + \mathrm{C3^2} \times \mathrm{Var_{Fault}} \quad (4\text{-}17)$$

where,
$Var(IRI_{INPUTS})$= Variance in IRI due to measurement errors for each distresses and initial IRI (estimated from field measurements)
Var_{IRIi} = Variance in initial IRI
Var_{CRK} = Variance in transverse cracking
Var_{Spall} = Variance in joint spalling
Var_{Fault} = Variance in joint faulting
$C1$, $C2$, $C3$ = IRI model coefficients

Using Equations (4-15 to 4-17), $Var(model + pure\ error)$ can be determined, which is used to predict the standard deviation in IRI at any predicted value. The global standard error equations for each model are summarized in Table 4-5.

Table 4-5 Global calibration reliability equations for each distress and smoothness model

Pavement Type	Pavement performance prediction model	Standard error equation
Flexible pavements	Fatigue cracking (bottom-up)	$s_{e(bottom-up)} = 1.13 + \frac{13}{1+e^{7.57-15.5\times Log(FC_{Bottom}+0.0001)}}$
	Fatigue cracking (top-down)	$s_{e(top-down)} = 0.3657 \times FC_{top} + 3.6563$
	Rutting	$s_{e(HMA)} = 0.24(\Delta_{HMA})^{0.8026} + 0.001$ $s_{e(Base)} = 0.1477(\Delta_{Base})^{0.6711} + 0.001$ $s_{e(SG)} = 0.1235(\Delta_{SG})^{0.5012} + 0.001$
	Transverse cracking	$s_e = 0.14 \times TC + 168$
	IRI	Estimated internally by the software
Rigid pavements	Transverse cracking	$s_{e(CRK)} = 3.5522(CRK)^{0.3415} + 0.75$
	Faulting	$s_{e(Fault)} = 0.07162(Fault)^{0.368} + 0.00806$
	IRI	Initial IRI S_e = 5.4 Estimated internally by the software

4.8 SUMMARY

This chapter detailed the calibration approach used for each Pavement-ME prediction model. Transfer functions have been calibrated based on whether they calculate the distresses directly or calculate them based on cumulative damage. It also discusses the different calibration resampling techniques and optimization methods. No sampling, bootstrapping, traditional split sampling, and repeated split sampling techniques have been used for calibration. For calibration validation, traditional and repeated split sampling are used. The chapter also outlined the process of local calibration.

CHAPTER 5 - LOCAL CALIBRATION

5.1 INTRODUCTION

The calibration process adjusts the Pavement-ME model parameters to match observed data better to ensure that the model outputs are reliable and useful for decision-making. The Pavement-ME models' calibration process can be challenging because of their complexity and the large number of parameters involved. However, technological advancements and data collection methods have made the calibration process more efficient and effective. For instance, pavement data can now be collected using automated methods such as laser-based measurements (sensors), which provide high-resolution data that can calibrate the Pavement-ME models accurately.

This chapter discusses the different options and the calibration results of each model. These data sets are formed using combinations of different MDOT pavements, i.e., reconstruct and rehabilitation sections. The options with varying combinations of the dataset are:

Option 1: Reconstruct sections only
Option 2: Reconstruct and rehabilitation sections combined
Option 3: Rehabilitation sections only

The different statistical techniques used for calibration are:

a. No sampling (include all data) – calibration
b. Traditional and repeated split sampling – calibration-validation
c. Bootstrapping – calibration

No sampling and bootstrapping approaches were used for calibration only, whereas traditional split and repeated split sampling were used for calibration and validation. The team recalibrated the following performance models in the Pavement-ME for Michigan conditions.

- Flexible pavements
  - Fatigue cracking (bottom-up)
  - Fatigue cracking (top-down)
  - Rutting
  - Transverse (thermal) cracking
  - IRI
- Rigid pavements
  - Transverse cracking
  - Faulting
  - IRI

It is important to note that the thermal cracking model for flexible sections and the joint faulting model for rigid sections were calibrated in the Calibration Assistance Tool (CAT).

For other performance models, the Pavement-ME was initially used to determine the damage with all available inputs (material, traffic, and climate). Then, the calibration approaches mentioned above were implemented using the outputs from the Pavement-ME program. A predicted vs. measured distress plot was generated for each model with a line of equality at 45 degrees. These plots can be used to visually inspect a model's SEE and bias. For an ideal model, all the points should lie on the line of equality. The calibration approach used the hypothesis tests outlined in the local calibration guide.

The local calibration results are presented for both flexible and rigid pavement performance prediction models and are compared among the different statistical techniques and the data set options mentioned above.

5.2 LOCAL CALIBRATION OF FLEXIBLE PAVEMENT MODELS

The detailed results for the local calibration of the fatigue cracking, rutting, transverse (thermal) cracking, and IRI models are presented in this section.

5.2.1 Fatigue Cracking Model – Bottom-up

The bottom-up cracking model was calibrated for reconstruct sections only (Option 1). This is because the Pavement-ME did not predict any damage and, therefore, any bottom-up cracking for rehabilitated sections. The number of reconstruct sections showing bottom-up cracking is relatively lower. Therefore, sections with even two measured points have been included in the calibration. More points can be added as more measured data becomes available in the future. Two different approaches were used for the calibration of the bottom-up cracking model:

a) Combining measured bottom-up and top-down fatigue cracking in the wheel path. This option reduces the assumption of crack type and the potential for incorrect type assignment. It is difficult to determine visually if a crack has initiated from the top or bottom of the pavement surface. This option is also helpful, as there are more measured points for longitudinal compared to alligator cracking.
b) Using measured bottom-up fatigue cracking only.

5.2.1.1. Option 1a: Reconstruct only

The team evaluated global calibration coefficients for SEE, bias, and hypothesis tests for each calibration technique. This was accomplished by comparing the measured bottom-up cracking (combined bottom-up cracking and top-down cracking considered bottom-up cracking) with predicted bottom-up cracking using global calibration coefficients. This comparison shows the efficiency of the global model and the need for local calibration.

No Sampling

In no sampling, the entire dataset was used for calibration. The error was minimized between the predicted and measured fatigue cracking. Figure 5-1 shows the predicted versus measured bottom-up for the global and locally calibrated models. The global model under predicts bottom-up cracking. Table 5-1 shows the local calibration results. The SEE is reduced from

8.28 to 8.08, whereas the bias is reduced from -4.90 to 0.17. Table 5-2 shows the results of the hypothesis tests. Although two out of three hypothesis tests are rejected, the SEE and bias values significantly improve. Figure 5-2 shows the fatigue damage curve and the measured and locally predicted bottom-up cracking with time. These measured and predicted cracking values are for the same sections and at the same ages. Figure 5-2 shows that local predictions are close to the measured values.

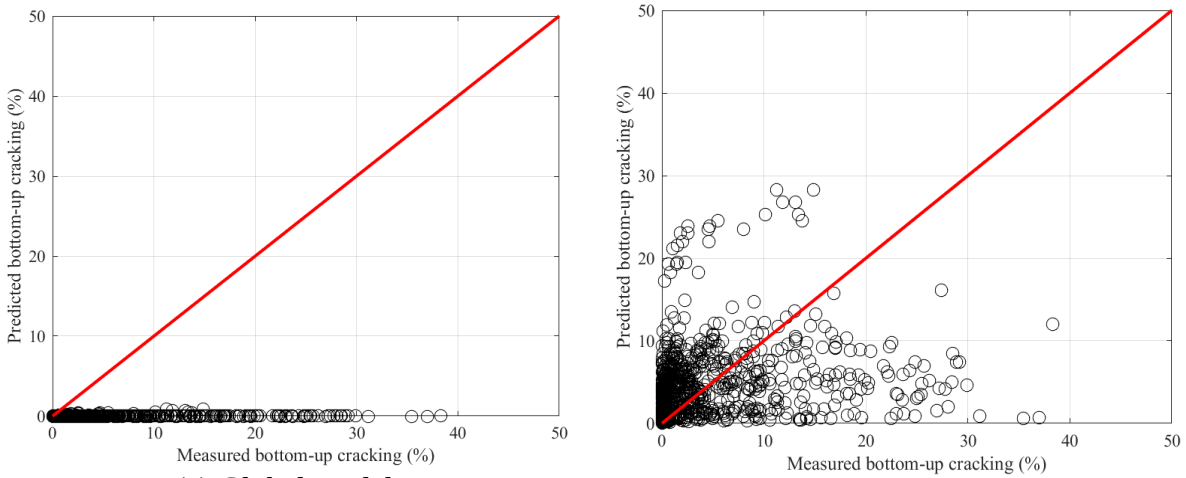

(a) Global model (b) Local model

Figure 5-1 Predicted vs measured bottom-up cracking (No sampling)

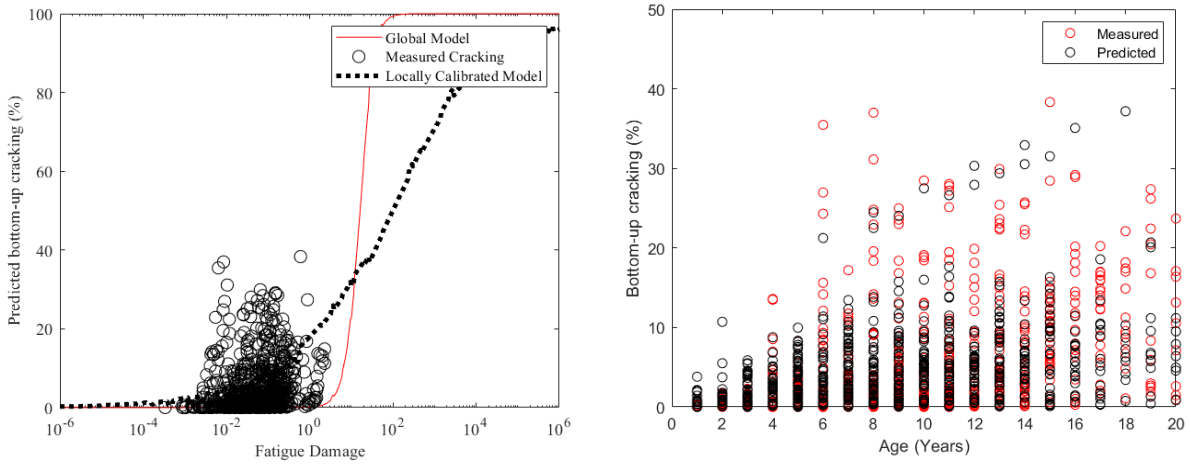

(a) Fatigue damage (b) Measured and predicted time series

Figure 5-2 Local calibration results for bottom-up cracking (No sampling)

Table 5-1 Local calibration summary for bottom-up cracking (No sampling)

Parameter	Global model	Local model
SEE (% total lane area)	8.28	8.08
Bias (% total lane area)	-4.90	0.17
C_1	1.31	0.22
C_2 (h_{ac} < 5 in.)	2.1585	0.66
C_2 (5 in. <= h_{ac} <=12 in.)	(0.867+0.2583* h_{ac})*1	(0.867+0.2583* h_{ac})*0.22

Table 5-2 Hypothesis testing results for bottom-up cracking (No sampling)

Hypothesis test	Global model	Local model
Mean difference = 0	0.00	0.55
Intercept = 0	0.02	0.00
Slope = 1	0.00	0.00

Split Sampling

Split sampling was used with a random split of 70% sections for the calibration set and the rest 30% for the validation set. Figure 5-3 shows the predicted vs. measured bottom-up cracking for the calibration and validation set. The validation set shows a similar trend as the calibration set. Table 5-3 summarizes the local calibration results. Though SEE is higher than the global model, bias is significantly improved from -4.54 to 0.7018 in the validation set. Overall, the validation results are satisfactory.

Table 5-3 Local calibration summary for bottom-up cracking (split sampling)

Parameter	Global model	Local model	Validation
SEE (% total lane area)	7.76	7.11	11.2955
Bias (% total lane area)	-4.54	-0.47	0.7018
C_1	1.31	0.19	0.19
C_2 (h_{ac} < 5 in.)	2.1585	0.78	0.78
C_2 (5 in. <= h_{ac} <=12 in.)	(0.867+0.2583*hac)*1	(0.867+0.2583*hac)*0.26	(0.867+0.2583*hac)*0.26

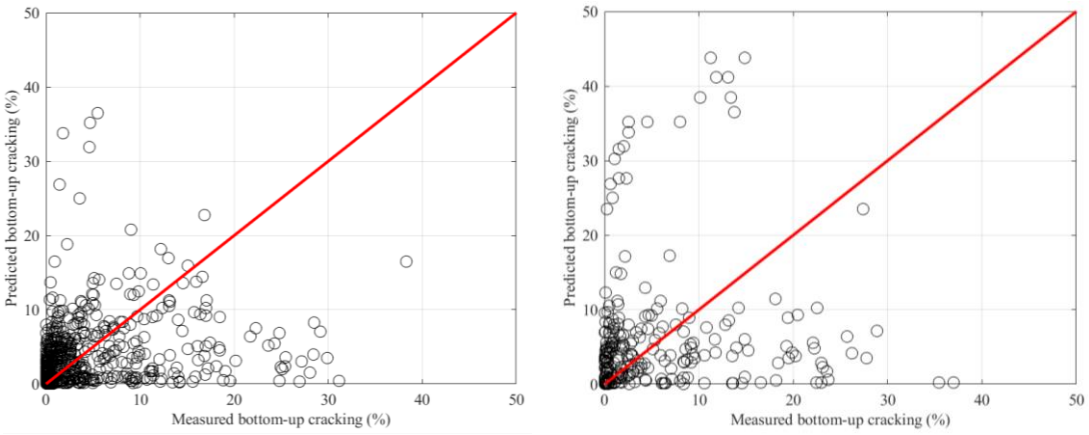

(a) Calibration set (b) Validation set

Figure 5-3 Local calibration results for bottom-up cracking (split sampling)

Repeated Split Sampling

Like split sampling, repeated split sampling was used with a random split of 70% sections for the calibration set and the remaining 30% for the validation set. This process was repeated 1000 times, where a new random set of calibration and validation sets was picked each time. Repeated split sampling is used to estimate the distribution of different parameters instead of optimizing for a point estimate. Confidence intervals (CI) for each parameter can also be obtained. Tables 5-4 to 5-6 show the summary for the global model, calibration, and validation sets, respectively. It is important to note that coefficient C_2 is a function of total HMA thickness (h_{ac}). For estimating the confidence intervals and distribution of C_2, it was converted to a single value for all HMA thicknesses. Figures 5-4 and 5-5 present the distribution of model parameters for calibration and validation sets. In Figures 5-4 and 5-5, the solid blue line shows the median, the dashed red line shows the mean, the solid black line shows the cumulative distribution and the dashed red lines on both sides show the 2.5th and 97.5th percentiles. The mean SEE is reduced from 8.29 to 7.90 for the calibration and 7.93 for the validation set. Similarly, bias was improved from -4.91 to -0.02 for the calibration and 0.03 for the validation set.

Table 5-4 Global model summary (Repeated split sampling)

Parameter	Global model mean	Global model median	Global model lower CI	Global model upper CI
SEE (% total lane area)	8.29	8.29	7.63	8.84
Bias (% total lane area)	-4.91	-4.91	-5.35	-4.47
C_1	1.31	1.31	-	-
C_2 (h_{ac} < 5 in.)	2.1585	2.1585	-	-
C_2 (5 in. <= h_{ac} <=12 in.)	(0.867+0.2583* h_{ac})*1	(0.867+0.2583* h_{ac})*1	-	-

Table 5-5 Calibration set summary (Repeated split sampling)

Parameter	Local model mean	Local model median	Local model lower CI	Local model upper CI
SEE (% total lane area)	7.90	7.73	6.49	9.93
Bias (% total lane area)	-0.02	0.00	-0.51	0.42
C_1	0.26	0.25	0.13	0.42
C_2 (h_{ac} < 5 in.)	0.60	0.60	0.29	0.89
C_2 (5 in. <= h_{ac} <=12 in.)	(0.867+0.2583* h_{ac})* 0.19	(0.867+0.2583* h_{ac})* 0.19		

Table 5-6 Validation set summary (Repeated split sampling)

Parameter	Local model mean	Local model median	Local model lower CI	Local model upper CI
SEE (% total lane area)	7.93	7.68	6.01	10.88
Bias (% total lane area)	0.03	0.02	-2.04	2.27
C_1	0.26	0.25	0.13	0.42
C_2 (h_{ac} < 5 in.)	0.60	0.60	0.29	0.89
C_2 (5 in. <= h_{ac} <=12 in.)	(0.867+0.2583* h_{ac})* 0.19	(0.867+0.2583* h_{ac})* 0.19		

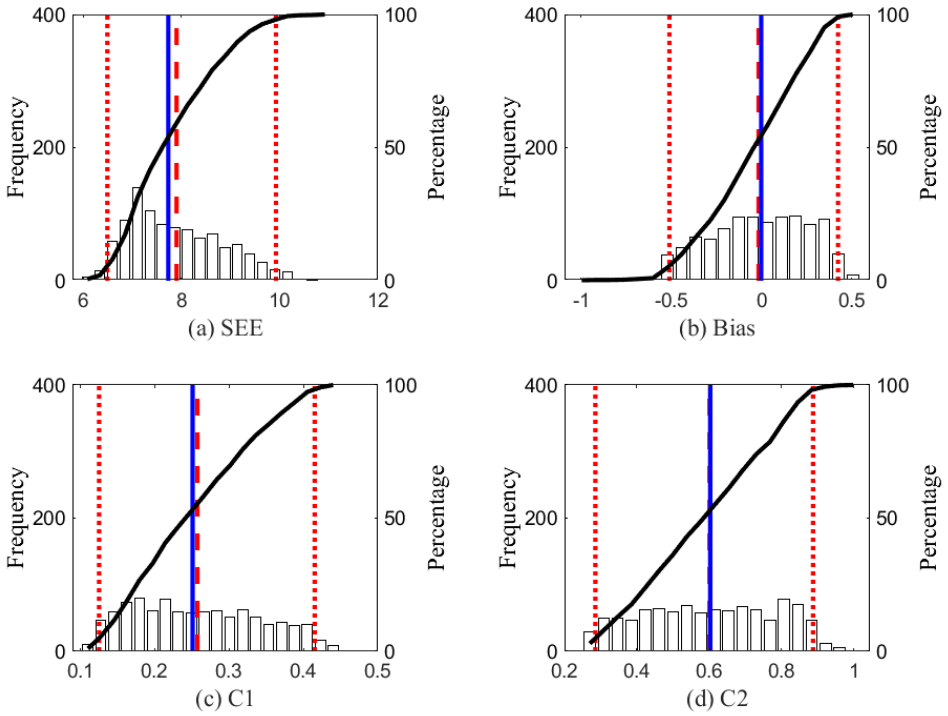

Figure 5-4 Distribution of local calibration parameters – calibration dataset (repeated split sampling)

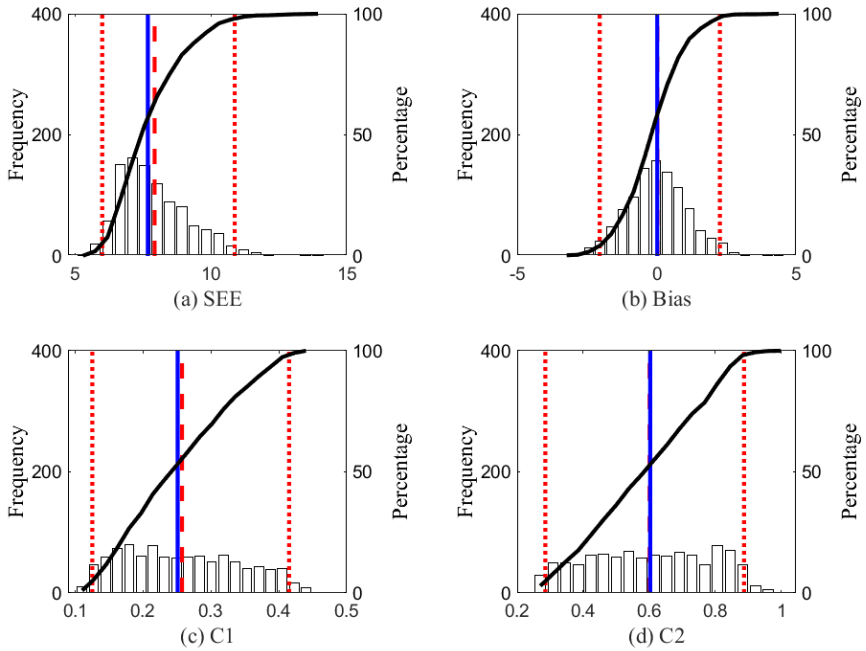

Figure 5-5 Distribution of local calibration parameters – validation dataset (repeated split sampling)

Bootstrapping

Bootstrapping was used as a resampling technique to calibrate the bottom-up cracking model. One thousand bootstrap samples were created, randomly sampling with replacement. Unlike repeated split sampling, in bootstrap, the samples were not split; instead, the entire dataset was used. Bootstrapping also generated CI and distribution of model parameters. Tables 5-7 and 5-8 summarize the model parameters for global and local models, respectively. SEE is slightly increased, whereas bias is significantly improved after local calibration. Figure 5-6 shows the distribution of parameters for the 1000 bootstrap samples.

Table 5-7 Bootstrapping global model summary

Parameter	Global model mean	Global model median	Global model lower CI	Global model upper CI
SEE (% total lane area)	8.30	8.30	7.38	9.20
Bias (% total lane area)	-4.91	-4.91	-5.53	-4.33
C_1	1.31	1.31	-	-
C_2 (h_{ac} < 5 in.)	2.1585	2.1585	-	-
C_2 (5 in. <= h_{ac} <=12 in.)	(0.867+0.2583*h_{ac})*1	(0.867+0.2583* h_{ac})*1	-	-

Table 5-8 Bootstrapping local calibration results summary

Parameter	Local model mean	Local model median	Local model lower CI	Local model upper CI
SEE (% total lane area)	8.73	8.30	6.21	12.83
Bias (% total lane area)	0.00	-0.03	-0.80	0.68
C_1	0.23	0.20	0.01	0.54
C_2 (h_{ac} < 5 in.)	0.70	0.73	0.04	1.29
C_2 (5 in. <= h_{ac} <=12 in.)	(0.867+0.2583* h_{ac})* 0.22	(0.867+0.2583* h_{ac})* 0.23		

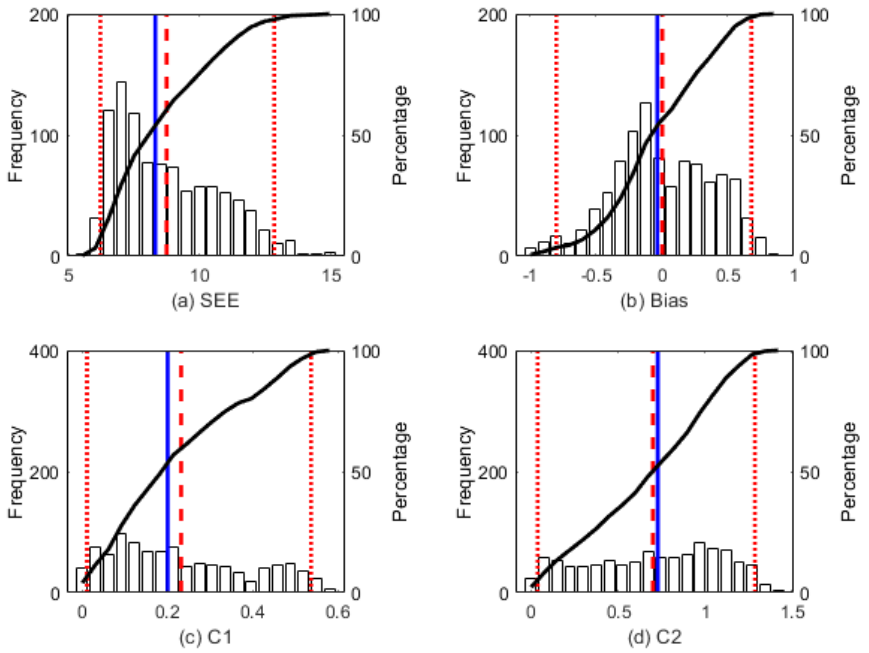

Figure 5-6 Distribution of local calibration parameters (bootstrapping)

Summary

All calibration approaches have significantly improved the bottom-up cracking model. Table 5-9 shows the summary of all sampling techniques. It should be noted that these calibrations were performed with specific limits on the calibration coefficients taken from the literature, as mentioned in Chapter 2. These limits ensure that we get reasonable and practical calibration results.

Table 5-9 Summary of results for all sampling techniques (Option 1a)

Sampling technique	SEE	Bias	C_1	*C2 (hac < 5 in.)*	*C2 (5 in. <= hac <=12 in.)*
No sampling	8.08	0.17	0.22	0.66	(0.867+0.2583* h_{ac})*0.21
Split sampling	7.11	-0.47	0.19	0.78	(0.867+0.2583* h_{ac})*0.26
Repeated split sampling	7.90	-0.02	0.26	0.60	(0.867+0.2583* h_{ac})*0.20
Bootstrapping	8.73	0.00	0.23	0.70	(0.867+0.2583* h_{ac})*0.22

5.2.1.2. Option 1b: Reconstruct only (measured bottom-up cracking only)

In this option, the bottom-up cracking model was calibrated using only bottom-up alligator cracking. This option has fewer measured data points available compared to Option 1a. Figure 5-7 shows global and local models' measured vs. predicted bottom-up cracking. Table 5-10 summarizes all calibration approaches and the model parameters. All approaches have improved the bottom-up cracking model. Bootstrap has the minimum bias followed by repeated split sampling.

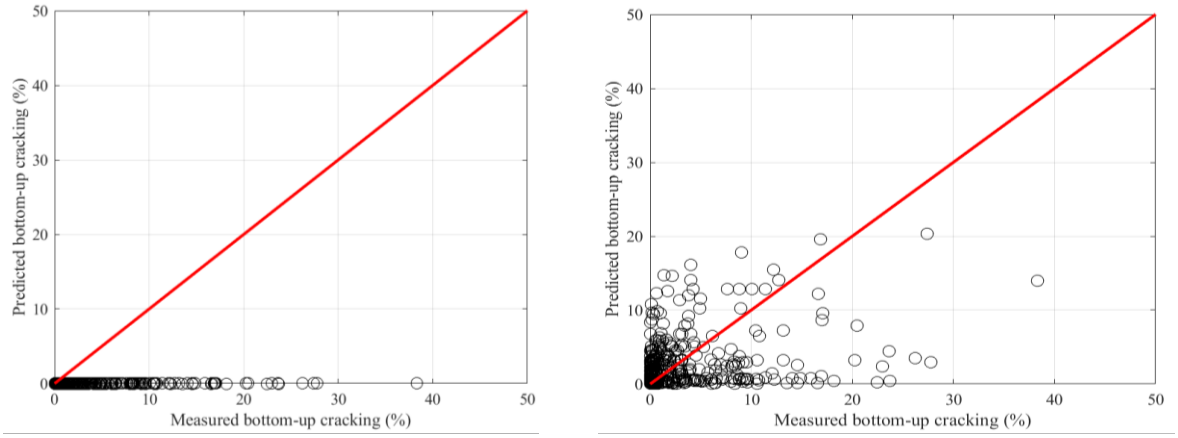

(a) Global model (b) Local model

Figure 5-7 Predicted vs measured bottom-up cracking (No sampling)

Table 5-10 Summary of results for all sampling techniques (Option 1b)

Sampling Technique	SEE	Bias	C_1	*C2 (hac < 5 in.)*	*C2 (5 in. <= hac <=12 in.)*
No sampling	5.81	-0.82	0.23	0.78	0.28
Split sampling	5.87	-0.75	0.20	0.83	0.31
Repeated split sampling	5.78	-0.71	0.26	0.70	0.25
Bootstrapping	5.92	-0.60	0.25	0.73	0.27

It is difficult to identify the initiation of a crack (bottom-up vs. top-down). Also, considering the limited data available for Option 1b, Option 1a should be preferred when bottom-up and top-down cracking data are not differentiated.

5.2.1.3. Reliability for the bottom-up cracking models

The calibration process and the Pavement-ME predictions are obtained at a reliability of 50%. The concept of reliability and method are discussed in detail in Chapter 4. The measured and predicted cracking were sorted in bins based on the expected cracking. The next step was to develop a relationship between the standard deviation of the measured cracking and the mean predicted cracking. Tables 5-11 and 5-12 summarize the standard error equations for Options 1a and 1b.

Table 5-11 Reliability summary for Option 1a

Sampling technique	Global model equation	Local model equation
No Sampling	$s_{e(Alligator)} = 1.13 + \frac{13}{1 + e^{7.57 - 15.5 \times log(D + 0.0001)}}$	$s_{e(Alligator)} = 0.2166 + \frac{6.5879}{1 + e^{0.5604 - 6.3472 \times log(D)}}$
Split Sampling		$s_{e(Alligator)} = 0.2696 + \frac{8.4309}{1 + e^{0.0837 - 1.4108 \times log(D)}}$
Repeated split sampling		$s_{e(Alligator)} = 0.0995 + \frac{13.7673}{1 + e^{0.3303 - 0.3123 \times log(D)}}$
Bootstrapping		$s_{e(Alligator)} = 0.2262 + \frac{14.2350}{1 + e^{0.2958 - 0.1441 \times log(D)}}$

Table 5-12 Reliability summary for Option 1b

Sampling technique	Global model equation	Local model equation
No Sampling	$S_{e(Alligator)} = 1.13 + \frac{13}{1+e^{7.57-15.5\times log(D+0.0001)}}$	$S_{e(Alligator)} = 4.6633 + \frac{10.8653}{1+e^{3.2725-2.0882\times log(D)}}$
Split Sampling		$S_{e(Alligator)} = 5.0476 + \frac{18.6624}{1+e^{12.1108-9.4293\times log(D)}}$
Repeated split sampling		$S_{e(Alligator)} = 4.7465 + \frac{20.5426}{1+e^{4.9276-2.6720\times log(D)}}$
Bootstrapping		$S_{e(Alligator)} = 4.4396 + \frac{25.4391}{1+e^{4.3119-2.2778\times log(D)}}$

5.2.2 Fatigue Cracking Model – Top-down

The following section shows the calibration of the top-down cracking model. The model contains crack initiation and crack propagation models. Since the actual crack initiation time is not known, it was not possible to calibrate the crack initiation model separately. So, a single function was used by substituting the crack initiation function with the crack propagation function. Initially, an attempt was made to change all eight coefficients simultaneously. This approach had some challenges:

- The model has some mathematical limitations. High values for C_3 give mathematical errors in the Pavement-ME output.
- There is no current literature available for the top-down cracking model. Therefore, estimating the range for each coefficient to be used in optimization was difficult.
- The model has numerous coefficients with coefficient values ranging from 0.011 to 64271618. This makes the optimization challenging to converge.

The top-down cracking model was calibrated in Microsoft excel by combining engineering judgment and the solver function. Four coefficients from the crack initiation function (*kL2, kL3, kL4, kL5)* and two from the crack propagation function (C_1, C_2) have been calibrated. Only no sampling method was used for this calibration.

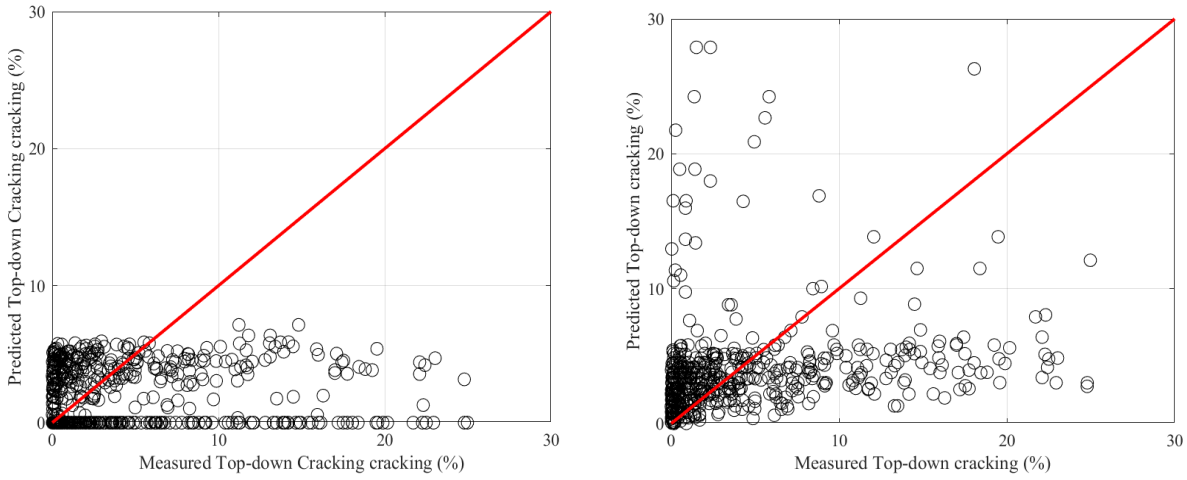

(a) Global model (b) Local model

Figure 5-8 Predicted vs. measured top-down cracking (No sampling)

Figure 5-8 shows only the predicted vs. measured top-down cracking for reconstruction sections (Option 1). Figure 5-9 shows the predicted and measured top-down cracking with time. The predicted and measured top-down cracking does not follow similar trends. Most top-down cracking predictions are limited to a specific time series curve. Table 5-13 summarizes model parameters for Option 1. The SEE and bias are improved. Table 5-14 shows the summary of calibrations for all options. The reliability of the top-down cracking model is estimated by developing a relationship between the standard deviation of the measured cracking, and the mean predicted cracking. Table 5-15 outlines the standard error equations for all options.

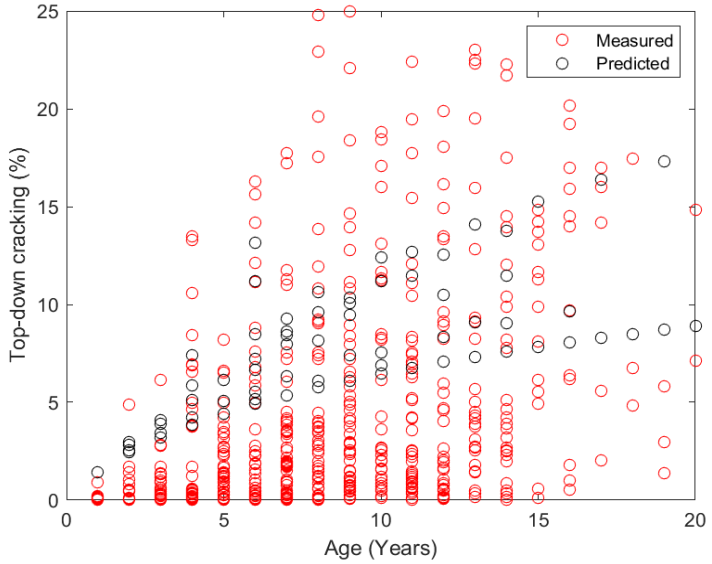

Figure 5-9 Measured and predicted top-down-cracking (time series)

Table 5-13 Calibration results for top-down cracking (Option 1)

Parameters	Global model	Local model
SEE	6.37	5.59
Bias	-2.36	1.60
K_{L2}	0.2855	0.90
K_{L3}	0.011	0.09
K_{L4}	0.01488	0.101
K_{L5}	3.266	3.260
C_1	2.5219	0.30
C_2	0.8069	1.155

Table 5-14 Summary of calibration results for top-down cracking

Parameters	Option 1	Option 2	Option 3 (HMA over HMA)	Option 3 (Composite)
SEE	5.59	7.51	4.10	5.32
Bias	1.60	0.25	0.00	0.16
K_{L2}	0.90	0.4887	0.714	0.475
K_{L3}	0.09	0.0956	0.093	0.097
K_{L4}	0.101	0.101	0.102	0.104
K_{L5}	3.260	0.1895	0.191	0.206
C_1	0.30	0.0855	0.084	0.104
C_2	1.155	1.9583	2.007	1.635

Table 5-15 Reliability summary for top-down cracking

MDOT Pavement options	Global model equation	Local model equation
Option 1	$s_{e(Top-down)} = 0.3657 \times TOP + 3.6563$	$s_{e(Top-down)} = 0.6417 \times TOP + 0.5014$
Option 2		$s_{e(Top-down)} = 0.1467 \times TOP + 1.6998$
Option 3 (HMA over HMA)		$s_{e(Top-down)} = 0.838 \times TOP + 0.0269$
Option 3 (Composite)		$s_{e(Top-down)} = 0.9236 \times TOP + 0.6452$

5.2.3 Rutting Model

Rutting in the Pavement-ME is a sum of permanent deformations from individual layers. The research team adopted the following two different approaches:

1. *Method 1: Individual layer rutting calibrations* — For this approach, the measured rutting from individual layers was matched against the predictions from Pavement-ME (β_{1r}, $\beta_{s1,}$ and β_{sg1} were calibrated separately). The total measured rutting was multiplied by the percent contribution from each layer to get measured rutting for the individual layer. The percentage contribution was estimated using transverse pavement profile analysis, as shown in Figure 4-4. The contribution of AC layer rutting is over 70% for all pavement types. The standard error equations for rutting in the Pavement-ME are separate for individual layers. This method was used to evaluate the standard error equations for rutting in each layer.
2. *Method 2: Total surface rutting calibration* — The total measured rutting was calibrated against the sum of individual predicted rutting (β_{1r}, $\beta_{s1,}$ and β_{sg1} were calibrated simultaneously).

It is worth noting that composite sections do not show any rutting predictions for the base and subgrade layers. Therefore, composite sections were only calibrated for AC rutting. Similarly, for Option 2, AC rutting was only calibrated. The individual layer contribution to total rutting was estimated using the transverse profiles for each pavement section based on the transverse profile analysis presented in Chapter 4.

5.2.3.1. Option 1: Reconstruct pavements only – Method 1

This section outlines the calibration of individual layer rutting using reconstruct sections only.

No Sampling

Pavement-ME predictions for individual layer rutting were matched against measured rutting determined by using the transverse profile analysis results, as discussed in Chapter 4. Figures 5-10 to 5-12 show the predicted vs. measured rutting for AC, base, and subgrade layers, respectively. The Pavement-ME under-predicts AC rutting and over-predicts base and subgrade rutting. Table 5-16 shows the hypothesis results for each layer. None of the hypotheses met for both global or local models. Table 5-17 shows the SEE and bias, whereas Table 5-18 shows the calibrated coefficients. Both SEE and bias significantly improved for all layers.

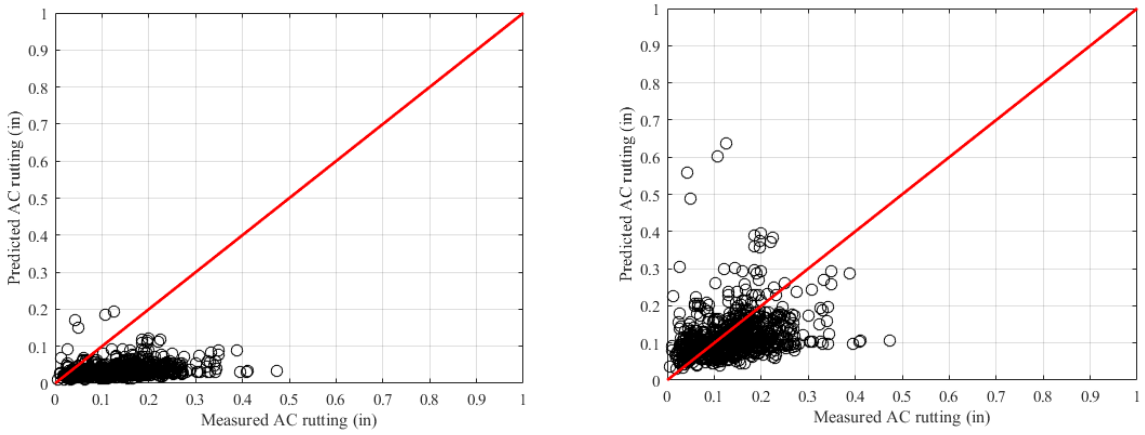

(a) Global model (b) Local model

Figure 5-10 Predicted vs. measured AC rutting (No sampling)

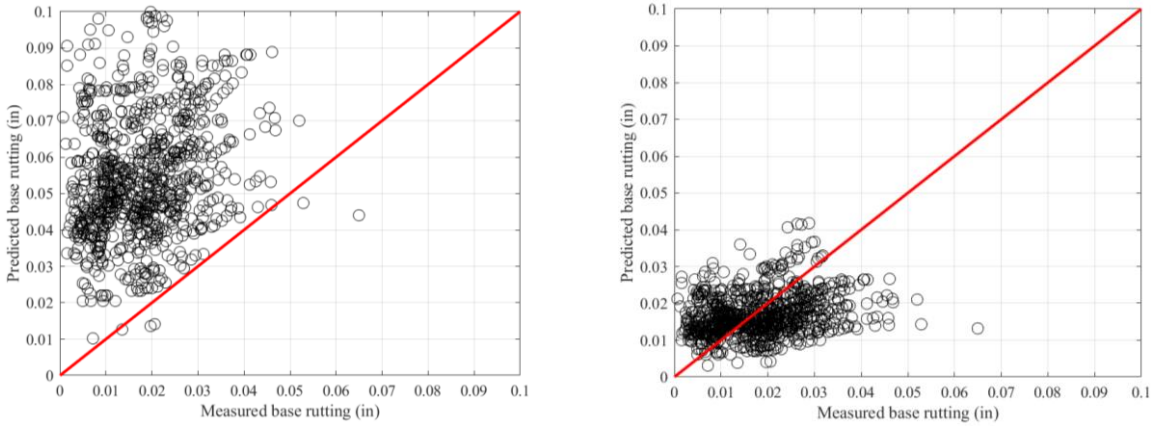

(a) Global model (b) Local model

Figure 5-11 Predicted vs. measured base rutting (No sampling)

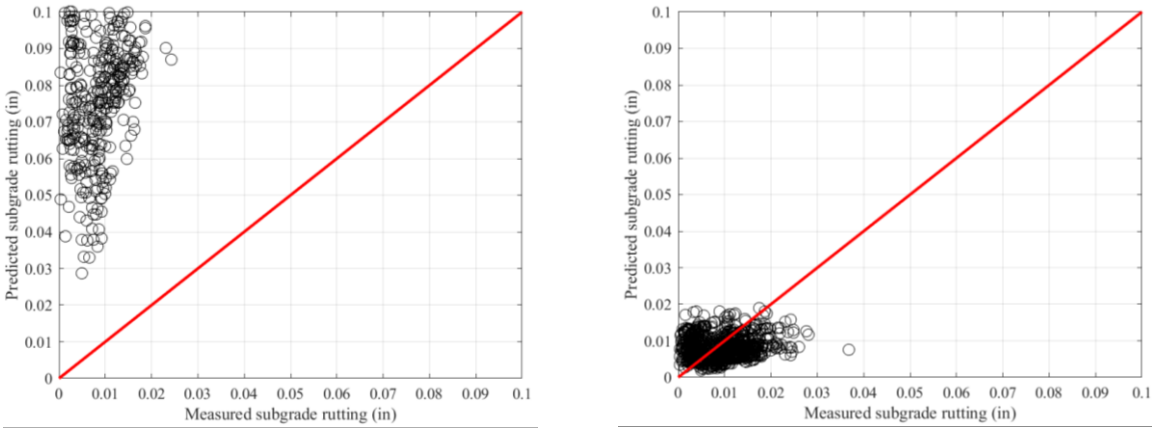

(a) Global model (b) Local model

Figure 5-12 Predicted vs. measured subgrade rutting (No sampling)

Table 5-16 Rutting models hypothesis testing results

Layer	Global model			Local model		
	t-test *p*-value	Intercept *p*-value	Slope = 1 *p*-value	t-test *p*-value	Intercept *p*-value	Slope = 1 *p*-value
HMA rut	0.0000	0.0000	0.0000	0.0000	0.0000	0.0000
Base rut	0.0000	0.0000	0.0000	0.0010	0.0000	0.0000
Subgrade	0.0000	0.0000	0.0000	0.0000	0.0000	0.0000

Table 5-17 Rutting models SEE and bias

Layer	Global model		Local model	
	SEE (in.)	Bias (in.)	SEE (in.)	Bias (in.)
HMA rut	0.2579	0.2015	0.0812	-0.0138
Base rut	0.0426	0.0380	0.0099	-0.0011
Subgrade	0.1184	0.1095	0.0062	-0.0009

Table 5-18 Rutting model calibration coefficients

Calibration coefficient	Global model	Local model
HMA rutting (br1)	0.4	0.1466
Base rutting (bs1)	1.0000	0.3003
Subgrade rutting (bsg1)	1.0000	0.0691

Split Sampling

Split sampling was performed on 70% of the sections for the calibration set and 30% for the validation set. Figures 5-13 to 5-15 show the predicted vs. measured for calibration and validation set for different layers. All layers show reasonable validation results. Table 5-19 shows the SEE, bias, and model parameters for the global model, and Table 5-20 shows the same for the calibration-validation set. Both SEE and bias significantly improved for all layers.

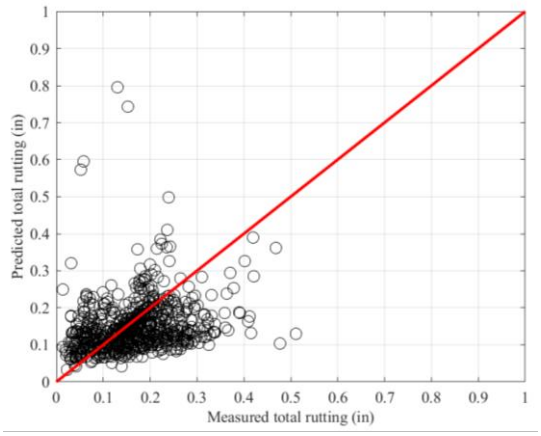

(a) Calibration set

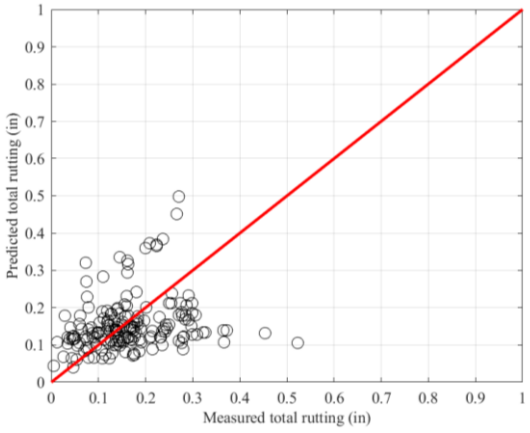

(b) Validation set

Figure 5-13 Predicted vs measured AC rutting (Split sampling)

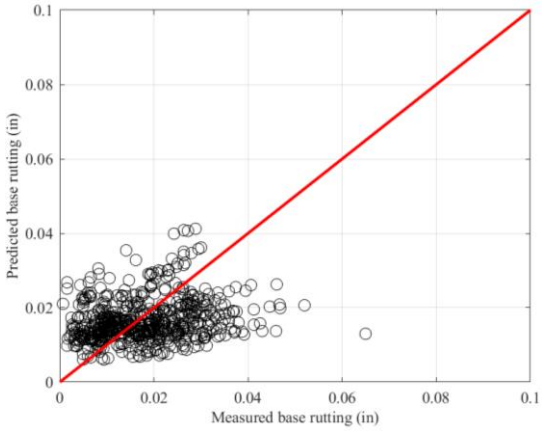

(a) Calibration set

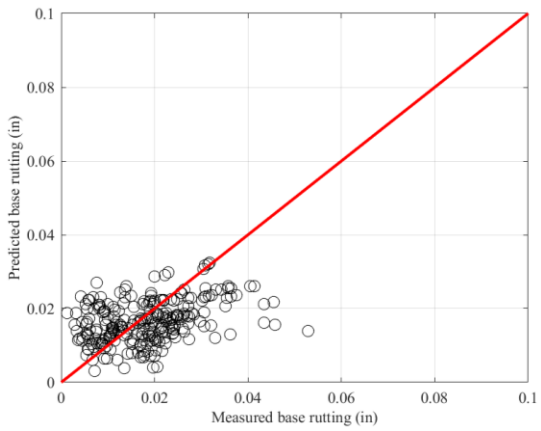

(b) Validation set

Figure 5-14 Predicted vs measured Base rutting (Split sampling)

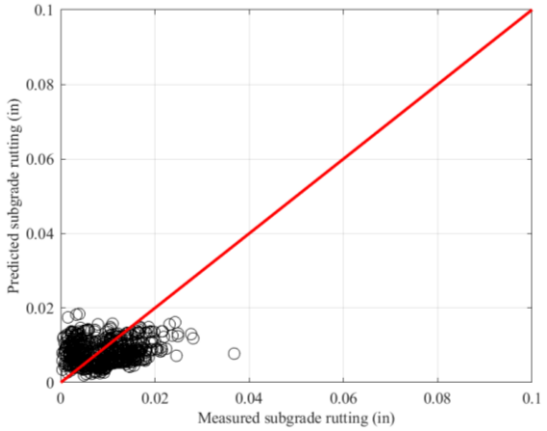

(a) Calibration set

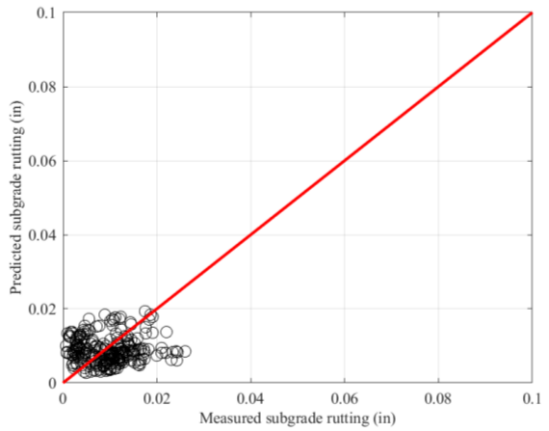

(b) Validation set

Figure 5-15 Predicted vs measured Subgrade rutting (Split sampling)

Table 5-19 Rutting global model results

Layer	SEE	Bias	Coefficient
HMA rut	0.2454	0.1759	0.4
Base rut	0.0872	-0.0138	1.0000
Subgrade	0.1153	0.1071	1.0000

Table 5-20 Rutting local model results

Layer	Calibration set			Validation set		
	SEE	Bias	Coefficient	SEE	Bias	Coefficient
HMA rut	0.0962	-0.0165	0.0705	0.1008	-0.0117	0.0705
Base rut	0.0102	-0.0012	0.2955	0.0092	-0.0018	0.2955
Subgrade	0.0061	-0.0008	0.0705	0.0064	-0.0007	0.0705

Repeated Split Sampling

Repeated split sampling was performed for 1000 split samples with new calibration and validation sets. Figures 5-16 to 5-18 show the distribution of model parameters for calibration and validation set for different layers. Tables 5-21 to 5-23 show the SEE, bias, model parameters, CI for the global model, and the calibration and validation sets, respectively. The rutting model significantly improved after local calibration.

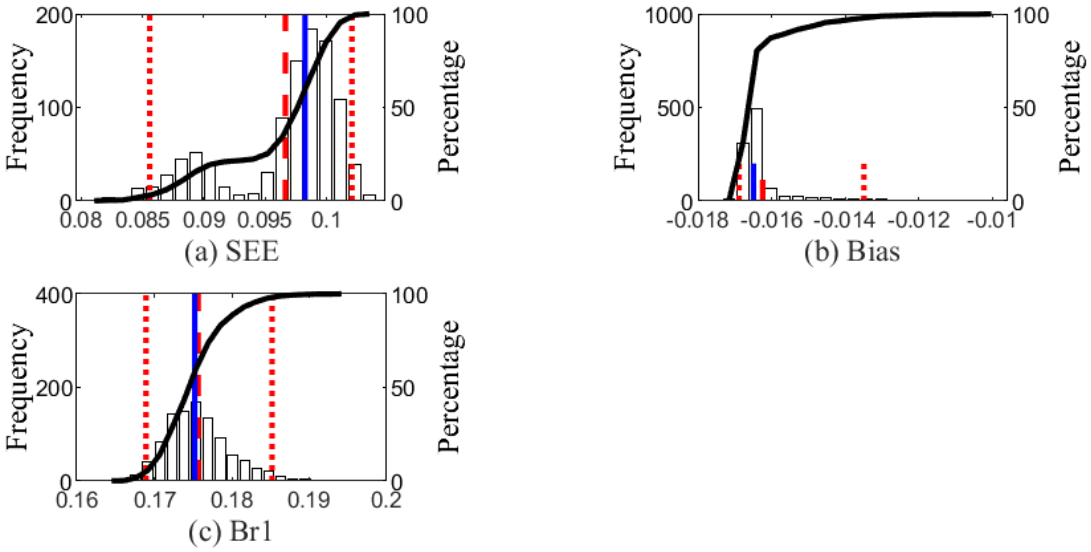

(a) Calibration set

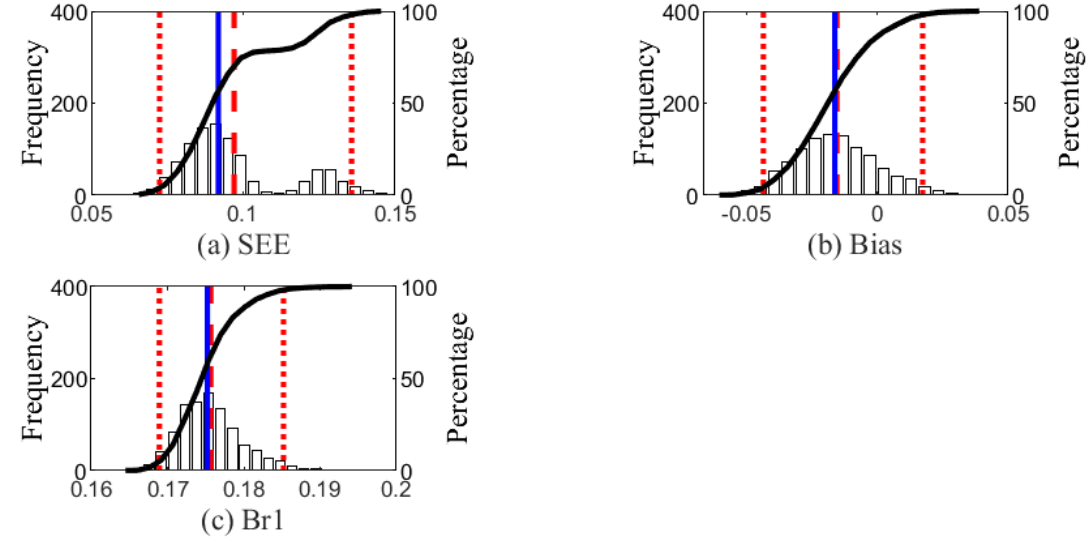

(b) Validation set

Figure 5-16 Distribution of calibration parameters - AC rutting (Repeated split sampling)

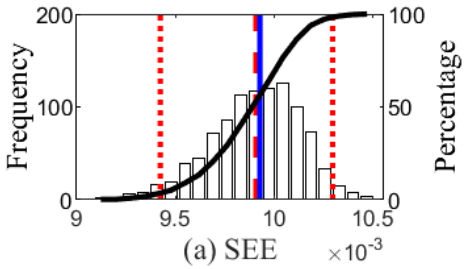

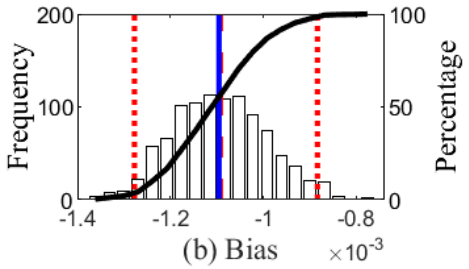

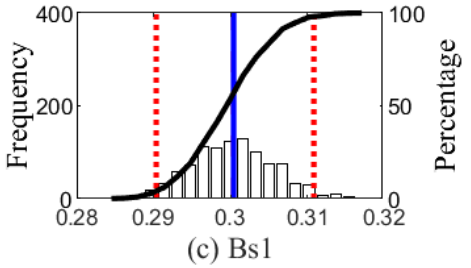

(a) Calibration set

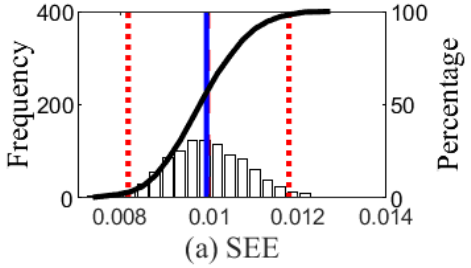

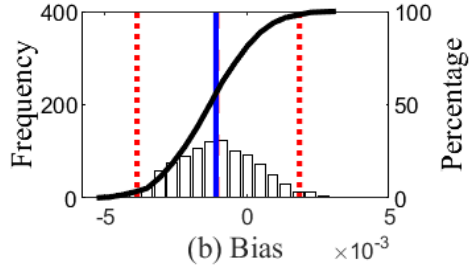

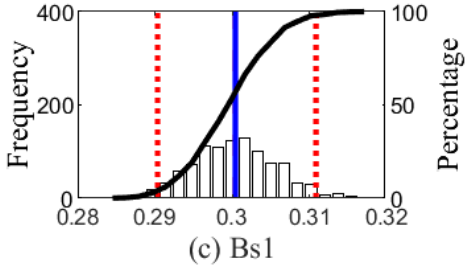

(b) Validation set

Figure 5-17 Distribution of calibration parameters - Base rutting (Repeated split sampling)

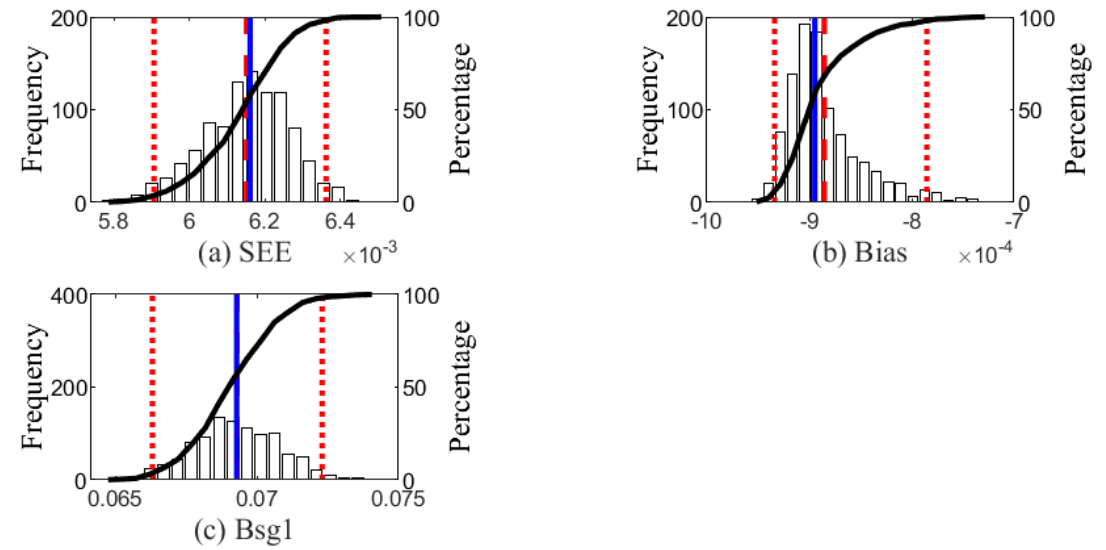

(a) Calibration set

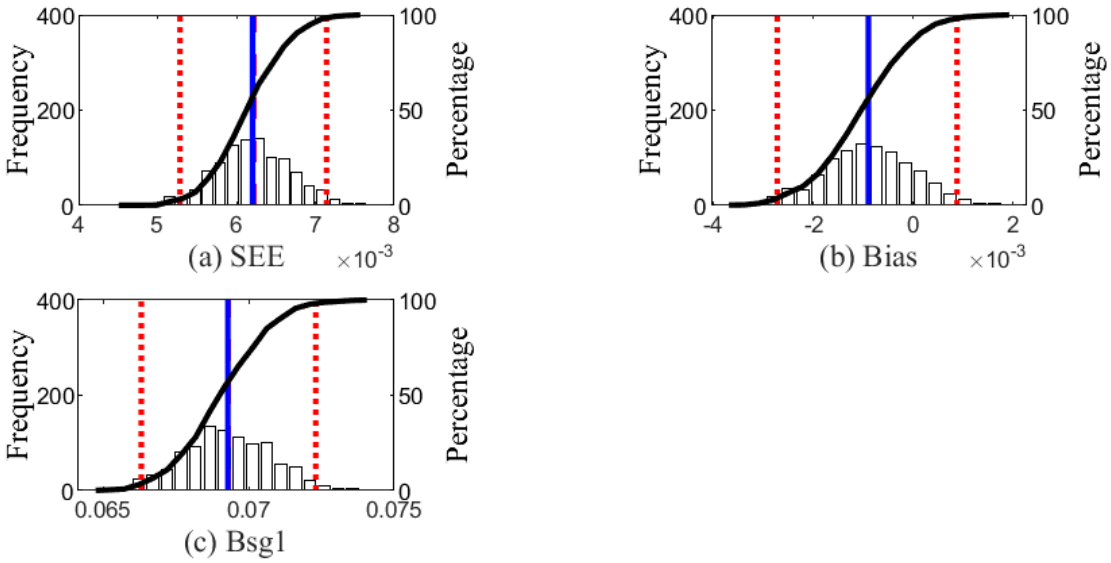

(b) Validation set

Figure 5-18 Distribution of calibration parameters - Subgrade rutting (Repeated split sampling)

Table 5-21 Global model results (repeated split sampling)

Layer	Average SEE	SEE Lower CI	SEE Upper CI	Average bias (in.)	Bias Lower CI	Bias Upper CI
HMA	0.2387	0.2097	0.2540	0.1743	0.1617	0.1853
Base	0.0426	0.0409	0.0440	0.0380	0.0367	0.0394
Subgrade	0.1185	0.1150	0.1216	0.1095	0.1064	0.1126

Table 5-22 Local model calibration results (repeated split sampling)

Statistics	HMA rutting	Base rutting	Subgrade rutting
Average SEE	0.0966	0.0099	0.0062
SEE Lower CI	0.0856	0.0094	0.0059
SEE Upper CI	0.1021	0.0103	0.0064
Average bias (in.)	-0.0162	-0.0011	-0.0009
Bias Lower CI	-0.0169	-0.0013	-0.0009
Bias Upper CI	-0.0135	-0.0009	-0.0008
Average calibration coefficient	0.1757	0.3003	0.0693
Calibration coefficient Lower CI	0.1689	0.2897	0.0663
Calibration coefficient Upper CI	0.1852	0.3115	0.0723

Table 5-23 Local model validation results (repeated split sampling)

Statistics	HMA rutting	Base rutting	Subgrade rutting
Average SEE	0.0971	0.0100	0.0062
SEE Lower CI	0.0725	0.0084	0.0053
SEE Upper CI	0.1358	0.0119	0.0071
Average bias (in.)	-0.0153	-0.0011	-0.0009
Bias Lower CI	-0.0434	-0.0041	-0.0027
Bias Upper CI	0.0174	0.0017	0.0009
Average calibration coefficient	0.1757	0.3003	0.0693
Calibration coefficient Lower CI	0.1689	0.2897	0.0663
Calibration coefficient Upper CI	0.1852	0.3115	0.0723

Bootstrapping

Bootstrapping was performed with 1000 bootstrap samples with replacement. Figures 5-19 to 5-21 show the distribution of model parameters for AC, base, and subgrade rutting. Tables 5-24 and 5-25 summarize the calibration results for the global and local models. Model parameter distribution and CI provide a more reliable estimate of model coefficients. Moreover, SEE and bias significantly improved for all layers.

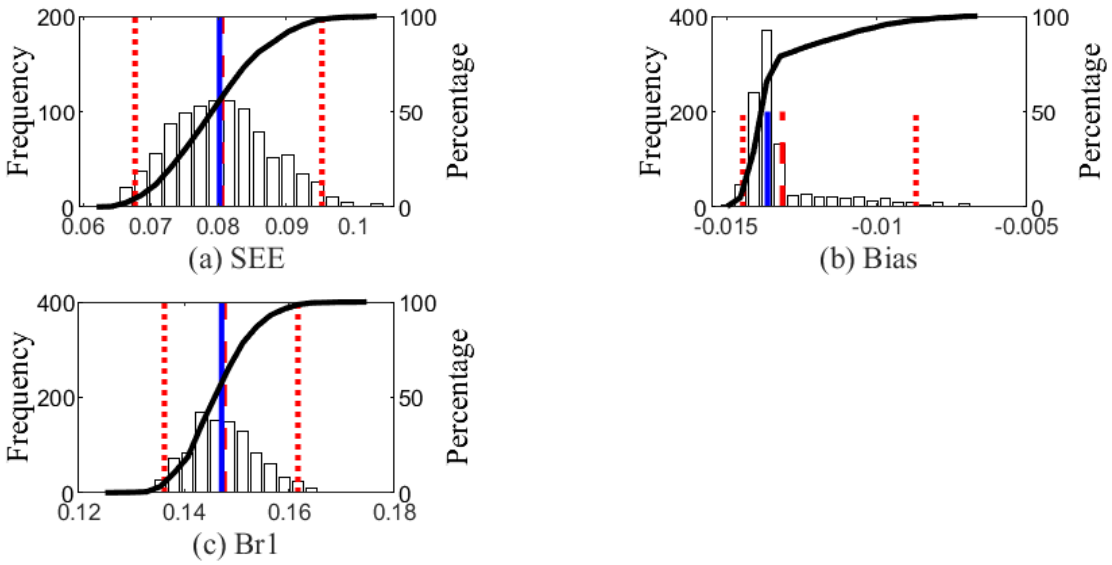

Figure 5-19 Distribution of calibration parameters - AC rutting (Bootstrapping)

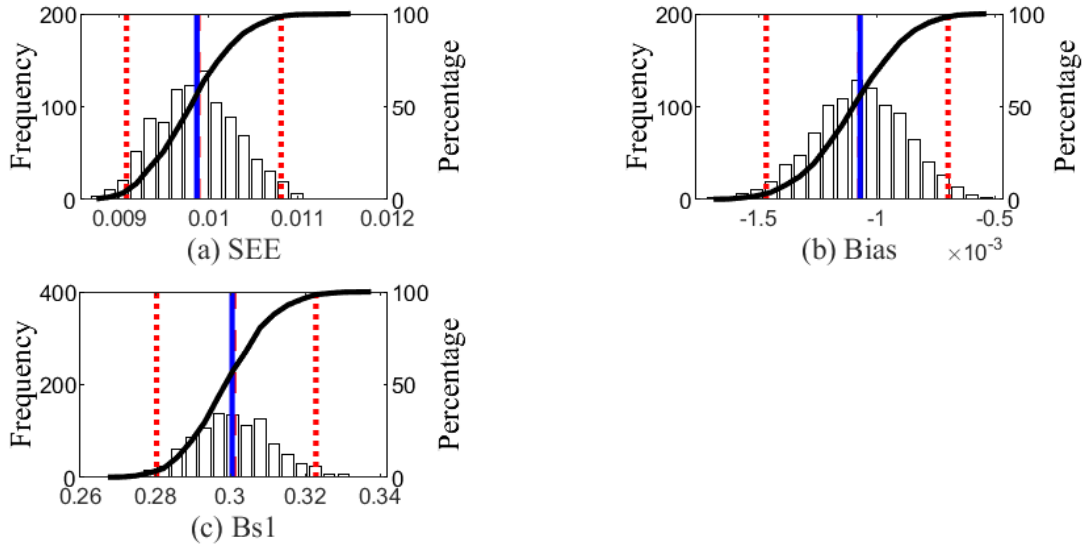

Figure 5-20 Distribution of calibration parameters - Base rutting (Bootstrapping)

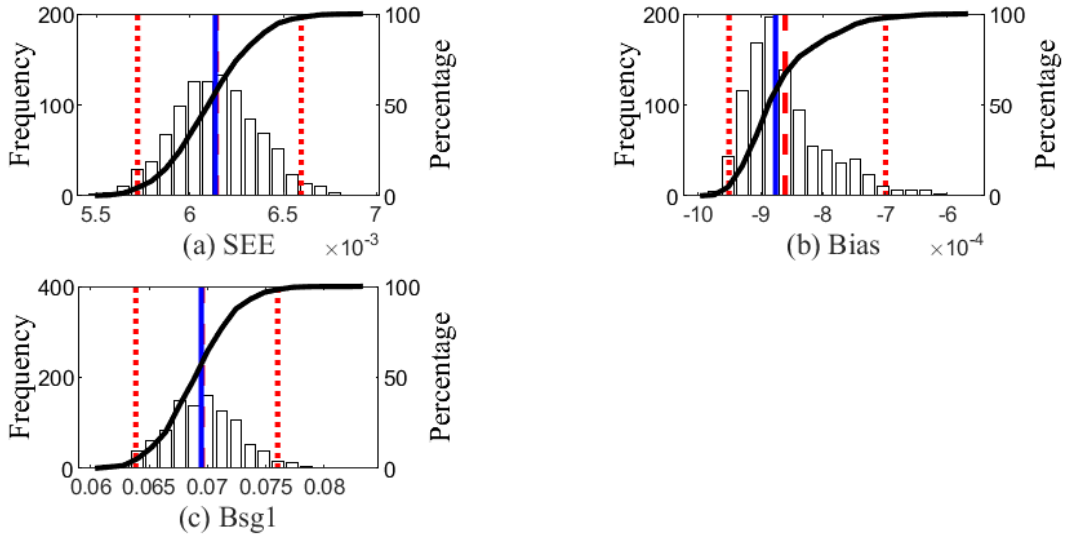

Figure 5-21 Distribution of calibration parameters-Subgrade rutting (Bootstrapping)

Table 5-24 Global rutting model

Layer type	Average SEE	SEE Lower CI	SEE Upper CI	Average bias (in.)	Bias Lower CI	Bias Upper CI
HMA	0.2565	0.2174	0.3047	0.2010	0.1796	0.2238
Base	0.0425	0.0396	0.0456	0.0380	0.0355	0.0408
Subgrade	0.1183	0.1117	0.1251	0.1094	0.1032	0.1159

Table 5-25 Local rutting model

Statistics	HMA rutting	Base rutting	Subgrade rutting
Average SEE	0.0805	0.0099	0.0061
SEE Lower CI	0.0677	0.0091	0.0057
SEE Upper CI	0.0953	0.0108	0.0066
Average bias (in.)	-0.0131	-0.0011	-0.0009
Bias Lower CI	-0.0145	-0.0015	-0.0010
Bias Upper CI	-0.0087	-0.0007	-0.0007
Average calibration coefficient	0.1476	0.3009	0.0696
Calibration coefficient Lower CI	0.1363	0.2803	0.0639
Calibration coefficient Upper CI	0.1616	0.3228	0.0760

Summary

Results for method 1 are summarized in Table 5-26. All calibration approaches have improved the SEE and bias. Bootstrap shows the lowest SEE and bias for all layers.

Table 5-26 Rutting model calibration results summary – Option 1 Method 1

Sampling Technique	Pavement layer rutting	SEE	Bias	Calibration coefficient
No sampling	HMA	0.0812	-0.0138	0.1466
	Base	0.0099	-0.0011	0.3003
	Subgrade	0.0062	-0.0009	0.0691
Split sampling	HMA	0.0962	-0.0165	0.0705
	Base	0.0102	-0.0012	0.2955
	Subgrade	0.0061	-0.0008	0.0705
Repeated split sampling	HMA	0.0971	-0.0153	0.1757
	Base	0.0099	-0.0011	0.3003
	Subgrade	0.0062	-0.0009	0.0693
Bootstrapping	HMA	0.080	-0.013	0.148
	Base	0.010	-0.001	0.301
	Subgrade	0.006	-0.001	0.070

5.2.3.2. Option 1: Reconstruct pavements only – Method 2

In this method, the measured total rutting was calibrated against predicted total rutting. Total predicted rutting is simply the sum of rutting predictions for individual layers. Calibration coefficients of all layers were simultaneously changed to match the total predicted rutting with measured rutting. Table 5-27 shows the results of the hypothesis tests. Two out of three tests fail for the local model. Figure 5-22 shows the predicted vs. measured total rutting for the global and local models. Table 5-28 shows the calibration results for the global and local models. The SEE is reduced from 0.3935 to 0.0782, whereas the bias is reduced from 0.3491 to -0.0035.

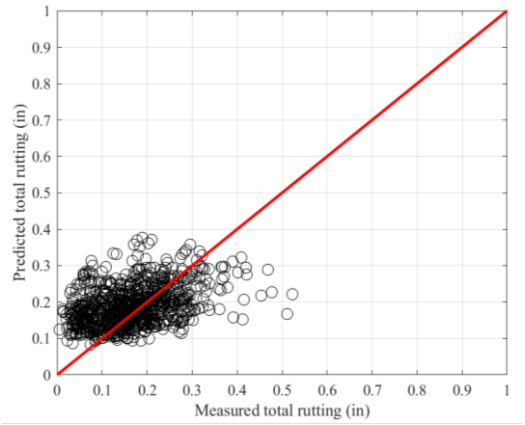

(a) Global model

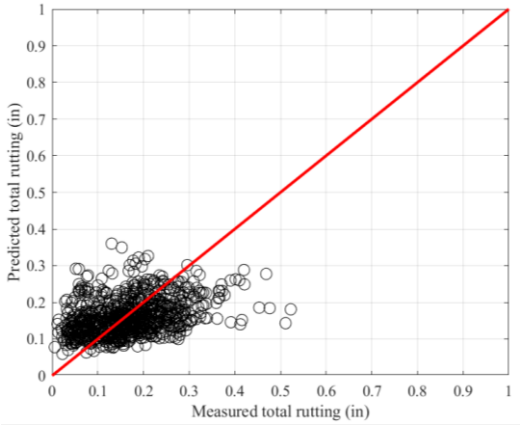

(b) Local model

Figure 5-22 Predicted vs measured Total rutting (No sampling)

Table 5-27 Hypothesis testing results for total rutting

Layer	Global model	Local model
t-test p-value	0.0000	0.1859
Intercept p-value	0.0000	0.0000
Slope = 1 p-value	0.0000	0.0000

Table 5-28 total rutting model calibration results

Layer	Global model	Local model
SEE	0.3935	0.0782
Bias	0.3491	-0.0035
HMA rutting (br1)	0.4000	0.0372
Base rutting (bs1)	1.0000	0.9910
Subgrade rutting (bsg1)	1.0000	0.6308

Figure 5-23 shows the measured and predicted total rutting with time. The predictions are close to the measured values for most of the rutting range.

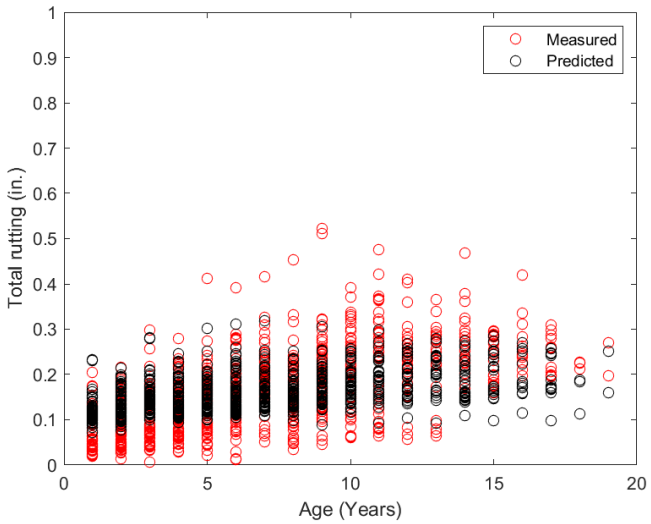

Figure 5-23 Measured and predicted total rutting-Time series

Summary

Like method 1, all four calibration approaches were applied to method 2. Table 5-29 summarizes the SEE, bias, and calibration coefficients for all sampling techniques. The SEE and bias improved for all calibration approaches.

Table 5-29 Summary results for all sampling techniques

Sampling Technique	SEE	Bias	β_{1r}	β_{s1}	β_{sg1}
No sampling	0.0782	-0.0035	0.0372	0.9910	0.6308
Split sampling	0.0851	-0.0094	0.0470	1.0002	1.0287
Repeated split sampling	0.0858	-0.0071	0.0962	0.6907	0.6768
Bootstrapping	0.085	-0.008	0.061	0.921	0.963

5.2.3.3. Option 2: Reconstruct and rehabilitated pavements – Method 1

As explained before, only AC rutting was calibrated under this option. Table 5-30 summarizes the SEE, bias, and calibration coefficients.

Table 5-30 Summary of AC rutting for all sampling techniques

Sampling technique	SEE	Bias	Calibration coefficient
No sampling	0.0742	-0.0185	1.3200
Split sampling	0.0752	-0.0127	1.3651
Repeated split sampling	0.0742	-0.0127	1.3884
Bootstrapping	0.0738	-0.0204	1.2978

5.2.3.4. Option 3: HMA over HMA pavements only – Method 1

Table 5-31 shows all calibration approaches' SEE, bias, and calibration coefficients.

Table 5-31 Summary of calibration results (Option 3 – Method 1)

Sampling Technique	Pavement layer rutting	SEE	Bias	Calibration coefficient
No sampling	HMA	0.0555	-0.0076	1.0295
	Base	0.0138	-0.0022	0.3760
	Subgrade	0.0061	-0.0003	0.1208
Split sampling	HMA	0.0592	-0.0098	1.1278
	Base	0.0133	-0.0022	0.3898
	Subgrade	0.0067	-0.0004	0.1236
Repeated split sampling	HMA	0.0553	-0.0074	1.0336
	Base	0.0137	-0.0020	0.3795
	Subgrade	0.0060	-0.0003	0.1208
Bootstrapping	HMA	0.0548	-0.0074	1.0423
	Base	0.0135	-0.0020	0.3824
	Subgrade	0.0059	-0.0003	0.1213

5.2.3.5. Option 3: HMA over HMA pavements only – Method 2

The results for this option are presented in Table 5-32.

Table 5-32 Summary of calibration results (Option 3 – Method 2)

Sampling technique	SEE	Bias	br1	bs1	bsg1
No sampling	0.0693	-0.0041	0.6145	0.4547	0.5353
Split sampling	0.0815	-0.0116	0.6862	0.8814	1.1995
Repeated split sampling	0.0781	-0.0075	0.4405	0.7913	0.8325
Bootstrapping	0.077	-0.009	0.510	0.752	0.738

5.2.3.6. Option 3: Composite pavements only – Method 1

The results for Option 3 – Method 2 are presented in Table 5-33. As mentioned before, composite pavements were calibrated for AC rutting only.

Table 5-33 Calibration results for composite pavements – Method 1

Sampling technique	SEE	Bias	Calibration coefficient
No sampling	0.0622	-0.0170	1.1400
Split sampling	0.0629	-0.0107	1.4742
Repeated split sampling	0.0618	-0.0106	1.5295
Bootstrapping	0.0614	-0.0102	1.5351

5.2.3.7. Reliability for the rutting model

The rutting predictions using the calibrated model are at 50% reliability. The standard error equations were formulated using the standard deviation of the measured cracking and mean predicted cracking to incorporate reliability in the model. Tables 5-34 to 5-37 show the standard error equation for Option 1 using different calibration approaches.

Table 5-34 Rutting model reliability for Option 1 – Method 1 – No sampling

Pavement layer	Global model equation	Local model equation
HMA rutting	$s_{e(HMA)} = 0.24(Rut_{HMA})^{0.8026} + 0.001$	$s_{e(HMA)} = 0.137(Rut_{HMA})^{0.3728}$
Base rutting	$s_{e(base)} = 0.1477(Rut_{base})^{0.6711} + 0.001$	$s_{e(base)} = 0.0597(Rut_{base})^{0.4484}$
Subgrade	$s_{e(subgrade)} = 0.1235\left(Rut_{subgrade}\right)^{0.5012} + 0.001$	$s_{e(subgrade)} = 0.0815\left(Rut_{subgrade}\right)^{0.5662}$

Table 5-35 Rutting model reliability for Option 1 – Method 1 – Split sampling

Pavement layer	Global model equation	Local model equation
HMA rutting	$s_{e(HMA)} = 0.24(Rut_{HMA})^{0.8026} + 0.001$	$s_{e(HMA)} = 0.1315(Rut_{HMA})^{0.2833}$
Base rutting	$s_{e(base)} = 0.1477(Rut_{base})^{0.6711} + 0.001$	$s_{e(base)} = 0.0318(Rut_{base})^{0.2877}$
Subgrade	$s_{e(subgrade)} = 0.1235\left(Rut_{subgrade}\right)^{0.5012} + 0.001$	$s_{e(subgrade)} = 0.149\left(Rut_{subgrade}\right)^{0.688}$

Table 5-36 Rutting model reliability for Option 1 – Method 1 – Repeated split sampling

Pavement layer	Global model equation	Local model equation
HMA rutting	$s_{e(HMA)} = 0.24(Rut_{HMA})^{0.8026} + 0.001$	$s_{e(HMA)} = 0.1324(Rut_{HMA})^{0.3184}$
Base rutting	$s_{e(base)} = 0.1477(Rut_{base})^{0.6711} + 0.001$	$s_{e(base)} = 0.0582(Rut_{base})^{0.4427}$
Subgrade	$s_{e(subgrade)} = 0.1235\left(Rut_{subgrade}\right)^{0.5012} + 0.001$	$s_{e(subgrade)} = 0.0341\left(Rut_{subgrade}\right)^{0.3988}$

Table 5-37 Rutting model reliability for Option 1 – Method 1 - Bootstrap

Pavement layer	Global model equation	Local model equation
HMA rutting	$s_{e(HMA)} = 0.24(Rut_{HMA})^{0.8026} + 0.001$	$s_{e(HMA)} = 0.1481(Rut_{HMA})^{0.4175}$
Base rutting	$s_{e(base)} = 0.1477(Rut_{base})^{0.6711} + 0.001$	$s_{e(base)} = 0.0411(Rut_{base})^{0.3656}$
Subgrade	$s_{e(subgrade)} = 0.1235\left(Rut_{subgrade}\right)^{0.5012} + 0.001$	$s_{e(subgrade)} = 0.0728\left(Rut_{subgrade}\right)^{0.5456}$

5.2.4 Transverse (thermal) Cracking Model

The thermal cracking model was calibrated for Level 1 inputs in the Pavement-ME. The model calibration only considered sections with Performance Grade (PG) binder type. Calibration approaches for different options are discussed in the following sections. The thermal cracking model for Option 1 was calibrated as a single *K*-value by running Pavement-ME multiple times. Thermal cracking and Reflective cracking models for Option 3 were calibrated using CAT. Since rehabilitation sections have combined thermal cracking and reflective cracking, which cannot be separated, the thermal cracking model was not calibrated for Option 2.

5.2.4.1. Option 1: Reconstruct pavements only

Although calibration coefficient *K* is a function of mean annual air temperature (MAAT), it was calibrated as a single value similar to the previous version of Pavement-ME (version 2.3). For this purpose, the Pavement-ME was run at different *K* values (0.25,0.65,0.75,0.85, 0.95 and 1.35). SEE and bias were determined for each value of *K*. Table 5-38 summarizes the SEE and bias for the global model and for different *K* values. Based on the SEE and bias, a value of 0.85 is recommended. Recalibration improved the SEE and bias, but thermal cracking predictions still show high variability. Figure 5-24 shows the predicted vs. measured thermal cracking for the global and local models at *K*=0.85. As previously explained in Chapter 3, measured thermal cracking values have been capped at 2112 feet/mile. This means any measured value of more than 2112 feet/mile for sections has been removed from the calibration data.

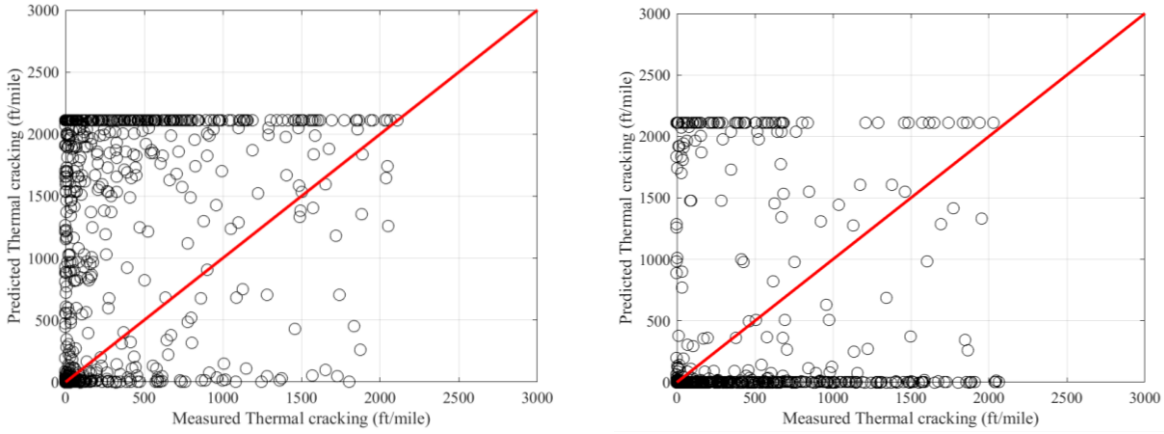

(a) Global model (b) Local model

Figure 5-24 Option 1 measured versus predicted transverse (thermal) cracking, (local at *K=0.85*)

Table 5-38 Transverse thermal cracking results – Option 1

Parameter	SEE	Bias
Global model	1225	-812
K = 0.25	650	272
K = 0.65	760	172
K = 0.75	813	106
K = 0.85	851	20
K = 0.95	893	-71
K = 1.35	1077	-471

5.2.4.2. Option 3: HMA over HMA pavements only

Both thermal cracking and reflective cracking coefficients were calibrated for HMA over HMA sections. Figure 5-25 shows the predicted vs. measured thermal with reflective cracking for the global and local models. Table 5-39 summarizes global and local mode's SEE, bias, and calibration coefficients. The local model has improved the SEE and bias.

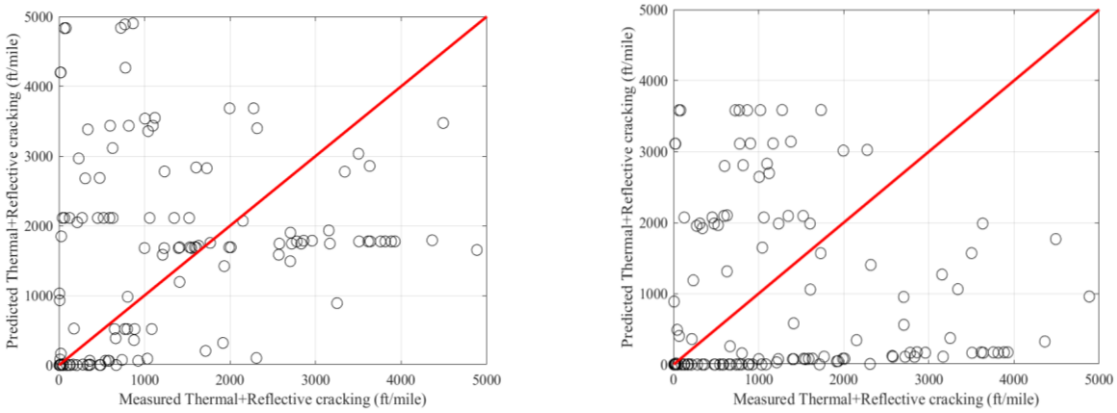

(a) Global model (b) Local model

Figure 5-25 Option 3 measured versus predicted thermal cracking-HMA over HMA

Table 5-39 Transverse (thermal) cracking results – Option 3 (HMA over HMA)

Parameter	Global model	Local model
SEE	1856	1720
Bias	504	-28
K	$K = (3 * POW(10,-7)) * Pow(MAAT, 4.0319)) * 1 + 0$	$K = (3 * POW(10,-7)) * Pow(MAAT, 4.0319)) * 0.55 + 0$
C1	3.22	3.25
C2	25.7	25
C3	0.1	0.14
C4	133.4	180

5.2.4.3. Option 3: Composite pavements only

Like HMA over HMA sections, both thermal and reflective cracking coefficients were calibrated for composite sections. The entire dataset (no sampling) was used for model calibration. Figure 5-26 shows the predicted vs. measured thermal +reflective cracking for the global and local models. Table 5-40 summarizes global and local mode's SEE, bias, and calibration coefficients. The local calibration has improved the SEE and bias.

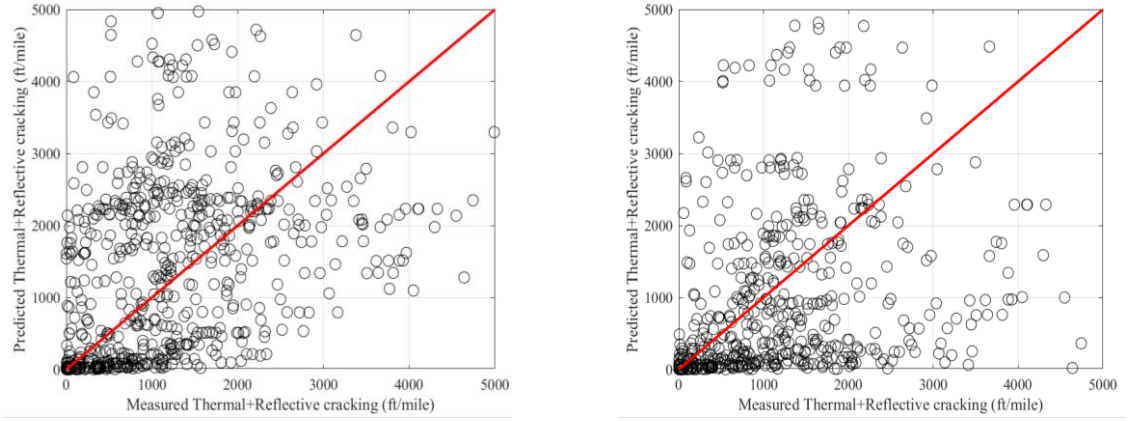

(a) Global model (b) Local model

Figure 5-26 Measured versus predicted transverse (thermal) cracking-Composite

Table 5-40 Transverse (thermal) cracking results – Option 3 – Composite

Parameter	Global model	Local model
SEE	1426	1357
Bias	265	-220
K	$K = (3 * POW(10,-7)) * Pow(MAAT, 4.0319)) * 1 + 0$	$K = (3 * POW(10,-7)) * Pow(MAAT, 4.0319)) * 0.55 + 0$
C1	0.1	0.2833
C2	0.52	0.7333
C3	3.1	2.5
C4	79.5	70

5.2.4.4. Reliability for thermal cracking model

The standard error equations were developed using the standard deviation of the measured cracking and mean predicted cracking, as explained in Chapter 4. Table 5-41 summarizes the standard error equations for all dataset options.

Table 5-41 Reliability summary for thermal cracking

Data set option	Global model equation	Local model equation
Option 1	$s_e = 0.14(TC) + 168$	$s_e = 0.1223(TC) + 400.9$
Option 3 – HMA over HMA	$s_{e(TC)} = 70.98(TC)^{0.2998} + 30.12$	$s_{e(TC)} = 338.59(TC)^{0.0849}$
Option 3 – Composite	$s_{e(TC)} = 5.1025(TC)^{0.6513} + 30.12$	$s_{e(TC)} = 308.74(TC)^{0.1063}$

5.2.5 Flexible Pavement Roughness (IRI) Model

IRI is a linear function of initial IRI, rut depth, total fatigue cracking, transverse cracking, and site factor. The IRI model was calibrated after the local calibration of the fatigue and, transverse cracking, and rutting models. Table 5-42 shows the hypothesis results for the global and local models for Option 1. None of the tests passed for the global model, whereas the local model passed one test. Figure 5-27 shows the predicted vs. measured IRI for the global and local models for Option 1. Table 5-43 shows the summary of model parameters using no sampling technique for Option 1. SEE is slightly improved, whereas bias is significantly enhanced from local calibration. Figure 5-28 shows the measured and predicted IRI with time for Option 1.

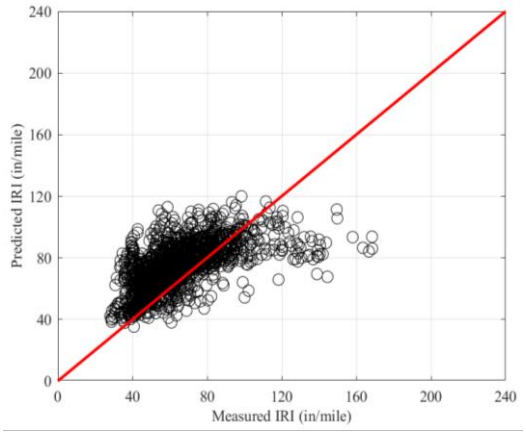

(a) Global model

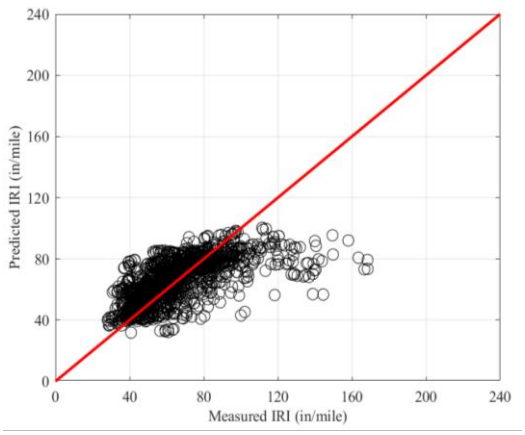

(b) Local model

Figure 5-27 Measured vs predicted IRI (No sampling)

Table 5-42 IRI model hypothesis testing results

Layer	Global model	Local model
t-test p-value	0.0000	1.0000
Intercept p-value	0.0000	0.0000
Slope = 1 p-value	0.0000	0.0000

Table 5-43 IRI model calibration results (No sampling)

Model coefficient	Global model	Local model
SEE	20.4152	18.8897
Bias	5.1769	0.0000
C1	40.0000	42.5829
C2	0.4000	0.0989
C3	0.0080	0.0078
C4	0.0150	0.0030

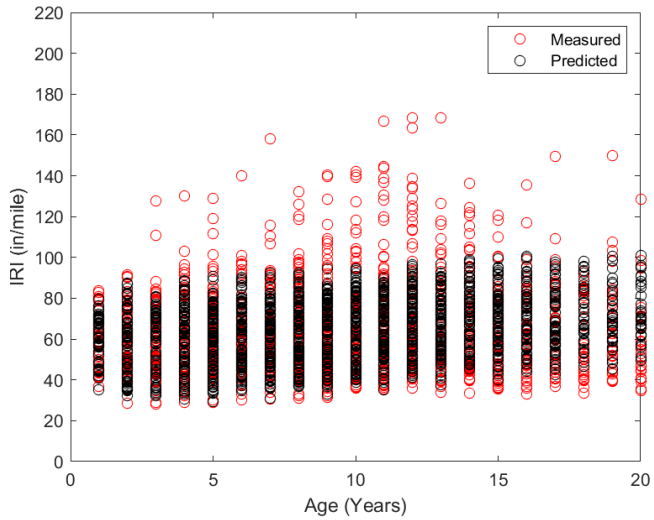

Figure 5-28 Measured and predicted IRI-Time series

The entire dataset was split into two parts, with 70% of the sections used for calibration and 30% for validation using a split sampling approach. Figure 5-29 shows the predicted vs. measured IRI for calibration and validation. Table 5-44 summarizes the model parameters for the global model, calibration, and validation set. A calibration summary for all other options with different calibration approaches is given in Tables 5-45 to 5-48.

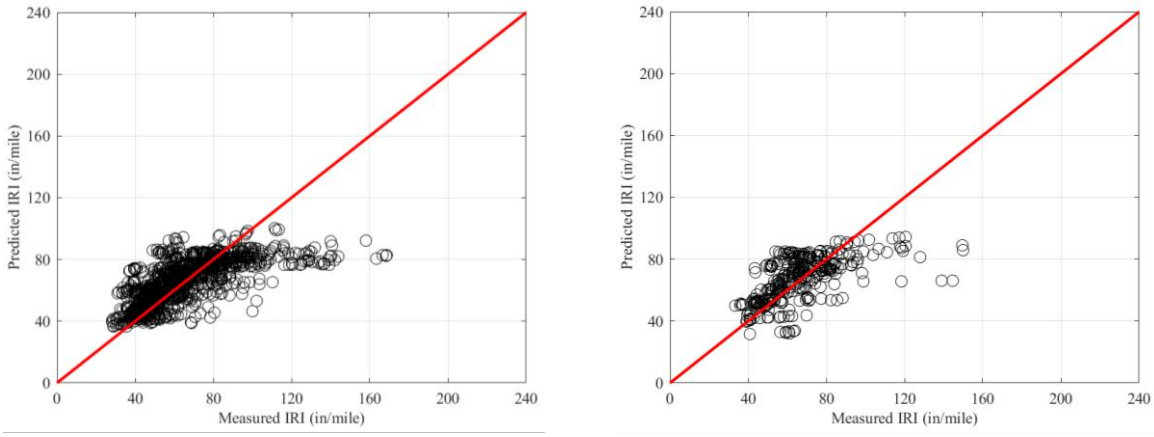

(a) Calibration set (b) Validation set

Figure 5-29 Measured vs predicted IRI (Split sampling)

Table 5-44 IRI model validation results (Split sampling)

Model coefficient	Global model	Calibration set	Validation set
SEE	22.2411	16.0074	15.7971
Bias	14.1373	0.4807	0.6950
C1	40.0000	40.0000	40.0000
C2	0.4000	0.0928	0.0928
C3	0.0080	0.0046	0.0046
C4	0.0150	0.0001	0.0001

Table 5-45 Flexible IRI local calibration – Option 1

Sampling Technique	Parameter	SEE	Bias	C1	C2	C3	C4
No Sampling	Global model	20.4152	5.1769	40.0000	0.4000	0.0080	0.0150
	Local model	18.8897	0.0000	42.5829	0.0989	0.0078	0.0030
Split sampling	Global model	22.2411	14.1373	40.0000	0.4000	0.0080	0.0150
	Local model calibration	16.0074	0.4807	40.0000	0.0928	0.0046	0.0001
	Local model validation	15.7971	0.6950	40.0000	0.0928	0.0046	0.0001
Repeated split sampling	Global Model Mean	22.2317	14.3096	40.0000	0.4000	0.0080	0.0150
	Global Model Median	22.3077	14.3351	40.0000	0.4000	0.0080	0.0150
	Global model lower CI	21.1240	13.2566	-	-	-	-
	Global model upper CI	23.0352	15.2865	-	-	-	-
	Local Model Mean	15.9637	0.8438	40.0068	0.0912	0.0046	0.0007
	Local Model Median	15.9671	0.6881	40.0000	0.0901	0.0046	0.0002
	Local model lower CI	14.9453	0.1598	40.0000	0.0900	0.0026	0.0000
	Local model upper CI	16.8554	2.7574	40.0009	0.1002	0.0063	0.0042
	Local Model Mean – validation	16.0524	0.8401	40.0068	0.0912	0.0046	0.0007
	Local Model Median – validation	16.0454	0.7630	40.0000	0.0901	0.0046	0.0002
	Local model lower CI	12.4582	-3.2269	40.0000	0.0900	0.0026	0.0000
	Local model upper CI	19.8453	5.3700	40.0009	0.1002	0.0063	0.0042
Bootstrapping	Global Model Mean	20.3790	5.0900	40.0000	0.4000	0.0080	0.0150
	Global Model Median	20.3518	5.0744	40.0000	0.4000	0.0080	0.0150
	Global model lower CI	17.6560	1.6677	-	-	-	-
	Global model upper CI	23.2553	8.5022	-	-	-	-
	Local Model Mean	18.7441	0.0718	42.8739	0.1025	0.0081	0.0030
	Local Model Median	18.7652	0.0000	41.8644	0.1005	0.0080	0.0028
	Local model lower CI	15.6545	0.0000	40.0000	0.0900	0.0005	0.0000
	Local model upper CI	22.0126	0.7193	51.9628	0.1362	0.0161	0.0082

Table 5-46 Flexible IRI local calibration – Option 2

Sampling Technique	Parameter	SEE	Bias	C1	C2	C3	C4
No Sampling	Global model	20.5763	9.2791	40.0000	0.4000	0.0080	0.0150
	Local model	17.4521	-0.2463	38.3082	0.1891	0.0085	0.0132
Split sampling	Global model	21.1270	9.8825	40.0000	0.4000	0.0080	0.0150
	Local model calibration	17.4968	0.0000	8.3289	0.2632	0.0043	0.0167
	Local model validation	16.9318	1.3313	8.3289	0.2632	0.0043	0.0167
Repeated split sampling	Global Model Mean	21.2009	10.1284	40.0000	0.4000	0.0080	0.0150
	Global Model Median	21.2416	10.1364	40.0000	0.4000	0.0080	0.0150
	Global model lower CI	20.3079	9.1769	-	-	-	-
	Global model upper CI	21.8170	11.0794	-	-	-	-
	Local Model Mean	17.6014	-0.0058	12.5117	0.2571	0.0049	0.0147
	Local Model Median	17.5504	0.0000	11.8115	0.2499	0.0042	0.0155
	Local model lower CI	16.5606	0.0000	2.6969	0.0542	0.0000	0.0042
	Local model upper CI	19.2750	0.0000	29.9810	0.5538	0.0149	0.0188
	Local Model Mean – validation	17.6260	-0.0178	12.5117	0.2571	0.0049	0.0147
	Local Model Median – validation	17.5344	-0.1271	11.8115	0.2499	0.0042	0.0155
	Local model lower CI	14.9296	-4.3172	2.6969	0.0542	0.0000	0.0042
	Local model upper CI	20.9412	4.3502	29.9810	0.5538	0.0149	0.0188
Bootstrapping	Global Model Mean	20.7289	9.2211	40.0000	0.4000	0.0080	0.0150
	Global Model Median	20.7020	9.2194	40.0000	0.4000	0.0080	0.0150
	Global model lower CI	19.3371	7.3110	-	-	-	-
	Global model upper CI	22.2711	11.1433	-	-	-	-
	Local Model Mean	17.4568	-0.0779	23.9779	0.2695	0.0051	0.0153
	Local Model Median	17.3895	0.0000	20.9565	0.2584	0.0043	0.0163
	Local model lower CI	15.8643	-1.4507	10.3702	0.0485	0.0000	0.0043
	Local model upper CI	19.4972	0.0000	46.4457	0.5787	0.0180	0.0203

Table 5-47 Flexible IRI local calibration results – Option 3 (HMA over HMA)

Sampling Technique	Parameter	SEE	Bias	C1	C2	C3	C4
No Sampling	Global model	20.1973	14.0240	40.0000	0.4000	0.0080	0.0150
	Local model	16.1774	0.0000	13.8154	0.1420	0.0188	0.0153
Split sampling	Global model	16.0194	10.1876	40.0000	0.4000	0.0080	0.0150
	Local model calibration	12.6546	0.0000	23.7284	0.3814	0.0000	0.0126
	Local model validation	17.0559	-10.7765	23.7284	0.3814	0.0000	0.0126
Repeated split sampling	Global Model Mean	15.2512	7.4582	40.0000	0.4000	0.0080	0.0150
	Global Model Median	15.3534	7.4361	40.0000	0.4000	0.0080	0.0150
	Global model lower CI	13.5598	5.3490	-	-	-	-
	Global model upper CI	16.3405	9.8181	-	-	-	-
	Local Model Mean	14.0406	0.0038	15.5939	0.3044	0.0058	0.0187
	Local Model Median	13.3539	0.0000	14.8974	0.0257	0.0001	0.0193
	Local model lower CI	11.0362	0.0000	0.6498	0.0000	0.0000	0.0031
	Local model upper CI	21.4628	0.0000	34.1755	1.9447	0.0394	0.0291
	Local Model Mean – validation	14.9061	0.2665	15.5939	0.3044	0.0058	0.0187
	Local Model Median – validation	13.6036	-0.3974	14.8974	0.0257	0.0001	0.0193
	Local model lower CI	7.3846	-11.4536	0.6498	0.0000	0.0000	0.0031
	Local model upper CI	30.9044	14.2806	34.1755	1.9447	0.0394	0.0291
Bootstrapping	Global Model Mean	20.1818	14.1091	40.0000	0.4000	0.0080	0.0150
	Global Model Median	20.2509	14.2055	40.0000	0.4000	0.0080	0.0150
	Global model lower CI	17.0255	9.2613	-	-	-	-
	Global model upper CI	22.8855	18.7346	-	-	-	-
	Local Model Mean	12.5726	-0.0187	15.0723	0.1404	0.0035	0.0192
	Local Model Median	12.5141	0.0000	14.5163	0.1317	0.0003	0.0188
	Local model lower CI	9.3166	-0.1178	0.9376	0.0000	0.0000	0.0045
	Local model upper CI	16.5425	0.0000	43.4113	0.3858	0.0267	0.0318

Table 5-48 Flexible IRI local calibration results – Option 3 (Composite)

Sampling Technique	Parameter	SEE	Bias	C1	C2	C3	C4
No Sampling	Global model	17.2970	-1.2161	40.0000	0.4000	0.0080	0.0150
	Local model	17.1593	0.0000	11.3635	1.1727	0.0082	0.0299
Split sampling	Global model	18.0032	-1.7024	40.000	0.400	0.008	0.0150
	Local model calibration	17.2114	0.0000	6.8318	0.0004	0.0044	0.0348
	Local model validation	15.2017	0.0870	6.8318	0.0004	0.0044	0.0348
Repeated split sampling	Global Model Mean	17.7332	-1.2839	40.0000	0.4000	0.0080	0.0150
	Global Model Median	17.8173	-1.2738	40.0000	0.4000	0.0080	0.0150
	Global model lower CI	16.2719	-2.7816	-	-	-	-
	Global model upper CI	18.8935	0.2160	-	-	-	-
	Local Model Mean	18.4618	-1.0226	22.6459	0.3105	0.0138	0.0282
	Local Model Median	17.3958	0.0000	16.9068	0.0137	0.0056	0.0323
	Local model lower CI	15.5516	-5.9992	0.2381	0.0000	0.0000	0.0035
	Local model upper CI	28.9063	0.0001	47.6492	2.1974	0.0682	0.0377
	Local Model Mean – validation	18.9384	-0.8073	22.6459	0.3105	0.0138	0.0282
	Local Model Median – validation	18.4499	-0.7487	16.9068	0.0137	0.0056	0.0323
	Local model lower CI	11.9388	-10.0187	0.2381	0.0000	0.0000	0.0035
	Local model upper CI	30.5810	8.2058	47.6492	2.1974	0.0682	0.0377
Bootstrapping	Global Model Mean	17.7369	-1.4326	40.0000	0.4000	0.0080	0.0150
	Global Model Median	17.6578	-1.4073	40.0000	0.4000	0.0080	0.0150
	Global model lower CI	15.2874	-4.5392	-	-	-	-
	Global model upper CI	20.6130	1.6390	-	-	-	-
	Local Model Mean	16.3822	-0.0983	14.9112	2.4596	0.0112	0.0212
	Local Model Median	16.0084	0.0000	11.9195	2.4095	0.0078	0.0218
	Local model lower CI	13.4634	-1.6002	0.1771	0.7930	0.0000	0.0031
	Local model upper CI	22.0754	0.0011	45.8747	4.5607	0.0489	0.0313

5.3 LOCAL CALIBRATION OF RIGID PAVEMENT MODELS

The local calibration results for the transverse cracking model, joint faulting model, and IRI in rigid pavements are presented in this section. Chapter 4 includes the details of the calibration approach for each model. The local calibration was performed using different sets of data. These sets include reconstruct and rehabilitation sections in various combinations, as given below:

1. Option 1: JPCP reconstruct sections only
2. Option 2: JPCP reconstruct and unbonded overlay pavement sections
3. Option 3: Unbonded overlay pavement sections

5.3.1 Transverse Cracking Model

The transverse cracking model was calibrated by minimizing the error between measured and predicted cracking. The number of available unbonded overlay sections is small and lower than the number of reconstructed JPCP sections. Therefore, Option 2 calibration results are recommended and will be discussed in detail in the following sections.

5.3.1.1. Option 2: JPCP reconstruct and unbonded overlay sections

No Sampling

All available sections were considered in the no-sampling approach. Figure 5-30 shows the predicted versus measured transverse cracking for the global and locally calibrated models. The global model underpredicts transverse cracking. Table 5-49 shows the hypothesis test results. The global model passes none of the tests, whereas one of the tests passed in the case of the local model. Table 5-50 shows the local calibration results. The SEE is reduced from 5.99 to 3.95, whereas the bias is reduced from -2.39 to -0.4. Although two out of three hypothesis tests were rejected, the SEE and bias values significantly improved. Figure 5-31 shows the fatigue damage curve and the measured and locally predicted transverse cracking with time. Figure 5-31 shows that local predicted and measured cracking follows a similar trend with time.

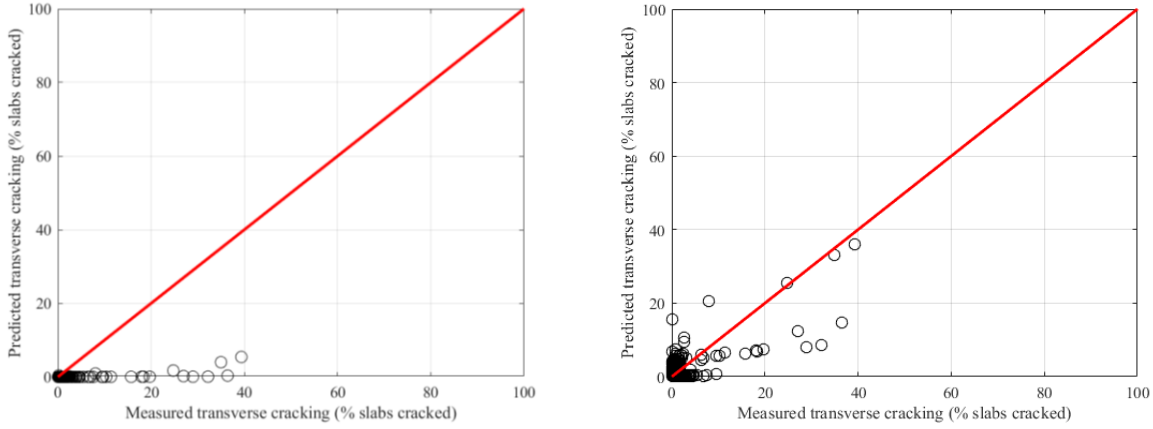

(a) Global model (b) Local model

Figure 5-30 Local calibration results using the entire dataset

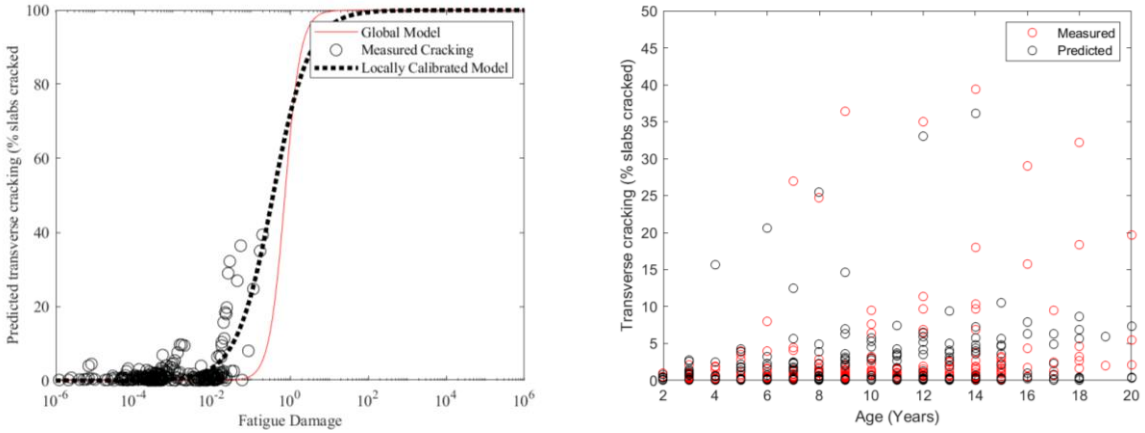

(a) Fatigue damage (b) Measured and predicted time series

Figure 5-31 Local calibration results for transverse cracking (No sampling)

Table 5-49 Global model hypothesis testing results

Hypothesis test	Global model	Local model
t-test p-value	0.0000	0.1055
Intercept p-value	0.0125	0.0004
Slope = 1 p-value	0.0000	0.0000

Table 5-50 Local calibration results using the entire dataset (No sampling)

Parameter	Global model	Local model
SEE (% slabs cracked)	5.99	3.95
Bias (% slabs cracked)	-2.39	-0.40
C_4	0.52	0.39
C_5	-2.17	-0.93

Split sampling

The split sampling technique was utilized to calibrate and validate the transverse cracking model, with 70% of the sections used for calibration and 30% for validation. Figure 5-32 shows the predicted vs. measured transverse cracking for the calibration and validation sets. Table 5-51 shows the calibration results using split sampling. The SEE and bias are improved with local calibration. Also, validation results show good agreement with the calibration results.

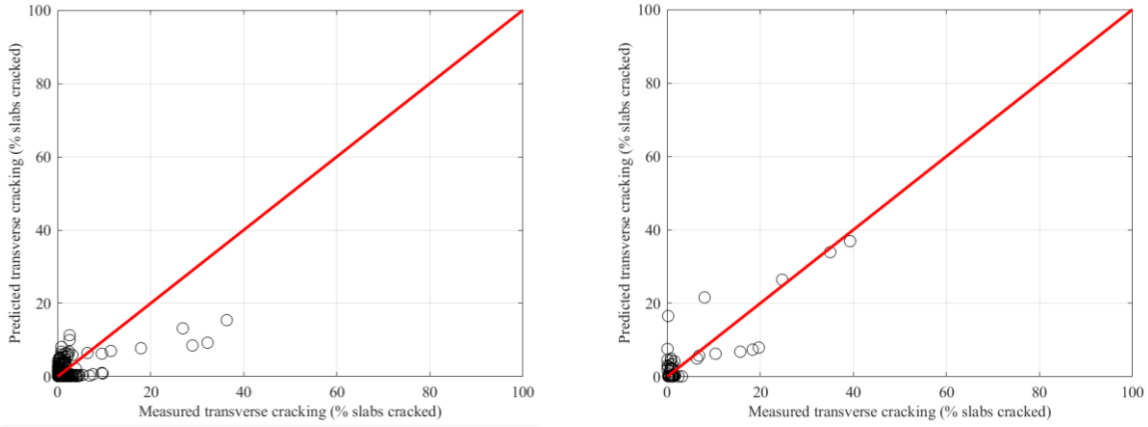

(a) Calibration set (b) Validation set

Figure 5-32 Split sampling local calibration results

Table 5-51 Split sample calibration results

Hypothesis test	Global model	Local model	Validation
SEE (percent slabs cracked)	4.99	3.86	4.68
Bias (percent slabs cracked)	-1.86	-0.19	-1.08
C4	0.52	0.60	0.60
C5	-2.17	-0.82	-0.82

Repeated split sampling

In repeated split sampling, multiple split samples are created where the sections in the calibration and validation sets can change each time. Split sampling is repeated 1000 times. This generates a distribution of model parameters, which are more robust than split sampling. Tables 5-52 and 5-53 show the calibration summary for the calibration and validation sets. Figures 5-33 and 5-34 show the distribution of model parameters. The validation results are satisfactory compared to the calibration set. The validation results showed a slightly higher SEE and less bias than the calibration dataset; however, these values are lower than for the case of a single split sample, especially for the bias.

Table 5-52 Repeated split sampling results for the calibration set

Parameter	Local model mean	Local model median	Local model lower CI	Local model upper CI
SEE (percent slabs cracked)	3.95	4.08	2.77	4.65
Bias (percent slabs cracked)	-0.41	-0.37	-0.91	-0.09
C_4	0.40	0.41	0.06	0.70
C_5	-0.97	-0.92	-1.48	-0.75

Table 5-53 Repeated split sampling results for the validation set

Parameter	Local model mean	Local model median	Local model lower CI	Local model upper CI
SEE (percent slabs cracked)	4.12	3.90	1.56	7.78
Bias (percent slabs cracked)	-0.38	-0.39	-2.71	2.27
C_4	0.40	0.41	0.06	0.70
C_5	-0.97	-0.92	-1.48	-0.75

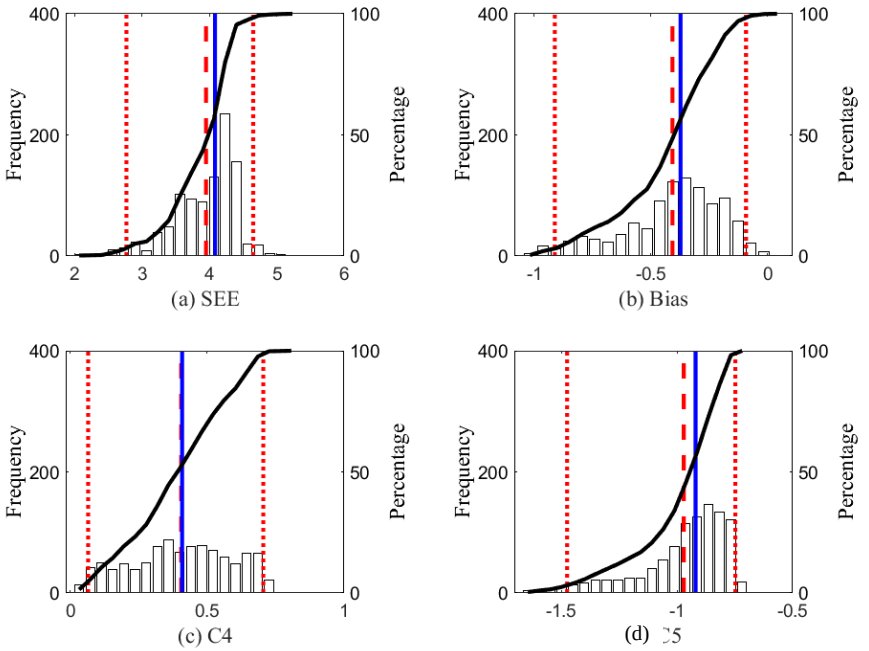

Figure 5-33 Repeated split sampling frequency distributions – calibration set

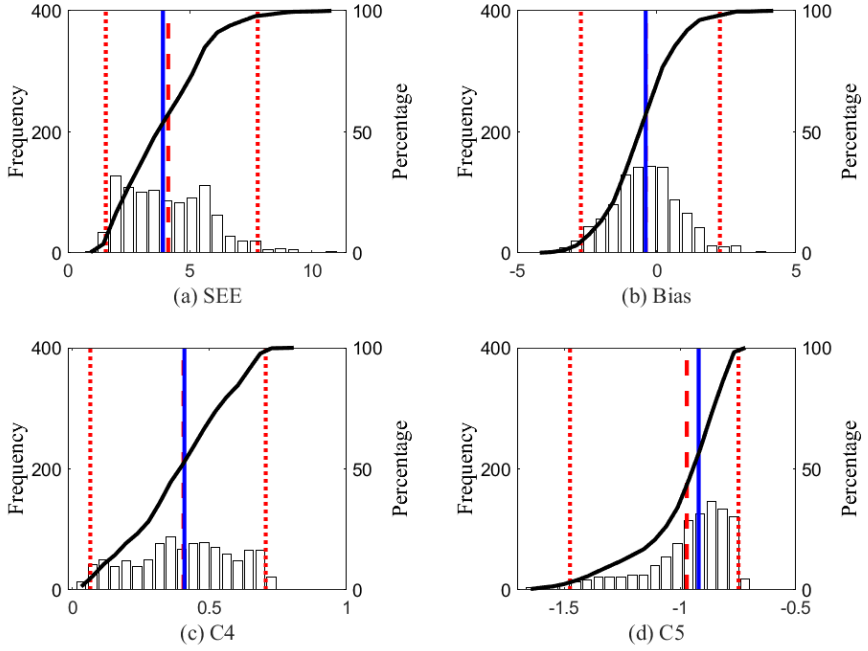

Figure 5-34 Repeated split sampling frequency distributions – validation set

Bootstrapping

Bootstrapping was used to calibrate the transverse cracking model, with 1000 bootstrap samples with replacement. Unlike repeated split sampling, in bootstrap, the samples were not split; instead, the entire dataset was used for calibration. Bootstrapping also generated CI and distribution of model parameters. Figure 5-35 shows the predicted vs. measured transverse

cracking for the local model. Table 5-54 summarizes the model parameters for local calibration. Figure 5-36 shows the distribution of SEE, bias, and model coefficients. Bootstrap provides mean, median, and CI for the model parameters.

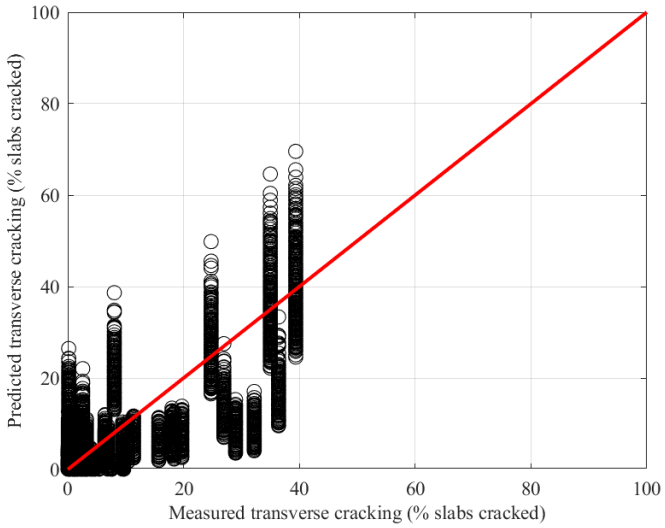

Figure 5-35 Bootstrap sampling predicted vs. measured results (1000 bootstraps)

Table 5-54 Bootstrap sampling calibration results summary (1000 bootstraps)

Parameter	Local Model Mean	Local Model Median	Local model lower CI	Local model upper CI
SEE (percent slabs cracked)	3.85	3.84	2.21	5.29
Bias (percent slabs cracked)	-0.36	-0.36	-0.92	0.11
C4	0.426	0.433	0.074	0.718
C5	-0.953	-0.911	-1.455	-0.716

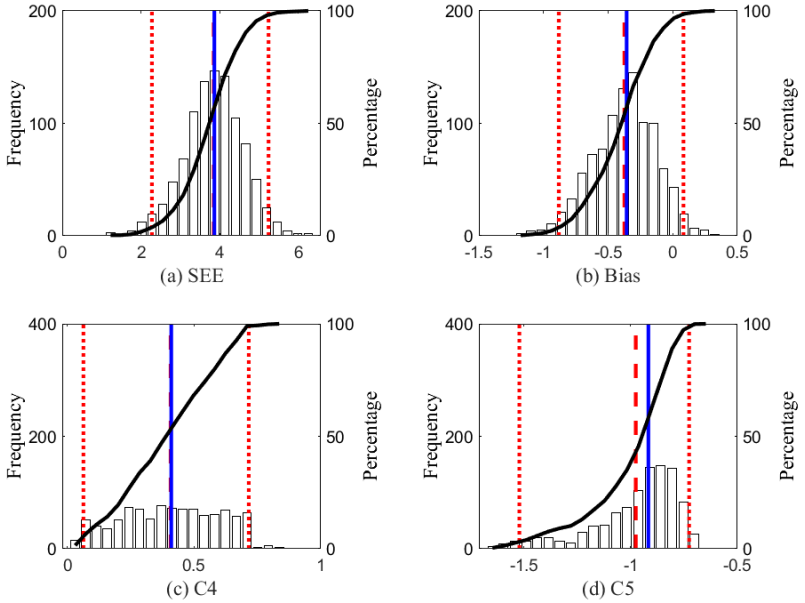

Figure 5-36: Bootstrap sampling calibration results (1000 bootstraps)

Summary

The global model alone underpredicts concrete transverse cracking for the MDOT sections. Conversely, the SEE and bias improved in all calibration approaches. Also, split sampling and repeated split sampling validate the calibrated model. The calibration results for all options are summarized in Tables 5-55 to 5-58. Table 5-58 shows the results for a special case of Option 2. In this case, all widened lane sections (lane width = 14 feet) were assigned a lane width of 12.5 feet while designing using the Pavement-ME. This calibration alternative was provided for MDOT's consideration as they have found that the widened slab input is extremely sensitive and not practical for their designs. Due to this sensitivity, MDOT currently uses a thickness adjustment to the standard width (12 feet) designs when a widened slab is planned. This calibration alternative would allow MDOT to input 12.5 feet for widened slab width to represent 14 feet widened slab configurations, therefore allowing direct use of the widened slab input and providing more practical results.

Table 5-55 Summary of Option 1 local calibration – Transverse cracking model

Sampling technique	Parameter	SEE	Bias	C4	C5
No Sampling	Global model	6.97	-2.96	0.52	-2.17
	Local model	3.77	-0.02	0.59	-0.66
Split sampling	Global model	7.38	-2.84	0.52	-2.17
	Local model calibration	4.02	-0.38	0.41	-0.76
	Local model validation	3.25	-0.52	0.41	-0.76
Repeated split sampling	Global Model Mean	6.95	-2.97	0.52	-2.17
	Global Model Median	6.95	-2.97	0.52	-2.17
	Global model lower CI	5.05	-3.55	-	-
	Global model upper CI	7.90	-2.11	-	-
	Local Model Mean	3.98	-0.35	0.40	-0.84
	Local Model Median	4.06	-0.33	0.42	-0.76
	Local model lower CI	2.55	-1.00	0.05	-1.44
	Local model upper CI	5.81	0.36	0.72	-0.59
	Local Model Mean - validation	4.03	-0.29	0.40	-0.84
	Local Model Median - validation	3.44	-0.55	0.42	-0.76
	Local model lower CI	1.00	-2.76	0.05	-1.44
	Local model upper CI	10.84	3.42	0.72	-0.59
Bootstrapping	Global Model Mean	6.86	-2.99	0.52	-2.17
	Global Model Median	6.97	-2.96	0.52	-2.17
	Global model lower CI	3.22	-4.70	-	-
	Global model upper CI	9.72	-1.60	-	-
	Local Model Mean	3.80	-0.28	0.40	-0.83
	Local Model Median	3.80	-0.30	0.41	-0.75
	Local model lower CI	2.07	-1.04	0.04	-1.48
	Local model upper CI	6.03	0.57	0.75	-0.57

Table 5-56 Summary of Option 2 local calibration – Transverse cracking model

Sampling technique	Parameter	SEE	Bias	C4	C5
No Sampling	Global model	5.99	-2.39	0.52	-2.17
	Local model	3.95	-0.40	0.39	-0.93
Split sampling	Global model	4.99	-1.86	0.52	-2.17
	Local model calibration	3.86	-0.19	0.60	-0.82
	Local model validation	4.68	-1.08	0.60	-0.82
Repeated split sampling	Global model mean	5.93	-2.38	0.52	-2.17
	Global model median	5.93	-2.38	0.52	-2.17
	Global model lower CI	4.08	-2.83	-	-
	Global model upper CI	6.77	-1.64	-	-
	Local model mean	3.95	-0.41	0.40	-0.97
	Local model median	4.08	-0.37	0.41	-0.92
	Local model lower CI	2.77	-0.91	0.06	-1.48
	Local model upper CI	4.65	-0.09	0.70	-0.75
	Local model mean - validation	4.12	-0.38	0.40	-0.97
	Local model median - validation	3.90	-0.39	0.41	-0.92
	Local model lower CI - validation	1.56	-2.71	0.06	-1.48
	Local model upper CI - validation	7.78	2.27	0.70	-0.75
Bootstrapping	Global Model mean	5.83	-2.39	0.52	-2.17
	Global Model median	5.82	-2.32	0.52	-2.17
	Global model lower CI	2.82	-3.72	-	-
	Global model upper CI	8.55	-1.32	-	-
	Local Model mean	3.85	-0.36	0.43	-0.95
	Local Model median	3.84	-0.36	0.43	-0.91
	Local model lower CI	2.21	-0.92	0.07	-1.45
	Local model upper CI	5.29	0.11	0.72	-0.72

Table 5-57 Summary of Option 3 local calibration – Transverse cracking model

Sampling technique	Parameter	SEE	Bias	C4	C5
No Sampling	Global model	1.15	-0.81	0.52	-2.17
	Local model	0.73	-0.07	0.91	-1.09
Split sampling	Global model	1.19	-0.84	0.52	-2.17
	Local model calibration	0.84	-0.14	0.41	-1.27
	Local model validation	0.39	0.14	0.41	-1.27
Repeated split sampling	Global Model Mean	1.15	-0.81	0.52	-2.17
	Global Model Median	1.15	-0.81	0.52	-2.17
	Global model lower CI	0.87	-1.02	-	-
	Global model upper CI	1.37	-0.59	-	-
	Local Model Mean	0.74	-0.11	0.55	-1.24
	Local Model Median	0.78	-0.11	0.57	-1.21
	Local model lower CI	0.50	-0.24	0.18	-1.50
	Local model upper CI	0.89	-0.03	0.86	-1.08
	Local Model Mean - validation	0.82	-0.09	0.55	-1.24
	Local Model Median - validation	0.76	-0.11	0.57	-1.21
	Local model lower CI - validation	0.42	-0.70	0.18	-1.50
	Local model upper CI - validation	1.27	0.55	0.86	-1.08
Bootstrapping	Global Model Mean	1.14	-0.81	0.52	-2.17
	Global Model Median	1.14	-0.80	0.52	-2.17
	Global model lower CI	0.80	-1.13	-	-
	Global model upper CI	1.47	-0.51	-	-
	Local Model Mean	0.72	-0.11	0.56	-1.23
	Local Model Median	0.71	-0.10	0.57	-1.21
	Local model lower CI	0.46	-0.25	0.19	-1.49
	Local model upper CI	1.03	-0.01	0.87	-1.06

Table 5-58 Summary of Option 2 local calibration – Transverse cracking model (Widened Lane = 12.5 feet)

Sampling technique	Parameter	SEE	Bias	C4	C5
No Sampling	Global model	5.99	-2.39	0.52	-2.17
	Local model	3.96	-0.38	0.42	-0.91
Split sampling	Global model	5.63	-2.33	0.52	-2.17
	Local model calibration	4.12	-0.23	0.58	-0.77
	Local model validation	3.99	1.57	0.58	-0.77
Repeated split sampling	Global Model Mean	5.96	-2.40	0.52	-2.17
	Global Model Median	5.96	-2.40	0.52	-2.17
	Global model lower CI	4.20	-2.83	-	-
	Global model upper CI	6.76	-1.69	-	-
	Local Model Mean	3.97	-0.42	0.41	-0.97
	Local Model Median	4.08	-0.38	0.40	-0.92
	Local model lower CI	2.87	-0.95	0.07	-1.47
	Local model upper CI	4.64	-0.09	0.71	-0.75
	Local Model Mean - validation	4.04	-0.35	0.41	-0.97
	Local Model Median - validation	3.84	-0.35	0.40	-0.92
	Local model lower CI - validation	1.45	-2.81	0.07	-1.47
	Local model upper CI - validation	7.72	2.08	0.71	-0.75
Bootstrapping	Global Model Mean	5.78	-2.37	0.52	-2.17
	Global Model Median	5.81	-2.32	0.52	-2.17
	Global model lower CI	2.85	-3.69	-	-
	Global model upper CI	8.46	-1.33	-	-
	Local Model Mean	3.82	-0.38	0.42	-0.97
	Local Model Median	3.85	-0.37	0.42	-0.91
	Local model lower CI	2.14	-0.93	0.07	-1.48
	Local model upper CI	5.29	0.11	0.71	-0.73

5.3.1.2. Reliability for the transverse cracking model

The standard error of the calibrated cracking models was used to establish the relationship between the standard deviation of the measured cracking and mean predicted cracking, as explained in Chapter 4. These relationships are used to calculate the cracking for specific reliability. Tables 5-59 to 5-62 summarize the standard error equations for different options.

Table 5-59 Transverse cracking reliability – Option 1

Sampling technique	Global model equation	Local model equation
No Sampling	$s_{e(CRK)} = 3.5522(CRK)^{0.3415} + 0.75$	$s_{e(CRK)} = 1.3627(CRK)^{0.7473}$
Split Sampling		$s_{e(CRK)} = 1.9369(CRK)^{0.6374}$
Repeated split sampling		$s_{e(CRK)} = 1.9545(CRK)^{0.5617}$
Bootstrapping		$s_{e(CRK)} = 1.9194(CRK)^{0.572}$

Table 5-60 Transverse cracking reliability – Option 2

Sampling technique	Global model equation	Local model equation
No Sampling	$s_{e(CRK)} = 3.5522(CRK)^{0.3415} + 0.75$	$s_{e(CRK)} = 1.9455(CRK)^{0.5842}$
Split Sampling		$s_{e(CRK)} = 1.3362(CRK)^{0.4923}$
Repeated split sampling		$s_{e(CRK)} = 2.4683(CRK)^{0.5266}$
Bootstrapping		$s_{e(CRK)} = 2.8285(CRK)^{0.5205}$

Table 5-61 Transverse cracking reliability – Option 3

Sampling technique	Global model equation	Local model equation
No Sampling	$s_{e(CRK)} = 3.5522(CRK)^{0.3415} + 0.75$	$s_{e(CRK)} = 0.6855(CRK)^{0.2987}$
Split Sampling		$s_{e(CRK)} = 0.7295(CRK)^{0.2664}$
Repeated split sampling		$s_{e(CRK)} = 0.6259(CRK)^{0.1831}$
Bootstrapping		$s_{e(CRK)} = 0.642(CRK)^{0.1269}$

Table 5-62 Transverse cracking reliability – Option 2 (Widened Lane = 12.5 ft)

Sampling technique	Global model equation	Local model equation
No Sampling	$s_{e(CRK)} = 3.5522(CRK)^{0.3415} + 0.75$	$s_{e(CRK)} = 1.7334(CRK)^{0.6185}$
Split Sampling		$s_{e(CRK)} = 2.9024(CRK)^{0.6226}$
Repeated split sampling		$s_{e(CRK)} = 2.9801(CRK)^{0.5147}$
Bootstrapping		$s_{e(CRK)} = 2.9004(CRK)^{0.5074}$

5.3.2 Faulting Model

The research team performed calibration of the faulting model using the CAT tool. No sampling technique was used for the calibration. In the first step, the most sensitive coefficients, C_1 and C_6 were simultaneously calibrated. In the next step, C_1 and C_6 were kept at the calibrated value, and C_2 was calibrated. All other coefficients (C_3, C_4, C_5, C_7 and C_8) were not calibrated and kept at the global values. All coefficients could not be simultaneously calibrated because of the limited run time and the total combinations of coefficients that can be calibrated simultaneously. It should be noted that the measured faulting was cut to 0.4 inches, as mentioned in Chapter 3. This means that any 0.1-mile section with mean faulting above 0.4 inches was removed from calibration. CAT cannot be used to calibrate models for different pavement types. Therefore, the faulting model was not calibrated for Option 2 since the JPCP and unbonded overlays cannot be calibrated together in CAT. Figure 5-37 shows the predicted vs. measured joint faulting for Option 1. Figure 5-38 shows the measured and predicted joint faulting with time for Option 1. In Figure 5-38, the predicted faulting is in the same range as measured faulting except for high values for measured faulting. Table 5-63 summarizes local calibration and the corresponding model parameters. SEE and bias are significantly improved for both options. The calibration results for widened slabs can be found in Appendix-A.

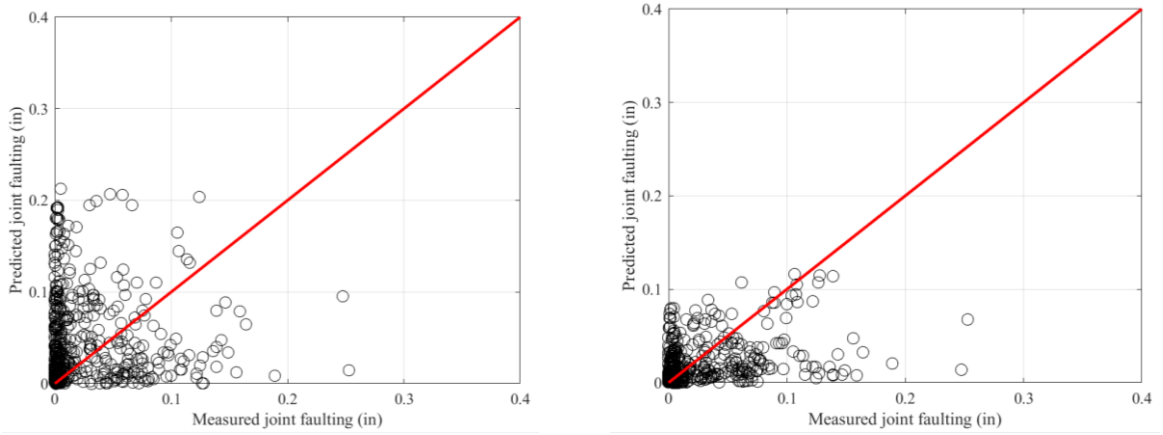

(a) Global model (b) Local model

Figure 5-37 Calibration results for joint faulting – Option 1

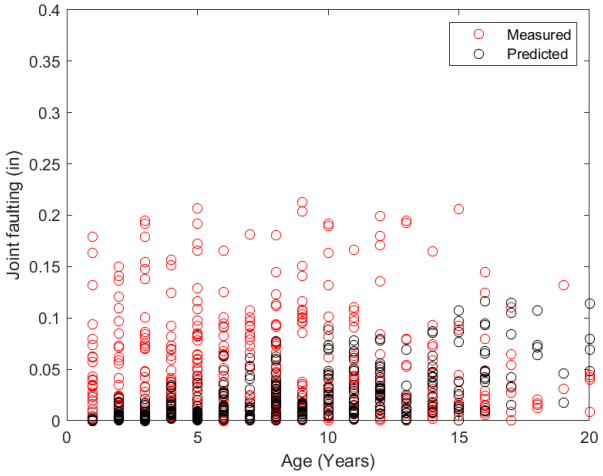

Figure 5-38 Measured and predicted joint faulting-Time series

Table 5-63 Summary of faulting model calibration

Parameter	Option 1		Option 3	
	Global	Local	Global	Local
SEE	0.06	0.03	0.02	-0.003
Bias	0.01	0.00	0.02	0.000
C_1	0.595	0.8	0.595	0.667
C_2	1.636	1.3889	1.636	1.5789
C_3	0.00217	0.00217	0.00217	0.00217
C_4	0.00444	0.00444	0.00444	0.00444
C_5	250	250	250	250
C_6	0.47	0.2	0.47	0.5
C_7	7.3	7.3	7.3	7.3
C_8	400	400	400	400

5.3.2.1. Reliability for faulting model

The standard errors of the calibrated faulting models were used to establish the relationship between the standard deviation of the measured faulting and mean predicted faulting, as explained in Chapter 4. Table 5-89 summarizes standard error equations for the faulting model.

Table 5-64 Faulting model reliability

Data option	Global model equation	Local model equation
Option 1	$s_{e(Fault)} = 0.07162(Fault)^{0.368} + 0.00806$	$s_{e(Fault)} = 0.0902(Fault)^{0.2038}$
Option 3		$s_{e(Fault)} = 0.2457(Fault)^{0.6267}$

5.3.3 Rigid Pavement Roughness (IRI) Model

IRI in rigid pavements is a linear function of initial IRI, transverse cracking, joint spalling, joint faulting, and site factor. Transverse cracking and faulting models were calibrated before calibrating the IRI model. All options and calibration approaches were considered. Figure 5-39 shows the predicted vs. measured IRI for Option 2 using no sampling approach. Figure 5-

40 shows the measured and predicted IRI with time using no sampling approach. The local model predictions are well within the range of measured values. Table 5-65 shows the calibration results for Option 2 using no sampling. The SEE reduced from 19.72 to 10.31, and the bias reduced from 11.70 to 0.00.

A split sampling approach has been used for model validation, with 70% of the sections used for calibration and the rest 30% for validation. Figure 5-47 shows the predicted vs. measured IRI using the calibration and validation sets. Table 5-66 summarizes the validation results for Option-2 using split sampling. The bias is significantly reduced for the validation set.

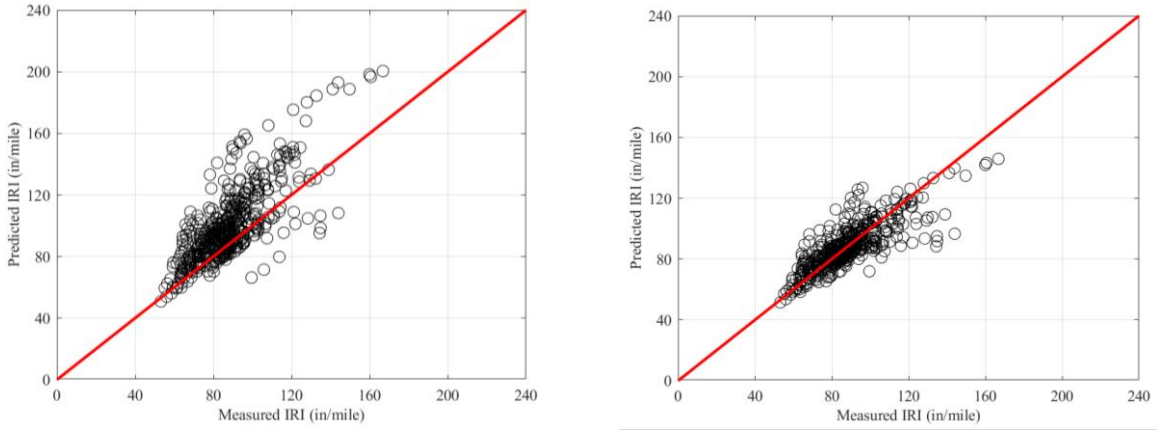

(a) Global model (b) Local model

Figure 5-39 IRI calibration results using no sampling (Option-2)

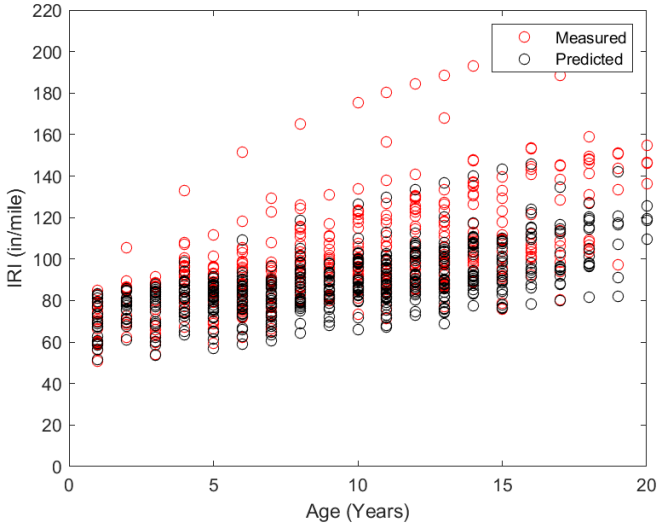

Figure 5-40 Measured and predicted IRI-Time series (Option-2)

Table 5-65 Calibration results for IRI (No sampling)

Parameters	Global model	Local model
SEE	19.72	10.31
Bias	11.70	0.00
C1	0.8203	0.0943
C2	0.4417	1.9384
C3	1.4929	1.5660
C4	25.2400	25.8398

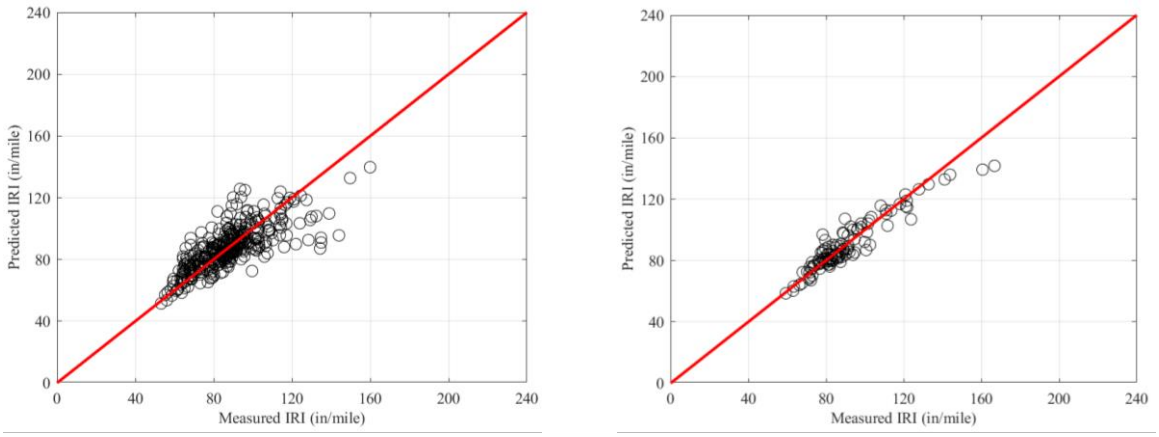

(a) Calibration set (b) Validation set

Figure 5-41 IRI calibration results (Split sampling)

Table 5-66 Validation results for IRI (Split sampling)

Parameters	Calibration set	Validation set
SEE	11.18	6.61
Bias	0.00	-0.34
C1	0.0547	0.0547
C2	1.9405	1.9405
C3	1.4654	1.4654
C4	29.4003	29.4003

The calibration results for all options are summarized in Tables 5-67 to 5-70. Table 5-70 shows the results for a special case of Option 2. In this case, all widened lane sections (lane width = 14 feet) were assigned a lane width of 12.5 feet while designing in the Pavement-ME.

Table 5-67 Summary of Option 1 local calibration – Rigid IRI model

Sampling technique	Parameter	SEE	Bias	C1	C2	C3	C4
No sampling	Global model	21.19	14.47	0.8203	0.4417	1.4929	25.2400
	Local model	9.28	0.00	0.3330	1.3057	1.5239	27.5491
Split sampling	Global model	21.40	13.65	0.8203	0.4417	1.4920	25.2400
	Local model	9.91	0.00	0.3105	2.1219	1.4660	27.9766
	Validation	6.50	2.07	0.3105	2.1219	1.4660	27.9766
Repeated split sampling	Global model	21.15	14.44	0.8203	0.4417	1.4920	25.2400
	Local model mean	9.21	0.00	0.2801	1.3888	1.5076	28.1599
	Local model median	9.26	0.00	0.2790	1.1173	1.5040	28.2544
	Local model lower CI	8.15	0.00	0.0521	0.0154	1.1818	21.9759
	Local model upper CI	10.01	0.00	0.5907	4.1613	1.8325	33.8194
Bootstrapping	Global model	21.06	14.48	0.8203	0.4417	1.4920	25.2400
	Local model mean	8.98	-0.02	0.3951	1.9102	1.4585	26.9081
	Local model median	9.00	0.00	0.2615	1.4629	1.4750	27.4054
	Local model lower CI	7.24	-0.32	0.0488	0.0000	0.8806	16.4521
	Local model upper CI	10.70	0.00	2.3081	6.9607	1.9434	34.6775

Table 5-68 Summary of Option 2 local calibration – Rigid IRI model

Sampling technique	Parameter	SEE	Bias	C1	C2	C3	C4
No sampling	Global model	19.722	11.698	0.820	0.442	1.493	25.240
	Local model	10.310	0.000	0.094	1.938	1.566	25.840
Split sampling	Global model	19.585	11.328	0.820	0.442	1.492	25.240
	Local model	11.180	0.000	0.055	1.941	1.465	29.400
	Validation	6.605	-0.341	0.055	1.941	1.465	29.400
Repeated split sampling	Global model	19.720	11.696	0.820	0.442	1.492	25.240
	Local model mean	10.284	-0.001	0.075	1.986	1.625	24.147
	Local model median	10.349	0.000	0.055	2.017	1.609	24.261
	Local model lower CI	9.075	0.000	0.046	0.603	1.396	17.324
	Local model upper CI	11.149	0.000	0.177	3.261	1.908	30.354
Bootstrapping	Global model	19.664	11.730	0.820	0.442	1.492	25.240
	Local model mean	10.103	-0.007	0.100	2.061	1.634	22.998
	Local model median	10.131	0.000	0.057	1.968	1.642	23.733
	Local model lower CI	8.318	-0.065	0.046	0.017	1.153	11.046
	Local model upper CI	11.915	0.000	0.432	4.604	2.133	31.378

Table 5-69 Summary of Option 3 local calibration – Rigid IRI model

Sampling technique	Parameter	SEE	Bias	C1	C2	C3	C4
No sampling	Global model	15.92	5.23	0.8203	0.4417	1.4929	25.2400
	Local model	11.53	0.00	0.0220	1.2694	2.6059	0.1009
Split sampling	Global model	16.20	4.86	0.8203	0.4417	1.492	25.24
	Local model	12.07	0.00	0.0565	1.0031	2.7863	1.4285
	Validation	9.95	3.94	0.0565	1.0031	2.7863	1.4285
Repeated split sampling	Global model	15.92	5.19	0.8203	0.4417	1.4920	25.2400
	Local model mean	11.55	0.00	0.0561	1.0031	2.6455	1.8916
	Local model median	11.86	0.00	0.0525	0.8717	2.7175	0.0201
	Local model lower CI	9.06	0.00	0.0456	0.0164	1.8600	0.0000
	Local model upper CI	12.91	0.00	0.0953	2.7470	3.2280	13.1302
Bootstrapping	Global model	15.76	5.15	0.8203	0.4417	1.4920	25.2400
	Local model mean	11.00	-0.01	0.0758	1.1684	2.5115	3.9195
	Local model median	11.11	0.00	0.0533	0.8624	2.5489	0.0123
	Local model lower CI	6.94	-0.22	0.0455	0.0000	0.8600	0.0000
	Local model upper CI	14.57	0.00	0.1896	3.7691	3.8412	21.5708

Table 5-70 Summary of Option 2 local calibration – Rigid IRI model (widened lane = 12.5 feet)

Sampling technique	Parameter	SEE	Bias	C1	C2	C3	C4
No sampling	Global model	19.82	10.80	0.8203	0.4417	1.4929	25.2400
	Local model	12.00	0.00	0.0852	1.2782	1.6878	29.2462
Split sampling	Global model	18.30	10.04	0.8203	0.4417	1.4920	25.2400
	Local model	11.93	0.00	0.0583	0.1857	2.0373	28.8017
	Validation	13.45	2.87	0.0583	0.1857	2.0373	28.8017
Repeated split sampling	Global model	19.84	10.91	0.8203	0.4417	1.4920	25.2400
	Local model mean	11.74	0.00	0.0942	1.5471	1.7970	23.7529
	Local model median	11.71	0.00	0.0549	1.4435	1.7991	24.3162
	Local model lower CI	8.94	0.00	0.0455	0.0000	1.2894	12.0122
	Local model upper CI	14.64	0.00	0.3433	4.1531	2.3469	31.6348
Bootstrapping	Global model	19.84	10.91	0.8203	0.4417	1.4920	25.2400
	Local model mean	11.74	0.00	0.0942	1.5471	1.7970	23.7529
	Local model median	11.71	0.00	0.0549	1.4435	1.7991	24.3162
	Local model lower CI	8.94	0.00	0.0455	0.0000	1.2894	12.0122
	Local model upper CI	14.64	0.00	0.3433	4.1531	2.3469	31.6348

5.4 SUMMARY OF FINDINGS

This chapter outlines the calibration results for different dataset options and uses different calibration approaches. Once all the models are locally calibrated and validated, the final model statistics and coefficients are summarized for each model within the various data subsets and by each pavement type considered in the study. The following are the recommended final results for the locally calibrated models for Michigan conditions. It was found that the bootstrapping technique leads to the most robust calibration with minimum standard error and bias for most cases. Therefore, results from bootstrapping have been recommended. The calibration results for widened sections in rigid pavements are summarized in Appendix A.

5.4.1 Flexible Pavements

Tables 5-71 to 5-75 summarize the global and locally calibrated model coefficients for each flexible pavement performance model considered in this study within each data subset (or option). The local models SEE, bias, and coefficients are highlighted in grey.

Table 5-71 Locally calibrated model coefficients — Bottom-up cracking (Flexible)

Option	Model type	SEE	Bias	C_1	*C2 (hac < 5 in.)*	*C2 (5 in. <= hac <=12 in.)*
Option 1a	Global model	8.30	-4.91	1.31	2.1585	$(0.867+0.2583* h_{ac})*1$
	Local model	8.73	0.00	0.2320	0.6998	$(0.867+0.2583* h_{ac})*0.2204$

Table 5-72 Locally calibrated model coefficients — Top-down cracking (Flexible)

Option	Model type	SEE	Bias	K_{L2}	K_{L3}	K_{L4}	K_{L5}	C_1	C_2
Option 1	Global model	-2.36	0.2855	0.011	0.01488	3.266	2.5219	0.8069	-2.36
	Local model	1.6	0.9	0.09	0.101	3.26	0.3	1.155	1.6

Table 5-73 Locally calibrated model coefficients — Rutting (Flexible)

Option	Model type	SEE	Bias	Br1	Bs1	Bsg1
Option 1	Global model	0.3935	0.3491	0.4	1	1
	Local model	0.085	-0.008	0.1476	0.3009	0.0696
Option 3-HMA over HMA	Global model	0.081	0.009	0.4	1	1
	Local model	0.077	-0.009	1.0423	0.3824	0.1213
Option 3-Composite	Global model	0.107	-0.092	0.4	1	1
	Local model	0.061	-0.010	1.5351	-	-

Table 5-74 Locally calibrated model coefficients — Thermal cracking (Flexible)

Option	Model type	SEE	Bias	K
Option 1	Global model	1225	-812	$K = (3 * POW(10,-7)) * Pow(MAAT, 4.0319)) * 1 + 0$
	Local Model	851	20	0.85
Option 3-HMA Over HMA	Global model	1856	1720	$K = (3 * POW(10,-7)) * Pow(MAAT, 4.0319)) * 0.55 + 0$
	Local Model	504	-28	$K = (3 * POW(10,-7)) * Pow(MAAT, 4.0319)) * 1 + 0$
Option 3-Composite	Global model	1426	1357	$K = (3 * POW(10,-7)) * Pow(MAAT, 4.0319)) * 1 + 0$
	Local Model	265	-220	$K = (3 * POW(10,-7)) * Pow(MAAT, 4.0319)) * 0.55 + 0$

Table 5-75 Locally calibrated model coefficients — IRI (Flexible)

Options	Model type	SEE	Bias	C_1	C_2	C_3	C_4
Option 1	Global model	20.3790	5.0900	40.0000	0.4000	0.0080	0.0150
	Local model	18.7441	0.0718	42.8739	0.1025	0.0081	0.0030
Option 2	Global model	20.7289	9.2211	40.0000	0.4000	0.0080	0.0150
	Local model	17.4568	-0.0779	23.9779	0.2695	0.0051	0.0153
Option 3-HMA Over HMA	Global model	20.1818	14.1091	40.0000	0.4000	0.0080	0.0150
	Local model	12.5726	-0.0187	15.0723	0.1404	0.0035	0.0192
Option 3-Composite	Global model	17.7369	-1.4326	40.0000	0.4000	0.0080	0.0150
	Local model	16.3822	-0.0983	14.9112	2.4596	0.0112	0.0212

5.4.2 Rigid Pavements

Tables 5-76 to 5-78 summarize the global and locally calibrated model coefficients for each rigid pavement performance model considered in this study within each data subset (or option). The local models SEE, bias, and coefficients are highlighted in grey.

Table 5-76 Locally calibrated model coefficients — Transverse cracking (Rigid)

Options	Model type	SEE	Bias	C_4	C_5
Option 1	Global model	6.86	-2.99	0.52	-2.17
	Local model	3.80	-0.28	0.40	-0.83
Option 2	Global model	5.83	-2.39	0.52	-2.17
	Local model	3.85	-0.36	0.43	-0.95
Option 3	Global model	1.14	-0.81	0.52	-2.17
	Local model	0.72	-0.11	0.56	-1.23

Table 5-77 Locally calibrated model coefficients — Faulting (Rigid)

Option	Model type	SEE	Bias	C_1	C_2	C_6
Option 1	Global model	0.06	0.01	0.595	1.636	0.47
	Local model	0.03	0.00	0.8	1.3889	0.2
Option 3	Global model	0.02	0.02	0.595	1.636	0.47
	Local model	-0.003	0.00	0.667	1.5789	0.5

Table 5-78 Locally calibrated model coefficients — IRI (Rigid)

Option	Model type	SEE	Bias	C_1	C_2	C_3	C_4
Option 1	Global model	21.06	14.48	0.8203	0.4417	1.4920	25.2400
	Local model	8.98	-0.02	0.3951	1.9102	1.4585	26.9081
Option 2	Global model	19.664	11.730	0.820	0.442	1.492	25.240
	Local model	10.103	-0.007	0.100	2.061	1.634	22.998
Option 3	Global model	15.76	5.15	0.8203	0.4417	1.4920	25.2400
	Local model	11.00	-0.01	0.0758	1.1684	2.5115	3.9195

5.5 IMPACT OF CALIBRATION ON PAVEMENT DESIGN

Local calibration aims to optimize the transfer function coefficients and minimize the error between measured and predicted performance. The calibrated model will impact the local design practices. In this section, supplementary flexible and rigid pavements (not part of the calibration) with various Michigan traffic and climate types are designed to evaluate the impact of the locally calibrated models. The designs are based on calibrated model coefficients and standard error equations. It is important to note that the subsequent design thicknesses are based on the current MDOT criteria for final designs, which include the following:

- The minimum thicknesses are 6.5" for flexible, 9" for JPCP freeway, and 8" for JPCP non-freeway sections.
- A maximum difference of ± 1 inch from the AASHTO 93 minimum thickness limits.
- JPCP widened slab sections were designed as standard width (12 feet), and design thicknesses were reduced by a maximum of 1 inch depending on whether the previous conditions were met. This practice is followed because the slab width is a sensitive parameter in the Pavement-ME, giving impractical (very thin) designs.
- The design trials were stopped when a pavement reached a maximum thickness of 16". Few designs fail at even 16", but further increasing the thicknesses leads to impractical designs. This occurs because a particular design may have inputs (material, traffic, climate) that aren't well represented in the global (or local) dataset. Therefore, the Pavement-ME has difficulty providing a practical design outcome. These designs may require changes in the Pavement-ME inputs, and simply changing the thickness cannot achieve a passing design. Furthermore, MDOT is limited by design changes (construction, materials, budget, and design procedures). Therefore, changing the inputs may not be practical.

Forty-four (44) flexible sections were designed in the Pavement-ME using the new calibrated models in v2.6 and the coefficients from the previous calibration effort in v2.3. Table 5-79 shows the average final design thickness for the 44 flexible sections using AASHTO 93, previous, and new local calibration model coefficients. For the new local calibration coefficients, these results are based on Option 1a for fatigue cracking (combining bottom-up and top-down cracking). Option 1 was used for other performance models. The average design thickness using the newly calibrated models is closer to the AASHTO 93 design, compared to the previous model calibration, with an average thickness reduction of 0.22 inches. Table 5-80 shows the summary of distress predictions using previous calibration coefficients and new calibration coefficients. The percentage change in Table 5-80 was

calculated as the change in predicted distress (new model – previous model) as a percentage of the previous calibrated model. Fatigue cracking controlled 25%, and thermal cracking was the dominant distress for 59% of designs. None of the sections failed in IRI, and total rutting controlled only one section.

Table 5-79 Summary of flexible pavement design

Design method	Design thickness (in)	
	Average	Standard deviation
AASHTO 93	9.17	2.20
Pavement-ME v2.3 previous local calibration model	8.86	1.78
Pavement-ME v2.6 new local calibration model	8.95	2.27

Note: The design ESALs range is between 1 and 41 million, and MR ranges from 3.7 to 6.5 ksi. Design reliability = 95%

Table 5-80 Summary of flexible pavement design distresses

Predicted distress		Previous, v2.3 local calibration model	New, v2.6 local calibration model	Percentage change
Fatigue cracking	Average	18.2	18.4	1.1%
	SD	2.3	2.8	21.7%
Total rutting	Average	0.4	0.3	-25%
	SD	0.07	0.07	0%
Thermal cracking	Average	1587	1792	12.9%
	SD	1498	1058	-29.4%
IRI	Average	149	133	-10.7%
	SD	7.8	9.6	23.1%

SD = standard deviation

Forty-four (44) rigid sections were designed using AASHTO 93, global, and new calibrated model coefficients. It is important to note that MDOT found the v2.3 global coefficients more suitable than the previous v2.3 local coefficients for their designs. Therefore, the v2.3 global coefficients were used for comparison in the case of rigid sections. Table 5-81 summarizes PCC pavement design thicknesses using the AASHTO 93, the 2.3 global, and the v2.6 locally calibrated models. Interestingly, for unrestricted designs using the global model, five sections reached the design thickness of 16 inches, and another five sections reached the design thickness of 6 inches. However, for the unrestricted design using the locally calibrated model, only one section has a design thickness of 16 inches. IRI and joint faulting are critical distress types. Overall, the average design thickness using the locally calibrated models is slightly lower than those using the v2.3 global model or AASHTO 93. Moreover, it eliminates the extreme design thicknesses.

Table 5-81 Summary of rigid pavement design

Design method	Design thickness (in)	
	Average	Standard deviation
AASHTO 93	10.07	1.67
Pavement-ME v2.3 global model	9.83	1.63
Pavement-ME v2.6 new local calibration model (14 ft)	9.64	1.45
Pavement-ME v2.6 new local calibration model (12.5 ft)	9.63	1.44

Note: The design ESALs range is between 1 and 64 million, and MR ranges from 3.7 to 6.5 ksi. Design reliability = 95%

CHAPTER 6 - MATERIAL TESTING AND TESTING PROTOCOLS

6.1 INTRODUCTION

Task 4 of this project was to conduct laboratory characterization of pavement materials collected from different projects for the development/updation of the material property database. The material properties would be inputs in pavement designs and future Pavement-ME model calibration efforts. In addition, several field tests were suggested as part of this project to develop testing protocols for future projects. This chapter also documents the sample collection and field testing efforts conducted under this project, along with the results of material characterization and field test data analyses. As part of this project, eight projects, four each year from the 2020 and 2021 construction seasons, were selected. The team performed laboratory testing on the HMA, PCC, and unbound materials collected from the construction sites. In addition, several field tests such as Falling Weight Deflectometer (FWD), Light Weight Deflectometer (LWD), and Dynamic Cone Penetrometer (DCP) were conducted on different pavement layers during construction. The criteria selected for new projects selection included:

- Pavement surface type (flexible vs. rigid)
- Project length (adequate for developing testing protocols, including the in-situ and laboratory testing)
- Pavement type (reconstruct, overlay, or crush and shape)
- Road class (Interstate vs. state routes or freeway vs. nonfreeway)
- Traffic volumes (low, medium, and high)

Based on the construction schedule and the willingness of regions for data collection and sampling, eight projects were selected (see Figure 6-1). Table 6-1 presents the details of the projects chosen for 2020. Similarly, Table 6-2 shows the selected projects for the year 2021.

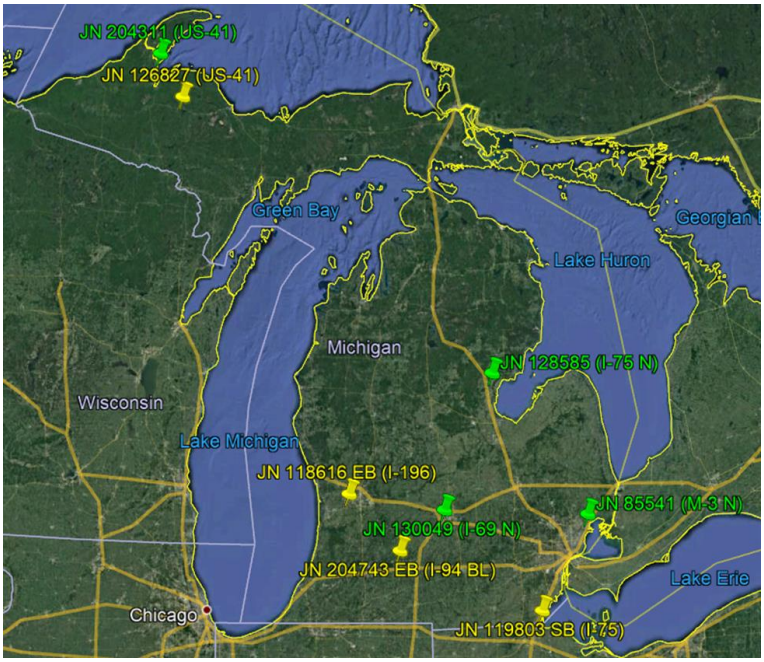

Figure 6-1 Location of the selected projects in 2020 and 2021

Table 6-1 Selected projects for the year 2020 construction season

Project No.	Surface type	Region	Job number	Route	Pavement type description	Road class	Project length	Total lane miles	Two-way AADT	Two-way AADTT
1	Rigid	University	119803	I-75 SB	JPCP Reconstruction	Freeway	5.06	15.731	28,414	9,645
2	Rigid	Grand	118616	I-196 EB	JPCP Reconstruction	Freeway	4.950	11.800	29,757	2,007
3	Flexible	Superior	126827	US-41	HMA Reconstruction and HMA Overlay of existing HMA	Non-freeway	5.250	10.621	2,561	310
4	Flexible	Southwest	204743	I-94BL	Milling and Two-Course HMA Overlay of existing PCC	Non-freeway	2.916	8.789	8,801	434

Table 6-2 Selected projects for the year 2021 construction season

Project No.	Surface type	Region	Job number	Route	Pavement type description	Road class	Project length	Total lane miles	Two-way AADT	Two-way AADTT
1	Flexible	University	125869	I-69 WB	HMA Reconstruction	Freeway	5.00	10.25	16,181	2,091
2	Flexible	Superior	204311	US-41	HMA Reconstruction and Aggregate Grade Lift with Asphalt Resurfacing	Non-freeway	4.39	8.78	2,561	310
3	Flexible	Metro	85541	M-3 NB	HMA Reconstruction	Non-freeway	3.44	14.17	65,122	1,113
4	Flexible	Bay	128585	I-75 NB	HMA over Rubblized PCC	Freeway	4.53	9.30	8,497	783

6.2 FIELD CHARACTERIZATION OF MATERIALS

Material testing in the field involved conducting in-situ tests like FWD, LWD, and DCP on different pavement layers of the 2020 and 2021 projects. In addition, Albedo measurements were performed to estimate the asphalt and concrete pavement's shortwave absorptivity. This section summarizes the field testing data analysis for all the projects tested under this project. The details for each test type are included in Appendix B.

6.2.1 Falling Weight Deflectometer Testing

MDOT provided FWD deflection data from the selected 2020 and 2021 projects. This section presents the summary of the backcalculation results for each project.

6.2.1.1. I-75 Southbound (SB) JPCP (2020) Project

FWD deflection data for the mainline I-75 SB JPCP (from stations 119+67 to 396+03) project were analyzed to determine the PCC layer modulus (*E*) and the modulus of subgrade reaction (*k*-value) using the AREA method. The joints' load transfer efficiency (LTE) was also estimated using the FWD deflections measured at joints in the outer wheel path (OWP). The FWD deflection data were received from three locations, i.e., 500 feet sections at the start, middle, and end of the total project length. FWD deflections are available at three locations along SB I-75 on three different days with a pass, each in the morning (am) and the afternoon (pm). Table 6-3 summarizes the backcalculation results.

Table 6-3 FWD backcalculation results – SB I-75 JPCP project

Parameter	Section	Station from	Station to	FWD date	Testing time	No. of FWD points	Mean	Std.	Min.	Max.
E (ksi)	1	372+00	367+00	10/27/20	am	7	11,582	1,219	9,669	13,158
	1	372+00	367+00	10/27/20	pm	7	10,589	1,609	8,420	13,268
	2	293+00	297+00	10/5/20	am	5	8,642	504	8,113	9,496
	2	293+00	288+00	10/5/20	pm	5	7,666	311	7,121	8,046
	3	176+00	171+00	10/7/20	am	7	12,395	1076	10,146	13,214
	3	176+00	171+00	10/7/20	pm	7	10,418	737	8,161	10,269
Dynamic *k*-value (pci)	1	372+00	367+00	10/27/20	am	7	244	16	211	260
	1	372+00	367+00	10/27/20	pm	7	265	11	231	263
	2	293+00	297+00	10/5/20	am	5	370	49	329	465
	2	293+00	288+00	10/5/20	pm	5	349	50	290	422
	3	176+00	171+00	10/7/20	am	7	270	24	255	318
	3	176+00	171+00	10/7/20	pm	7	284	20	278	337
LTE (%)	1	372+00	367+00	10/27/20	am	7	85	4	78	91
	1	372+00	367+00	10/27/20	pm	7	84	5	78	92
	2	293+00	288+00	10/5/20	am	5	92	2	88	94
	2	293+00	288+00	10/5/20	pm	5	89	3	85	92
	3	176+00	171+00	10/7/20	am	7	88	4	81	95
	3	176+00	171+00	10/7/20	pm	7	88	5	79	95

Note: Std. = Standard deviation, Min. = Minimum, Max. = Maximum.

Figure 6-2 displays the backcalculation results from the three sections. The results in Figure 6-2(a) show higher *E* values with higher spatial variability (indicated by error bars) for

sections 1 and 3, irrespective of the time of the day compared to section 2. Figure 6-2(b) displays the modulus of the subgrade reaction values backcalculated for each section. Sections 1 and 3 have lower *k*-value values than Section 2; however, Section 2 also displays a higher variability in the *k*-values. The LTE values for all three sections are similar, with very low spatial variability. Appendix B includes the plots for *E*, *k*, and LTE values with stationing for each section.

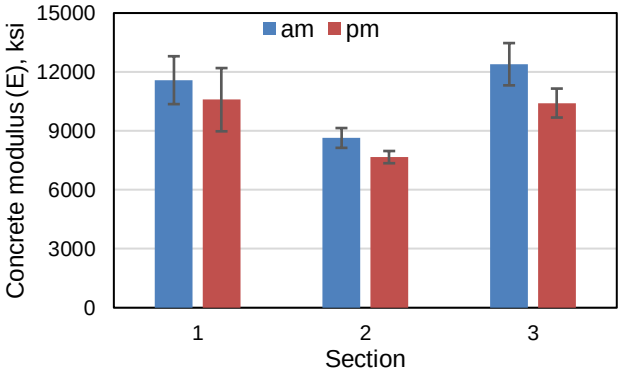

(a) Concrete elastic modulus

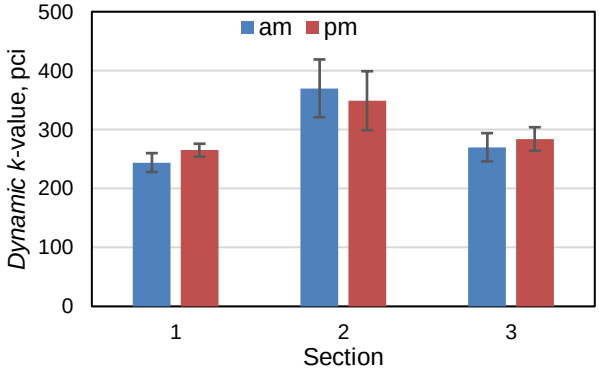

(b) *k*-value

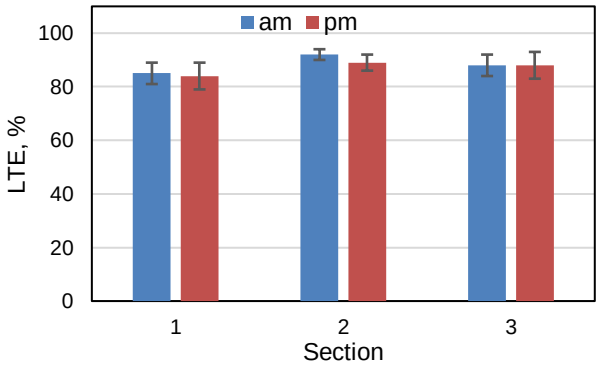

(c) LTE

Figure 6-2 Backcalculation results – I-75 SB JPCP project

6.2.1.2. I-196 Eastbound (EB) JPCP (2020) Project

Table 6-4 displays the backcalculated *E*, *k*, and LTE values using FWD deflections data for the mainline I-196 EB JPCP (from stations 952+52 to 1217+45). Like the I-75 project, the FWD deflection data were collected on three locations, i.e., 500 feet sections at the start, middle, and end of the total project length, a pass each morning (am), and the afternoon (pm). Figure 6-3 compares the concrete's modulus, *k*-value, and LTE of the three sections at different times of the day. The concrete's modulus values for this project are much lower than the I-75 SB project. Section 1 has the highest E values compared to the other two sections, with no considerable variations between the morning and evening values [see Figure 6-3(a)]. No significant variability is observed in the elastic modulus values of the concrete from all three sections. Figure 6-3(b) shows that the *k*-values for section 3 are the highest of all sections. Also, the *k*-values display considerable variability for all three sections. Figure 6-3(c) shows the LTE values for the project. Section 1 has the highest LTE values compared to the other sections; however, the project has low LTE values for a newly constructed pavement.

Table 6-4 FWD backcalculation results – EB I-196 JPCP project

Parameter	Section	Station from	Station to	FWD date	Testing time	No. of FWD points	Mean	Std.	Min.	Max.
E (ksi)	1	988+00	992+74	10/12/20	am	7	4,421	277	4,081	4,911
	1	988+00	992+74	10/12/20	pm	7	4,422	276	4,141	5,045
	2	1073+00	1077+11	10/15/20	am	8	3,371	359	2,815	3,885
	2	1073+00	1077+11	10/15/20	pm	4	3,103	231	2,724	3,346
	3	1204+00	1210+27	10/12/20	am	10	2,982	197	2,603	3,258
	3	1204+00	1210+27	10/12/20	pm	10	3,682	101	3,466	3,810
Dynamic *k*-value (pci)	1	988+00	992+74	10/12/20	am	7	279	69	173	391
	1	988+00	992+74	10/12/20	pm	7	266	67	165	375
	2	1073+00	1077+11	10/15/20	am	8	346	45	286	421
	2	1073+00	1077+11	10/15/20	pm	4	372	16	363	399
	3	1204+00	1210+27	10/12/20	am	10	435	58	347	521
	3	1204+00	1210+27	10/12/20	pm	10	385	46	303	449
LTE (%)	1	988+00	992+74	10/12/20	am	6	85	9	75	95.5
	1	988+00	992+74	10/12/20	pm	6	86	7.5	76	95
	2	1073+00	1077+11	10/15/20	am	5	77	5	71.5	83
	2	1073+00	1077+11	10/15/20	pm	5	73.5	5	67	81
	3	1204+00	1210+27	10/12/20	am	10	72	7	63	83
	3	1204+00	1210+27	10/12/20	pm	10	71	6	60.5	77.5

Note: Std. = Standard deviation, Min. = Minimum, Max. = Maximum.

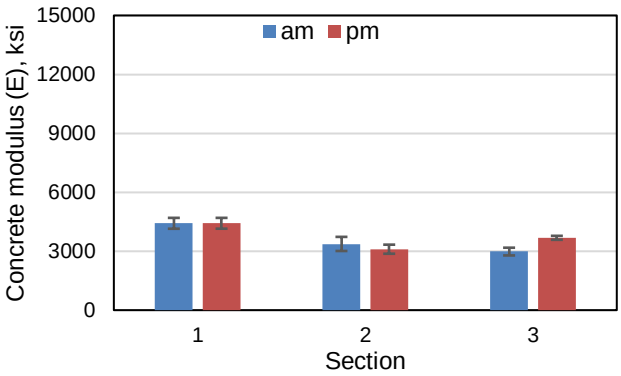

(a) Concrete elastic modulus

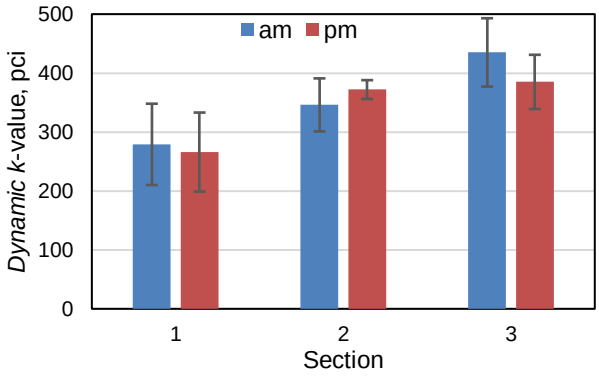

(b) *k*-value

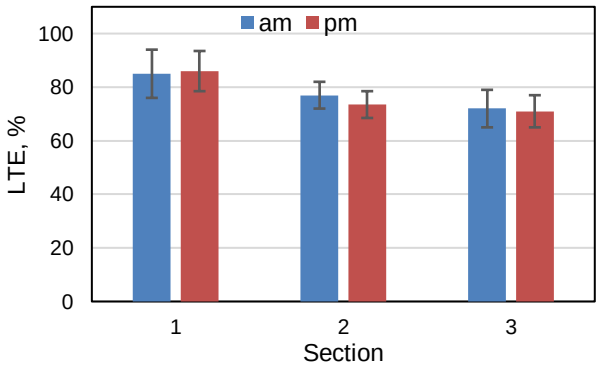

(c) LTE

Figure 6-3 Backcalculation results – I-196 EB JPCP project

6.2.1.3. US-41 HMA Reconstruction and HMA Overlay of existing HMA (2020) Project

Some sections of this project were full-depth HMA reconstruction, and others were HMA overlays on existing HMA pavement. FWD deflection data on the milled surface and leveling course were available for the US-41 flexible pavement project, and both were analyzed considering a three-layered structure, as shown in Table 6-5, to estimate the modulus of the asphalt concrete (AC), base/subbase, and subgrade layers using MICHBACK software. The FWD data were collected on the milled surface between stations 2012+00 and 2127+50 of the project. The existing AC layer thickness for the stations where FWD testing was conducted on the milled surface (i.e., after milling the existing HMA layer) ranges from 3 to

7 inches. Considering a mean AC thickness of 5 inches with 2 inches milled off, the backcalculation was performed with a 3-inch AC layer. For the analysis of FWD data collected over the leveling course, the structure used in the backcalculation process included an AC layer of 5 inches after laying a 2-inch leveling course. It is noted that the FWD measurements taken over the leveling course were within the project bounds but outside the stations mentioned earlier for the milled surface. The 7-inch base and 4-inch subbase layers were combined into one composite base/subbase layer. The existing granular material layer (24 inches & varying) and the underlying reinforced concrete (about 9 inches thick) below the subbase layer was considered part of the subgrade layer in the backcalculation process.

Table 6-6 displays the descriptive statistics for the backcalculation results from the deflections measured on the milled surface of the project. The obtained AC layer moduli are high because, with a thin AC layer (i.e., 3-inch), the backcalculation process generally results in higher values. The combined base/subbase layer moduli are also high. Higher subgrade layer moduli can be due to 24-inch granular material and the underlying concrete layers beneath the subbase. The AC and the base/subbase layer moduli exhibit higher variability than the subgrade layer. Table 6-7 shows the layer moduli values obtained from FWD deflection measured on the leveling course. The obtained AC modulus values are reasonable; however, the base/subbase layer has some high values. Looking at the peak deflection under the load (D0), the locations resulting in higher base/subbase moduli had significantly lower deflections under the load than others.

Table 6-5 Structure used for backcalculation of layer moduli– US-41 project

Layer	Layer thicknesses used for backcalculation for FWD testing on the milled surface	Layer thicknesses used for backcalculation for FWD testing on the leveling course
AC layer	3 in	5 in
Base/subbase layer	11 in	11 in
Subgrade	Semi-infinite	Semi-infinite
Bedrock	Incorporated	Incorporated

Table 6-6 Backcalculation results for FWD over the milled surface – US-41 project

Layer	No. of points	Average	Standard deviation	Minimum	Maximum
AC layer, psi	10	4,109,430	147,7341	245,2480	6,427,234
Base/subbase layer, psi	10	63,476	17,727	24,216	84,192
Subgrade, psi	11	31,909	5,249	22,495	37,751

Table 6-7 Backcalculation results for FWD over leveling course – US-41 project

Layer	No. of points	Average	Standard deviation	Minimum	Maximum
AC layer, psi	19	475,574	79,732	354,472	608,842
Base/subbase layer, psi	19	72,563	93,200	11,419	278,480
Subgrade, psi	19	28,716	6,788	16,372	38,728

6.2.1.4. I-94BL Milling and Two-Course HMA Overlay of existing PCC(2020) Project

The FWD deflections data for the I-94 BL flexible pavement project included deflections measured on the pavement's surface before and after the milling and resurfacing operations in the Westbound (WB) and Eastbound (EB) directions. The deflection measurements after resurfacing involved FWD passes in the morning and the afternoon in either direction. The FWD data analyses considered a four-layered structure, as shown in Table 6-8, to estimate the modulus of the AC, existing PCC, subbase, and subgrade layers using MODULUS software. Table 6-9 displays the descriptive statistics of the backcalculation results from the deflections measured before milling in either direction. The obtained layer moduli values are within reasonable ranges. The backcalculated AC layer moduli and the corresponding variability are higher for the EB than the WB pavement, while the subgrade moduli do not vary much, which is expected. The subbase layer moduli also exhibit higher variability spatially.

Table 6-8 Structure used for backcalculation of layer moduli – I-94 BL project

Layer	Layer thicknesses used for backcalculation
AC layer	4 in
Existing PCC layer	9 in
Subbase layer	8 in
Subgrade	Semi-infinite
Bedrock	Incorporated

Table 6-9 Backcalculated layer moduli before milling – I-94 BL project

Layer	No. of points	Average	Standard deviation	Minimum	Maximum
Eastbound (EB)					
AC, ksi	50	706	314	200	1040
PCC, ksi		6032	5363	100	15000
Subbase, ksi		56	43	10	150
Subgrade, ksi		13	4	6	23
Westbound (WB)					
AC, ksi	36	520	254	340	1040
PCC, ksi		5898	4719	100	15000
Subbase, ksi		72	52	10	150
Subgrade, ksi		14	4	8	29

FWD testing was also conducted in both directions of the I-94 BL project after resurfacing the pavement. These tests included two FWD rounds, one in the morning and the other in the afternoon, in either direction of the pavement. Table 6-10 displays the backcalculated moduli values for the different pavement layers using the deflections measured after resurfacing. It is observed that the values obtained from the analyses are in reasonable ranges. The estimated AC moduli values for the new AC layer (shown in Table 6-10) are lower than the ones estimated for the existing AC layer (see Table 6-9) using FWD measurements taken before milling. This can be attributed to the increased stiffness of the existing AC layer due to aging. The mean AC moduli values are lower for the afternoon FWD round than the morning because of higher pavement surface temperatures (around 83°F in the morning versus 96°F in the afternoon).

Table 6-10 Backcalculated layer moduli after resurfacing – I-94 BL project

Layer	No. of points	Average	Standard deviation	Minimum	Maximum
Eastbound (EB) – morning (am) round					
AC, ksi	52	561	320	106	1040
PCC, ksi		6710	5692	100	15000
Subbase, ksi		44	41	10	150
Subgrade, ksi		14	4	5	22
Eastbound (EB) – afternoon (pm) round					
AC, ksi	42	329	242	66	1040
PCC, ksi		5930	6069	100	15000
Subbase, ksi		50	49	10	150
Subgrade, ksi		14	4	6	23
Westbound (WB) – morning (am) round					
AC, ksi	48	383	214	200	1040
PCC, ksi		4332	4935	100	15000
Subbase, ksi		65	54	10	150
Subgrade, ksi		14	4	3	26
Westbound (WB) – afternoon (pm) round					
AC, ksi	38	309	287	50	1040
PCC, ksi		3455	4139	50	14837
Subbase, ksi		70	55	10	150
Subgrade, ksi		14	5	5	28

6.2.1.5. I-69 HMA Reconstruction (2021) Project

The FWD deflections data for the I-69 WB flexible pavement project included deflections measured on the pavement's leveling and top surface. The analyses of the FWD deflection data conducted over the top surface for morning and afternoon runs are presented in this section. The FWD data analyses considered a four-layered structure, as shown in Table 6-11, to estimate the modulus of the AC, base, subbase, and subgrade layers using MODULUS software. Table 6-12 displays the descriptive statistics of the backcalculation results. The backcalculated AC layer moduli are high, as the FWD was conducted in December 2021 when the temperatures were low. Overall, the FWD results are consistent with similar variations among the AC moduli between the different stations.

Table 6-11 Structure used for backcalculation of layer moduli – I-69 WB project

Layer	Layer thicknesses used for backcalculation
AC	8.75 in
Base	6 in
Subbase	18 in
Subgrade	Semi-infinite

Table 6-12 Backcalculation results – I-69 WB project

Layer	No. of points	Average	Standard deviation	Minimum	Maximum
Morning (am) round					
AC, ksi	23	2476.4	376.8	1946.7	3341.4
Base, ksi		46.6	21.9	26.1	89.2
Subbase, ksi		20.6	7.8	11.0	46.3
Subgrade, ksi		24.1	4.7	12.2	32.1
Afternoon (pm) round					
AC, ksi	23	2161.8	400.7	1725.2	3326.4
Base, ksi		40.3	15.2	25.0	68.2
Subbase, ksi		19.5	6.5	10.0	31.9
Subgrade, ksi		22.4	4.3	15.7	28.1

6.2.1.6. US-41 HMA Reconstruction and Aggregate Grade Lift with Asphalt Resurfacing(2021) Project

Some sections of this project were full-depth HMA reconstruction and others were HMA with an aggregate base fill over existing composite pavement. The FWD deflections data for the US-41 flexible pavement project included deflections measured on the pavement's top surface in either direction, i.e., EB and WB. The backcalculation results presented in this section are from the EB direction, which had reconstruction along the entire length. Table 6-13 displays the structure used in the analyses, while Table 6-14 shows the backcalculation results. It is observed that the estimated layer moduli are in reasonable ranges; however, the base layer modulus is slightly high. Also, the base layer moduli are highly variable spatially compared to the subbase and subgrade moduli, which displayed low variability.

Table 6-13 Structure used for backcalculation of layer moduli – US-41 EB project

Layer	Layer thicknesses used for backcalculation
AC	6.5 in
Base	6 in
Subbase	18 in
Subgrade	Semi-infinite

Table 6-14 Backcalculation results – US-41 EB morning FWD round

Layer	No. of points	Average	Standard deviation	Minimum	Maximum
AC, ksi	7	564.4	141.5	363.6	674.7
Base, ksi		65.7	31.9	31.5	127.9
Subbase, ksi		26.7	7.4	19.1	39.4
Subgrade, ksi		28.9	5.0	23.1	36.4

6.2.1.7. M-3 HMA Reconstruction (2021) Project

The FWD deflections data for the M-3 flexible pavement project included deflections measured on the pavement's base course, leveling course, and top surface in the NB and SB directions. The analyses of the FWD deflection data conducted over the top surface are presented for morning and afternoon rounds. The FWD data analyses considered a four-

layered structure, as shown in Table 6-15, to estimate the modulus of the AC, base, subbase, and subgrade layers using MODULUS software. Table 6-16 displays the descriptive statistics of the backcalculation results. As the FWD measurements were taken in November 2021, the backcalculated AC layer moduli are slightly high with considerable variability.

Table 6-15 Structure used for backcalculation of layer moduli – M-3 project

Layer	Layer thicknesses used for backcalculation
AC	7 in
Base	16 in
Subbase	8 in
Subgrade	Semi-infinite

Table 6-16 Backcalculation results – M-3 project

Layer	No. of points	Average	Standard deviation	Minimum	Maximum
Northbound (NB) morning (am) round					
AC, ksi	21	3,038	778	1,174	4,000
Base, ksi		46.2	27.9	25.0	116.9
Subbase, ksi		39.3	20.4	10.7	82.9
Subgrade, ksi		17.5	3.6	11.0	23.8
Northbound (NB) afternoon (pm) round					
AC, ksi	21	2,552	639.4	1,297	3,500
Base, ksi		44.9	24.4	25.0	107.1
Subbase, ksi		38.4	16.8	12.8	71.8
Subgrade, ksi		16.4	3.1	10.9	22.3
Southbound (SB) morning (am) round					
AC, ksi	21	2,910	771.4	1,468	4,000
Base, ksi		44.9	22.8	30.0	115.3
Subbase, ksi		37.5	19.6	16.5	85.8
Subgrade, ksi		17.6	4.5	11.1	29.2
Southbound (SB) afternoon (pm) round					
AC, ksi	21	2,426	716.4	1,048	3,874
Base, ksi		45.7	16.6	30.0	92.4
Subbase, ksi		37.3	18.3	11.3	84.8
Subgrade, ksi		16.6	3.9	10.1	27.3

6.2.1.8. I-75 HMA over Rubblized PCC (2021) Project

The FWD data for the I-75 flexible pavement project included deflections measured on the pavement's rubblized PCC base, base course, leveling course, and top surface in the NB and SB directions. The analyses of the FWD deflection data conducted over the top surface are presented. The FWD data analyses considered a four-layered structure, as shown in Table 6-17, to estimate the modulus of the AC, base, subbase, and subgrade layers. Since the existing 9-inch PCC layer was rubblized and left over the existing 4-inch aggregate base layer, these were combined into a single base layer for backcalculation. Table 6-18 displays the descriptive statistics of the backcalculation results. The backcalculated AC layer moduli estimated from the morning round are higher than values in the afternoon round. The

difference in temperatures recorded due to FWD testing (68°F in the morning while 76°F in the afternoon) can explain this during morning and afternoon rounds.

Table 6-17 Structure used for backcalculation of layer moduli – I-75 project

Layer	Layer thicknesses used for backcalculation
AC	7 in
Rubblized PCC over an aggregate base	9 + 4 = 13 in
Subbase	10 in
Subgrade	Semi-infinite

Table 6-18 Backcalculation results – I-75 project

Layer	No. of points	Average	Standard deviation	Minimum	Maximum
Northbound (NB) morning (am) round					
AC, ksi	48	963.1	181.5	260.2	1,227
Base, ksi		62.7	25.0	35.0	161.5
Subbase, ksi		35.2	19.4	10.3	80.5
Subgrade, ksi		12.1	2.6	4.6	22.4
Northbound (NB) afternoon (pm) round					
AC, ksi	28	698.3	155.9	160.1	925.4
Base, ksi		48.3	9.9	35.0	67.7
Subbase, ksi		32.0	16.9	10.0	68.7
Subgrade, ksi		11.3	2.9	4.6	16.9
Southbound (SB) – afternoon (pm) round 1					
AC, ksi	43	1,872	479.8	933.5	3,000
Base, ksi		67.7	33.4	30.0	181.0
Subbase, ksi		28.1	15.0	12.0	74.9
Subgrade, ksi		12.7	2.7	7.8	17.8
Southbound (SB) afternoon (pm) round 2					
AC, ksi	42	1,415	298.4	732.6	2,000
Base, ksi		72.5	34.3	30.1	193.8
Subbase, ksi		27.2	22.0	10.3	101.1
Subgrade, ksi		12.5	2.2	8.7	18.0

6.2.2 Light Weight Deflectometer Testing

Light Weight Deflectometer (LWD) data were collected at several different layers of the 2020 and 2021 selected projects. Table 6-19 summarizes the available LWD data from all the selected projects. The force applied at each drop by the LWD was obtained using Equation (6-1). Boussinesq's elastic half-space equation was used to determine each test's LWD elastic modulus values using Equation (6-2) (*1*). Table 6-20 presents the descriptive statistics of the LWD-based layer moduli for all the projects, while Figure 6-4 compares them.

$$F_{LWD} = \sqrt{2mghC} \tag{6-1}$$

where;
F_{LWD} = force applied by the LWD equipment (N)
m = dropped mass (kg)
g = acceleration due to gravity (9.81 m/s^2)
h = drop height (m)
C = spring constant (362396.2 N/m)

$$E_{LWD} = \frac{(1 - \nu^2)\sigma_0 r}{d_0} f \quad (6\text{-}2)$$

where;
E_{LWD} = LWD elastic modulus (MPa)
ν = Poisson's ratio [0.35 and 0.40 for tests performed on base and subgrade layers, respectively]; σ_0 = applied stress (Mpa)
r = radius of the plate (mm)
d_0 = average deflection (mm)
f = shape factor [8/3 (rigid plate on granular material) and $\pi/2$ (rigid plate on material with intermediate characteristics) for tests performed on base and subgrade layers, respectively].

Table 6-19 Summary of the available LWD data

Project \ Layer	DGAB	Subbase	OGDC	Subgrade	Rubb. PCC base
I-75 SB (2020)	✓	✓	✓	✓	×
I-196 (2020)	×	×	✓	×	×
US-41 (2020)	✓	✓	×	✓	×
I-69 (2021)	✓	✓	×	✓	×
US-41 (2021)	✓	✓	×	✓	×
M-3 (2021)	×	✓	✓	✓	×
I-75 NB (2021)	×	×	×	×	✓

Note: ✓ data available, × data not available or layer not part of the structure, DGAB = Dense-graded aggregate base, OGDC = Open-graded drainage course, Rubb. = Rubblized.

Table 6-20 LWD-based layer moduli

Layer	No. of test locations	Average (psi)	Standard deviation (psi)	Minimum (psi)	Maximum (psi)
I-196 EB (2020 selected project)					
OGDC	19	9,287	2,562	4,303	14,606
DGAB	17	8,853	2,994	2,962	14,410
Subbase	23	4,230	2,269	1,334	9,963
I-75 SB (2020 selected project)					
OGDC	23	9,398	2,109	4,908	11,995
Subgrade	27	2,713	1,411	670	7,066
US-41 (2020 selected project)					
DGAB	18	9,090	1,270	7,017	12,062
Subbase	9	4,712	609	3,633	5,415
Subgrade	6	2,415	949	912	3,401
US-41 (2021 selected project)					
DGAB	23	5,727	1,349	3,176	8,782
Subbase	14	4,913	1,245	3,256	7,696
Subgrade	13	3,856	736	2,764	5,055
I-69 WB (2021 selected project)					
DGAB	11	9,521	2,421	6,516	14,859
Subbase	11	3,565	641	2,659	4,506
Subgrade	12	2,743	1,188	1,046	4,952
M-3 NB (2021 selected project)					
OGDC, psi	21	7,504	1,749	4,450	10,224
Subbase, psi	18	3,203	1,534	1,116	6,126
Subgrade, psi	20	1,725	1,059	363	3,798
I-75 NB (2021 selected project)					
Rubb. PCC base, psi	32	8,322	1,892	5,368	13,419

Note: DGAB = Dense-graded aggregate base, OGDC = Open-graded drainage course, Rubb. = Rubblized.

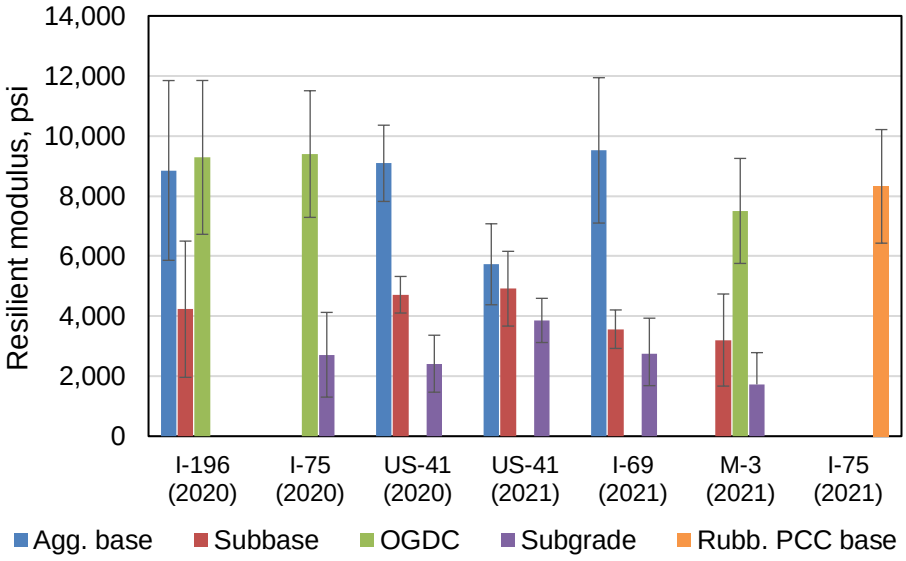

Figure 6-4 Comparison of LWD-based resilient moduli

Figure 6-4 shows that the dense-graded aggregate base (DGAB), open-graded drainage course (OGDC), and rubblized PCC base layers have similar resilient moduli from the different pavement projects. Similarly, the subbase layer moduli are close to 4,000 psi while the subgrade layers moduli range between 2,000 to 4,000 psi. All the layer moduli display considerable variability, with the highest in the DGAB, OGDC, and rubblized PCC base layers.

6.2.3 Dynamic Cone Penetrometer Testing

Table 6-21 summarizes the DCP data for the selected 2020 and 2021 projects. The following equations were used to analyze the data and determine the resilient moduli of the different layers. For using Equation (6-3), the California bearing ratio (CBR) is computed using one of Equation (6-5) through Equation (6-7). Table 6-22 through Table 6-27 display the DCP-based resilient moduli for each project, while Figure 6-5 compares them.

$$M_r\,(psi) = 2555 * CBR^{0.64} \qquad \text{(NCHRP 1-37A)} \qquad (6\text{-}3)$$

$$M_r\,(psi) = \frac{151.8}{DCP\left(\frac{mm}{blow}\right)^{1.096}} * 1000 \qquad \text{(DCP direct model)} \qquad (6\text{-}4)$$

where;
Mr = resilient modulus
CBR = California bearing ratio
DCP = dynamic cone penetrometer index in mm/blow

For all soils except for CL soils with CBR<10 and CH soils:

$$\text{CBR} = 292/\text{DCP}^{1.12} \qquad (6\text{-}5)$$

For CL soils with CBR<10:

$$CBR = \frac{1}{(0.017019 * DCP)^2} \qquad (6\text{-}6)$$

For CH soils:

$$CBR = \frac{1}{0.002871 * DCP} \qquad (6\text{-}7)$$

where;
DCP = dynamic cone penetrometer index in mm/blow.

Table 6-21 Summary of the available DCP data

Project \ Layer	Subbase	Subgrade
I-75 (2020)	✗	✓
I-196 (2020)	✓	✗
US-41 (2020)	✓	✓
I-69 (2021)	✓	✓
US-41 (2021)	✓	✓
M-3 (2021)	✓	✓
I-75 (2021)	✗	✗

Note: ✓ data available, ✗ data not available.

Table 6-22 DCP-based subgrade moduli, I-75 SB (2020) project

Statistics	DCP direct model, psi	NCHRP 1-37A, psi	DCP index, in/blow
Average	12,627	17,506	0.69
Standard deviation	10,118	8,623	0.38
Minimum	3,092	7,513	0.12
Maximum	51,814	43,376	1.51

Table 6-23 DCP-based subbase moduli, I-196 EB (2020) project

Statistics	DCP direct model, psi	NCHRP 1-37A, psi	DCP index, in/blow
Average	6,842	11,942	1.07
Standard deviation	5,337	5,194	0.53
Minimum	2,175	5,981	0.22
Maximum	28,745	31,446	2.56

Figure 6-5 shows the subbase layer on all projects except US-41 had a resilient modulus of about 5,000 psi, much lower than the subgrade moduli that range between 11,000 to 20,000 psi. However, the DCP-based subbase and subgrade layer moduli exhibit considerable variability for all the projects. A comparison between the different unbound layers moduli from all the field tests and laboratory-determined values will be presented later in the chapter.

Table 6-24 DCP-based estimated resilient moduli – US-41 (2020) project

	DCP direct model, psi	NCHRP 1-37A, psi	DCP index, in/blow
Subbase layer			
Average	16,090	20,664	0.47
Standard deviation	7,137	4,444	0.13
Minimum	7,589	13,036	0.32
Maximum	32,526	26,897	0.75
Subgrade layer			
Average	16,127	18,636	0.73
Standard deviation	12,587	8,427	0.64
Minimum	3,998	7,999	0.24
Maximum	33,629	30,830	1.98

Table 6-25 DCP-based resilient moduli, US-41 (2021) project

Statistics	DCP direct model, psi	NCHRP 1-37A, psi	DCP index, in/blow
Subbase layer			
Average	16,209	18,212	0.67
Standard deviation	14,382	7,543	0.28
Minimum	5,328	10,423	0.27
Maximum	55,260	29,551	1.05
Subgrade layer			
Average	20,706	24,942	0.34
Standard deviation	6,121	5,114	0.11
Minimum	8,381	14,243	0.19
Maximum	31,045	34,031	0.59

Table 6-26 DCP-based resilient moduli, I-69 WB (2021) project

Statistics	DCP direct model, psi	NCHRP 1-37A, psi	DCP index, in/blow
Subbase layer			
Average	4,582	9,066	1.58
Standard deviation	2,350	2,934	0.45
Minimum	1,739	5,220	1.17
Maximum	8,152	13,350	2.40
Subgrade layer			
Average	21,071	24,463	0.41
Standard deviation	9,152	7,018	0.21
Minimum	5,486	10,482	0.25
Maximum	34,766	31,788	0.96

Table 6-27 DCP-based resilient moduli, M-3 flexible pavement project

Statistics	DCP direct model, psi	NCHRP 1-37A, psi	DCP index, in/blow
Subbase layer			
Average	2,787	6,769	1.93
Standard deviation	1,349	1,899	0.70
Minimum	1,057	3,722	0.94
Maximum	7,272	12,495	3.91
Subgrade layer			
Average	11,427	16,324	0.81
Standard deviation	9,157	8,508	0.50
Minimum	3,034	7,198	0.26
Maximum	32,011	31,207	1.71

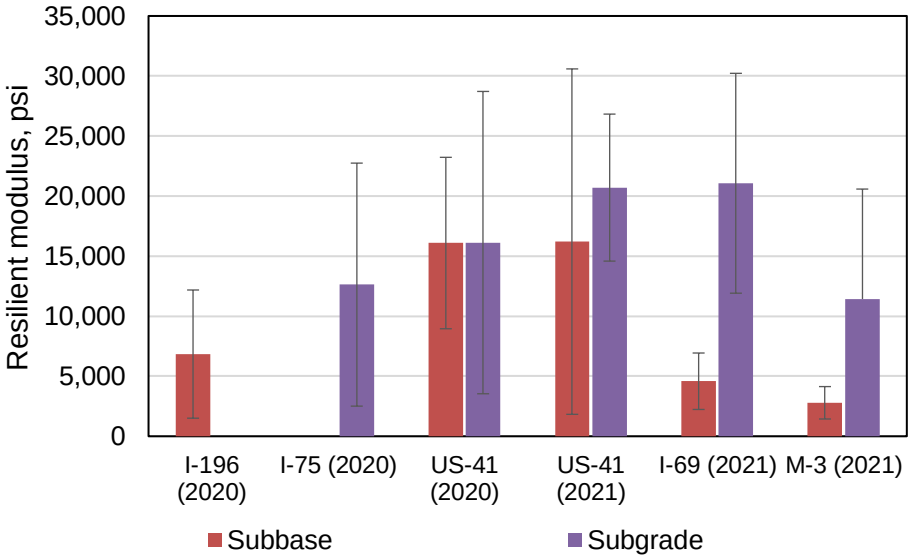

Figure 6-5 Comparison of DCP-based (using DCP direct model) resilient moduli

6.2.4 Albedo Measurements

The albedo measures how much light that hits a surface is reflected without being absorbed. It is a dimensionless value ranging between 0 and 1, where 0 represents the total absorbency (darker surfaces) and 1 the total reflectance (clearer surfaces). The albedometer or pyranometer is the apparatus recommended by the ASTM E1918-16 for measuring the solar reflectance of horizontal and low-sloped surfaces in the field (*2*).

Figure 6-6 shows the dual-pyranometer used for the tests conducted on I-69 and I-496 in August and October 2020, respectively. This instrument, produced by Novalynx (*3*), has a sensitivity to radiant energy in the 0.28-2.8 μm band and the advantage of having two domes. The dome on the top face measures the global (or incoming) radiation G [W/m2], while the dome on the bottom face measures the reflected radiation R [W/m2]. Both measurements are performed simultaneously, reducing the error that could result from flipping the pyranometer to take the second measurement. The dual-pyranometer is mounted on the arm connected to a tripod at 0.5 m (19.7 in) above the pavement surface to minimize the shadow's effect on the

measured reflected radiation (*2*). Following the standard, tests must be performed on clear sunny days (no clouds) between 9 am and 3 pm in summer and 10 am to 2 pm in winter. This ensures that the sun's angle to the normal from the surface is less than 45°. A minimum of three measurements were taken for each section. Data were recorded on a data logger connected to a computer, where the instrument's software was installed. During the measurements, pavement temperature was recorded using a digital infrared thermometer, while the air temperature and wind speed were taken with an anemometer. The albedo A is calculated as the ratio between the reflected radiation and the global radiation, as shown in Equation (6-8). The absorptivity S was calculated based on Equation (6-9).

$$Albedo\ A = \frac{R\left[{}^{W}/_{m^2}\right]}{G\left[{}^{W}/_{m^2}\right]} \tag{6-8}$$

$$Absorptivity\ S = 1 - A \tag{6-9}$$

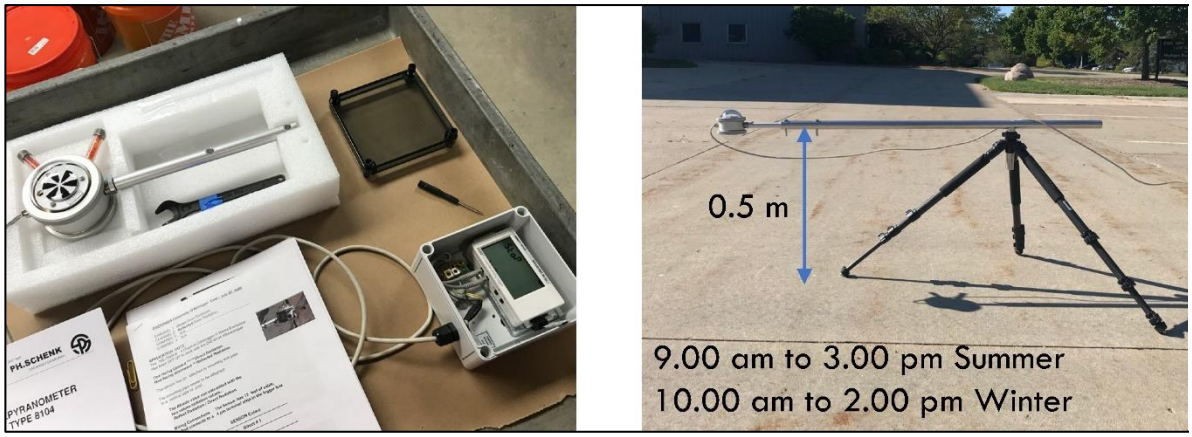

a) b)

Figure 6-6 The dual-pyranometer used to conduct the tests on the field. Part a) shows the instrument and the data logger; part b) shows a trial test on a concrete pavement of a parking lot at the MSU facility on Jolly Road.

On August 27, 2020, tests were conducted on I-69 EB, close to exit 123 (Segment 2) and on August 31, 2020, on the portion of I-69 EB, close to exit 113 (Segment 1), as indicated in Figure 6-7. Segment 1 included HMA cold milling (1.5") and single course resurfacing (1.5"). Segment 2 included paver placed surface seal and overband crack fill. Figure 6-9 shows the old and new surfaces where the tests were carried out. Figure 6-9(a) and (b) are related to segment 2, while c) and d) refer to segment 1. On October 13, 2020, tests were carried out on two sections of the I-496 (Figure 6-8). On the exit 97 ramp, measurements were taken on a new cement concrete surface and on the existing surface constructed in 1990. Close to exit 4 of the same Interstate, measurements were performed on two existing surfaces. This lane was constructed in cement concrete in 1960, while the shoulder was built in HMA (Figure 6-10). Table 6-28 presents the summarized climate, field conditions, and albedo measurements.

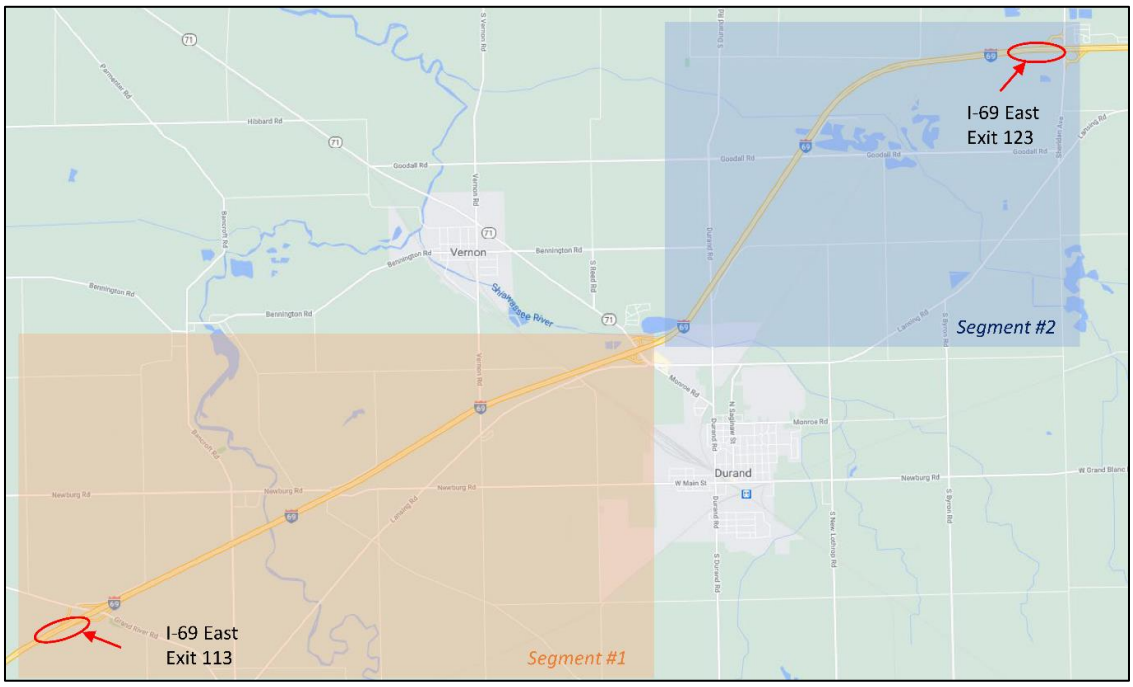

Figure 6-7 Location of the two tested sections of the I-69 east

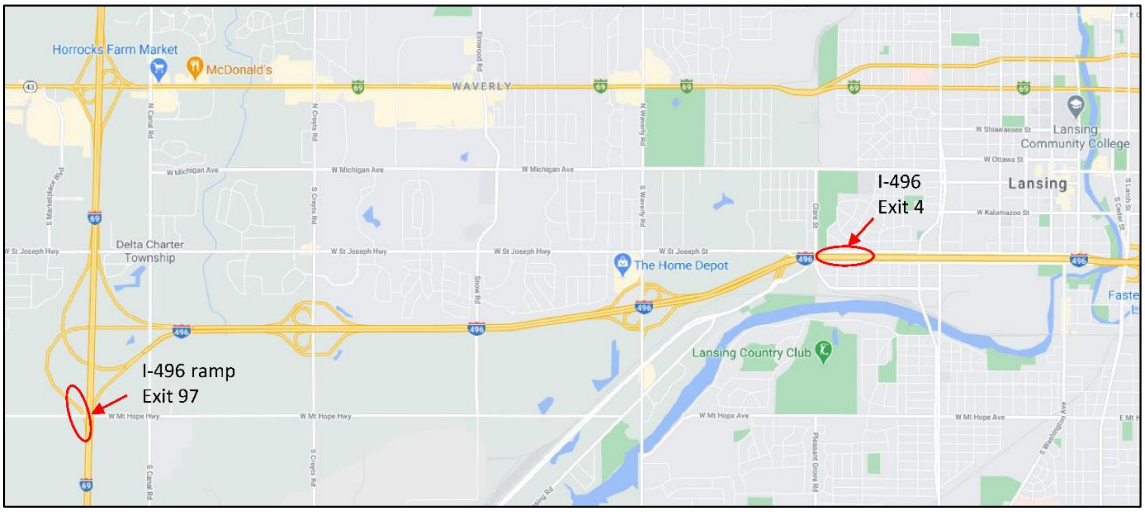

Figure 6-8 Location of the two tested sections of the I-496

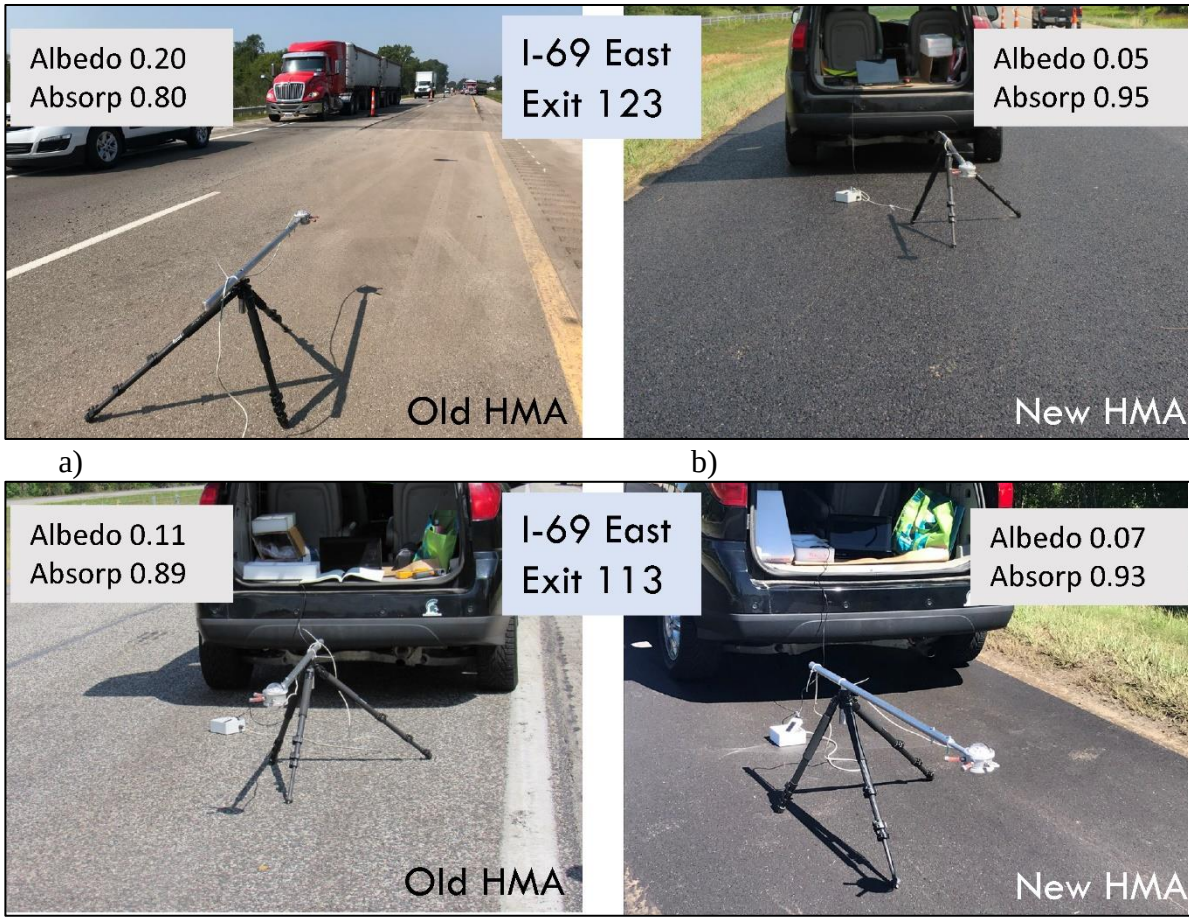

Figure 6-9 Test section on the I-69 segment 2 (exit 123): a) old surface in HMA, b) new reconstruction in HMA; test section on the I-69 segment 1 (exit 113): c) old surface in HMA, d) new reconstruction in HMA.

Figure 6-10 a) Test section on the ramp of the I-496 (exit 97), new and old cement concrete surfaces; b) test section on the I-496 (exit 4), old cement concrete and old HMA surfaces.

Table 6-28 Summary data on climate, field conditions, and measurements

Location	I-69 Exit 123		I-69 Exit 113		I-496 Exit 97		I-496 Exit 4	
Surface condition	Old HMA	New HMA	Old HMA	New HMA	Old PCC	New PCC	Old PCC	Old HMA
Date Time	8/27/2020 11:47	8/27/2020 12:28	8/31/2020 13:40	8/31/2020 14:31	10/13/2020 10:17	10/13/2020 10:30	10/13/2020 10:58	10/13/2020 11:07
Weather	Sunny with no cloud							
Air temperature [°C]	28.0	30.4	26.8	32.2	11.5	11.5	11.5	11.5
Wind speed [m/s]	2.00	1.80	1.16	0.70	0.05	0.05	0.50	0.50
Pavement temperature [°C]	37.0	49.0	38.0	48.6	11.6	12.0	10.4	11.4
SR Direct *G* [W/m²]	690.99	766.32	871.04	833.42	409.73	476.16	514.99	539.20
SR Reflected *R* [W/m²]	139.42	39.65	97.39	56.33	153.40	206.30	133.90	122.52
Albedo *A*	0.20	0.05	0.11	0.07	0.37	0.43	0.26	0.23
Absorptivity *S*	0.80	0.95	0.89	0.93	0.63	0.57	0.74	0.77

Note: HMA= Hot Mix Asphalt; PCC= Portland Cement Concrete.

6.3 LABORATORY CHARACTERIZATION OF MATERIALS

Several material samples, including loose HMA mixtures, asphalt binders, asphalt pavement cores, concrete pavement cylinders, beams, and cores, were collected from the selected 2020 and 2021 projects. In addition, loose asphalt mixtures and pavement cores from projects constructed in 2013 and 2014 were also provided by the MDOT. This section summarizes the laboratory characterization of all the provided materials.

6.3.1 HMA Material Testing

The MDOT provided HMA samples for 11 mix types and cores from 9 projects constructed between 2013-2014, in addition to those from 2020 and 2021 selected projects. Table 6-29 presents the details of the loose HMA mixes. Also, cores were provided for various projects, as shown in Table 6-30. This section summarizes the results of the HMA material testing. Laboratory characterization of HMA material considered the following tests on the loose mix samples and HMA cores received from the MDOT:

- Dynamic Modulus |*E**| Test (AASHTO PP60, AASHTO T342, AASHTO R84)
- Complex Shear Modulus of Binder (*G**) Test (AASHTO T315)
- Creep compliance D(t) and Indirect Tensile Strength (IDT) at low temperatures (AASHTO T322)
- Creep Compliance (Park, 1999)

Table 6-29 Summary of Loose Mix from MDOT

Mix type	Route	Sampling date
2E3	M-50	2013/8/13
3E30	I-94	2013/9/13
4E03	US-2	2014/9/16
4E1	M-26	2014/9/16
4E10HS	M-37	2013/9/18
5E3	US-12	2014/9/23
5E3	M-57	2013/2/26
5E3CR	M-57	2013/7/10
5E3PHS	M-57	2013/7/26
5E30	I-96	2014/10/2
HMASL	US-10	2013/7/19
4E3, 5E3	I-94	2020 selected project
3E30-B, 3E30-L, 5E30-T	I-69 WB	2021 selected project
3E3, 4E3, 5E3HS	M-3	2021 selected project
2E10, 3E10, 4E10, 5E10	I-75	2021 selected project
3E3, 4E3, 5E3	US-41	2020 and 2021 selected project

Table 6-30 Summary of field cores from MDOT

Mix type	Route
3E30	I-94 (2013)
4E03	US-2 (2014)
4E10HS	M-26 (2014)
4E10HS	M-37 (2013)
5E3	M-57 (2013)
5E3	US-12 (2014)
5E3	US-41 (2021 selected project)
5E3HS	M-3 (2021 selected project)
5E3P	M-57 (2013)
5E3CR	M-57 (2013)
5E3, 4E3	I-94 (2020 selected project)
5E10	I-75 (2021 selected project)
5E30	I-96 (2014)
5E30-T	I-69 (2021 selected project)

Note: At least 3 replicates for each project

6.3.1.1. Dynamic Modulus |E| Testing*

The |E*| tests were conducted to characterize the stiffness of the asphalt mixtures at different temperatures and loading frequencies following AASHTO T342. The average of three replicates was used to generate |E*| master curves, per AASHTO R84. Each replicate was tested in uniaxial compression mode at temperatures of -10, 10, 21, 37, and 54°C and loading frequencies of 25, 10, 5, 1.0, 0.5, and 0.1 Hz. Figure 6-11 through Figure 6-14 display the dynamic modulus master curves for HMA mixes from I-69, M-3, I-75, and US-41 (2021 selected) projects. Figure 6-11 shows that the 3E30-B mix is slightly stiffer, followed by the 3E30-L, and the 5E30 mix is the least stiff at all temperatures and frequencies. The 3E30-B mix used a softer PG 64-22 binder with 13% RAP content, while the 3E30-L and 5E30 mixes

included a polymer-modified PG 70-28 binder with 13% and 20% RAP contents, respectively. Although with a softer binder and lower RAP content, the higher stiffness of the 3E30-B mix can be attributed to the gradation of the mixes; 3E30-B was the coarser mix of the three, while 5E30 used a fine gradation.

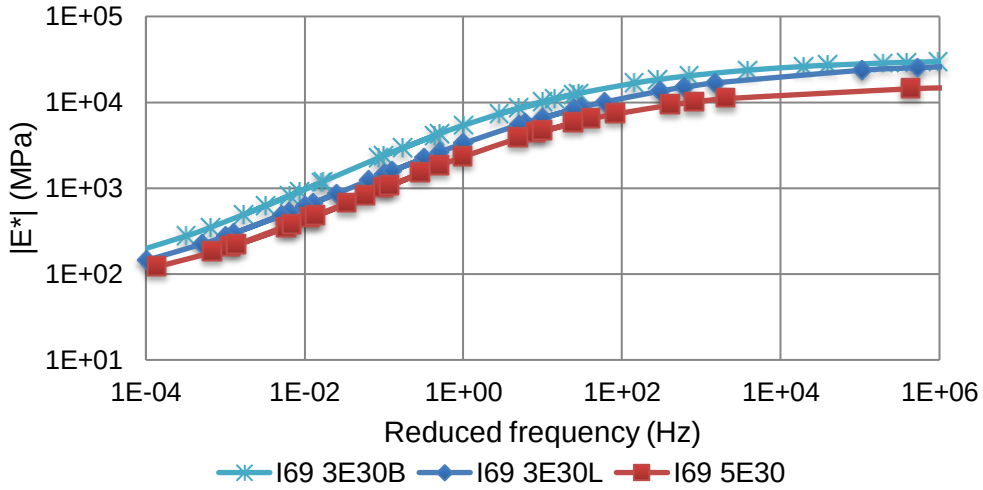

Figure 6-11 |*E| master curves for mixes from I-69 (2021) project**

Figure 6-12 compares the |*E**| master curves of the 3E3, 4E3, and 5E3 mixes of the M-3 (2021) project. The results show that the 4E3 mix is stiffer at high temperatures and low frequencies than the 3E3 and 5E3 mixes. However, at low temperatures and higher frequencies, the 4E3 mix performed similarly to the 3E3 mix. The |*E**| master curve for the 5E3 mix indicates its lowest stiffness for all temperatures and frequencies owing to a finer aggregate structure. Figure 6-13 displays the dynamic modulus master curves for the 2E10, 3E10, 4E10, and 5E10 mixes of the I-75 (2021) project. The 2E10 and 3E10 mixes included a PG 58-22 binder with 10% and 16% RAP contents, respectively. The 4E10 and 5E10 were PG 64-28 mixes with 18% and 20% RAP contents, respectively. However, the master curves indicate that all four mixes from the project are similar at all temperatures and frequencies. Figure 6-14 shows the |*E**| master curves for the HMA mixes from the US-41 (2020 & 2021) project. The figure shows that the 3E3 and 5E3 mixes have similar stiffnesses irrespective of the temperatures and frequencies. The 4E3 mix is similar in stiffness to the other two mixes at low temperatures and higher frequencies but is softer than them at the lower frequencies (and higher temperatures).

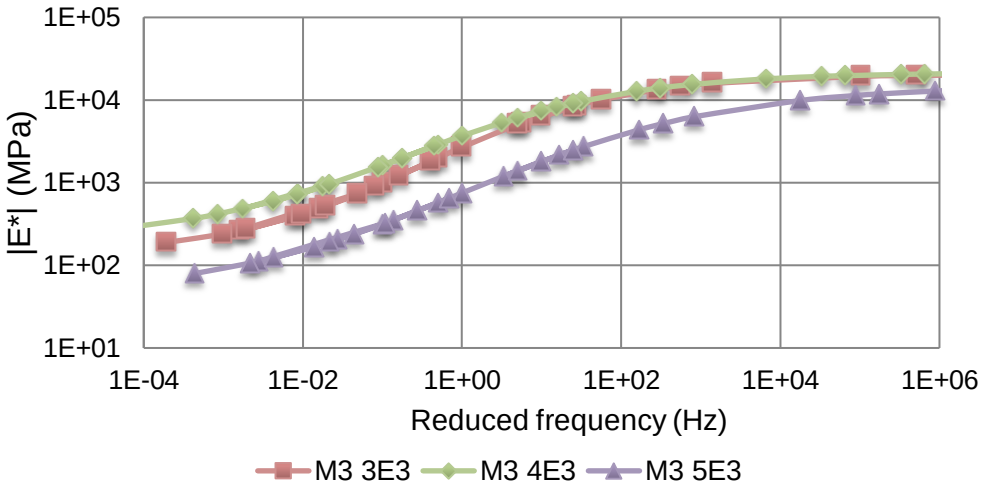

Figure 6-12 |*E| master curves for mixes from M-3 (2021 project)**

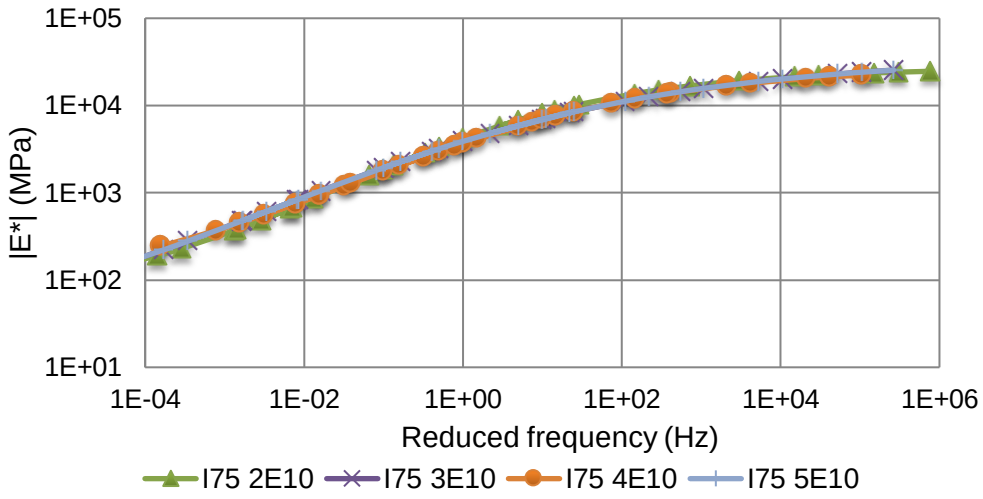

Figure 6-13 |*E| master curves for mixes from I-75 (2021) project**

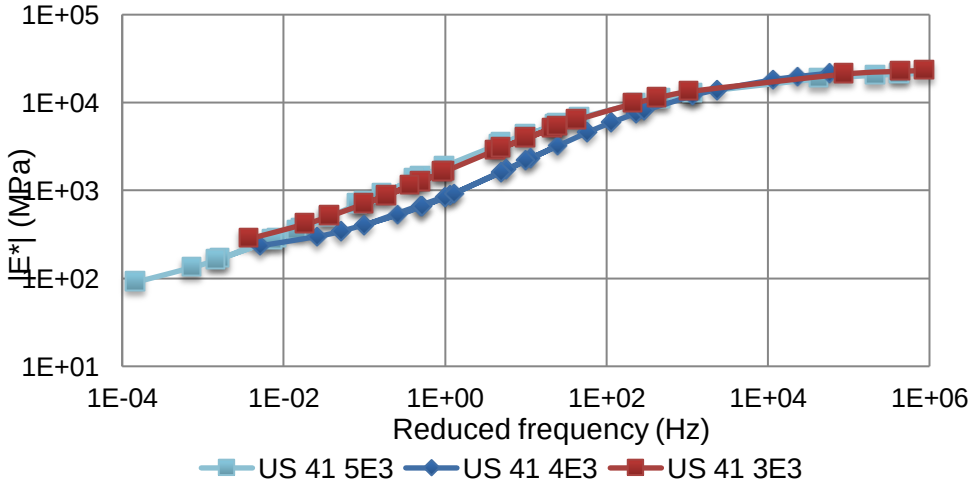

Figure 6-14 |*E| master curves for mixes from US-41 (2020 & 2021) project**

Figure 6-13 through Figure 6-15 display the |*E**| master curves for the HMA mixes from selected 2020 and earlier projects. Figure 6-13 shows the |*E**| master curves for the 3E30-B, 4E3, and 5E3 mixes from I-94 while the 5E30 mix from the I-96 project. The master curves show that the 3E30-B and 5E30 mixes are similar in performance and are stiffer than the 4E3 and 5E3 mixes for all frequencies and temperatures. All the mixes from I-94 have similar stiffness at high frequencies (and low temperatures); however, the 4E3 and 5E3 mixes have similar stiffness at low frequencies and are softer than the 5E30 mix. Figure 6-14 shows |*E**| master curves for the different HMA mixtures from the M-26, M-37, M-50, and M-57 projects. The 5E3 and 2E3 mixtures have similar |*E**| master curves and are stiffer than the 4E1 and 4E10HS mixtures at low frequencies. Figure 6-15 shows that the US-2, US-10, and US-12 project mixes have similar stiffness for all frequencies (and temperatures).

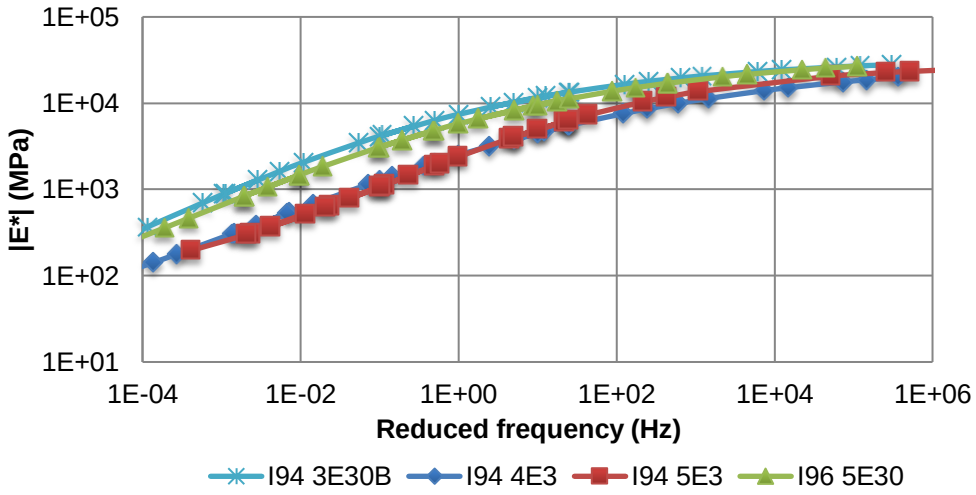

Figure 6-15 |*E| master curves for mixes, I-94 (2013 & 2020) and I-96 (2014) projects**

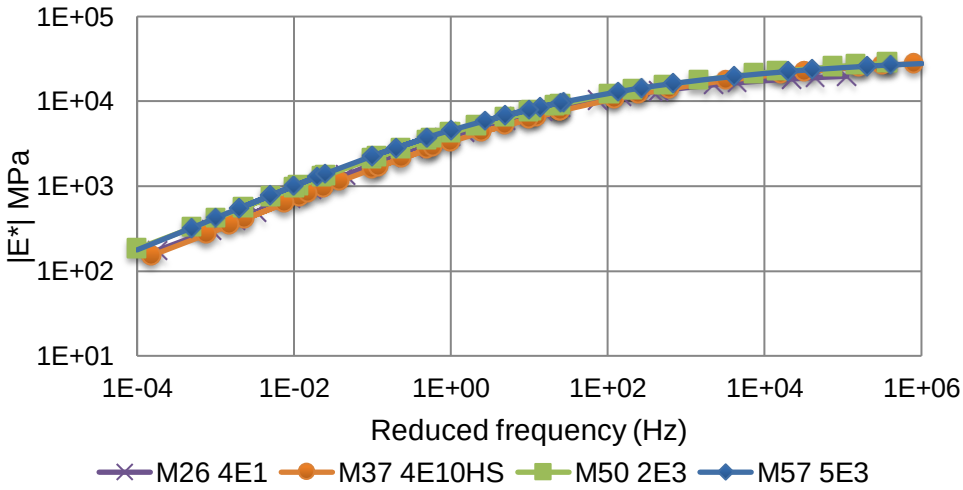

Figure 6-16 |*E| master curves for mixes, M-26 (2014), M-37, M-50, and M-57 (2013)**

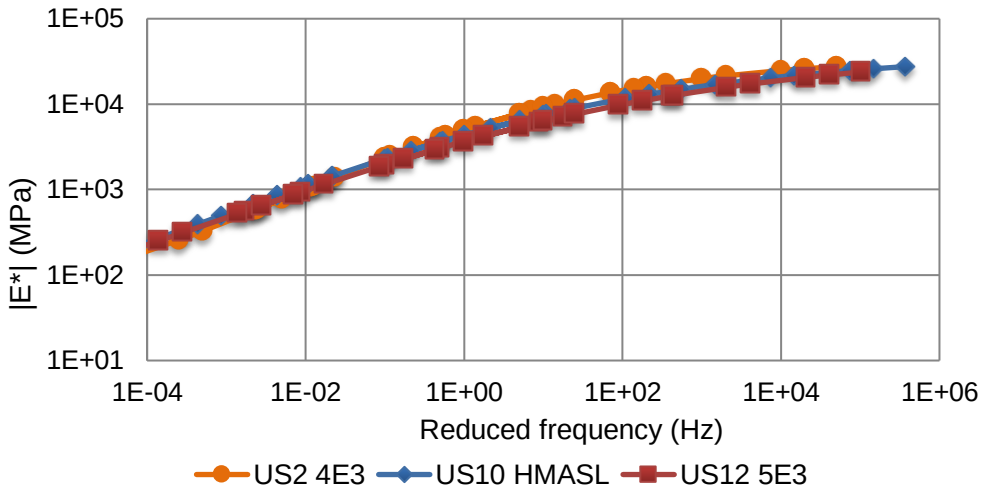

Figure 6-17 |*E| master curves for mixes, US-10 (2013), US-2, and US-12 (2014) projects**

6.3.1.2. Indirect Tensile Strength Testing

The indirect tensile test (IDT) evaluates the strength of asphalt mixtures and is associated with other performance tests to estimate its resistance to rutting deformation and cracking damage. Figure 6-18 displays the results of the IDT tests for all the projects whose cores were provided by the MDOT. Among the 2021 projects, the 5E30 mix from I-69 has the highest IDT strength, followed by M-3 and I-75, and US-41 has the lowest strength. The results for I-69 are reasonable since the mix is designed for a higher traffic volume than those from other projects. The I-75 was expected to have higher IDT strength than M3 and US41; however, many cores for I-75 were collected from the shoulder, resulting in lower IDT strength for the 5E10 mix from I-75. The 5E3 mix from the I-94 project showed the highest IDT strength, while the same mix from M-57 displayed the lowest strength. Overall, the average IDT strength for all mixtures ranges between 200 psi to 500 psi.

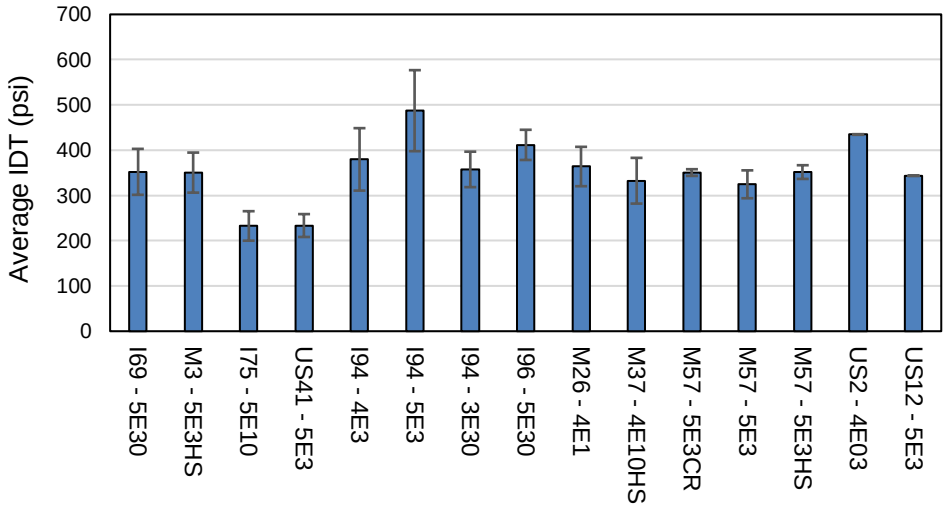

Figure 6-18 IDT strength results

6.3.1.3. Creep Compliance

The creep compliance results can represent the trend of asphalt mixtures from deformation to fracture. The creep compliance was determined at three temperatures, i.e., -4, 14, and 32°F, and the time nodes of 1, 2, 5, 10, 20, 50, and 100s. The values from three replicates of each mix were summarized and drawn into curves. Generally, the creep compliance value at high temperatures is higher than at low temperatures because the materials become soft when the temperature increases and reduces the stiffness. In addition, as time goes by, creep compliance will gradually increase. The trend is true for all four roadway materials. Figure 6-19 displays the creep compliance results for the 3E30-B, 3E30-L, and 5E30 mixes of the I-69 (2021) project. The 3E30-B mix displayed the least D(t) values. At the same time, 5E30 showed the highest creep compliance results indicating that the 3E30-B mix will accumulate permanent deformation slowly and perform better than the other mixes. Figure 6-20 shows the creep compliance results for the HMA mixes from the M-3 (2021) project. The creep compliance results indicate that the 5E3 mix performed inferior to the 3E3 and 4E3 mixes.

Figure 6-21 shows the results for the HMA mixes from the I-75 (2021) project. It is observed that the results can be divided into three parts: the top part of the figure shows the creep compliance at high temperatures, creep compliance at low temperatures is located at the bottom of the figure, and creep compliance values for the intermediate temperature are seen in the middle of the figure. The 4E10 has the lowest potential to accumulate permanent deformation at low temperatures. The 2E10, 3E10, and 4E10 mixes have similar performance at the intermediate temperature, while at high temperatures, the 3E10 and 5E10 have similar lowest creep compliance values.

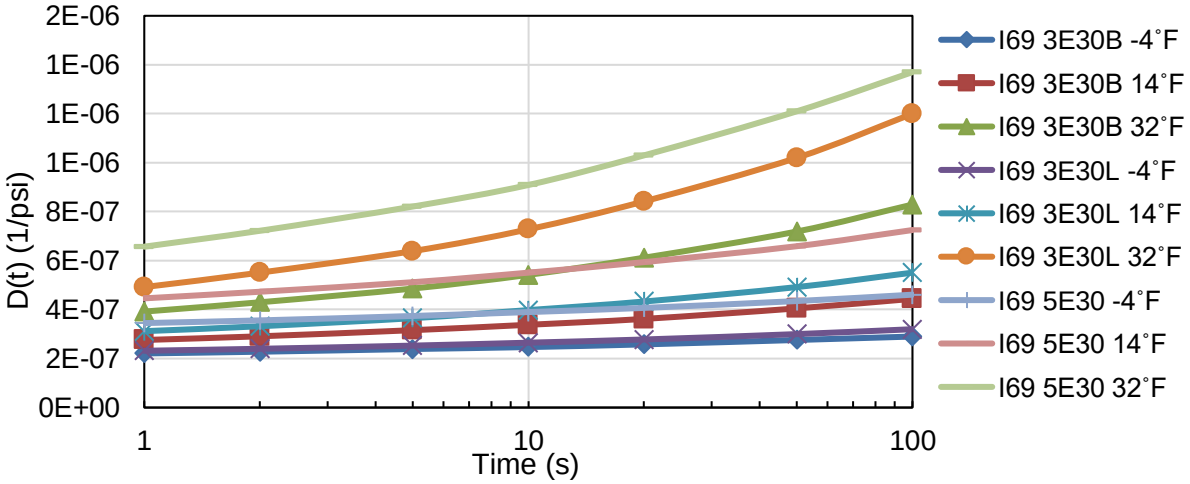

Figure 6-19 Creep compliance results – I-69 (2021) project

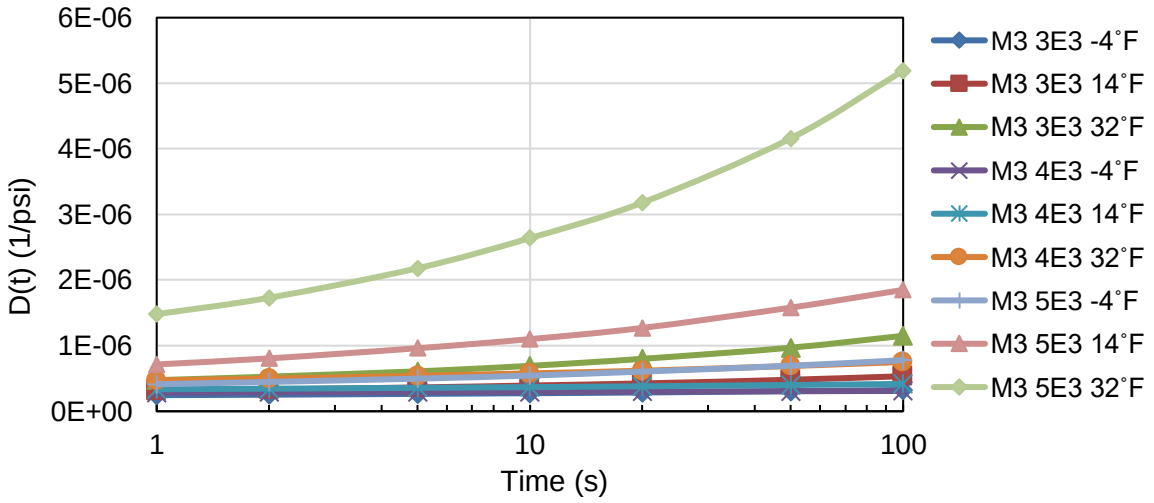

Figure 6-20 Creep compliance results – M-3 (2021) project

Figure 6-22 shows the creep compliance values for the US-41 project's 3E3, 4E3, and 5E3 HMA mixtures. The creep compliance values for all the mixes are smallest at low temperatures; however, at high temperatures, all mixtures, especially the 5E3, have a higher potential to deform permanently. Figure 6-23 through Figure 6-26 shows the creep compliance results of the HMA mixtures from projects from 2020 and earlier years.

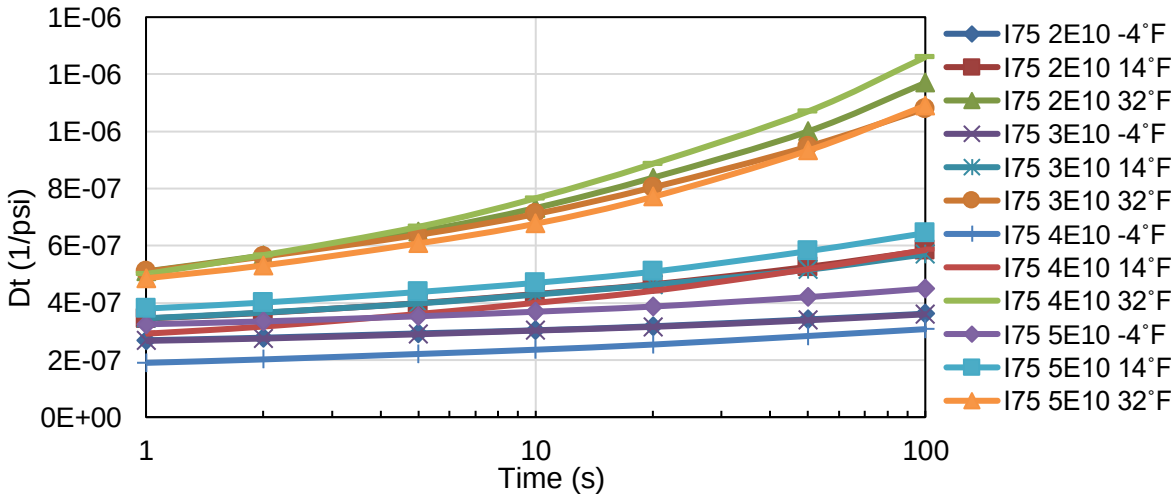

Figure 6-21 Creep compliance results – I-75 (2021) project

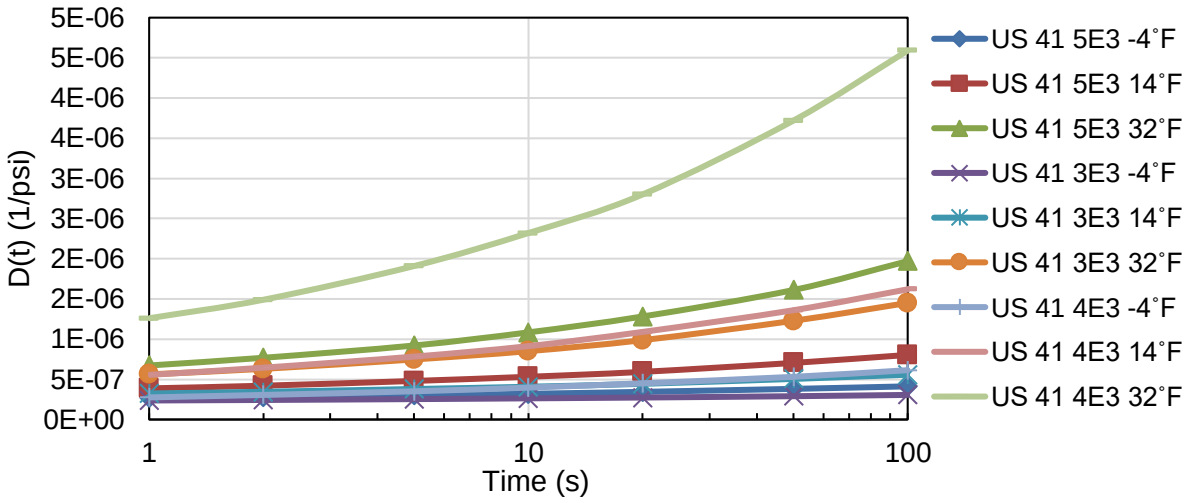

Figure 6-22 Creep compliance results – US-41 (2020 & 2021) project

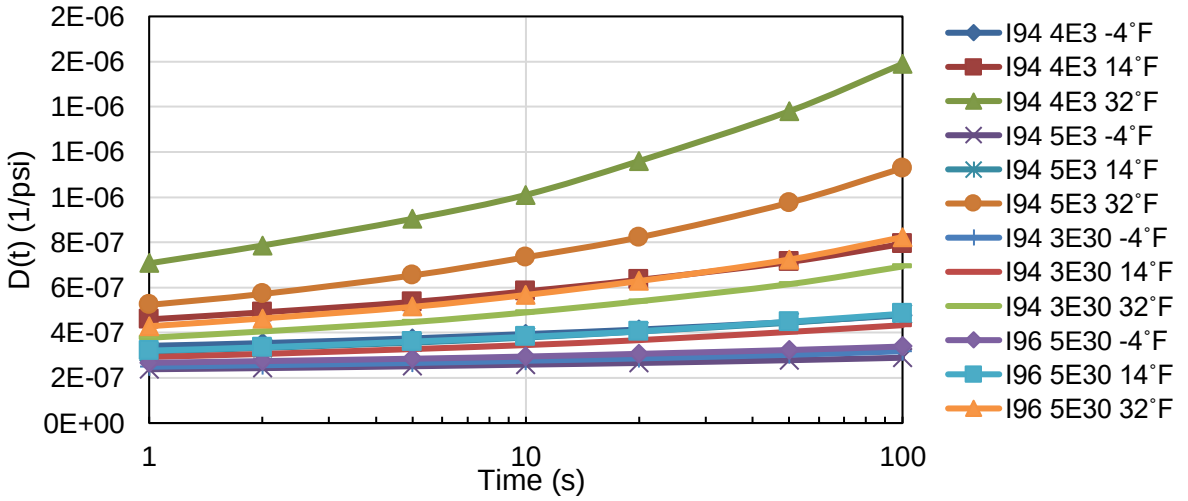

Figure 6-23 Creep compliance results – I-94 & I-96 projects

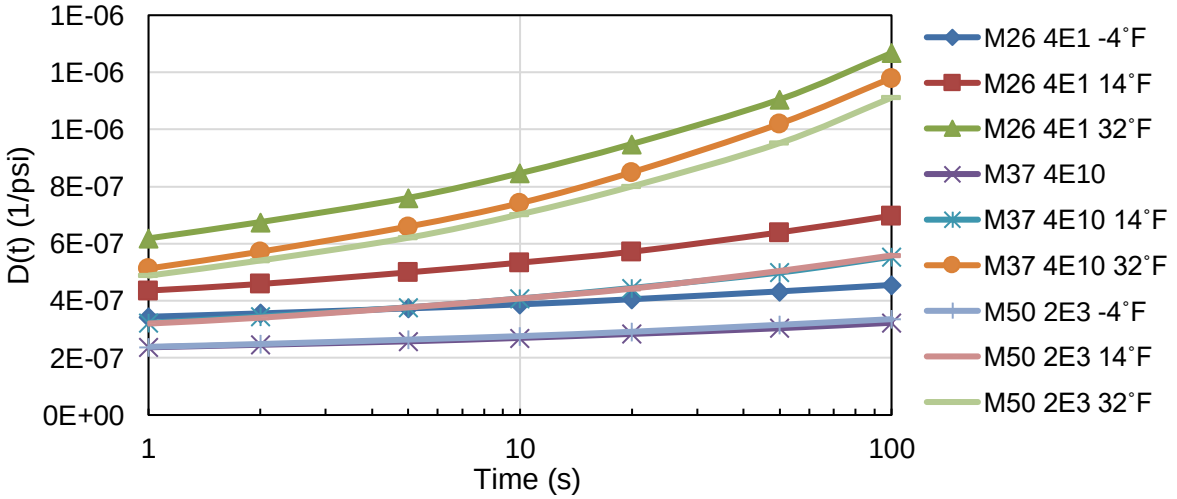

Figure 6-24 Creep compliance results of mixes from M-26, M-37, and M-50 projects

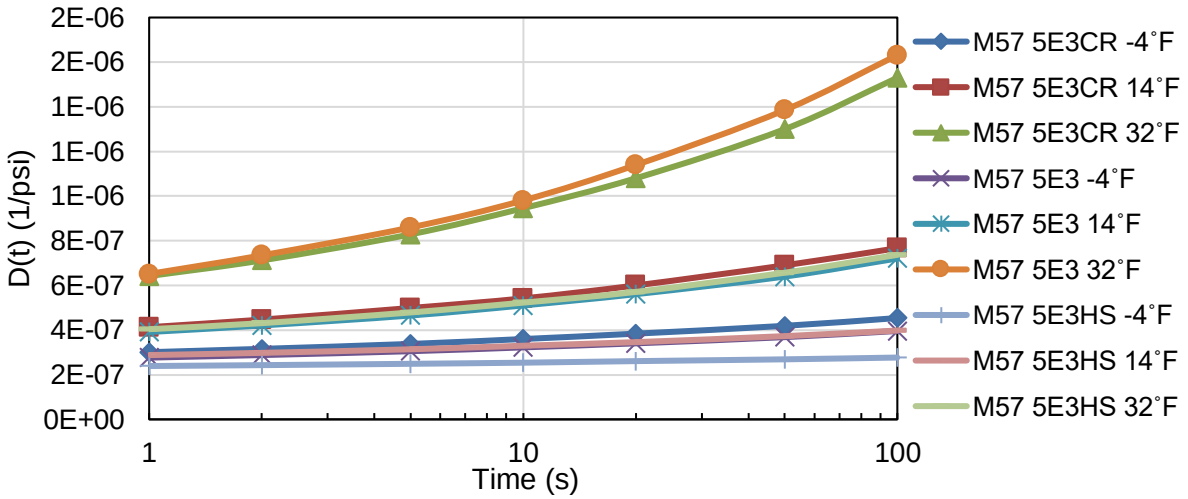

Figure 6-25 Creep compliance results of mixes from the M-57 project

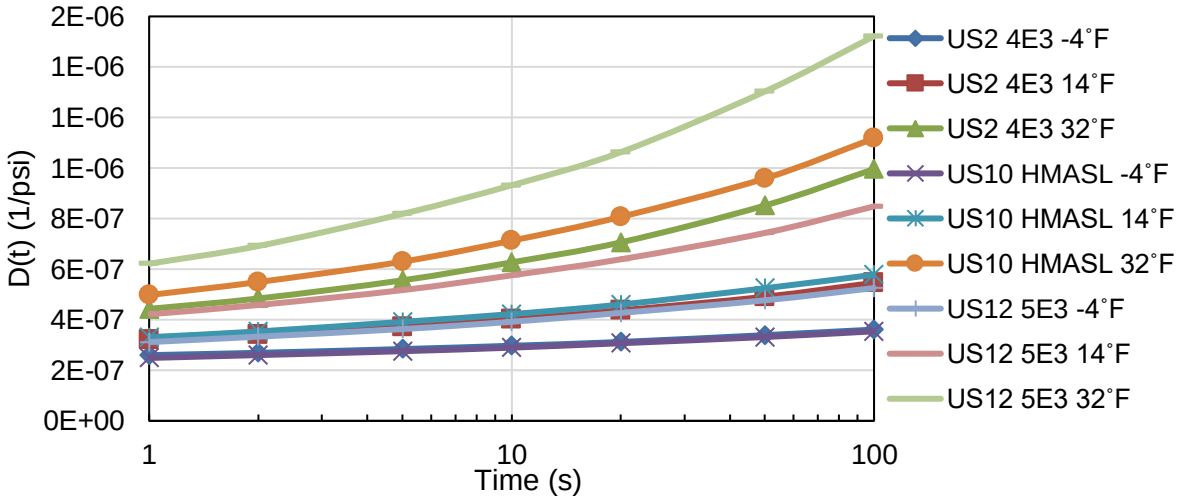

Figure 6-26 Creep compliance results of mixes from US-2, US-10, and US-12 projects

6.3.1.4. Asphalt Binder Complex Shear Modulus (|G|)*

Table 6-31 lists the different asphalt binders provided by the MDOT. The |*G**| testing was conducted per AASHTO T 315. The |*G**| master curves and phase angles were summarized. Just as dynamic modulus results discussed earlier, a higher |*G**| represents stiffer asphalt binder, and low frequency corresponds to higher temperatures and vice versa. A higher phase angle indicates a more viscous asphalt binder; a lower phase angle indicates a more elastic one.

Table 6-31 Summary of asphalt binders received from the MDOT

Project	Binder Type
I69	PG 64-22, PG 70-22P leveling, PG 70-22P top
M3	PG 58-28, PG 70-22P
I75	PG 58-22, PG64-28
Dickman road	PG 64-28
M37	PG 70-28P
I75	PG 58-22, PG 64-28
I94	PG 64-22
I96	PG 70-28P
M3	PG 58-28, PG 70-22P
M26	PG 58-28
US2	PG 58-28
US12	PG 58-34
US41	PG 58-28, PG 58-34

Figure 6-27 shows the |*G**| master curves for the three binders tested from the I-69 (2021) project. The |*G**| values of the PG70-22P binders are larger than PG64-22 at low frequency, indicating better performance in rutting. The PG70-22P binder also displayed smaller |*G**| values compared to PG 64-22 at high frequency, indicating a better performance potential in fatigue. Such behavior can be expected owing to the polymer modification of the PG70-22P binder. Figure 6-28 displays the phase angle of the binders from the I-69 project. The PG70-22P top and leveling binders had the same phase angle but were smaller than the PG64-22 for all frequencies, illustrating that the PG70-22P binders were more elastic than PG 64-22. The |*G**| master curves and the phase angle plots for the remaining binders can be found in Appendix B.

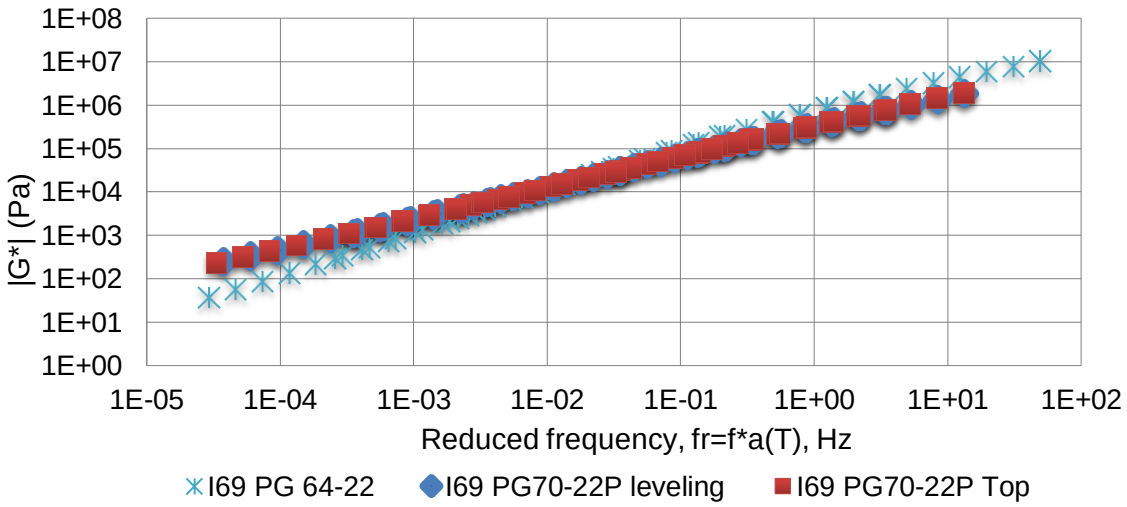

Figure 6-27 |*G| master curve of I-69 binders**

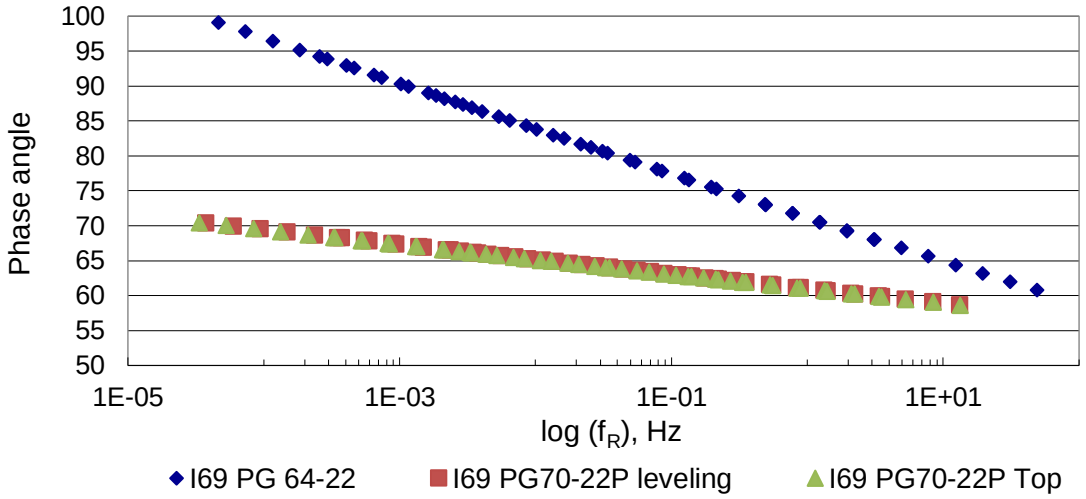

Figure 6-28 Phase angle for I-69 binders

6.3.1.5. IDEAL-CT Testing

As part of the NCHRP Innovations Deserving Exploratory Analysis (IDEA) Project No.195, a new test method known as the Indirect Tensile Asphalt Cracking Test (IDEAL-CT) was developed for asphalt mix design, quality control (QC), quality assurance (QA) purposes. The IDEAL-CT is very similar to the traditional IDT strength test. It is performed using the IDT strength test equipment at room temperature on laboratory-prepared cylindrical samples with various diameters (100 or 150 mm) and thicknesses (38, 50, 62, 75 mm, etc.). It can also be performed on field cores that can be directly tested without cutting, notching, coring, gluing, instrumentation, or any other sample preparation. IDEAL-CT is relatively simple, practical, quick, and completed within a minute, using a loading rate of 50 mm/min (*4, 5*)

The key performance-related cracking parameter derived from the measured load versus displacement curve using the IDEAL-CT is named the cracking test index (CT_{Index}). The index form is inspired by the well-known Paris' law and Bazant and Prat's work on crack propagation (*6, 7*). The CT_{Index} is calculated using Equation (6-10):

$$CT_{Index} = \frac{t}{62} \times \frac{G_f}{\frac{P}{l}} \times \left(\frac{l}{D}\right) \qquad (6\text{-}10)$$

where fracture energy G_f is calculated by dividing the work of fracture (the area under the curve of the load versus vertical displacement plot) by the area of the cracking face (diameter times the thickness); the term *P/l* is a modulus parameter (i.e., the slope of the load-displacement curve) and the term *l/D* is a strain tolerance parameter. For any load versus displacement curve, the G_f is constant; however, the parameters *P/l* and *l/D* change between different points; the asphalt mixtures are visco-elastic-plastic, where damage can occur because of micro- or macro cracking.

The macro-crack occurs in the post-peak load segment, which is accompanied by crack propagation and, thus, a reduction in the load-bearing capacity of the mixture. Hence, the

CT_{Index} calculations focus on the post-peak segment of the load versus displacement curve. For the determination of the *P/l* parameter, an analysis of more than 200 IDEAL-CT load-displacement curves was generated from a variety of asphalt mixes with varying gradation, binders, and RAP/RAS contents was undertaken. The results revealed that the post-peak load at the inflection points is 75 percent of the average value of the peak loads of those curves with a standard deviation of five ($\sigma = 5$). Hence, the use of post-peak point (PPP75), i.e., where the load is reduced to 75 percent of the peak load, for the determination of parameters *P/l* and *l/D* were found to be stable and consistent, recommended for use in the CT_{Index} calculations. Since the *P/l* parameter in the post-peak segment of the load versus displacement curve is not a true asphalt mix modulus parameter but an overall representative of the cracked asphalt mix's modulus, developers suggested using the absolute value of the slope between the post-peak point (PPP_{85}). That is where the load is reduced to 85 percent of the peak load and post-peak point (PPP_{65}) (i.e., where the load is reduced to 65 percent of the peak load). A detailed discussion on the selection and use of the parameters shown in the final calculations of the CT_{Index} as shown in Equation (6-11) can be found in the NCHRP IDEA-195 project report and excluded here for brevity (*4*).

$$CT_{Index} = \frac{t}{62} \times \frac{G_f}{|m_{75}|} \times \left(\frac{l_{75}}{D}\right) \tag{6-11}$$

where *t* is the specimen thickness (mm), G_f is fracture energy (Joules/m^2), $|m_{75}|$ is the absolute value of the slope between PPP_{85} and PPP_{65} (N/m), l_{75} is the displacement corresponding to the 75 percent of the peak load at the post-peak stage (mm), and *D* is the specimen diameter (mm).

The IDEAL-CT setup incorporated the use of a 6-inch diameter specimen IDT strength test fixture with the load applied such that a constant load-line displacement (LLD) rate of 50 ± 2 mm/min was obtained and maintained during the test's duration using a Material Testing System (MTS) (see Figure 6-29). As recommended, test specimens were conditioned in an environmental chamber for 2 hours at 25°C and tested within 4 minutes after removal from the chamber to maintain a uniform specimen temperature (*4*). The applied load and the sample displacement with time were recorded during the test until the load dropped below 100 N. Figure 6-29 displays the load versus displacement curves for all 43 cores obtained from the I-69, I-75, and M-3 projects (2021 construction) and tested. The mix volumetrics, aggregate gradations, and the measured air voids and thicknesses of the cores are given in Table 6-32. As recommended, a minimum of three cores were tested per asphalt mixture. One of the objectives of this work is to compare and assess the relative performance of the different mix types. This comparison was accomplished by considering the area under the load-displacement curve until the 10 mm displacement. Because beyond 10 mm, the curve showed a slight load increase. The broken sample was prevented from falling out of the IDT fixture until the MTS actuator was raised due to the fixture's vertical support. The resistance posed by the broken sample caused a slight jump in the load.

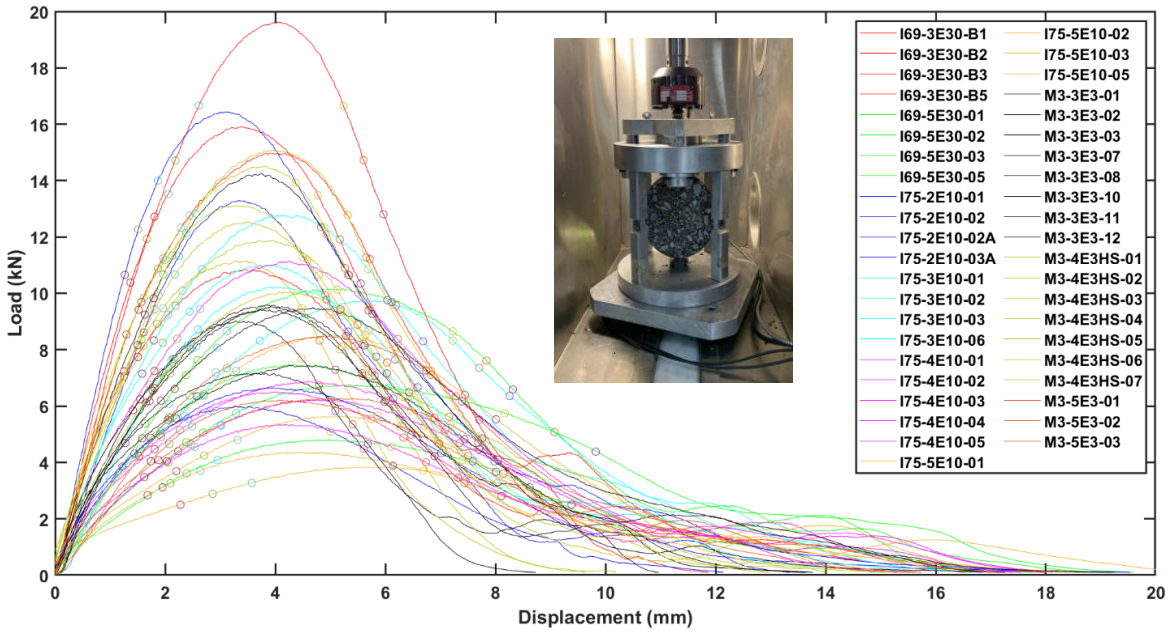

Figure 6-29 IDEAL-CT setup and load versus displacement curves for all samples

Using the load-displacement data obtained from the test, the CT_{Index} was determined for each mix along with other indexes such as flexibility index (FI), cracking resistance index (CRI), toughness index (TI), and the N_{flex} factor.

The FI was developed under the FHWA study that investigated testing protocols for testing engineering properties of AC mixtures with varying amounts of RAP and RAS. The developed FI was shown to differentiate well among the mixes concerning their fatigue cracking resistance (*8*). The FI describes the material's cracking behavior following the AASHTO TP124-16 specification. Mathematically, FI is defined as the ratio of the fracture energy (G_f) to the slope of the post-peak load-displacement curve at the inflection point, as shown by Equation (6-12):

$$FI = k \times \frac{G_f}{|m|} \tag{6-12}$$

where k is a scaling coefficient ($k = 0.01$) while $|m|$ is the absolute value of the post-peak slope at the inflection point of the load-displacement curve.

Table 6-32 Mix volumetrics, aggregate gradations, and measured thicknesses and air voids for the nine asphalt mix cores

Mix ID	**2E10**	**3E3**	**3E10**	**3E30-B**	**4E3HS**	**4E10**	**5E3HS**	**5E10**	**5E30**
Binder PG grade	58-22	58-22	58-22	64-22	70-22P	64-28	70-22P	64-28	70-28P
Binder content (%)	4.48	4.97	5.08	4.92	5.54	5.49	5.99	6.10	6.64
Design air voids (%)	3	3	3	3	3	3	3	3	3
VMA (%)	12.99	13.52	13.88	14.05	14.51	14.86	15.80	16.04	16.25
VFA (%)	76.90	77.80	78.38	78.69	79.33	79.82	81.01	81.29	81.50
RAP content (%)	10	24	16	13	27	18	24	20	15
NMAS (mm)	19	12.5	19	12.5	12.5	12.5	9.5	9.5	9.5
Aggregate gradation (% passing)									
P 1-1/2" (37.5mm)	100	100	100	100	100	100	100	100	100
P 1" (25.0 mm)	100	100	100	100	100	100	100	100	100
P 3/4" (19.0 mm)	89.2	100	94.1	100	100	100	100	100	100
P 1/2" (12.5 mm)	74.9	87.9	87.1	87.6	93.9	91.3	99.8	99.6	100
P 3/8" (9.5mm)	71.0	77.7	84.9	77.7	86.5	85.0	97.6	97.6	99.5
P No.4 (4.75mm)	62.8	58.4	71.2	61.8	76.5	74.2	77.2	84.4	79.4
P No.8 (2.36mm)	37.5	44.1	44.8	48.0	51.3	50.8	55.1	56.1	60.8
P No.16 (1.18mm)	23.4	33.4	30.3	34.8	39.0	34.8	39.5	38.5	41.6
P No.30 (600µm)	15.5	24.8	21.0	22.8	28.9	24.3	28.2	26.8	27.6
P No.50 (300µm)	10.3	14.6	12.6	12.3	16.8	14.6	16.9	15.8	16.8
P No.100 (150µm)	6.6	7.1	7.0	6.7	7.9	7.8	8.3	8.2	9.6
P No.200 (75µm)	4.5	4.5	4.9	4.5	4.9	5.4	5.1	5.6	5.7
Measured parameters									
Avg. air voids (%)	6.0	5.6	6.5	5.7	5.8	7.2	4.5	7.2	7.0
StDev. air voids (%)	1.1	0.9	1.4	0.4	0.5	1.6	2.2	1.3	1.5
Avg. thickness (mm)	55.0	55.0	59.0	57.8	54.1	53.3	33.9	43.6	41.5
StDev. thickness (mm)	22.7	14.3	7.3	7.7	8.2	6.8	4.4	10.4	8.2

Note: 3E30-B = 3E30 mix used as a base course, HS = High-stress mix, StDev. = Standard deviation.

The CRI is a cracking parameter derived from the load-displacement curve of an asphalt mixture aimed at discriminating between the mixes with different peak loads but similar fracture energies relative to their maximum strengths (*9*). Equation (6-13) shows the mathematical form of the CRI, which is a ratio between the G_f and the peak load (P_{max}).

$$CRI = \frac{G_f}{|\,P_{max}\,|} \tag{6-13}$$

The TI aims to capture the asphalt mixture's response during the crack propagation, i.e., within the post-peak segment of the load-displacement curve. Developed by Parez-Jimenez et al., the mathematical form of the TI is given by Equation (6-14) (*10*):

$$TI = \left(G_f - G_{f P_{max}}\right) - \left(\delta_{50P_{max}} - \delta_{P_{max}}\right) \times 10^{-3} \tag{6-14}$$

where G_{fPmax} is the fracture energy calculated until the peak load (P_{max}), δ_{50Pmax} is the post-peak displacement at a 50% reduction of the load, while δ_{Pmax} is the displacement at the peak load (P_{max}).

The Nflex is calculated by determining the toughness (T_{inf}) from the load-displacement curve up to the inflection point in the post-peak segment and dividing it by the absolute value of the slope of the curve at the inflection point as shown in Equation (6-15). The N_{flex} factor was introduced for the IDT strength test and has also been used for the SCB tests (*11*).

$$N_{flex} = \frac{T_{inf}}{|\, m \,|} \tag{6-15}$$

After obtaining the load-displacement curves for each specimen, the CT_{Index} was calculated. This study also used the same data to calculate each mix type's FI, CRI, TI, and N_{flex} factor for comparison purposes only. Figure 6-30 displays the bar charts for each of the determined cracking indexes. Figure 6-30(a) shows that the CT_{Index} values for the base course (2E & 3E) mixes are generally lower as compared to the leveling and surface course (4E & 5E) mixes, as expected. However, the coefficient of variation (CoV) for the 2E10, 3E3, and 5E30 mixes (see Table 2) is slightly higher than the maximum CoV of 23.5% reported for the laboratory-prepared samples in the NCHRP IDEA-195 report. Such variability can be attributed to testing field-extracted cores rather than laboratory-prepared samples that are more uniform in their composition. The 5E mixes show the highest crack resistance (i.e., higher CT_{Index}), which is expected as these mixes are binder-rich with more than 6% binder content. Among the base course mixes, the 3E30 has the lowest CT_{Index}, which can be explained by the stiffer binder and its lower content within this mix compared to the others. The 4E3HS mix with higher binder content shows lower CT_{Index} than the 4E10 mix because of higher RAP content.

The FI plot in Figure 6-30(b) shows similar trends to the CT_{Index}; however, with larger CoV, especially for the 2E10 mix. The CRI displayed lower variability than the CT_{Index} and the FI, as shown in Figure 6-30(c). The 5E3HS mix has a higher CRI than the other "5E" mixes. The G_f value for the 5E3HS mix was the highest among the surface course (5E) mixes, a possible reason for its highest CRI value, which is simply the ratio between the G_f and the peak load. It is worth mentioning that the 5E3HS mix specimens have the lowest air voids among the "5E" mixes. The TI has the lowest CoV among all the indexes (see Table 6-33), while the trends observed in Figure 6-30(d) are similar to the CT_{Index} ones for all mixes except the "5E" mixes that resemble the trends observed for TI. The highest variability (i.e., highest CoV) is observed in the N_{flex} values with mixed trends among all the mixes, as displayed in Figure 6-30(e). Overall, the CT_{Index} can differentiate between different mix types (*4*). The CT_{Index} displayed similar trends (and similar CoV) as the FI, which is the same observation made in the NCHRP IDEA-195 report about the two indexes. Among the indexes, the highest variability is observed in the N_{flex} values, followed by CRI, while TI had the lowest variability.

(a)

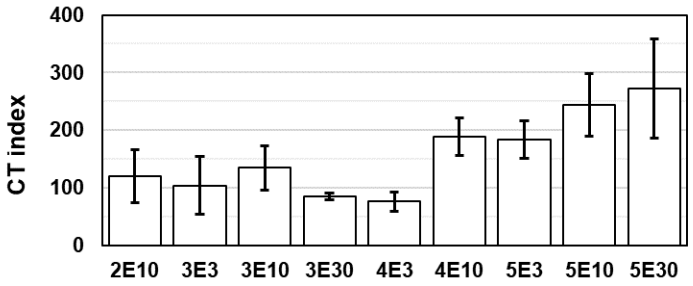

(b)

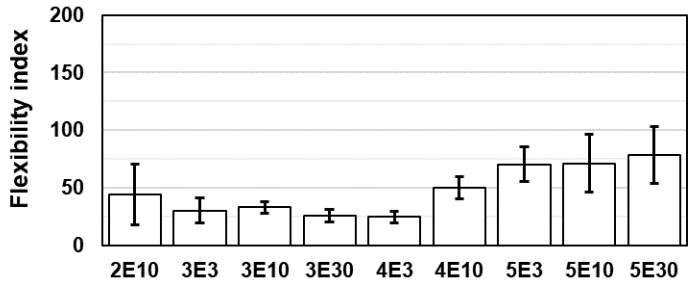

(c)

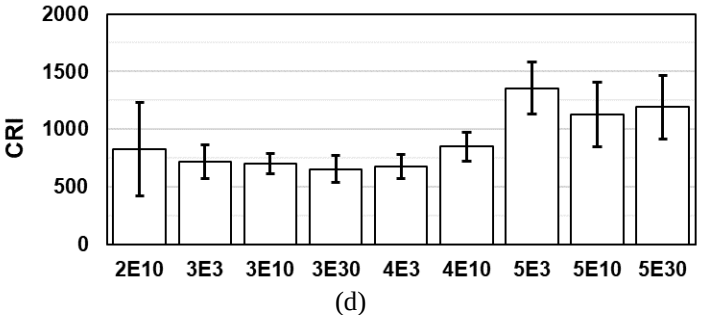

(d)

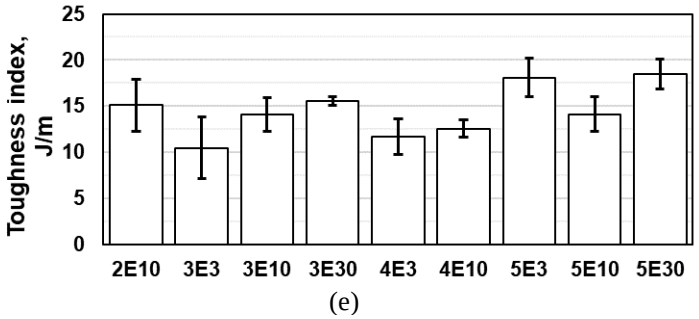

(e)

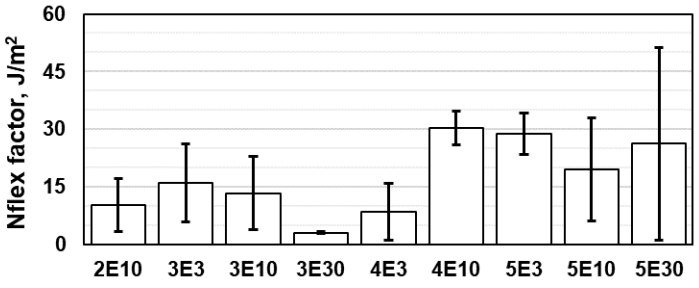

Figure 6-30 Load-displacement curve-based parameters for all mixes: (a) Cracking test index (CT_{Index}), (b) Flexibility index (FI), (c) Cracking resistance index (CRI), (d) Toughness index (TI), (e) N_{flex} factor

Table 6-33 Statistical details of the computed indexes for every mix

Mix ID		2E10	3E3	3E10	3E30-B	4E3HS	4E10	5E3HS	5E10	5E30
CT_{Index}	Average	119.4	103.8	134.5	84.5	75.7	188.3	184.0	243.4	272.1
	StDev.	46.3	50.7	38.6	6.2	16.5	33.2	32.6	54.4	85.9
	CoV (%)	39	49	29	7	22	18	18	22	32
FI	Average	44.2	30.2	33.1	25.6	24.6	49.9	70.3	71.2	78.6
	StDev.	26.5	10.8	5.1	5.6	4.7	9.7	14.9	24.9	24.9
	CoV (%)	60	36	15	22	19	19	21	35	32
CRI	Average	825.1	715.7	702.6	652.4	671.5	846.7	1354.5	1127.0	1189.2
	StDev.	407.1	148.9	87.7	114.7	103.5	125.1	224.1	281.0	275.7
	CoV (%)	49	21	12	18	15	15	17	25	23
TI (J/m)	Average	15.1	10.5	14.1	15.5	11.7	12.6	18.1	14.1	18.5
	StDev.	2.8	3.3	1.8	0.5	1.9	1.0	2.1	1.9	1.6
	CoV (%)	19	32	13	3	16	8	12	13	9
N_{flex} factor (J/m^2)	Average	10.2	16.0	13.3	3.0	8.5	30.3	28.8	19.5	26.2
	StDev.	6.8	10.1	9.6	0.3	7.4	4.4	5.4	13.3	25.1
	CoV (%)	67	63	72	8	87	14	19	68	96

Note: StDev. = Standard deviation, CoV = Coefficient of variation.

6.3.1.6. DynaMOD Predictions Evaluation

DynaMOD is a standalone software that serves as a database for HMA test results conducted under MDOT research projects. It is a convenient tool that can be used to quickly assess the material testing data and generate material inputs that can be directly used in the Pavement-ME design software. The test data from the material characterization conducted under this project was used to compare the $|E^*|$ predictions obtained from DynaMOD for the different HMA mixes of the 2020 and 2021 projects. Figure 6-31 compares the $|E^*|$ master curves obtained using the laboratory measured $|E^*|$ data and DynaMOD predicted $|E^*|$ values. It is observed that the DynaMOD predicted master curve is in close agreement with the one determined from laboratory test data, as shown by the bias and SE values reported in the figure.

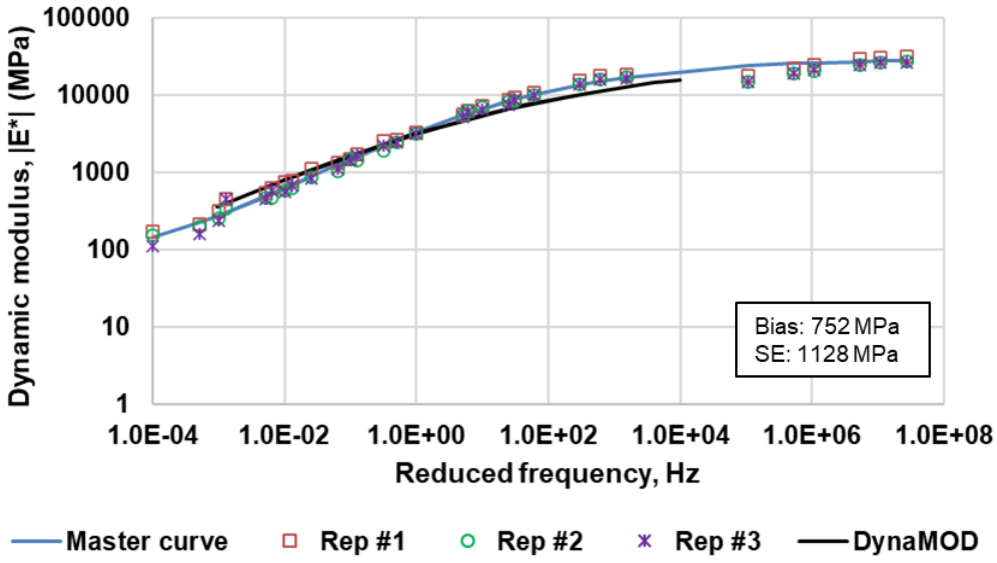

(a) I-69 3E30-L mix

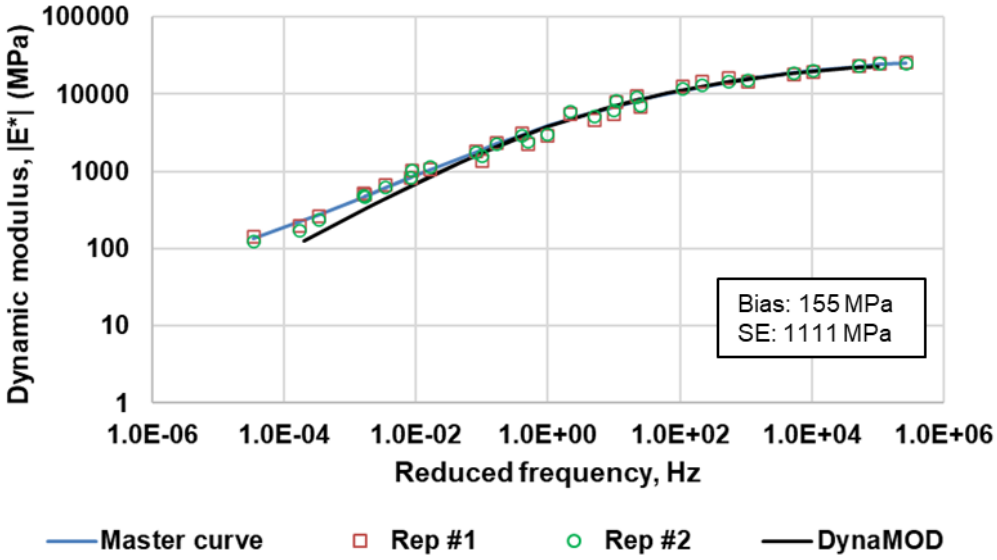

(b) I-75 3E10 mix

Figure 6-31 Measured vs. DynaMOD predicted |E*| comparison

6.3.2 PCC Material Testing

For the PCC materials, various material properties related to ME inputs include *E*, $f_c^{'}$, modulus of rupture (*MOR*), coefficient of thermal expansion (*CTE*), unit weight, and Poisson's ratio. Since *MOR* and *CTE* inputs significantly impact the predicted JPCP performance, these were measured in the laboratory for the PCC projects selected from the 2020 projects. Table 6-34 summarizes the total number of concrete samples received from the MDOT and those tested for the I-196 Eastbound (EB) and I-75 Southbound (SB) JPCP projects.

Table 6-34 Summary of concrete samples testing

Project	Beams		Cylinders		Cores	
	Received	Tested	Received	Tested	Received	Tested
I-196 EB	2	2	9	9	27	9
I-75 SB	2	2	9	9	24	12

6.3.2.1. Concrete Mechanical Properties

For the I-196 EB JPCP project, two concrete beams were tested for *MOR*. Both beams were subjected to 4-point loading using MDOT's portable beam tester, and failure occurred near the mid-point as expected (see Figure 6-32). Table 6-35 shows the *MOR* test results; a mean *MOR* of 683 psi was obtained from beam tests. Table 6-36 presents the estimated concrete's elastic modulus and compressive strengths from testing all nine cylinders. The average cylinder modulus is 4.33 x 106 psi, and the average compressive strength is 6,455 psi. The ratio between the mean *MOR* and the square root of the average compressive strength is 8.5, slightly lower than 9.5, which ACI suggests. The resultant coefficient for the modulus ratio to square root compressive strength is ~54,000, while it is 57,000 for the PMED equation based on a concrete unit weight of 144 lb/cft.

Figure 6-32 Typical beam break – I-196 EB JPCP project

Table 6-35 Flexural strength test results, I-196 EB JPCP project

Specimen number	Sampling date	Station	Test date	failure load (lbs)	MOR (psi)
1	7/1/2020	1121+75	8/28/2020	8,600	717
2	9/19/2020	1005+00	12/18/2020	7,800	650

Table 6-36 Cylinder compressive strength test results, I-196 EB JPCP project

Specimen number	Sampling date	Station	Test date	Modulus (psi)	Strength (psi)
1	7/1/2020	1111+00	8/21/2020	5,469,500	6,106
2	7/9/2020	1135+75	8/21/2020	4,388,967	5,766
3	7/12/2020	1151+00	6/21/2021	5,022,167	6,820
4	7/13/2020	1180+00	6/21/2021	4,106,400	6,358
5	7/15/2020	1204+44	6/21/2021	3,561,400	**3,071**
6	8/30/2020	955+00	6/21/2021	4,307,233	7,624
7	9/19/2020	989+00	12/17/2020	4,361,667	7,080
8	9/21/2020	1010+50	12/17/2020	3,729,367	6,066
9	9/23/2020	1032+00	12/17/2020	4,065,500	5,823
			Average	4,334,689	6,455
			Standard deviation	563,108	617
			Coefficient of variation, %	13.0	9.6

Note: Bold-faced strength value is not included in the average calculation as the sample broke during modulus testing. The strength was determined using the stress-strain curve and is an outlier.

Table 6-37 summarizes the compressive strength testing results of the nine concrete cores for the I-196 EB JPCP project. The remaining concrete cores were used for durability-related testing of the concrete. The stationing on the cores roughly corresponds to locations from the start (stations 900+00 to 1000+00), middle (stations 1000+00 to 1100+00), and end (stations 1100+00 to 1200+00) stations of the project. The table displays the average value for *E* and the $f_c^{'}$ for each of the three locations on the project. The results do not display much variation within the different locations.

Table 6-37 Compressive strength test results from cores, I-196 EB JPCP project

Specimen number	Station	Test date	Avg. dia. (in)	Avg. height (in)	Modulus (psi)	Strength (psi)	Correction factor	Corrected strength (psi)
280	967+36	6/21/2021	6	11.3	3,292,600	4,724	0.9768	4,614
284	959+01	6/21/2021	6	11.8	3,166,100	5,132	0.976	5,009
398	999+21	6/18/2021	6	11.7	3,512,333	4,752	0.9752	4,635
				Average	3,323,678			4,753
				Standard deviation	143,047			181
				Coefficient of variation, %	4.3			3.8
90	1100+34	12/22/2020	6	10.4	3,660,300	4,372	0.9832	4,298
413	1029+00	6/18/2021	6	11.7	4,041,300	4,752	0.996	4,733
436	1082+18	6/18/2021	6	11.7	3,295,000	4,774	0.996	4,755
				Average	3,665,533			4,595
				Standard deviation	304,698			210
				Coefficient of variation, %	8.3			4.6
63	1179+79	6/18/2021	6	10.4	2,740,400	4948	0.9784	4,841
78	1132+02	6/18/2021	6	10.4	3,824,300	5522	0.9784	5,403
83	1120+33	6/18/2021	6	10.6	3,280,533	5313	0.9776	5,194
				Average	3,281,744			5,146
				Standard deviation	442,501			232
				Coefficient of variation, %	13.5			4.5

For the I-75 SB JPCP project, two concrete beams were tested for MOR (from station 119+67 to station 396+03). The beams failed near the mid-point, as shown in Figure 6-33, once subjected to 4-point loading. Table 6-44 shows the *MOR* test results. The mean *MOR* recorded for the project was 758 psi. Table 6-45 presents the compressive strength test results using concrete cylinders. The average cylinder modulus is 4.76 x 10^6 psi, and the average compressive strength is 7,027 psi. The ratio between mean *MOR* and the square root of average compressive strength is 9, close to the ACI suggested value of 9.5. The resultant coefficient for the modulus ratio to square root compressive strength is 56,860, which is in excellent agreement with the PMED equation of 57,000 based on a concrete unit weight of 144 lb/cft.

Table 6-39 summarizes the compressive strength testing results of the twelve concrete cores for the I-75 SB JPCP project. The stationing on the cores roughly corresponds to locations from the project's start, middle, and end stations. The table displays the average modulus and compressive strengths for each of the three locations on the project. The obtained results for modulus and compressive strength from core testing between stations 100+00 to 200+00 are higher (average elastic modulus of 4.67 x 10^6 psi and average compressive strength of 6,208 psi) as compared to those obtained from stations 200+00 to 300+00 (average elastic modulus of 2.87 x 10^6 psi and average compressive strength of 5,550 psi) and 300+00 to 400+00 (average elastic modulus of 3.26 x 10^6 psi and average compressive strength of 5,011 psi).

Figure 6-33 Typical beam break – I-75 SB JPCP project

Table 6-38 Flexural strength test results, I-75 SB JPCP project

Specimen number	Specimen ID	Cast date	Test date	Failure load (lbs)	MOR (psi)
1	7011-1C	9/10/2020	3/26/2021	9,300	775
2	7011-1D	9/10/2020	3/26/2021	8,900	742

Table 6-39 Compressive strength test results from cylinders, I-75 SB JPCP project

Specimen ID	Cast date	Test date	Modulus (psi)	Corrected strength (psi)
3630	10/15/2020	5/4/2021	4,726,267	6,154
3981	10/27/2020	5/4/2021	4,590,133	7,000
4063	10/30/2020	5/4/2021	4,913,633	7,069
4156	11/3/2020	5/11/2021	5,153,400	7,579
4335	11/9/2020	5/11/2021	4,248,633	6,329
4263	11/6/2020	5/12/2021	4,312,367	6,587
4440	11/11/2020	5/11/2021	5,035,367	7,518
4531	11/13/2020	5/12/2021	4,773,400	7,302
4610	11/17/2020	5/12/2021	5,144,467	7,704
		Average	4,766,407	7,027
		Standard deviation	334,231	562
		Coefficient of variation, %	7.0	8.0

Table 6-40 Compressive strength test results from cores, I-75 SB JPCP project

Specimen number	Station	Test date	Avg. dia. (in)	Avg. height (in)	Modulus (psi)	Strength (psi)	Correction factor	Corrected strength (psi)
96	387+82	12/22/2020	5.8	11.5	3,584,567	5,262	0.9984	5,253
111	362+04	4/13/2021	6	12	3,055,933	4,825	1.0000	4,825
121	344+64	4/13/2021	6	11.9	3,158,800	4,964	0.9984	4,956
				Average	3,266,433			5,011
				Standard deviation	28,0271			219
				Coefficient of variation, %	8.6			4.4
364	273+11	12/22/2020	5.8	11.8	**5,028,800**	7,473	1.0024	7,491
367	282+99	4/13/2021	6	11.4	2,579,533	5,770	0.9920	5,724
314	225+00	5/4/2021	6	12	2,670,367	5,843	1.0000	5,843
310	229+10	5/6/2021	6	12.1	3,244,833	5,430	1.0016	5,439
370	293+70	5/6/2021	6	11.8	3,004,767	5,208	0.9976	5,196
				Average	2,874,875			5,550
				Standard deviation	30,7024			291
				Coefficient of variation, %	10.7			5.2
332	197+05	12/22/2020	5.9	11.3	4,567,367	6022	0.9936	5,983
327	205+01	5/4/2021	6	11.5	4,624,933	6426	0.9936	6,385
383	131+74	5/4/2021	6	11.8	**2,846,300**	6150	0.9976	6,135
337	187+17	5/6/2021	6	12.1	4,822,933	6317	1.0016	6,327
				Average	4,671,744			6,208
				Standard deviation	134,060			184
				Coefficient of variation, %	2.9			3.0

Note: Bold-faced modulus values are not included in the average calculation for the corresponding sections.

6.3.2.2. Concrete Coefficient of Thermal Expansion (CTE)

The *CTE* measures the concrete's contraction or expansion caused due to temperature changes. As the length change associated with the thermal expansion is small, it is usually expressed in microstrain (10^{-6}) per degree Celsius ($\mu\varepsilon/°C$) or microstrain per degree

Fahrenheit (με/ °F) units. The typical range of *CTE* for a PCC is about 7.2 to 13 με/ °C (4 to 7.2 με/ °F). However, the value may vary depending on the concrete's components, aggregate types, w/c ratio, cement fineness, etc. The *CTE* is an important parameter in the design of concrete pavements. Characterizing the effects of thermal properties on a concrete pavement's structure is to account for its thermal movements. *CTE* is represented as an average value rather than a mix-specific input in pavement design. This may lead to erroneous assumptions about the pavement's thermal response and possible distresses. Therefore, conducting *CTE* tests can help pavement design engineers better predict the impact of mix-specific thermal expansion on pavement behavior.

The American Association of State Highway and Transportation Officials (AASHTO) standard test T 336-15 was adopted to measure the concrete's *CTE*. The specimen is heated in a water bath from 10 to 50°C and then cooled down to 10 °C. The length and temperature of the specimen at 10°C and 50°C are recorded for *CTE* calculation for each heating and cooling segment. The *CTE* value of the test specimen is taken as the average of the heating and cooling segments, provided the two values are within 0.3 με/ºC. The standard method has a couple of limitations as follows:

- The actual curve of temperature versus length change is unknown within each segment.
- Only the water bath temperature is measured, which may not represent the concrete specimen's temperature.

Therefore, a few modifications were made at the U of M based on AASHTO T336-15 to achieve better accuracy. Summarized modifications are as follows:

- The length change of the specimen vs. temperature is monitored for the entire process.
- Two companion concrete specimens that have a thermal couple embedded at the center are introduced to simulate the real temperature change in the test specimens. The average temperature of the two companion concrete specimens was used as the temperature of the test specimen.

Two cores from the I-75 and I-196 concrete pavement (2020) projects were tested to estimate the concrete's *CTE*. The prepared specimens from both projects were conditioned by submersion in a limewater bucket for at least 48 hours. Table 6-41 summarizes the dimensions and *CTE* test results for both concrete pavement projects. The estimated *CTE* from cores from the I-75 project has an average of 9.35 με/°C (5.19 με/°F) after calibration. The average *CTE* estimated using cores from the I-196 project is 7.22 με/°C (4.01 με/°F). The test results showed that the concrete's length changed almost linearly with temperature changes, as shown in Figure 6-34 and Figure 6-35.

Table 6-41 Dimensions and CTE results of test specimens

Project	Core number	Length (in)	Diameter (in)	CTE test (AASHTO T336-15)	
				($\times 10^{-6}$ in/in/°C)	($\times 10^{-6}$ in/in/°F)
I-75	#99	11.811	5.920	9.378	5.210
	#106	12.405	5.934	9.321	5.178
I-196	#394	12.062	5.914	7.390	4.106
	#408	12.362	5.858	7.055	3.919

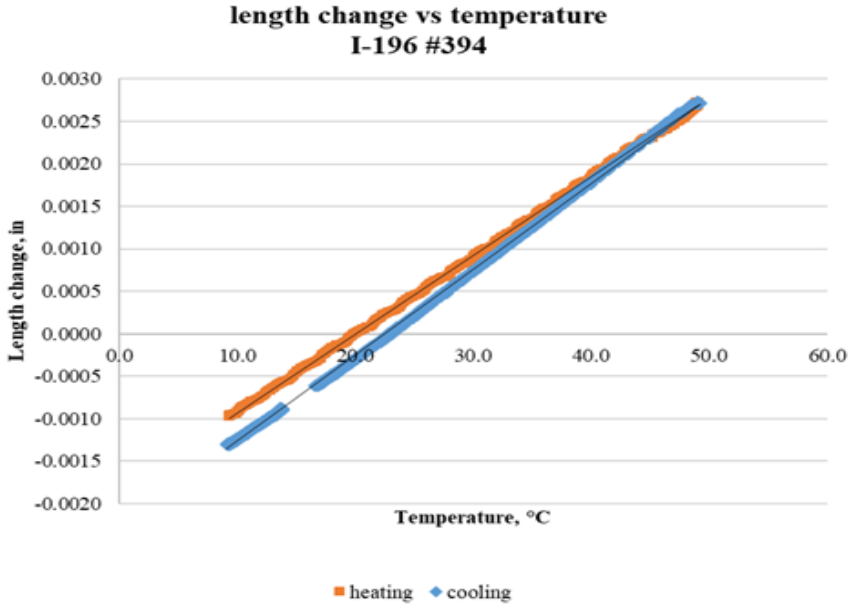

Figure 6-34 Length change vs. temperature for I-196 core #394

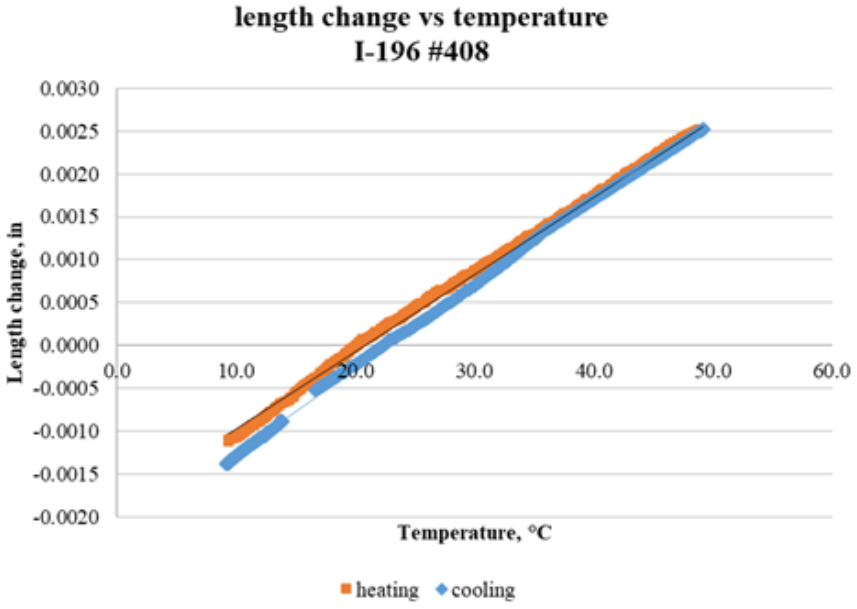

Figure 6-35 Length change vs. temperature for I-196 core #408

6.3.2.3. Concrete Surface Resistivity Testing

One of the key distresses in concrete pavements is joint spalling from deicer frost deterioration of the cement matrix combined with internal cracking in saturated concrete from insufficient air-void parameters (i.e., total air content in fresh concrete, spacing factor, and specific surface area in the hardened concrete). However, permeability requirements are also essential for concrete durability in addition to air content and hardened air-void properties. The concrete's durability can be measured in its ability to resist chloride ion penetration (AASHTO T 277 and ASTM C1202), commonly known as the rapid chloride permeability test (RCPT). However, research has shown that the surface resistivity (SR) test (AASHTO TP 95) is a promising alternative to the RCPT (*12*). Table 6-42 shows the relationship between the chloride ion penetrability and the SR test (AASHTO TP 95) that measures the electric resistivity of the concrete from concrete cylinders/cores. Table 6-43 summarizes the SR test results conducted on cores from the I-75 and I-196 JPCP (2020) projects. The concrete of the I-75 JPCP project falls under moderate to low, while that of the I-196 project falls under very low chloride ion penetrability.

Table 6-42 Comparison of chloride penetrability levels established for standards based on electric resistivity (AASHTO TP 95) and charge passed (ASTM C1202) (*12*)

Chloride ion penetrability	Electric resistivity, kΩ.cm	Electric charge passed, coulombs
High	<12	>4000
Moderate	12 to 21	2000 to 4000
Low	21 to 37	1000 to 2000
Very low	37 to 254	100 to 1000
Negligible	>254	<100

Table 6-43 Resistivity test results – 2020 concrete projects

Project	Core number	Resistivity (kΩ·cm)	
I-75	#99	33.9	Mean = 26.85
	#106	19.8	
I-196	#394	42.4	Mean = 41.25
	#408	40.1	

6.3.2.4. Concrete Water Sorption and Freeze-Thaw (F-T) Testing

This section presents the water sorption and freeze-thaw (F-T), durability testing on (100mm by 100mm, 70 mm thick) samples cut from cylinders/cores of the I-196 and I-75 concrete projects. The samples were dried for two weeks at 50°C before undergoing a 1-D sorption test for a week according to ASTM C 1585. The sorption test provided a near-full water saturation state before the start of F-T testing with the bottom surface continuously in contact with a 3% Sodium Chloride (NaCl) solution.

The theory according to ASTM C1585 is illustrated in Figure 6-36. The 1-D moisture uptake is plotted versus the square root of time in hours. The process consists of two near-linear portions starting with capillary suction followed by a slower diffusion process, which consists of partial moisture uptake of concrete air voids. The amount of moisture uptake corresponding to capillary suction is a measure of the capillary porosity of the cementitious binder. Moisture absorption by capillary forces is considered a major mode of transport in

unsaturated concrete. It is an important property for the F-T durability of concrete structures which largely depends on its resistance to the ingress of aggressive agents from the environment.

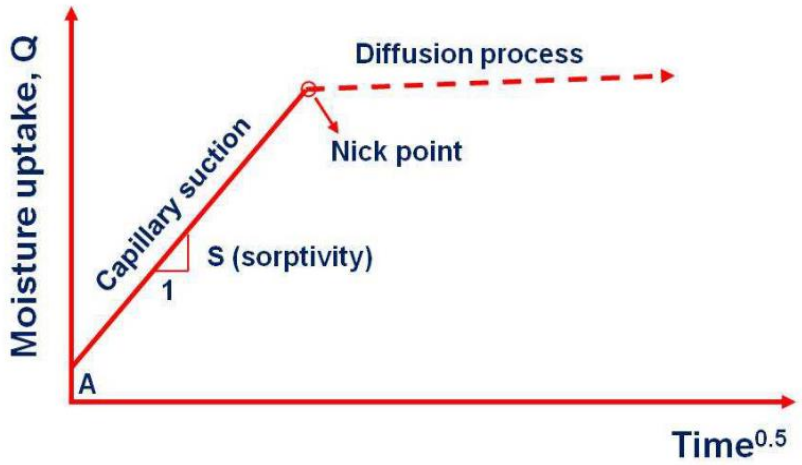

Figure 6-36 Idealized moisture uptake curve for concrete

Following the sorption test, the specimens were transferred to an F-T chamber [Figure 6-37(a)] with the bottom surface exposed to a 3% NaCl solution during the F-T cycle [Figure 6-37(b) and (c)]. A linear F-T temperature profile between 20°C and -20°C with a cycle of 12 hours is shown in Figure 6-37(d). This time-temperature profile allowed for a one-hour constant temperature period at 20°C for collection and weight measurement of the surface scaled material [see Figure 6-37(e)] along with the determination of the relative modulus [Figure 6-37(f)] for internal crack resistance. Typically, 28 F-T cycles are sufficient for determining deicer scaling resistance. In this study, 56 cycles were used to assess regular F-T resistance from relative dynamic modulus measurement (RDM) and deicer scaling resistance in terms of mass loss in g/m^2 units.

Duplicate samples from both the concrete projects (I-196 and I-75) were moisture conditioned according to the ASTM C 1585 procedure, whose results (i.e., the average mass gain of the replicate samples, in percentage) are plotted in Figure 6-38. Specimens #394 and #408 from the I-196 project were found to have a 2.41% and 2.46% total mass gain after about 7 days, respectively. These were slightly lower than the 2.75% and 3.12% for specimens #99 and #106, respectively from I-75. This suggests that I-196 concrete is slightly less porous than I-75 concrete. This finding is in line with the results of the SR tests on the I-196 concrete samples.

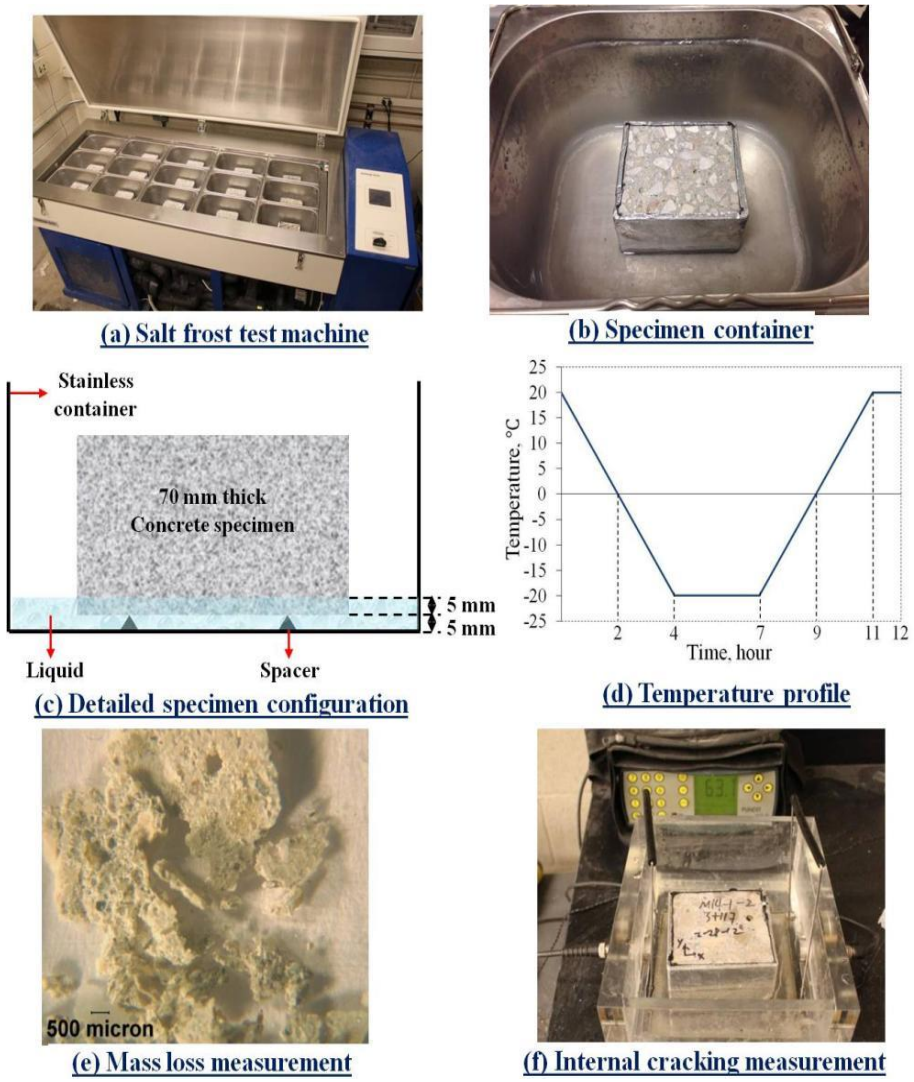

Figure 6-37 F-T test procedure

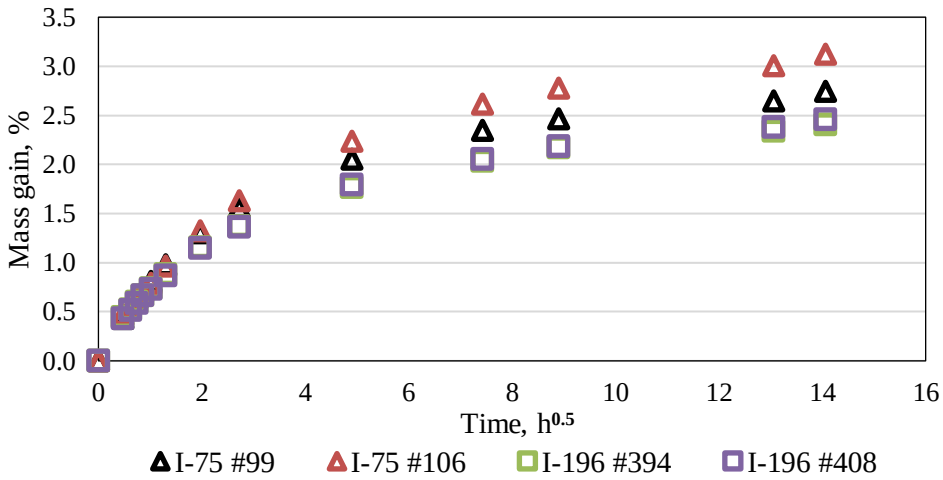

Figure 6-38 Moisture uptake results according to ASTM C1585

Deicer scaling results from samples from I-75 and I-196 had a similar trend of scaling development, as shown in Figure 6-39. All samples developed scaling linearly relating to F-T cycles, and the RILEM limit (1500 g/m^2 scaling limit at 28 cycles) was met. The scaling at the end of the test period (78 cycles) was about 1500 g/m^2, suggesting that they had good F-T scaling resistance. The surface exposure also demonstrates insignificant mass loss (see Figure 6-40) due to deicer scaling. Consistent with the low scaling results, the I-196 and I-75 concrete have an excellent regular F-T by RDM. All the samples have an RDM above 90%, suggesting that there is no internal cracking developed inside the concrete (see Figure 6-41).

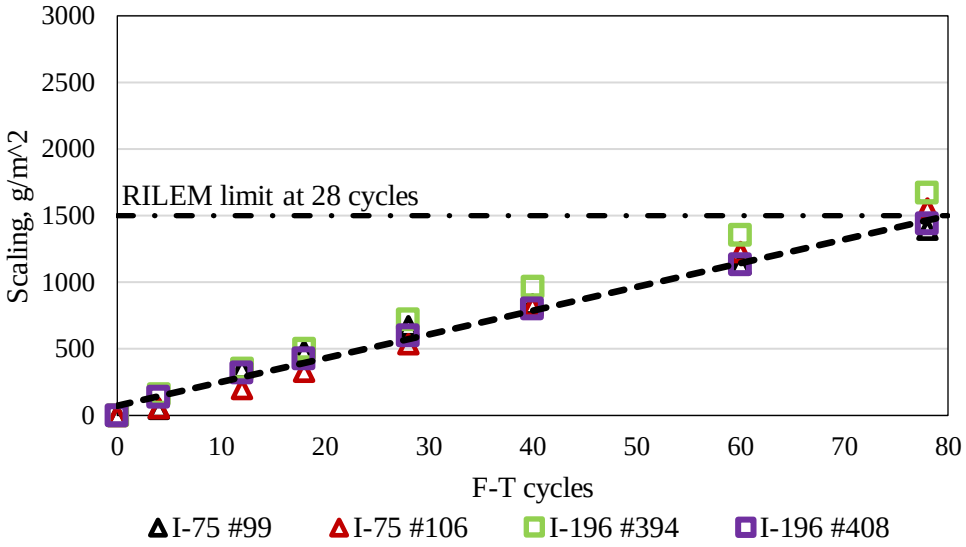

Figure 6-39 Deicer scaling results

(a) I-75 #106 (b) I-196 #394

Figure 6-40 Samples after the F-T test

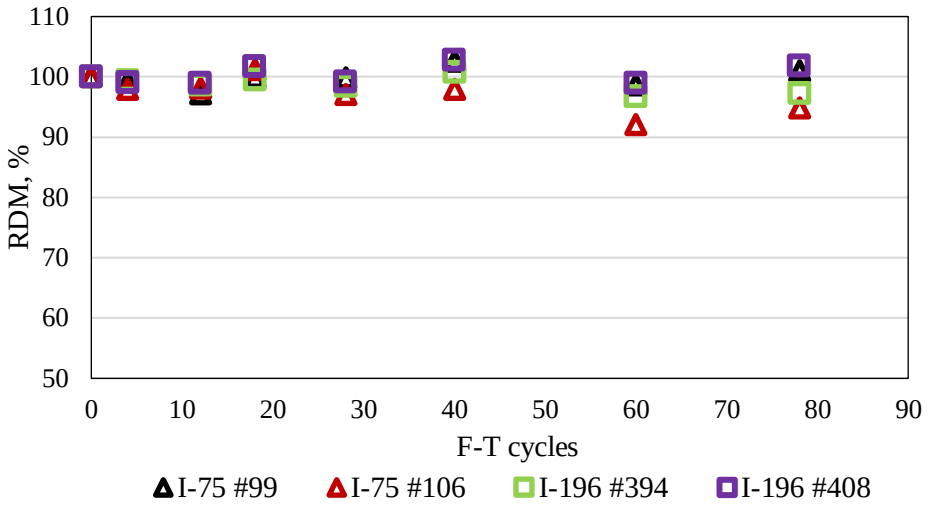

Figure 6-41 Relative Dynamic Modulus (RDM) results

6.3.2.5. Concrete Air Void Analysis

Based on ASTM C457, an air void analyzer is used to assess the air-void system in hardened concrete using point count procedures and the linear traverse method. 20mm thick square specimens with 100mm width and length are cut from the same beam specimens used for the F-T test. The specimens are first polished using silicon carbide abrasives to obtain a smooth surface. The point count procedure determines the volume fractions of air voids, paste, and aggregate on the polished surface by recording the number of stops over each phase under the crosshair of a microscope. The same scanned surface is used for the linear traverse test. Before starting the linear test, the surface was treated by coating it with barium sulfate to fill all the air voids, and the rest of the surface was painted black with caution so that the air voids could form a sharp contrast to the concrete matrix. The RapidAir 457 automatic image analyzer was used to scan the prepared surface for which the air void characteristics report was obtained. Table 6-44 shows the air void analysis results. The average hardened air content of samples from I-75 is 5.6% based on the point count results, which falls within the range of specified air (5.0% - 8.0%). The average spacing factor is 135 microns, which is way below the 200 microns limit recommended by ACI. The average hardened air content of samples from I-196 is 4.8%, with an average of 166.5 microns in the spacing factor.

Table 6-44 Air void analysis based on ASTM C 457

Project	Sample	Station	Point count			Linear traverse test			
						Air content, %		Spacing factor, µm	Specific surface, 1/mm
			Air	Paste	Aggregate	Entrained air <500 µm	Total air <4000 µm		
I-75	#99	382+70	5.4	22.2	72.4	4.2	5.4	133	31
	#106	368+18	5.8	23.9	70.4	3.6	5.4	137	32
I-196	#394	986+73	4.8	26.5	68.7	3.9	5.7	178	25
	#408	1018+04	5.8	28.9	65.3	5.1	6.8	155	27

6.3.3 Unbound Material Testing

Laboratory testing of unbound material samples included 67 geomaterials collected from I-69, I-196, I-75, M-3, and US-41. Overall, 46 geomaterials, including 16 base, 16 sub-base, and 25 subgrade materials, were tested for sieve analysis, compaction, resilient modulus, and Atterberg limits. Among the materials collected, 31 presented the same soil classification and index properties and belonged to the same gradation precision range. Those were merged according to AASHTO T 27-14 and ASTM C136-06. Summarized results are presented in this section, while detailed test results are included in Appendix B. Table 6-45 shows the summary resilient moduli (SM_R) values for the different pavement layers of all the 2020 and 2021 projects. Figure 6-42, Figure 6-43, and Figure 6-44 display the resilient moduli values for all the replicates of the base, subbase, and subgrade materials for all the projects. While Figure 6-45 shows the summary of the M_R results for the different layers of each project.

Table 6-45 Summary of the resilient moduli (SM_R) for each project

Layer	I-196		I-69		I-75		M-3		US-41	
	SM_R (ksi)	SD (ksi)	SM_R (ksi)	SD (ksi)	SM_R (ksi)	SD (ksi)	SM_R (ksi)	SD (ksi)	SM_R (ksi)	SD (ksi)
Base	36.04	NA	41.59	NA	30.58	NA	40.71	2.01	27.39	0.73
Subbase	21.71	NA	23.83	3.10	NA	NA	22.10	1.40	24.64	NA
Subgrade	NA	NA	12.87	2.19	14.67	4.30	11.98	1.52	13.10	0.94

SD = standard deviation.

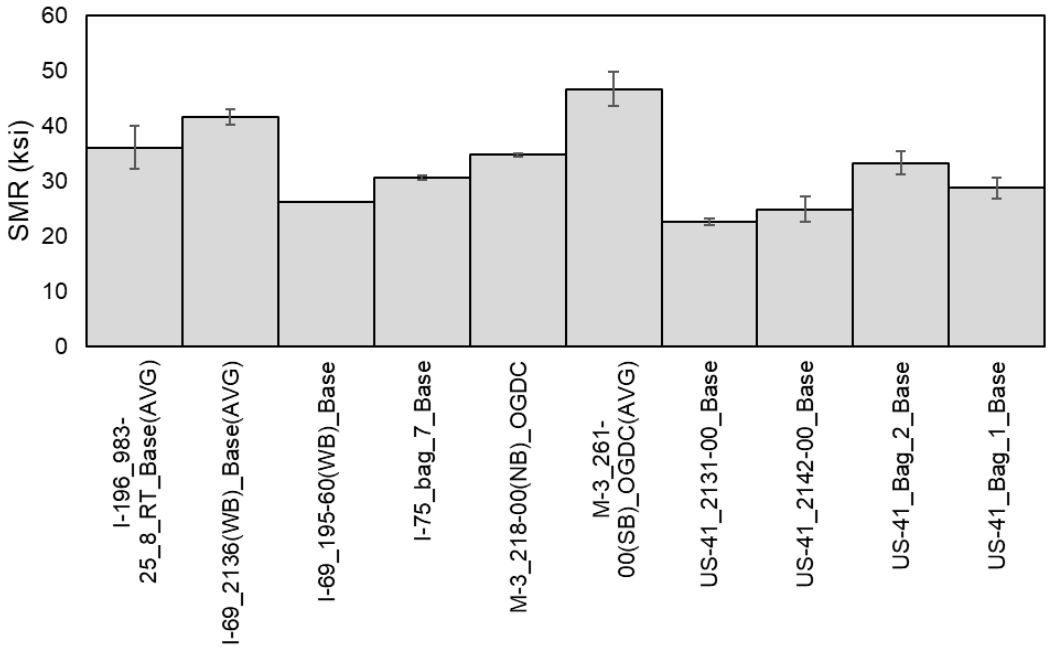

Figure 6-42 Summary resilient moduli (SM_R) values for base materials

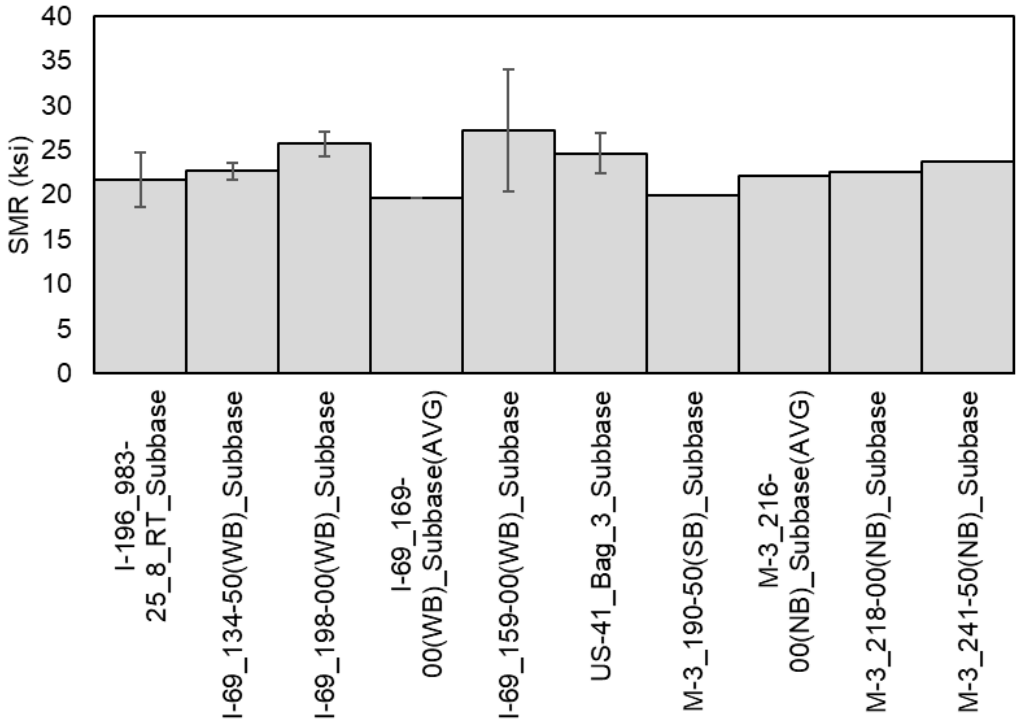

Figure 6-43 Summary resilient moduli (SM_R) values for sub-base materials

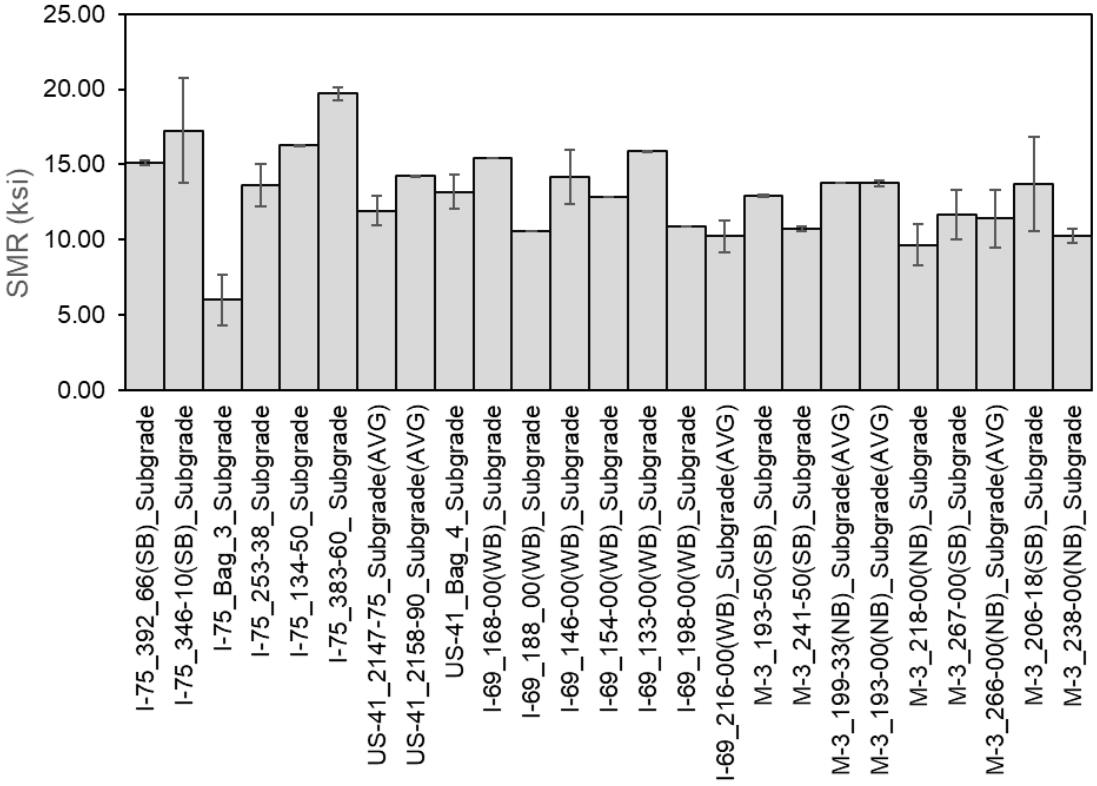

Figure 6-44 Summary resilient moduli (SM_R) values for subgrade materials

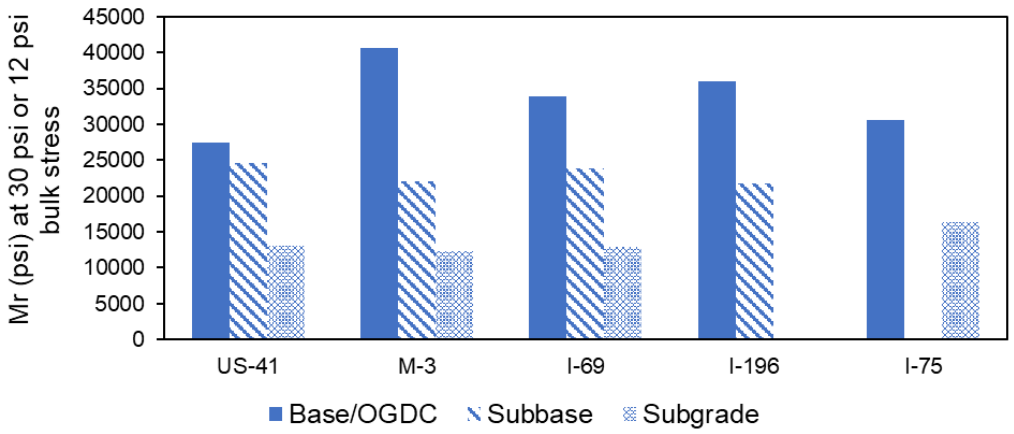

Figure 6-45 Summary resilient moduli (SM_R) values for different pavement layers

6.4 COMPARISON BETWEEN FIELD AND LAB MATERIAL PROPERTIES

The in-situ resilient or elastic moduli of pavement layers were estimated using various field tests—FWD, LWD, and DCP, conducted over different layers of the 2020 and 2021 selected projects. In addition, data from the "Evaluation of MDOT's Long-life Pilot Projects" project is also included in this section for comparison between the field and lab-measured moduli values for different pavement unbound layers. Figure 6-46 through Figure 6-48 show comparisons between the estimated moduli values for the different layers and the laboratory-measured summary resilient moduli (SM_R) values. The figures display the complete range of the moduli values for the different pavement unbound layers of each of the projects, irrespective of the testing/sampling locations. It is noted that the DCP direct model was utilized for calculating the resilient moduli of the materials in pavement layers.

Figure 6-46 shows boxplots comparing the subgrade moduli values of the different projects. The figure shows very few outlier values (represented by an asterisk symbol) within the data. The results show that the LWD resulted in the lowest subgrade moduli values. However, due to different stress levels, the general trends of the moduli values estimated from various field tests are expected to be similar. For example, the median subgrade modulus for the US-131 project is the highest among all projects from LWD and DCP data analyses. However, FWD data analyses show the highest subgrade moduli values for the US-41 project. The laboratory data show that the median subgrade moduli for all projects are between 12 to 17 ksi, with the values indicating the least variability. The LWD results also display minimal variability; however, the median moduli values from the LWD analysis are less than 5 ksi. The FWD and the DCP data estimated higher moduli for the subgrade layer for all projects with considerable variability.

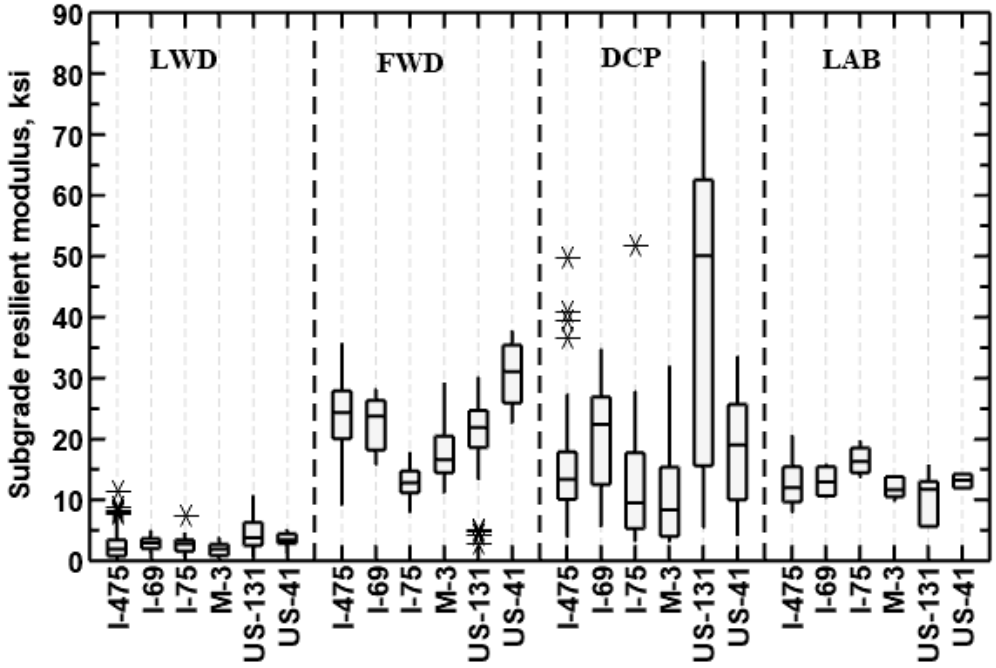

Figure 6-46 Comparison of subgrade resilient moduli determined from different field tests and laboratory-measured values

The median subbase moduli values determined in the laboratory range between 15 to 25 ksi for all projects, excluding the I-75 project with no subbase sample (see Figure 6-47). The LWD and DCP data display similar trends with median subbase moduli determined from field tests below 10 ksi for the I-475, I-69, M-3, and US-41 projects. The US-131 project has the highest median subbase modulus of 30 ksi estimated using DCP data. However, no LWD data was available for this project. FWD data analyses resulted in the highest subbase moduli values, slightly higher than the laboratory-determined subbase moduli values for the I-69, M-3, and US-41 projects. The FWD backcalculated subbase moduli for the I-475 and US-131 are not shown in the figure, as the subbase and base layers were combined for the analysis.

Figure 6-48 shows the boxplots for the estimated base moduli and the laboratory-measured values for the different projects. The LWD results show that the median base moduli range between 7 to 12 ksi, the lowest of the three test categories. The FWD-based results show that the median base moduli values range between 33 to 65 ksi while the lab-determined base moduli range between 30 to 40 ksi. Although the FWD data analyses resulted in the highest median moduli values, the laboratory-determined moduli are very close to them for all the projects (except I-75, for which no lab data was available). In addition, the moduli values from the FWD data analyses display a higher spatial variability, especially for the I-69, I-75, and US-41 projects.

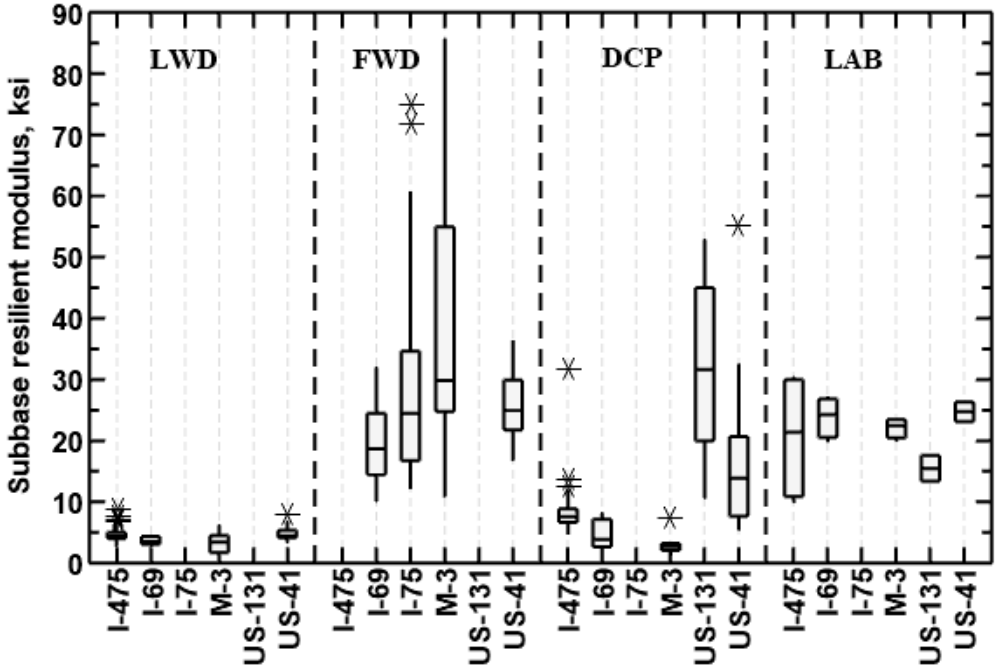

Figure 6-47 Comparison of subbase resilient moduli determined from different field tests and laboratory-measured values

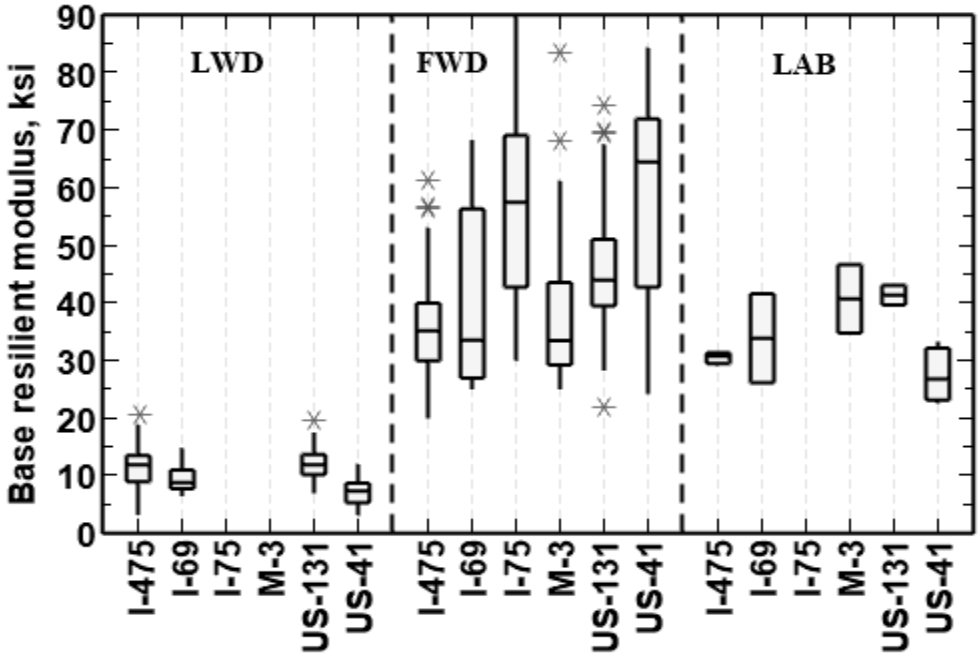

Figure 6-48 Comparison of base resilient moduli determined from different field tests and laboratory-measured values

Figure 6-49(a) displays that the subgrade SM_R ranges between 9 to 17 ksi while the LWD-based values range between 0.5 to 7 ksi. The plot displays that the LWD underestimates the subgrade moduli. Additionally, the data does not indicate any meaningful trend. Figure 6-49(b) shows a similar plot of the matched data between the SM_R values and FWD-based

moduli. While the lab SM_R values range between 5 to 17 ksi, FWD-based values have a range from 14 to 20 ksi. The figure displays that the FWD overestimates the subgrade moduli compared to the lab-determined SM_R values; however, it does not show any definite pattern. The matched lab and DCP-based data show that the laboratory-determined moduli range between 5 to 20 ksi; however, the DCP-based moduli display a wider range with values between 3 to 58 ksi [see Figure 6-49 (c)]. In addition, the data does not show any pattern. Figure 6-49(d) shows the range of the DCP penetration index for the subgrade layer. The DCP index values range between 0.1 to 1.1 inches/blow. The data from the plot can be used to roughly estimate the layer's modulus in the field while conducting the DCP test.

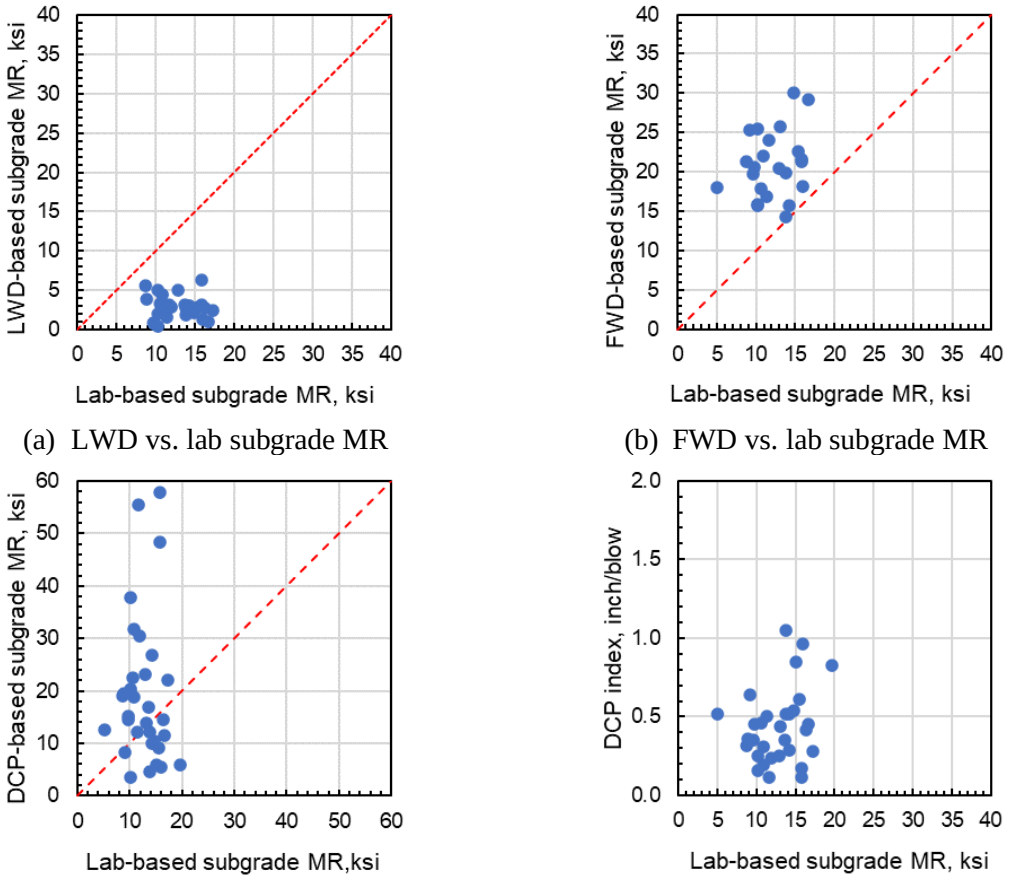

(a) LWD vs. lab subgrade MR

(b) FWD vs. lab subgrade MR

(c) DCP vs. lab subgrade MR

(d) DCP index vs. lab subgrade MR

Figure 6-49 Comparison of subgrade moduli determined from different field tests and laboratory SM_R values

Observing Figure 6-49, it is evident that a real correlation does not exist. Reasons for such behavior and differences between the moduli values estimated using the field tests and laboratory can be attributed to the difference in the testing conditions and analysis methods. The differences in the pavement layers' field moisture content (and density) at the time of testing and those used during the laboratory tests (i.e., optimum moisture content) are significant sources of variability in the results. In addition, the field gradation might not be like the laboratory-prepared samples even if the samples are prepared within the specification limits. As for the analysis method, the LWD estimates the elastic modulus of the different

pavement layers using the well-known Bousinnesq solution using the elastic half-space theory while assuming a specific stress distribution.

Similarly, FWD backcalculation also estimates the pavement layers' elastic moduli, considering them linearly elastic. The DCP data analyses, on the other hand, involved evaluating the different layer resilient moduli using an empirically derived (DCP direct) model. The laboratory-based resilient moduli of the various layers were determined using a repeated load triaxial test at a series of different combinations of deviatoric and confining stresses. Therefore, differences in the moduli values are expected. Since a real correlation is absent, correction factors can be used to estimate field moduli equivalent to lab-measured values.

Figure 6-50 displays similar correlation analyses for the subbase layer. Figure 6-50(a) shows that the laboratory-determined subbase resilient moduli values range between 11 to 30 ksi while they range between 1 to 10 ksi from the LWD data analysis. The LWD underestimates the subbase layer moduli as observed with the subgrade data. The FWD-based subbase moduli range between 11 and 50 ksi; corresponding laboratory SM_R values range between 20 and 28 ksi [see Figure 6-50(b)]. The moduli range between 1 to 10 ksi using DCP data, while the corresponding laboratory SM_R values range between 11 to 30 ksi [see Figure 6-50(c)]. Figure 6-50(d) shows that the DCP index values range between 0.1 to 2 inches/blow. As observed for the subgrade, Figure 6-50(a) through (c) does not display any meaningful trend for the same reason mentioned earlier.

Figure 6-51 shows similar one-to-one correlation plots for the laboratory-determined and field test-based estimated base layer resilient moduli. The LWD-based moduli range between 3 to 14 ksi; 31 to 50 ksi using FWD data [see Figures 6-51(a) and (b)]. The figures show that the laboratory-determined base resilient moduli range between 22 to 47 ksi for the data with matched stations. While the LWD underestimates the base moduli and does not display any useful correlation/trend, the FWD estimates base moduli very similar to the lab values. Table 6-46 summarizes the bias and the standard error of estimate (SEE) values between the lab- and the different field test-determined moduli values for different pavement unbound layers without correction. Among the three field tests, it can be observed that the FWD generally shows the lowest bias and SEE in estimating the layer moduli in comparison with the lab-determined values.

Table 6-46 Bias and SEE between lab- and field-measured moduli values

Layer	LWD		FWD		DCP	
	Bias	SEE	Bias	SEE	Bias	SEE
Subgrade	9.95	10.41	-8.77	9.82	-6.65	15.66
Subbase	17.10	18.21	-5.75	13.70	16.90	17.81
Base	26.99	27.94	-2.40	3.13	No data	

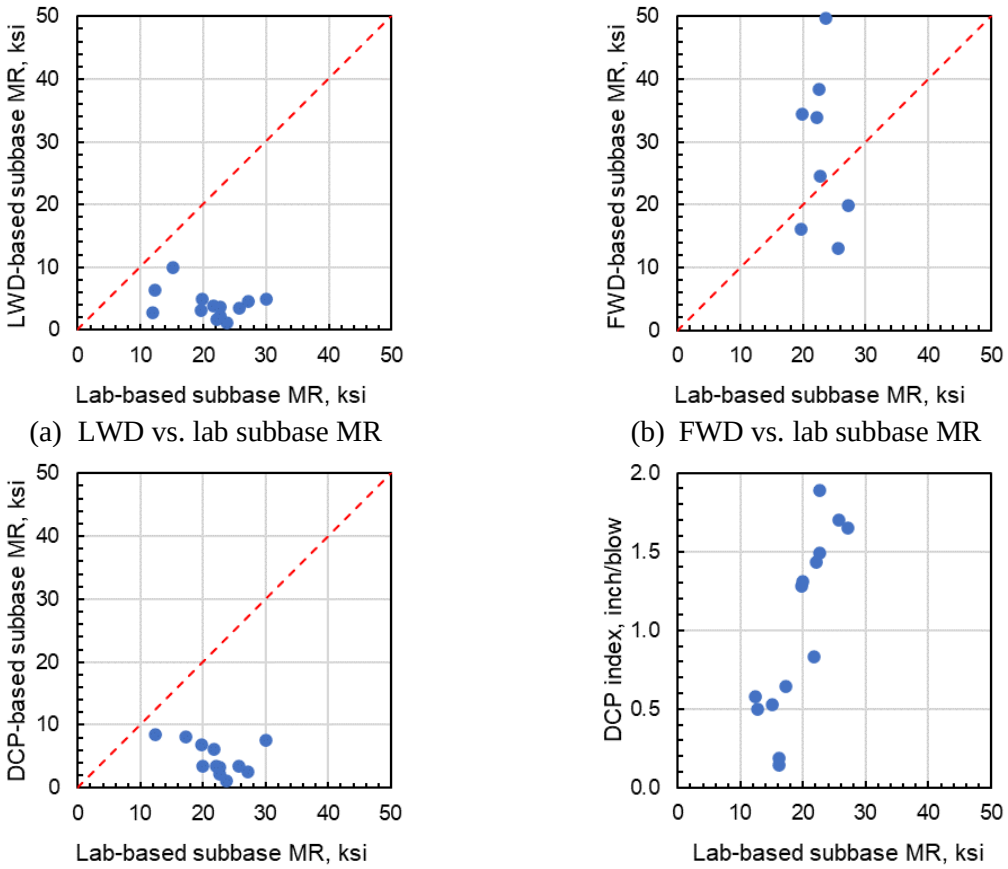

(a) LWD vs. lab subbase MR (b) FWD vs. lab subbase MR

(c) DCP vs. lab subbase MR (d) DCP index vs. lab subbase MR

Figure 6-50 Comparison of subbase resilient moduli determined from different field tests and laboratory-measured values

Table 6-47 summarizes the correction factors for each field test to estimate the lab subgrade moduli. Two different approaches were used to estimate the correction factors using the matched data presented earlier. Microsoft Excel® Solver was employed to estimate the best correction factor for each approach minimizing the SEE. Each method significantly reduced the bias and the SEE compared to the values shown in Table 6-46. The shaded rows in the table indicate the correction factors with the most negligible bias and SEE. Figures 6-52 through 6-54 visually display the performance of each approach in correcting the field test-determined moduli values and their comparison with the lab-determined ones. The figures reveal that the third correction approach (i.e., SG-L3, SG-F3, and SG-D3) best corrected the subgrade moduli to match the lab-determined SM_R values, irrespective of the field test.

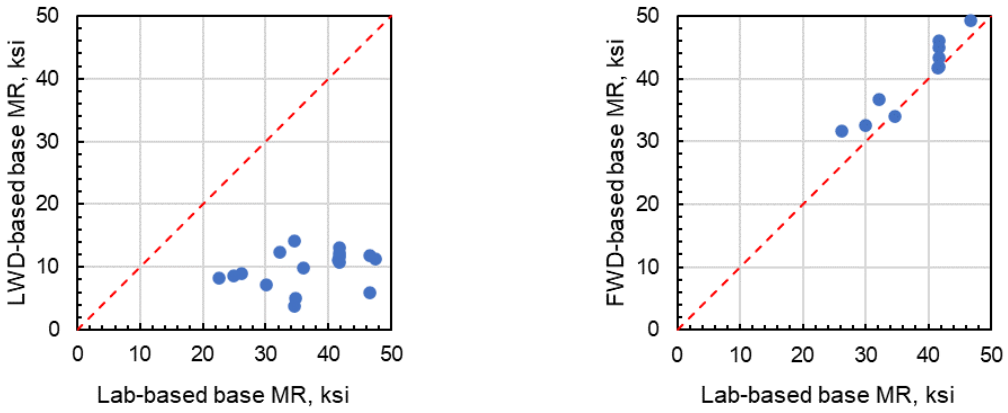

(a) LWD vs. lab base MR (b) FWD vs. lab base MR

Figure 6-51 Comparison of base resilient moduli determined from different field tests and laboratory-measured values

Table 6-47 Correction factors for estimating lab-measured subgrade moduli

Field test	Approach ID	Correction approach	Bias	SEE
LWD	SG-L1	$SG_{LAB} = 3.54 \times E_{LWD}$	2.73	6.51
	SG-L2	$SG_{LAB} = 7.30 \times \sqrt{E_{LWD}}$	0.95	4.34
	SG-L3	$SG_{LAB} = 2.82 \times E_{LWD} + \frac{7.41}{E_{LWD}}$	0.82	4.41
FWD	SG-F1	$SG_{LAB} = 0.57 \times E_{FWD}$	0.33	3.24
	SG-F2	$SG_{LAB} = 2.66 \times \sqrt{E_{FWD}}$	0.05	2.83
	SG-F3	$SG_{LAB} = 0.36 \times E_{FWD} + \frac{91.34}{E_{FWD}}$	-0.01	2.74
DCP	SG-D1	$SG_{LAB} = 0.67 \times E_{DCP}$	-0.26	9.80
	SG-D2	$SG_{LAB} = 2.71 \times \sqrt{E_{DCP}}$	1.45	5.38
	SG-D3	$SG_{LAB} = 0.30 \times E_{DCP} + \frac{74.03}{E_{DCP}}$	0.74	4.12

Also, correction factors are estimated for the subbase and base layers. Table 6-48 displays the bias and the SEE for each approach to correct subbase moduli values. The SEE has significantly reduced compared to Table 6-46 values after applying the correction to the field test-based subbase moduli. The bias, on the other hand, has decreased considerably as compared to the uncorrected subbase modulus values. Again, the third approach (i.e., SB-L3, SB-F3, and SB-D3) shows the lowest bias and SEE for correcting the values in the lab. Figures 6-55 through 6-57 display the performance of each approach in correcting the LWD, FWD, and DCP subbase moduli to the lab-determined SM_R values, and the third correction approach is the best. Table 6-49 summarizes each method's bias and SEE to correct the base layer moduli estimated from the LWD and FWD tests. For the FWD data, only two correction approaches were used as the third approach produced similar results as the first one (i.e., B-F1). While applying all the correction approaches reduced the bias and SEE for correcting the LWD base modulus to the laboratory SM_R values, these helped reduce the bias

with somewhat similar SEE for the FWD modulus data. The third approach (i.e., B-L3) proved to correct the LWD moduli values better; using a simple multiplier (i.e., B-F1) was able to reduce the bias in the FWD-based moduli values (see Figure 6-58 and Figure 6-59).

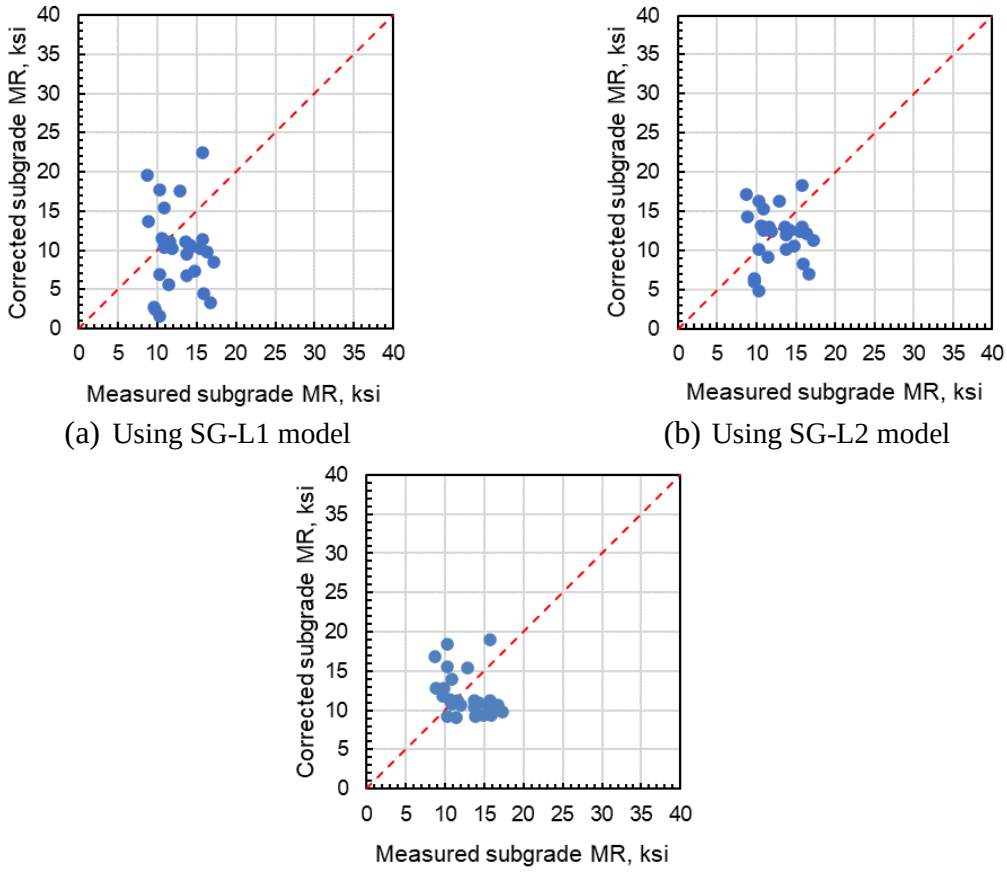

(a) Using SG-L1 model

(b) Using SG-L2 model

(c) Using SG-L3 model

Figure 6-52 Comparison of the measured and predicted subgrade moduli values using LWD tests

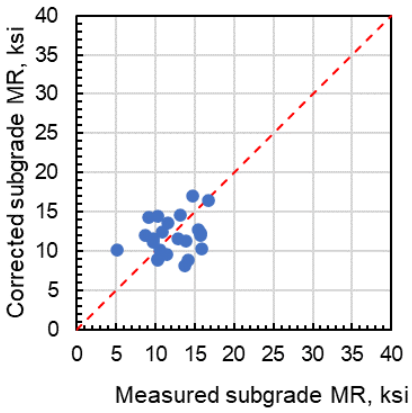

(a) Using SG-F1 model

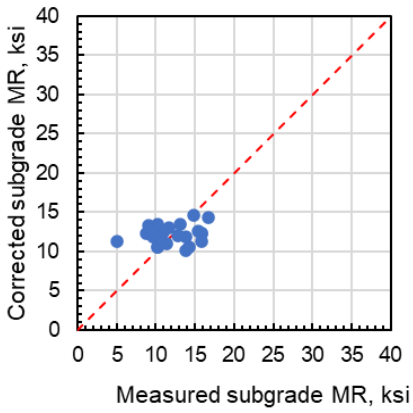

(b) Using SG-F2 model

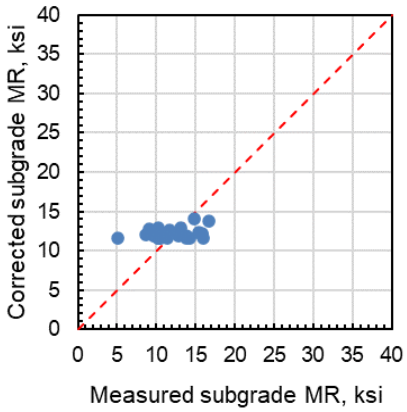

(c) Using SG-F3 model

Figure 6-53 Comparison of the measured and predicted subgrade moduli values using FWD tests

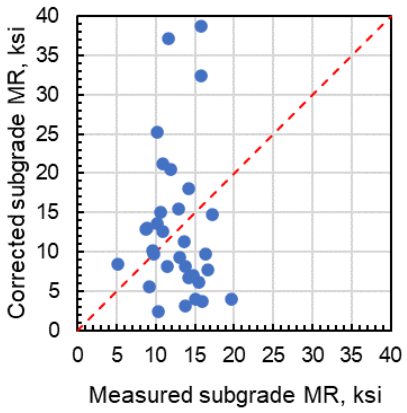

(a) Using SG-D1 model

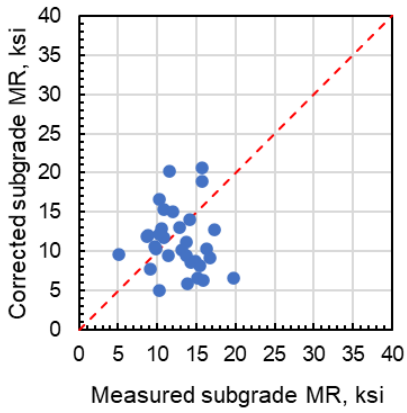

(b) Using SG-D2 model

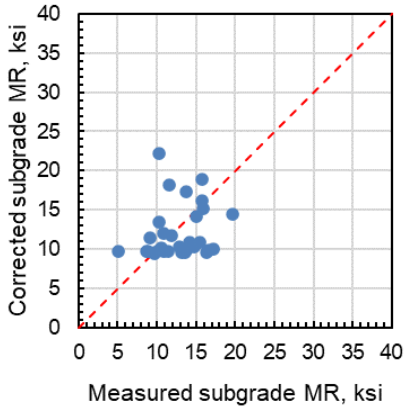

(c) Using SG-D3 model

Figure 6-54 Comparison of the measured and predicted subgrade moduli values using DCP tests

Table 6-48 Corrections for estimating lab-measured subbase moduli

Field test	Approach ID	Correction approach	Bias	SEE
LWD	SB-L1	$SB_{LAB} = 5.0 \times E_{LWD}$	0.90	13.56
	SB-L2	$SB_{LAB} = 9.97 \times \sqrt{E_{LWD}}$	1.76	8.49
	SB-L3	$SB_{LAB} = 2.29 \times E_{LWD} + \frac{33.50}{E_{LWD}}$	0.88	6.93
FWD	SB-F1	$SB_{LAB} = 0.75 \times E_{FWD}$	1.43	9.69
	SB-F2	$SB_{LAB} = 4.17 \times \sqrt{E_{FWD}}$	1.10	5.80
	SB-F3	$SB_{LAB} = 0.39 \times E_{FWD} + \frac{279.26}{E_{FWD}}$	0.09	2.57
DCP	SB-D1	$SB_{LAB} = 3.53 \times E_{DCP}$	5.50	12.56
	SB-D2	$SB_{LAB} = 9.59 \times \sqrt{E_{DCP}}$	2.08	8.70
	SB-D3	$SB_{LAB} = 2.36 \times E_{DCP} + \frac{32.88}{E_{DCP}}$	0.98	6.59

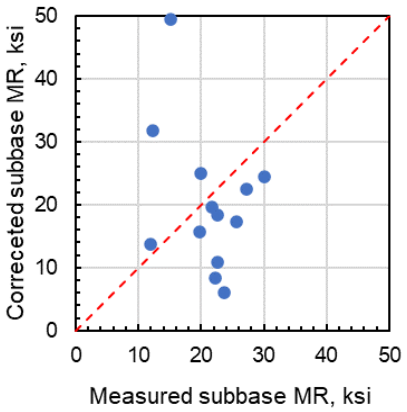

(a) Using SB-L1 model

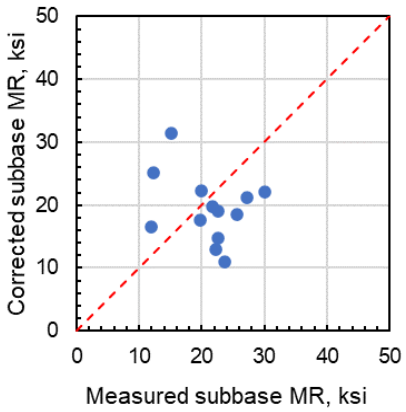

(b) Using SB-L2 model

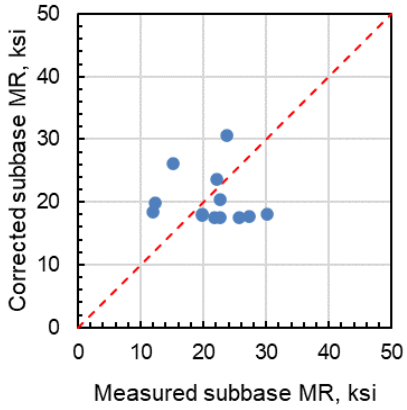

(c) Using SB-L3 model

Figure 6-55 Comparison of the measured and predicted subbase moduli values using LWD tests

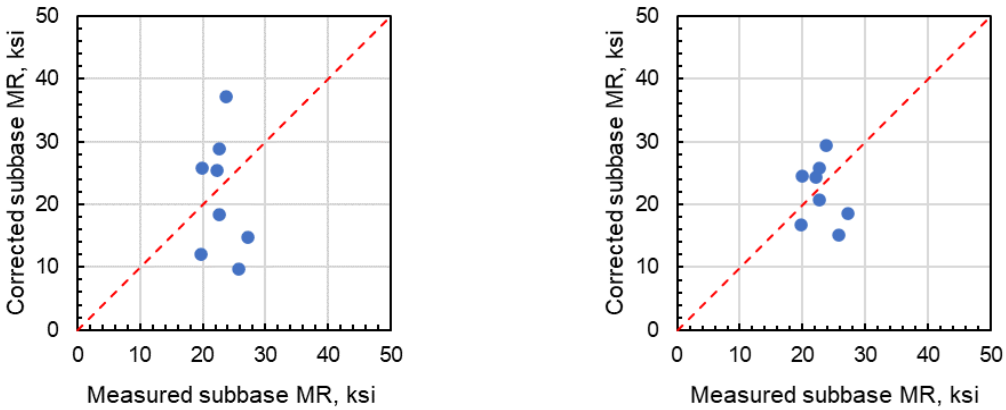

(a) Using SB-F1 model

(b) Using SB-F2 model

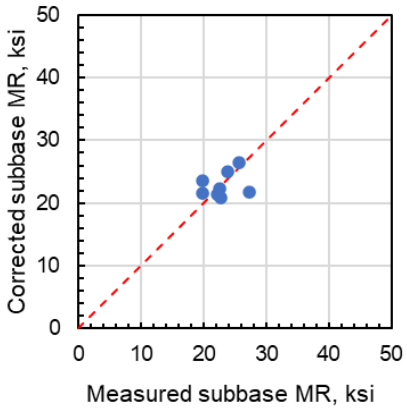

(c) Using SB-F3 model

Figure 6-56 Comparison of the measured and predicted subbase moduli values using FWD tests

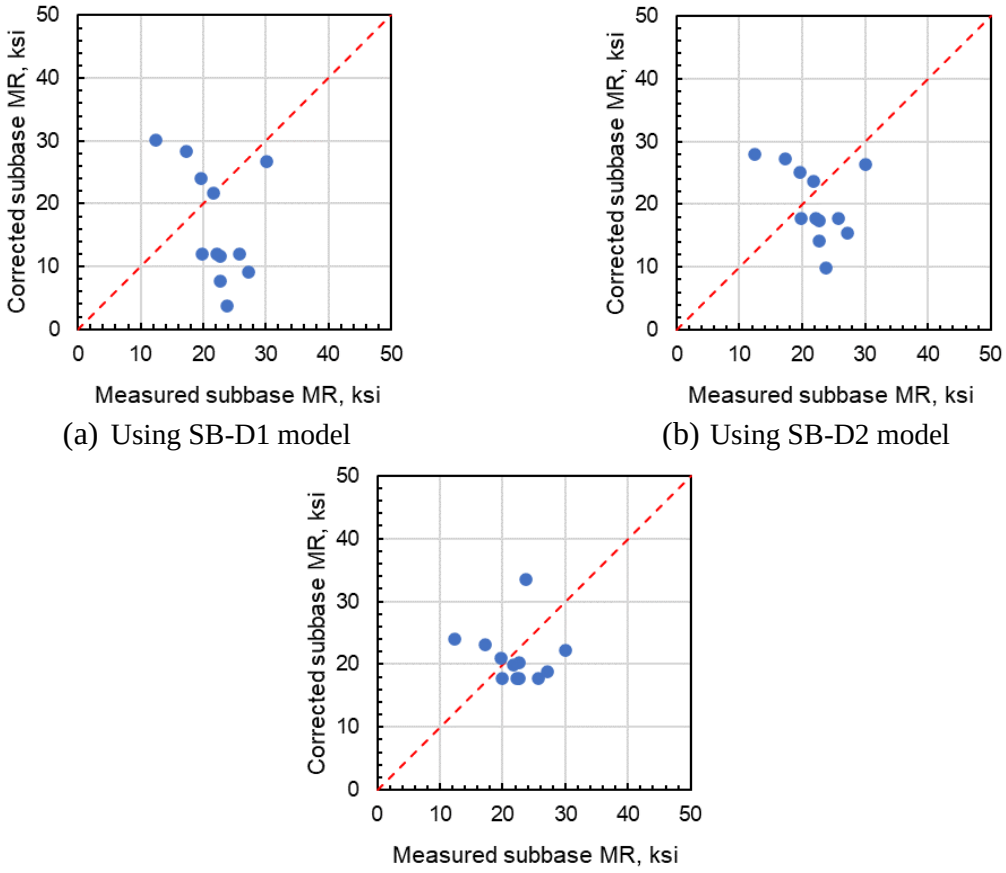

(a) Using SB-D1 model

(b) Using SB-D2 model

(c) Using SB-D3 model

Figure 6-57 Comparison of the measured and predicted subbase moduli values using DCP tests

The analysis presented in this section shows that the FWD backcalculation results in the lowest overall bias and SEE for different unbound layer moduli, especially for the base layer. This finding suggests FWD testing over the finished pavement surface reasonably estimates the unbound layer moduli for use in design. Additionally, the correction factors approach presented to obtain the actual layer's moduli should be used cautiously due to the factors that affect each test (field and laboratory). While laboratory material characterization is considered more accurate for pavement analysis & design, its replacement with field tests would require a large-scale experiment for better correlating lab versus field test results. The investigation would involve compacting different soils at varying moisture levels, conducting various field tests, and sampling immediately after testing to determine the resilient moduli in the lab without disturbing the sample's gradations and moisture content.

Table 6-49 Corrections for estimating lab-measured base moduli

Field test	Approach ID	Correction approach	Bias	SE
LWD	B-L1	$B_{LAB} = 3.80 \times E_{LWD}$	-0.35	11.23
	B-L2	$B_{LAB} = 11.72 \times \sqrt{E_{LWD}}$	0.59	8.14
	B-L3	$B_{LAB} = 2.51 \times E_{LWD} + \frac{105.78}{E_{LWD}}$	0.01	6.96
FWD	B-F1	$B_{LAB} = 0.94 \times E_{FWD}$	-0.06	2.05
	B-F2	$B_{LAB} = 6.02 \times \sqrt{E_{FWD}}$	-0.23	3.71

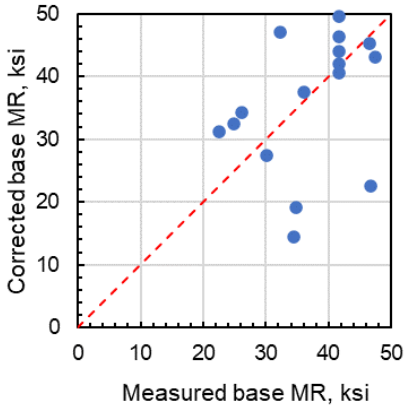

(a) Using B-L1 model

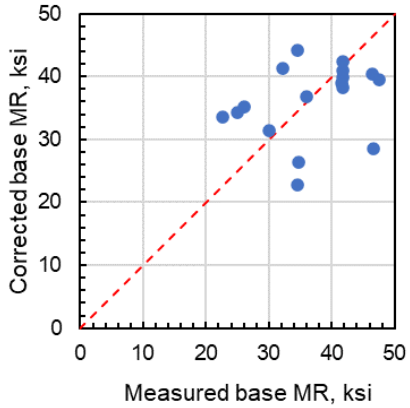

(b) Using B-L2 model

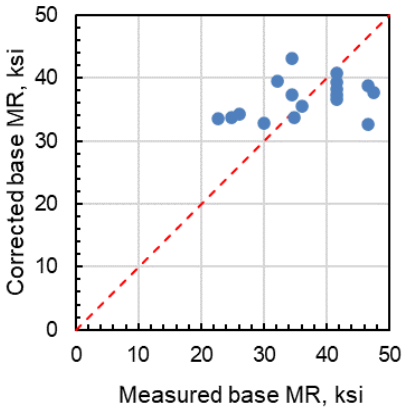

(c) Using B-L3 model

Figure 6-58 Comparison of the measured and predicted base moduli values using LWD tests

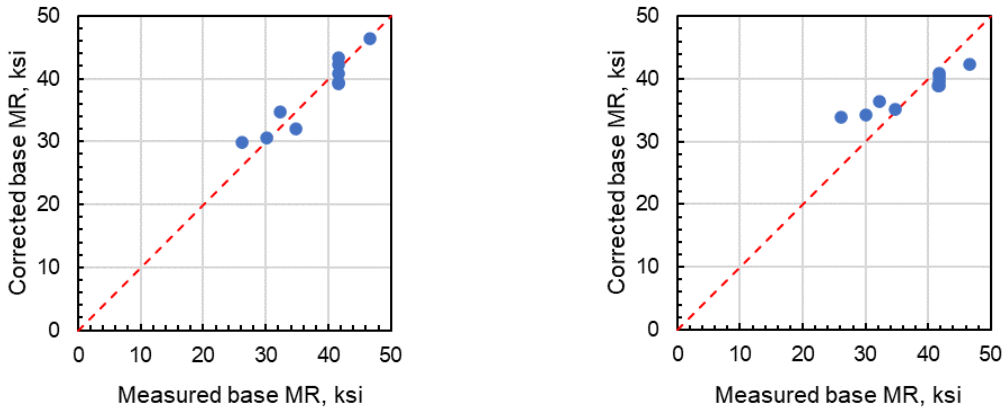

(a) Using B-F1 model (b) Using B-F2 model

Figure 6-59 Comparison of the measured and predicted base moduli using FWD tests

6.5 PROTOCOLS FOR MATERIAL SAMPLING AND TESTING

Since the as-constructed material properties are critical inputs in the Pavement-ME analysis and design, it is crucial to obtain such inputs during and after the construction of pavement sections. These properties can be a part of the database for future calibration of the performance models once sufficient performance data are available for the selected projects. Table 6-50 shows the general in-situ testing protocols for rigid and composite pavement sections.

Table 6-50 FWD testing protocols for the PCC layer

Field tests/material sampling	Sampling frequency	Layer/materials
FWD (Rigid Reconstruction)	Three subsections of 500 ft (project beginning, middle, and end, see Figure 6-60), FWD test at every 5th slab of each subsection at locations shown in Figure 6-61. • J1 (center of the slab) for uncracked slab • J4/J5 (LTE) with deflection time history (see Figure 6-62) • J2 (Void potential — a minimum of three load levels) • J3 (Edge support) Each of the above tests should be conducted in the morning on clear sunny days (8 to 10 am) and afternoon (1 to 3 pm) at the same slabs.	Top of PCC slab Tests = 14 per subsection per day (5 to 7 morning and 5 to 7 afternoon) Total = 42 per project
FWD temperature measurements for JPCP (temperature gradient)	Measure the temperature gradient in each subsection in the morning (8 to 10 am) and afternoon (1 to 3 pm). At the same location with three depths (top 1 to 2 inches, mid-depth, and 1 to 2 inches from the bottom), as shown in Figure 6-60.	PCC layer Three (3) temperature measurements each in the morning and afternoon at the same location (center of each subsection)
FWD (HMA overlay over JPCP)	Three subsections of 500 ft (project beginning, middle, and end, see Figure 6-60), FWD test at every 5th **uncracked slab** of each subsection at locations shown in Figure 6-61. • J1 (center of the slab) • J4/J5 (LTE) with deflection time history (see Figure 6-62) • J2 (Void potential — a minimum of three load levels) • J3 (Edge support)	Top of existing JPCP surface Total tests = 21 per project
	Every 1000 ft	Top of new HMA surface Total tests = 5 tests/mile/layer

Notes:

1. Testing should occur no earlier than 28 days after placement or a few days before opening to traffic.
2. J4/J5 (LTE) measurement with deflection time histories. Same for after the joint at OWP and EOM (i.e., beyond the dowel bar).
3. All testing is in the mainline outer lane wheel path.

Table 6-51 presents the in-situ testing protocols for flexible pavement sections. Table 6-52 illustrates the sampling protocols for material characterization and data collection frequencies for other standard destructive and non-destructive tests. Figure 6-60 through Figure 6-63 show the locations of temperature measurements (gradients), testing locations for JPCP, and testing and sampling locations for flexible pavements, respectively. Table 6-53 through Table 6-55 summarize different test methods used to characterize HMA, PCC, and unbound layer properties.

Table 6-51 FWD testing protocols for HMA layers

Field tests/material sampling	Sampling frequency	Layer/materials
Existing surface conditions (HMA overlay)	Fatigue and transverse cracking, rut depth, and IRI	Existing HMA and PCC surface obtained from the recent surface condition survey (PMS data)
FWD (HMA overlay over HMA)	Every 1000 ft (see Figure 6-63)	Top of existing HMA surface Top of base* & new HMA surface Total tests = 5 test/mile/layer
FWD (HMA Reconstruction)	Every 1000 ft (see Figure 6-63)	Top of base & HMA Total tests = 5 test/mile/layer
FWD temperature measurements for HMA	Obtain the temperature at the mid-depth of each HMA layer. Measure once during the morning (8 to 10 m) and once during the afternoon (1 to 3 pm) at the beginning, middle, and end of the project with FWD deflection time histories)	HMA layer

Note: All testing is in the mainline outer lane wheel path. *If all HMA layers are milled, and the base is exposed.

Table 6-52 In situ testing and the sampling frequency for unbound and bound layer materials

Field tests/ material sampling	Sampling frequency	Layer/materials	Estimated material property
LWD	Every 1000 ft	Top of the base, subbase, and subgrade Total tests = 5 test/layer If the project is more than a mile, one-mile section can be randomly selected for testing.	Base, subbase, and subgrade modulus
DCP	Every 1000 ft	Top of subbase, and subgrade Total tests = 5 tests/layer. If the project is more than a mile, one-mile section can be randomly selected for testing.	Base, subbase, and subgrade modulus and DCPI
Unbound material sampling (disturbed sample)	For the selected 1-mile section, collect 3 material samples, 2 bags (25 to 30 lb per bag) per sample. For the selected 1 mile collect sample every 1000 ft, 1 to 2 bags (25 to 30 lb per bag) per location.	Base and subbase Subgrade	Soil gradation, soil classification, maximum dry unit weight, OMC, index properties, and resilient modulus
HMA material sampling	For the selected 1 mile, cores at every 1000 ft (preferably entire HMA thickness with multiple lifts/layers) and GPR data for the entire project length.	HMA layer QA cores can be used within the selected 1 mile	IDT strength
	5 to 6 buckets per mix	HMA (Plant mix)	Dynamic modulus and creep compliance
	2 Gallon per mix	HMA (Binder)	Complex shear modulus
PCC material sampling	For the selected 1 mile, cores at every 1000 ft and GPR data for the entire project length	PCC layer QA cores can be used. If the project is more than a mile, a one-mile section can be randomly selected for testing.	$f_c^{'}$, IDT, and elastic modulus (*E*)
	9 cylinders (6” dia.) per project 3 beams (6” x 6” x 18”) per project	PCC mixture	$f_c^{'}$, IDT, *E*, and *CTE* Flexural strength (*MOR*)

Note: All testing and sampling are in the mainline outer lane wheel path. If the project is in both directions, the testing and sampling will apply for both directions if different materials are used.

Table 6-53 HMA material testing methods

Material Test Property	Test Method
Dynamic Modulus (E*)	AASHTO T342, and master curves generated in accordance with the AASHTO R 84
Complex Shear Modulus (G*) and Phase Angle (δ)	AASHTO T 315, and G*/δ master curves were generated at the loading frequencies and temperatures in accordance with MDOT RC-1593.
Asphalt Mixture Creep Compliance and IDT Strength	AASHTO T 322
Air Voids (%)	AASHTO T 166 / MTM 315
Effective Binder Content	AASHTO T 308
Theoretical Maximum Specific Gravity	ASTM D 2041
Layer Thickness	HMA core depth measure
Asphalt Binder Creep Compliance	AASHTO T 322, estimated (Park, 1999), or multiple stress creep recovery (MSCR) test using a DSR system in accordance with AASHTO T 350.
Fatigue Life (number of cycles to failure, Nf)	3PBC test as developed per NCHRP IDEA 20-30/IDEA 218 project, using cylindrical samples subjected to cyclic three-point bending.

Table 6-54 PCC material testing methods

Material Test Property	Test Method
Coefficient of Thermal Expansion (CTE)	AASHTO T 336-15
Modulus of Rupture (MOR)	ASTM C 78 (third-point loading beam method)
Compressive Strength	ASTM C 39
Elastic Modulus	ASTM C 469
PCC Surface Resistivity	AASHTO TP 95
Water Sorption and Freeze/Thaw Resistance	ASTM C 1585 for water sorption testing. The water sorption test provided a near full water saturation state before freeze-thaw (F-T) testing with the bottom surface continuously in contact with deionized water. Scaling resistance of concrete surfaces exposed to deicing chemicals using ASTM C672 ASTM C215 was used to evaluate changes in the Relative Dynamic Modulus (RDM) of the saturated concrete samples.
Air Voids	ASTM C 457
Layer Thickness	PCC core depth measure
Unit Weight	ASTM C 138

Table 6-55 Unbound material testing methods

Material Property	Test Method
Material Classification	The particle size distribution of the granular materials was determined in accordance with ASTM C136, D6913, and D7928. Atterberg limits determined in accordance with the ASTM D4318 Classification according to the Unified Soil Classification System (USCS) (ASTM D2487) and the American Association of State Highway and Transportation Officials (AASHTO) soil classification system (AASHTO M 145)
Proctor Compaction	The maximum dry unit weight (MDU) and optimum moisture content (OMC) are determined in accordance with: • ASTM D1557-12 (method C) technical standard for aggregate base materials • *ASTM D7382-20 (method 2A) if D1557-12 cannot be used* • ASTM D698-12 (methods A and B) for sand subbase and non-stabilized subgrade materials • ASTM D558/D558M-19 (method A) for cement-stabilized subgrade materials

Resilient Modulus (MR)	AASHTO T 307
	• If unbound material is not stiff enough to withstand the standard testing sequences, use a reduced stress sequence.
	
	Data Analysis and Test Results –
	• MEPDG model to determine MR using the elastic deformations recorded during the last five cycles of each testing sequence.
	• SM_R values per NCHRP Project 1-28A.
	  ○ For stiff materials (i.e., base), the bulk stress (θ) and the octahedral shear stress (τ_{oct}) values correspond to the 6th sequence to calculate SM_R (θ = 30 psi and τ_{oct} = 7 psi).
	  ○ For the reduced stress sequence (low stiffness), the stresses corresponding to the 13th sequence to calculate SM_R (θ = 12 psi and τ_{oct} = 3 psi)

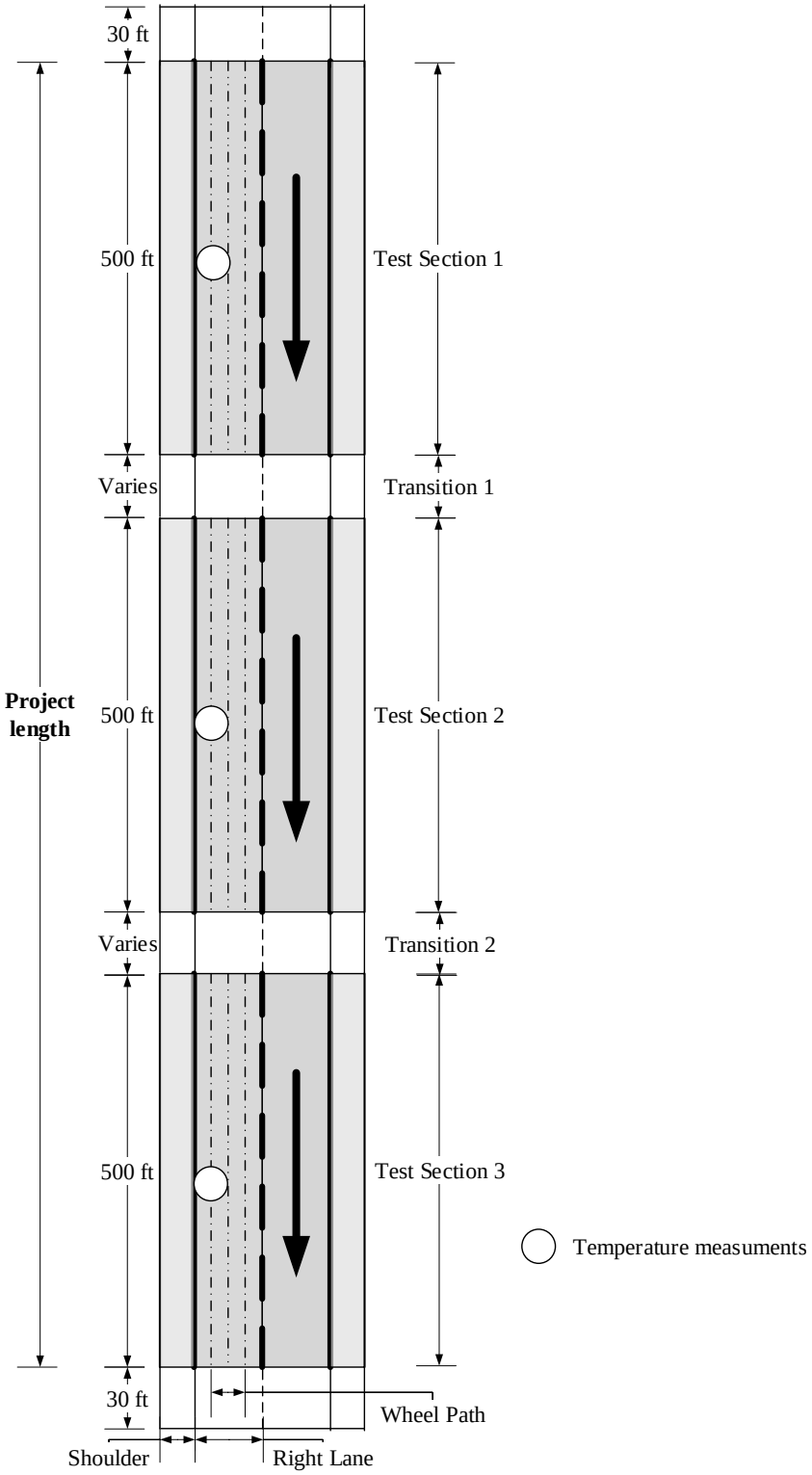

Figure 6-60 JPCP testing and sampling plan

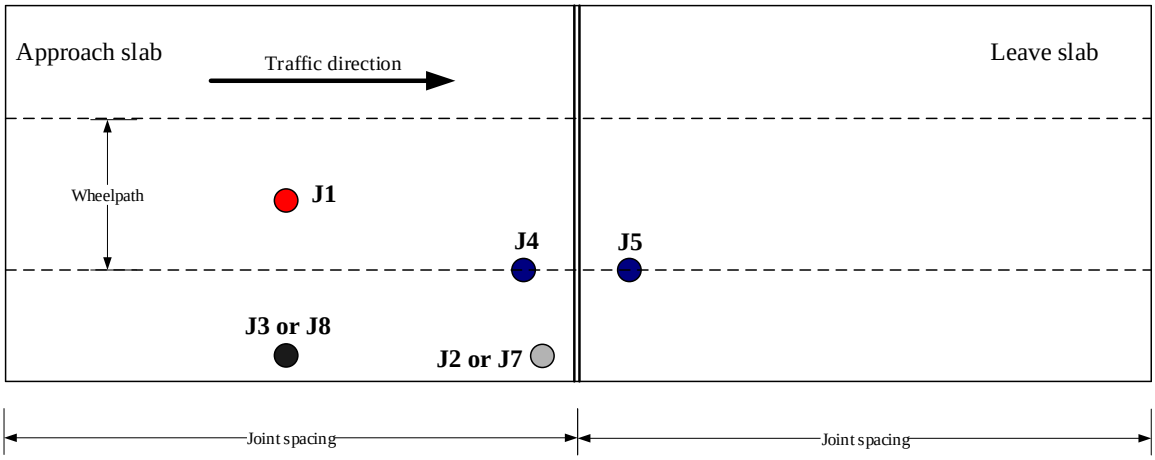

Figure 6-61 JPCP FWD per slab

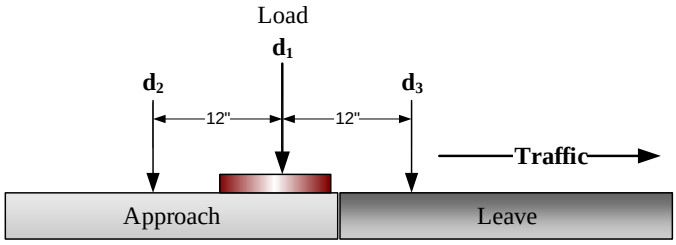

J4 Deflection (Approach LTE)

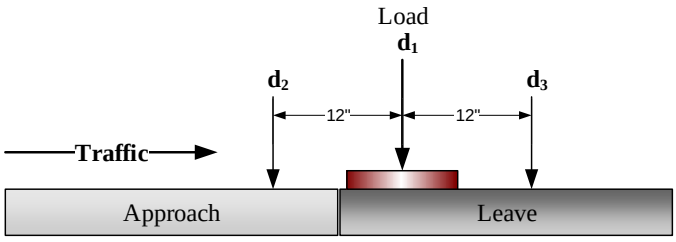

J5 Deflection (Leave LTE)

Figure 6-62 JPCP LTE testing

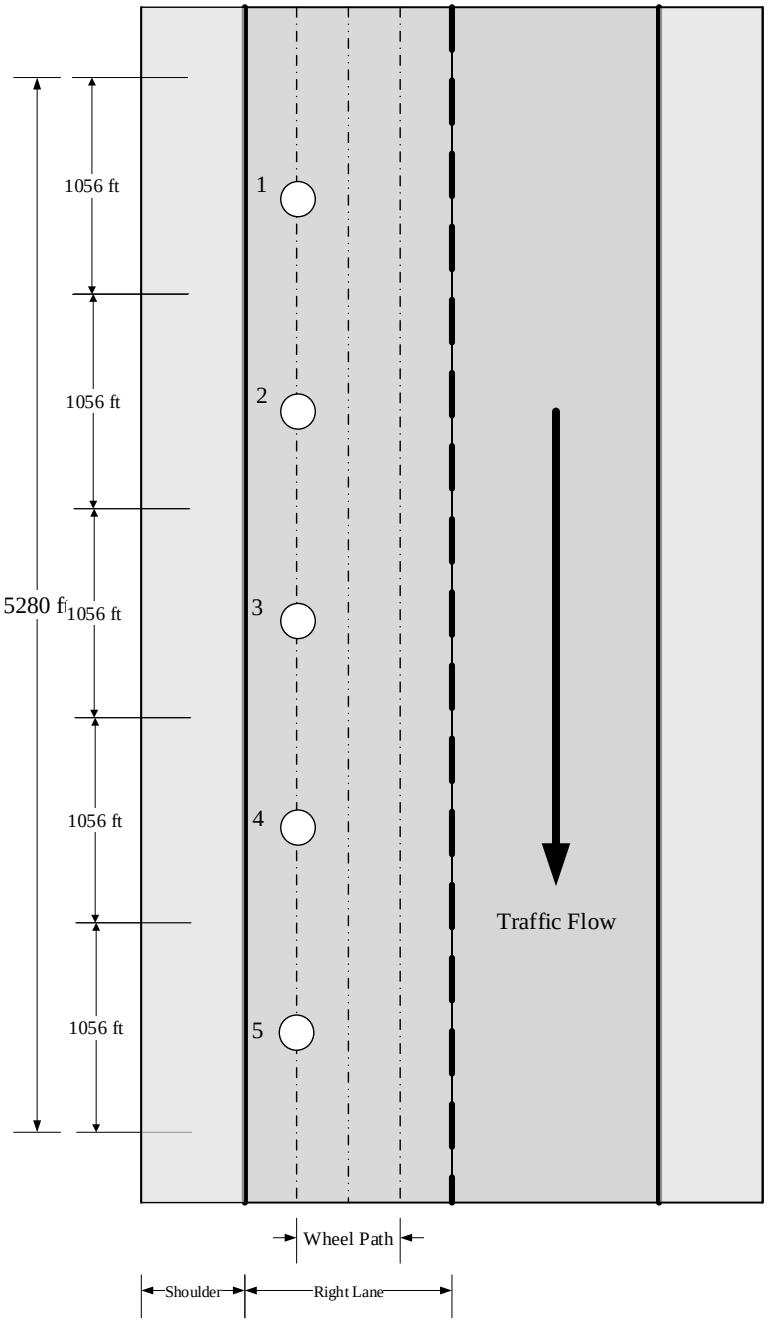

FWD, LWD and DCP test location and HMA/PCC cores (all layers) (locations 1 through 5)
Subgrade soil samples (locations 1 through 5)
Base & subbase samples (locations 1, 3, and 5)

Figure 6-63 Flexible pavement testing and sampling plan per mile

6.6 SUMMARY

This chapter presents the selection of eight projects, four each from the 2020 and 2021 construction seasons, along with the collected material samples and field-testing data. Protocols for material sampling and testing were established for these projects and for future data collection. Subsequently, pavement cross-section layers' moduli were estimated using the field-collected FWD, LWD, and DCP data. These were compared with the unbound material characterization results from the laboratory. Irrespective of the station locations, the subgrade SM_R values were relatively comparable to the median FWD- and DCP-determined moduli. Similarly, the subbase and base layer SM_R values were in close agreement with the moduli estimated using FWD data. To estimate potential correlations between the lab- and field test-based layer moduli, one-to-one correlation plots are presented. When the exact sampling locations were unavailable for these correlations, the median moduli estimated from the different field tests were compared to their laboratory-determined values. However, where available, the moduli values for samples with known locations were matched with the estimated moduli from the field test locations. Since an accurate correlation was not found between the different layer moduli obtained using field and laboratory tests, correction factors were obtained to estimate them from the field-testing data. The bias and SEE were determined for the field test-based moduli and the laboratory-determined SM_R values. The comparison showed that the FWD data results in moduli values with negligible bias and SEE, even without correction, among the three field tests evaluated.

The basic aim of finding the correction factors for estimating resilient moduli using field test data is to minimize the need for sampling and laboratory testing. Three approaches determined correction factors for each pavement layer and field tests. The evaluation showed that the third approach (i.e., SG-L3, SG-F3, SG-D3 for subgrade, etc.) significantly reduces the bias and the SEE for all pavement layers and field tests (except for the base layer and FWD test). However, the FWD-based base layer moduli were comparable to the lab value but slightly higher. Hence, using a single multiplier approach (i.e., B-F1) significantly reduced the bias with little reduction in the SEE. Therefore, correction factors should be carefully reviewed for the most accurate interpretation of moduli and not simply select the correct factor with the lowest bias and SEE as this may not practically represent the range of moduli.

The relationships presented in this chapter showed that the FWD testing reasonably estimates the layer moduli without using the correction factors. Therefore, FWD testing should be used to estimate the modulus of different materials for the post-construction design. Additionally, exercise caution in applying the correction factors for assessing the lab-based moduli values from field tests, especially LWD and DCP, due to differences in soil conditions (density, moisture content, and gradations) in the field and the laboratory. LWD and DCP testing can be used to quantify individual layers' stiffness to identify the weaker areas during construction.

CHAPTER 7 - CONCLUSIONS AND RECOMMENDATIONS

7.1 SUMMARY

This study aims to calibrate and validate the Pavement-ME performance models for Michigan as per Pavement-ME version 2.6. In addition, it outlines the testing protocols for field and laboratory material testing for collecting material input data for future calibrations. The research team selected 163 new flexible projects (i.e., 288 sections) and 121 flexible rehabilitation projects (i.e., 176 sections). For design purposes, new flexible projects are those construction practices used in Michigan that include HMA reconstruction, HMA over crushed & shaped HMA, and HMA over rubblized PCC pavements. In contrast, flexible rehabilitation fixes are those that are HMA over existing HMA and HMA over existing PCC (including existing composite pavement). Similarly, the team selected 46 new JPCP projects (i.e., 85 sections) and 11 unbonded overlay projects (i.e., 28 sections) for rigid pavements. These projects were selected considering different regions, materials, traffic, performance data, and pavement age. Chapter 3 outlines the selection process and details of each input. The main objectives of this project were:

- Evaluate projects used in previous calibration efforts and identify new potential projects for local calibration (*1*).
- Verify the adequacy of global models in the Pavement-ME and the need for local calibration.
- Perform local calibration of performance models for Michigan conditions.
- Provide the most suitable calibration coefficients for different pavement types.
- Recommend future local calibration guidelines and data needs.
- Recommend testing protocol guidelines for field and laboratory material testing.

The research team extracted the Pavement-ME inputs for the selected projects from MDOT construction records and other databases and obtained the performance data from MDOT PMS data. Some MDOT distress units are incompatible with the Pavement-ME outputs; therefore, the team considered necessary conversions. Calibration was performed for different combinations of MDOT sections as follows:

Option 1: Reconstruction sections only
Option 2: Reconstruction and rehabilitation sections
Option 3: Rehabilitation sections only

The team used several statistical techniques for the calibrations—no sampling, bootstrapping, split sampling, and repeated split sampling. Verification using global models shows that global models could not provide reasonable predictions, and there was a need for local calibration. The number of sections and performance data records has increased since the previous calibration effort. Also, some performance models have changed, and the last calibration results are no longer valid for those models. These developments further indicated a need for a new model calibration effort. Local recalibration results show that the performance model predictions improve significantly after calibration for Michigan

conditions. Resampling methods provide better predictions for most of the performance models. This report documents the calibration results, input data, future local calibration guidelines, and data needs.

7.2 LOCAL CALIBRATION FINDINGS

Several conclusions are drawn based on the local calibration results and input data requirements to the Pavement-ME. These conclusions are categorized into the following three parts:

- Data collection for the selected pavement sections
- Local calibration process
- Catalog of the local calibration coefficients

7.2.1 Data Needs for Local Calibration

Data collection for local calibration is challenging and includes collecting observed performance and input data for the selected pavement sections. The team ensured adequate data availability for enough pavement sections within each distress type. Chapter 3 outlines the process for pavement selection for local calibration sources for each input data. The data needed for the local calibration are:

1. Readily available MDOT-measured condition data
2. Project selection criteria
3. Pavement cross-section information
4. Traffic inputs
5. Construction materials inputs
6. Climate inputs

Table 7-1 summarizes the inputs and corresponding levels for the available data.

7.2.2 Process for Local Calibration

The local calibration guide describes the calibration process for local conditions (*2*). Local calibration aims to minimize the SEE and bias between the measured and predicted distress. SEE shows the scatter of data with respect to the line of equality, whereas bias shows the constant underprediction or overprediction by performance models. This study improved the SEE and bias values for all performance models. In general, the local calibration of the performance models involves the following steps:

1. Select an adequate number of projects based on performance and statistical requirements to a minimum number of projects. These projects should represent typical local construction practices and a wide range of Pavement-ME inputs.
2. Collect performance data and Pavement-ME inputs for the selected sections.
3. Run Pavement-ME analysis and extract critical responses and predicted distresses.
4. Compare the predicted distress with measured distress based on SEE, bias, and hypothesis tests.

5. Based on the results from step 4, test the accuracy of the global models and the need for local calibration.
6. If global models are satisfactory (see Table 7-2 for minimum requirements), local calibration is not required. If the global model has significant bias and standard error, recalibrate the models for local conditions.
7. Validate calibration results by applying them to an independent set of sections not used for calibration.
8. Estimate the reliability equations based on the calibrated model predictions and measured distress.

Table 7-1 Summary of input levels and data source

Input			Pavement-ME input level	Data source level	Input source
Traffic	Vehicle class distribution		1	2	MDOT specified traffic per cluster data
	Hourly distribution		1	2	
	Monthly adjustment factor		1	2	
	Number of axles per truck		1	2	
	Single, tandem, tridem, and quad axle load distribution		1	2	
	AADTT		1	1	From design drawings
	Vehicle class 9 percentage		1	1	MDOT TDMS website
Cross-section layers (new and existing)	HMA thickness		1	1	Project-specific HMA thicknesses based on design drawings
	PCC thickness		1	1	Project-specific PCC thicknesses based on design drawings
	Base thickness		1	1	Project specific base thicknesses based on design drawings
	Subbase thickness		1	1	Project-specific subbase thicknesses based on design drawings
Layer materials	HMA	Mix properties	1	Mix of 2 and 3	MDOT HMA mixture characterization study (DYNAMOD database)
		HMA mixture aggregate gradation	1	1 or 3	Project-specific mixture gradation data obtained from data collection or average statewide values
		Binder properties	1	3	MDOT HMA mixture characterization study (DYNAMOD database)
	PCC	Strength (f'_c, MOR)	3	1 or 3	Project-specific testing values or average statewide value
		CTE	1	2	MDOT recommended values
	Base/ subbase	MR	3	3	Recommendations from MDOT unbound material study
	Subgrade	MR	3	3	Soil-specific MR values per MDOT subgrade soil study
		Soil properties	Mix of all levels	1	Location-based soil type per MDOT subgrade soil study
Climate			1	1	Closest available climate station

Note: Data source Level 1 is project-specific data. Data source Level 2 inputs are based on regional averages in Michigan. Data source Level 3 inputs are based on statewide averages in Michigan.

Table 7-2 Recommended initial values for tolerable bias and standard deviation of the measured distress

Type	Distress/performance parameter	Tolerable Bias	Standard deviation of maximum measured distress
Flexible	Fatigue cracking (% total lane area)	1.5	5
	Rutting (inches)	0.075	0.2
	Thermal cracking (ft/mile) Thermal Reflection cracking	200	650
	IRI (inch/mile)	20	65
Rigid	Transverse cracking (% slabs cracked)	4	15
	Faulting (inch)	0.02	0.07
	IRI (inch/mile)	20	65

7.2.3 Coefficients for the Locally Calibrated Models

Final coefficients for calibration models were selected based on the efficiency of different calibration approaches for a combination of datasets. Mostly, bootstrapping provided the lowest SEE and bias. Also, bootstrapping provides a more robust optimization with CI. Therefore, recommended model coefficients are primarily using bootstrapping. For flexible sections, the team selected adequate sections for new and rehabilitation sections. A separate set of calibration coefficients is recommended for new flexible (Option 1), HMA over HMA, and composite sections (Option 3). Option 2 (new and overlay sections) is recommended for rigid pavements. CAT tool was used to calibrate thermal cracking and faulting models, which were calibrated using no sampling technique only. Tables 7-3 to 7-6 summarize the recommended model coefficients and standard error equations for flexible sections, whereas Tables 7-7 and 7-10 show the same for rigid sections. Some of the observations from calibration results are as follows:

- Global model underpredicted bottom-up cracking. For a measured value of 38%, the global model predictions were close to zero.
- Option 1a (which combines all cracking, bottom-up and top-down cracking to represent bottom-up cracking) provided better predictions compared to option 1b (which uses the estimated bottom-up cracking alone) for bottom-up cracking. It is difficult to estimate the origin of a crack (bottom-up or top-down); hence, combining bottom-up and top-down cracking reduces assumptions. Also, option 1a has more sections and measured data available.
- Top-down cracking model calibration improved the SEE and bias but did not provide realistic results. Option 1a is valuable for incorporating top-down cracking into calibration options. However, it should be noted that if option 1a is adopted for alligator cracking, the longitudinal cracking model should not be used because such measured cracking is already included in option 1a.
- Rutting calibration using method 2 minimizes the error for total rutting, but it is difficult to keep track of predictions for individual layers. Method 1 for rutting provides more realistic predictions and is recommended.
- The Pavement-ME limits the thermal cracking prediction to 2112 ft/mile, but the measured data showed several records of thermal cracking above 2112 ft/mile. Also,

the thermal cracking coefficient in the current version is changed and is a function of MAAT. This made the calibration of the thermal cracking model challenging. A single value of 0.85 was finally recommended. The SEE and bias were improved after local calibration, but the thermal cracking model still showed high prediction variability. Notably, sections with Superpave mixes were only considered to calibrate the thermal cracking model.

- Transverse cracking model for rigid pavements underpredicts using global coefficients.
- Joint faulting model for rigid pavements overpredicts using global coefficients. It is challenging to separate faulting at joints and cracks. Further, MDOT sensor data had records with more faulted joints than the number of joints. Joint faulting was cut off at 0.4 inches, and the maximum number of faults to 36 for any 0.1-mile sections to accurately estimate the measured joint faulting.
- IRI models for both flexible and rigid models provided good results after calibrating their components. Local calibration of these IRI models further improved the SEE and bias.

Table 7-3 Summary of flexible pavement performance models (reconstruct pavements)

Data Subset	Performance prediction model		Performance models and transfer functions	Local coefficient
Option 1a (Combined data for bottom-up & top-down)	Fatigue cracking (bottom-up)		$FC_{Bottom} = \left(\frac{1}{60}\right)\left(\frac{6000}{1+e^{C_1C_1^*+C_2C_2^*Log(DI_{Bottom}\cdot 100)}}\right)$	$C_1 = 0.2320$ $C_2 = 0.6998$ (hac <5 in) $C_2 = (0.867 + 0.2583 * hac) * 0.2204$ (5 in <= hac <=12 in) $C_2 = 0.8742$ (hac >12 in)
Option 1b (only bottom-up data)				$C_1 = 0.2540$ $C_2 = 0.7303$ (hac <5 in) $C_2 = (0.867 + 0.2583 * hac) * 0.2692$ (5 in <= hac <=12 in) $C_2 = 1.0678$ (hac >12 in)
Option 1	Fatigue cracking (top-down)		$t_0 = \frac{K_{L1}}{1 + e^{K_{L2}\times 100\times(a_0/2A_0)+K_{L3}\times HT+K_{L4}\times LT+K_{L5}\times \log_{10} AADTT}}$ $FC_{Top} = Lmax \times e^{-(\frac{C_1\rho}{t-C_3to})^{C_2\beta}}$	$K_{L2} = 0.90$ $K_{L3} = 0.09$ $K_{L4} = 0.101$ $K_{L5} = 3.260$ $C_1 = 0.30$ $C_2 = 1.155$
Option 1	Rutting	HMA	$\Delta_{p(HMA)} = \varepsilon_{p(HMA)}h_{HMA} = \beta_{1r}k_z\varepsilon_{r(HMA)}10^{k_{1r}}n^{k_{2r}\beta_{2r}}T^{k_{3r}\beta_{3r}}$	$\beta_{1r} = 0.148$ $\beta_{2r} = 0.7$ $\beta_{3r} = 1.3$
		Base/subgrade	$\Delta_{p(soil)} = \beta_{s1}k_{s1}\varepsilon_v h_{soil}\left(\frac{\varepsilon_o}{\varepsilon_r}\right)e^{-\left(\frac{\rho}{n}\right)^{\beta}}$	$\beta_{s1} = 0.301$ $\beta_{sg1} = 0.070$
Option 1	Thermal cracking		$A = 10^{k_t\beta_t(4.389-2.52Log(E_{HMA}\sigma_m\eta))}$	$K = 0.85$
Option 1	IRI		$IRI = IRI_o + C_1(RD) + C_2(FC_{Total}) + C_3(TC) + C_4(SF)$	$C_1 = 42.874, C_2 = 0.102$ $C_3 = 0.0081, C_4 = 0.003$

Note: Option 1 = Reconstruct pavements, Option 2 = Combined reconstruct and rehabilitated pavements, Option 3 = Rehabilitated pavements. The model coefficients in red color show the locally calibrated new coefficients. Option 1a uses bottom-up and top-down cracking; therefore, if Option 1a is used, the top-down model should not be used.

Table 7-4 Summary of flexible pavement performance models (rehabilitation pavements)

Data Subset	Performance prediction model		Performance models and transfer functions	Local coefficient
Option 3 (HMA over HMA)	Fatigue cracking (top-down)		$t_0 = \frac{K_{L1}}{1 + e^{K_{L2}\times 100\times(a_0/2A_0)+K_{L3}\times HT+K_{L4}\times LT+K_{L5}\times \log_{10} AADTT}}$	$K_{L2} = 0.714$ $K_{L3} = 0.093$ $K_{L4} = 0.102$ $K_{L5} = 0.191$ $C_1 = 0.084$ $C_2 = 2.007$
Option 3 (HMA over PCC)			$FC_{Top} = Lmax \times e^{-(\frac{C_1\rho}{t-C_3 to})^{C_2\beta}}$	$K_{L2} = 0.475$ $K_{L3} = 0.097$ $K_{L4} = 0.104$ $K_{L5} = 0.206$ $C_1 = 0.104$ $C_2 = 1.635$
Option 3 (HMA over HMA)	Rutting	HMA	$\Delta_{p(HMA)} = \varepsilon_{p(HMA)} h_{HMA} = \beta_{1r} k_z \varepsilon_{r(HMA)} 10^{k_{1r}} n^{k_{2r}\beta_{2r}} T^{k_{3r}\beta_{3r}}$	$\beta_{1r} = 1.0422$
		Base/subgrade	$\Delta_{p(soil)} = \beta_{s1} k_{s1} \varepsilon_v h_{soil} \left(\frac{\varepsilon_o}{\varepsilon_r}\right) e^{-\left(\frac{\rho}{n}\right)^{\beta}}$	$\beta_{s1} = 0.3823$ $\beta_{sg1} = 0.1212$
Option 3 (HMA over PCC)		HMA	$\Delta_{p(HMA)} = \varepsilon_{p(HMA)} h_{HMA} = \beta_{1r} k_z \varepsilon_{r(HMA)} 10^{k_{1r}} n^{k_{2r}\beta_{2r}} T^{k_{3r}\beta_{3r}}$	$\beta_{1r} = 1.535$
Option 3 (HMA over HMA)	Thermal + Reflective cracking		$A = 10^{k_t\beta_t(4.389-2.52Log(E_{HMA}\sigma_m\eta))}$ $\Delta D = \frac{C_1 k_1 \Delta_{bending} + C_2 k_2 \Delta_{shearing} + C_3 k_3 \Delta_{thermal}}{h_{OL}}$ $RCR = \left(\frac{100}{C4 + e^{c5 log D}}\right) * EXCRK$	$K = (3 * POW(10,-7)) * Pow(MAAT, 4.0319)) * 0.55 + 0$ $C_1 = 3.25, C_2 = 25$ $C_3 = 0.14, C_4 = 180$
Option 3 (HMA over PCC)				$K = (3 * POW(10,-7)) * Pow(MAAT, 4.0319)) * 0.55 + 0$ $C_1 = 0.2833, C_2 = 0.7333$ $C_3 = 2.5, C_4 = 70$
Option 3 (HMA over HMA)	IRI		$IRI = IRI_o + C_1(RD) + C_2(FC_{Total}) + C_3(TC) + C_4(SF)$	$C_1 = 15.072, C_2 = 0.140$ $C_3 = 0.004, C_4 = 0.0192$
Option 3 (HMA over PCC)				$C_1 = 14.911, C_2 = 2.460$ $C_3 = 0.011, C_4 = 0.0212$

Note: Option 1 = Reconstruct pavements, Option 2 = Combined reconstruct and rehabilitated pavements, Option 3 = Rehabilitated pavements. The model coefficients in red color show the locally calibrated new coefficients.

Table 7-5 Summary of flexible pavement performance model standard errors (reconstruct pavements)

Data Subset	Performance prediction model		Standard error
Option 1a	Fatigue cracking (bottom-up)		$s_{e(Alligator)} = 0.2262 + \frac{14.2349}{1 + \exp(0.2958 - 0.1441 \log(Crack))}$
Option 1b			$s_{e(Alligator)} = 4.4396 + \frac{25.4391}{1 + \exp(4.3119 - 2.2778 \log(Crack))}$
Option 1	Fatigue cracking (top-down)		$s_{e(Longitudinal)} = 0.6417 \times TOP + 0.5014$
Option 1	Rutting	HMA	$s_{e(HMA)} = 0.1481(RUT_{HMA})^{0.4175}$
		Base/subgrade	$s_{e(base)} = 0.0411(RUT_{base})^{0.3656}$ $s_{e(subgrade)} = 0.0728(RUT_{subgrade})^{0.5456}$
Option 1	Thermal cracking		$s_{e(TC)} = 0.1223(TC) + 400.9$
Option 1	IRI		Internally determined by the software

Table 7-6 Summary of flexible pavement performance model standard errors (rehabilitation pavements)

Data Subset	Performance prediction model		Standard error
Option 3- HMA over HMA	Fatigue cracking (top-down)		$s_{e(Longitudinal)} = 0.838 \times TOP + 0.0269$
Option 3- Composite			$s_{e(Longitudinal)} = 0.9236 \times TOP + 0.6452$
Option 3-HMA over HMA	Rutting	HMA	$s_{e(HMA)} = 0.272(RUT_{HMA})^{0.6939}$
		Base/subgrade	$s_{e(base)} = 0.0236(RUT_{base})^{0.184}$ $s_{e(subgrade)} = 0.1706(RUT_{subgrade})^{0.7269}$
Option 3- Composite		HMA	$s_{e(HMA)} = 0.2336(RUT_{HMA})^{0.7763}$
Option 3: HMA over HMA	Thermal + Reflective cracking		$s_{e(TC)} = 338.59(TC)^{0.0849}$
Option 3-Composite			$s_{e(TC)} = 308.74(TC)^{0.1063}$
Option 3- HMA over HMA	IRI		Internally determined by the software
Option 3- Composite			

Table 7-7 Summary of rigid pavement performance models (reconstruct and rehabilitation pavements: widened lane width = 14 ft)

Data Subset	Performance prediction model	Performance models and transfer functions	Local coefficient
Option 2	Transverse cracking	$CRK_{BU/TD} = \frac{100}{1 + C_4 (DI_F)^{C_5}}$	$C_4 = 0.426$ $C_5 = -0.953$
Option 2	Transverse joint faulting	$Fault_m = \sum_{i=1}^{m} \Delta Fault_i$ $\Delta Fault_i = C_{34} \times (FAULTMAX_{i-1} - Fault_{i-1})^2 \times DE_i$ $FAULTMAX_i = FAULTMAX_0 + C_7 \times \sum_{j=1}^{m} DE_j \times Log(1 + C_5 \times 5.0^{EROD})^{C_6}$ $FAULTMAX_0 = C_{12} \times \delta_{curling} \times \left[Log(1 + C_5 \times 5.0^{EROD}) \times Log(\frac{P_{200} \times WetDays}{p_s}) \right]^{C_6}$ $C_{12} = C_1 + C_2 \times FR^{0.25}$ $C_{34} = C_3 + C_4 \times FR^{0.25}$	$C_1 = 0.8$ $C_2 = 1.3889$ $C_3 = 0.00217$ $C_4 = 0.00444$ $C_5 = 250$ $C_6 = 0.2$ $C_7 = 7.3$ $C_8 = 400$
Option 2	IRI	$IRI = IRI_I + C_1 \times CRK + C_2 \times SPALL + C_3 \times TFAULT + C_4 \times SF$	$C_1 = 0.1$ $C_2 = 2.0611$ $C_3 = 1.6338$ $C_4 = 22.9978$

Note: Option 1 = Reconstruct pavements, Option 2 = Combined reconstruct and rehabilitated pavements, Option 3 = Rehabilitated pavements. The model coefficients in red color show the local calibrated new coefficients.

Table 7-8 Summary of rigid pavement performance model standard errors (reconstruct and rehabilitation pavements: widened lane width = 14 ft)

Data Subset	Performance prediction model	Reliability
Option 2	Transverse cracking	$S_{e(CRK)} = 2.8285(CRK)^{0.5205}$
Option 2	Transverse joint faulting	$S_{e(Fault)} = 0.0902(Fault)^{0.2038}$
Option 2	IRI	Internally determined by the software

Table 7-9 Summary of rigid pavement performance models (reconstruct and rehabilitation pavements: widened lane width = 12.5 ft)

Data Subset	Performance prediction model	Performance models and transfer functions	Local coefficient
Option 2	Transverse cracking	$CRK_{BU/TD} = \frac{100}{1 + C_4 (DI_F)^{C_5}}$	$C_4 = 0.415$ $C_5 = -0.965$
Option 2	Transverse joint faulting	$Fault_m = \sum_{i=1}^{m} \Delta Fault_i$ $\Delta Fault_i = C_{34} \times (FAULTMAX_{i-1} - Fault_{i-1})^2 \times DE_i$ $FAULTMAX_i = FAULTMAX_0 + C_7 \times \sum_{j=1}^{m} DE_j \times Log(1 + C_5 \times 5.0^{EROD})^{C_6}$ $FAULTMAX_0 = C_{12} \times \delta_{curling} \times \left[Log(1 + C_5 \times 5.0^{EROD}) \times Log(\frac{P_{200} \times WetDays}{p_s}) \right]^{C_6}$ $C_{12} = C_1 + C_2 \times FR^{0.25}$ $C_{34} = C_3 + C_4 \times FR^{0.25}$	$C_1 = 0.6$ $C_2 = 1.611$ $C_3 = 0.00217$ $C_4 = 0.00444$ $C_5 = 250$ $C_6 = 0.2$ $C_7 = 7.3$ $C_8 = 400$
Option 2	IRI	$IRI = IRI_I + C_1 \times CRK + C_2 \times SPALL + C_3 \times TFAULT + C_4 \times SF$	$C_1 = 0.0942$ $C_2 = 1.5471$ $C_3 = 1.7970$ $C_4 = 23.7529$

Note: Option 1 = Reconstruct pavements, Option 2 = Combined reconstruct and rehabilitated pavements, Option 3 = Rehabilitated pavements. The model coefficients in red color show the local calibrated new coefficients.

Table 7-10 Summary of rigid pavement performance model standard errors (reconstruct and rehabilitation pavements: widened lane width = 12.5 ft)

Data Subset	Performance prediction model	Reliability
Option 2	Transverse cracking	$S_{e(CRK)} = 2.9004(CRK)^{0.5074}$
Option 2	Transverse joint faulting	$S_{e(Fault)} = 0.0919(Fault)^{0.2249}$
Option 2	IRI	Internally determined by the software

7.3 MATERIAL CHARACTERIZATION & TESTING PROTOCOLS

The in-situ and laboratory-resilient moduli of pavement layers were estimated using field (FWD, LWD, and DCP) and lab tests conducted for various layers per projects conducted in 2020 and 2021. The following are the conclusions based on the test results:

- LWD resulted in the lowest moduli values for all pavement layers (base, subbase, and subgrade).
- The laboratory results show that the median subgrade moduli for all projects are between 12 to 17 ksi. The FWD and the DCP data estimated higher moduli for the subgrade layer for all projects with considerable spatial variability.
- The median subbase moduli values determined in the laboratory range between 15 to 25 ksi for all projects. The LWD and DCP data display similar trends with median subbase moduli determined from field tests below 10 ksi. FWD data analyses resulted in the highest subbase moduli values, slightly higher than the laboratory-determined median subbase moduli values.
- The laboratory determined median base moduli range between 30 to 40 ksi. FWD data analyses resulted in the highest moduli values for all the projects.
- Among the three field tests evaluated (DCP, LWD, and FWD), when comparing field to laboratory results, FWD data results in moduli values with the most negligible bias and SEE. Still, an exact correlation was not found for the unbound layers.
- To potentially minimize the need for sampling and laboratory testing of unbound layers, correction factors were provided to estimate them from the field-testing data. However, MDOT should exercise caution in applying the correction factors for estimating and assessing the lab-based moduli values from field tests, especially LWD and DCP, due to potential differences in soil conditions (density, moisture content, and gradations) in the field versus those in the laboratory. Furthermore, correction factors should be carefully reviewed for the most accurate interpretation of moduli and not simply use the correct factor with the lowest bias and SEE, as this may not practically represent the range of moduli.
- The results of material characterizations for HMA, PCC, and unbound materials can be used to validate the design inputs used in the Pavement-ME and/or future calibration efforts.
- Protocols for in-situ testing frequency and material sampling quantity and frequency are developed for collecting material library data in the future.
- DynaMOD was expanded to include the material testing results for concrete and unbound materials, in addition to its inclusion of asphalt materials for input into Pavement-ME.

7.4 RECOMMENDATIONS

The following are the recommendations based on the findings of this study:

1. HMA bottom-up cracking is defined as alligator cracking in the wheel path. The PDs 234, 235, 220, 221, 730, and 731 match this requirement in the MDOT PMS database. The PDs have units of miles; however, to make those compatible with the

Pavement-ME alligator cracking units, conversion to the percent of the total area is needed. The lane width was assumed to be 12 ft. The typical wheelpath width of 3 feet was assumed. The conversion is shown in Equation (7-1):

$$\%AC_{bottom-up} = \frac{\text{Length of cracking (miles)} \times \text{width of wheelpaths (feet)}}{\text{Length of section (miles)} \times \text{Lane width (feet)}} \times 100 \quad (7\text{-}1)$$

2. HMA top-down cracking is load-related longitudinal cracking in the wheel path. The PDs 204, 205, 724, and 725 were assumed to correspond to the top-down cracking in the MDOT PMS database because those may not have developed an interconnected pattern that indicates alligator cracking. Those cracks may show an early stage of fatigue cracking, which could also be bottom-up. Since estimating such cracking based on the PMS data is difficult, these cracks were first converted to % area crack and then categorized into bottom-up or top-down cracking based on the HMA thicknesses. The PDs are recorded in miles and need conversion to % area. Data from the wheelpaths were summed into one value and divided by the total project length, as shown in Equation (7-2). The lane width was assumed to be 12 ft. The typical wheel path width of 3 feet was assumed.

$$\%\, AC_{top-down} = \frac{\text{Length of cracking (miles)} \times \text{width of wheelpaths (feet)}}{\text{Length of section (miles)} \times \text{Lane width (feet)}} \times 100 \quad (7\text{-}2)$$

The calculated top-down cracking using Equation (7-2) is assigned as either bottom-up or top-down based on the total AC layer thickness. If the thickness is greater than a certain threshold, the cracking is considered top-down cracking; else, it is categorized as bottom-up cracking. For example, If the HMA thickness is greater than 5 inches for new flexible pavement, the cracking should be considered top-down. Table 7-11 presents the minimum threshold thicknesses for top-down cracking to apply for each surface type.

Table 7-11 Minimum thicknesses for top-down cracking

Surface type	Threshold thickness (in)
Bituminous overlay on rubblized concrete	6
Composite overlay	6
Crush and shape	4
HMA over HMA overlay	6
New or reconstruct	5

3. HMA thermal cracking corresponds to transverse cracking in flexible pavements. The transverse cracking is recorded as the number of occurrences, but the Pavement-ME predicts thermal cracking in feet/mile. To convert transverse cracking into feet/mile, the number of occurrences was multiplied by 3 feet for PDs 114 and 701 because these PDs are defined as "tears" (short cracks) that are less than half the lane width. For all other PDs, the number of occurrences was multiplied by the lane width (12 ft).

All transverse crack lengths were summed and divided by the project length to get feet/mile, as shown in Equation (7-3).

$$TC = \frac{\sum \text{No. of Occurrences} \times \text{Lane Width (ft)}}{\text{Section Length (miles)}} \quad (7\text{-}3)$$

Thermal cracking predictions in the Pavement-ME are restricted to a maximum value of 2112 ft/mile due to a minimum crack spacing limit of 30 feet. It means Pavement-ME predictions at 50% reliability cannot exceed 2112 ft/mile. Due to this limitation and ARA recommendations, the research team decided to have a 2112 ft/mile cutoff where any measured data for a section above 2112 ft/mile was not used for calibration.

4. Total rutting is the total amount of HMA surface rutting all the pavement layers and unbound sub-layers contribute. The average rutting (left & right wheel paths) was determined for the entire project length. No conversion was necessary. The individual layer rutting was obtained using the transverse profile analysis approach from the previous calibration effort (*1*).
5. MDOT does not have any specific PDs for reflective cracking in flexible pavements. Therefore, separating thermal and reflective cracks at the surface is challenging. Thus, the total measured transverse cracking was considered a combination of thermal and reflective cracking, and bother models were calibrated.
6. The IRI measurements in the MDOT sensor database are compatible with those in the Pavement-ME. Therefore, no conversion or adjustments were needed, and data can be used directly.
7. Transverse cracking in rigid pavements is predicted as % slabs cracked in the Pavement-ME. However, MDOT measures transverse cracking as the number of transverse cracks. PDs 112 and 113 correspond to transverse cracking. The estimated transverse cracking needs conversion to the percent slabs cracked using Equation (7-4).

$$\%\ \text{Slabs Cracked} = \frac{\sum PD_{112,113}}{\left(\frac{\text{Section Length (miles)} \times 5280\ ft}{\text{Joint Spacing (ft)}}\right)} \times 100 \quad (7\text{-}4)$$

8. In the Pavement-ME, rigid pavement faulting is predicted as average per joint. MDOT's sensor data records the number of faults (FaultNum), average faulting (avgFault), and the maximum faulting (FaultMax) for every 0.1-mile segment. The faulting values had some inconsistencies. For the years between 2000 and 2011, faulting values are maximum fault callouts only (not average values). For 2012 and after, both average and maximum fault values are available. To resolve this issue, a correlation was developed between the maximum and average faulting values using data from 2013 to 2017. The team used these correlations to estimate the average faulting from 2000 to 2011. Table 7-12 shows the regression equations between average and maximum faulting using the data from 2013 to 2017. These equations are based on the number of faults. It is important to note that ideally, the number of faults

cannot be greater than the number of joints, but the number of faults in the database has records where they are more than the number of joints. These pseudo-fault values might come from cracking, spalling, bridge segments, etc. Therefore, the maximum number of fault counts was restricted to 36, and the average faulting for a section was cut off at 0.4 inches to address this issue. Accordingly, any 0.1-mile section above these restricted faulting values was omitted (cut) from the calibration data.

Table 7-12 Correlation equations based on the number of faults

FaultNum		Equation	R^2
From	To	(y is avgFault, x is FaultMax)	(2013 to 2017data)
0	1	y=x	1
2	4	y = 0.3438x + 0.03	0.7189
5	40	y = 0.2132x + 0.0377	0.6074
41	ALL	y = 0.0936x + 0.0777	0.2476

The average joint faulting is calculated based on the number of faulting in a 0.1-mile section. It is assumed that if the number of faults is less or equal to the number of joints, faulting occurs at the joints only. In that case, the faulting unit conversion equation is as shown in Equation (7-5). If, for any 0.1-mile section, the number of faults is greater than the number of joints, that section is removed (cut) from the calibration data, as previously mentioned.

$$Fault = \frac{\text{FAULnum} \times \text{FAULi}}{\text{N}_{\text{joints}}} \quad (7\text{-}5)$$

where,

FAULnum = number of faults in a 0.1 mile

FAULi =(FAULT_(Avg_Right) + FAULT_(Avg_Left))/2 = Average faulting in a 0.1 mile (inches)

N_{joints} is the number of joints in 0.1-mile (528 ft) segments, i.e., N_{joints}=528/Joint Spacing.

9. More sections should be added to the calibration database with additional performance data. This is specifically applicable to the limited number of concrete overlay projects for rigid sections and HMA over HMA rehabilitation for flexible sections.
10. The as-constructed data for the existing layer for most overlay projects are unavailable. It is recommended to obtain the best possible inputs for these sections using field coring, FWD, and other relevant tests.
11. The calibration process using different combinations of MDOT sections and statistical techniques is recommended for future calibration.
12. It is recommended that local calibrations should be performed every six years. Pavement sections will likely have three additional performance data points for local calibration in six years.
13. It is recommended that at least FWD testing can be performed at the finished surface on all future projects as part of in situ evaluation. However, some material samples should be collected to validate the FWD results.
14. Specifying a minimum 1,000 ft section within a project for material sampling and in-situ testing for the selected projects is also recommended for all pavement layers.

REFERENCES

CHAPTER 1

1. NCHRP 1-37A, "Guide for Mechanistic-Empirical Design of New and Rehabilitated Pavement Structures," 2004.
2. AASHTO, *Guide for Design of Pavement Structures*, vol. 1: AASHTO, 1993.
3. AASHTO, *Guide for the Local Calibration of the Mechanistic-Empirical Pavement Design Guide*, 2010.
4. Kutay, M. E. and A. Jamrah, "Preparation for Implementation of the Mechanistic-Empirical Pavement Design Guide in Michigan: Part 1 – HMA Mixture Characterization.," RC-1593, 2013.
5. Coban, H., B. Cetin, W. Likos, and T. Edil, "Construction Evaluation of Recycled Aggregate Bases and Large Stone Subbases," presented at Proceedings of the 99th Annual Meeting of the Transportation Research Board, Washington, DC, 2019, pp.
6. Chatti, K., M. E. Kutay, N. Lajnef, I. Zaabar, S. Varma, and H. S. Lee, "Enhanced analysis of falling weight deflectometer data for use with mechanistic-empirical flexible pavement design and analysis and recommendations for improvements to falling weight deflectometer," Turner-Fairbank Highway Research Center 2017.
7. Kutay, M. E., K. Chatti, and L. Lei, "Backcalculation of dynamic modulus mastercurve from falling weight deflectometer surface deflections," *Transportation Research Record*, vol. 2227, pp. 87-96, 2011.
8. Buch, N., K. Chatti, S. W. Haider, G. Baladi, W. Brink, and I. Harsini, "Preparation for implementation of the mechanistic-empirical pavement design guide in Michigan : part 2 - evaluation of rehabilitation fixes.," RC-1594, 2013.
9. Haider, S. W., N. Buch, W. Brink, K. Chatti, and G. Baladi, "Preparation for implementation of the mechanistic-empirical pavement design guide in Michigan, part 3 : local calibration and validation of the pavement-ME performance models.," RC-1595, 2014.

CHAPTER 2

1. NCHRP 1-37A, "Guide for Mechanistic-Empirical Design of New and Rehabilitated Pavement Structures," 2004.
2. Li, Q., D. X. Xiao, K. C. Wang, K. D. Hall, and Y. Qiu, "Mechanistic-empirical pavement design guide (MEPDG): a bird's-eye view," *Journal of Modern Transportation*, 2011.
3. Kang, M., T. Adams, and A. Kang, "Local calibration for fatigue cracking models used in the Mechanistic-empirical pavement design guide," 2007.
4. Von Quintus, H. L. and J. S. Moulthrop, "Mechanistic-Empirical Pavement Design Guide Flexible Pavement Performance Prediction Models for Montana--Volume I Executive Research Summary," 2007.
5. Muthadi, N. R. and Y. R. Kim, "Local Calibration of Mechanistic-Empirical Pavement Design Guide for Flexible Pavement Design," *Transportation Research Record*, vol. 2087, pp. 131-141, 2008.

6. Haider, S. W., G. Musunuru, N. Buch, and W. C. Brink, "Local Recalibration of JPCP Performance Models and Pavement-ME Implementation Challenges in Michigan," *Journal of Transportation Engineering, Part B: Pavements*, vol. 146, pp. 04019037, 2020.
7. Tabesh, M. and M. S. Sakhaeifar, "Local calibration and Implementation of AASHTOWARE Pavement ME performance models for Oklahoma pavement systems," *International Journal of Pavement Engineering*, pp. 1–12, 2021.
8. Dong, S., J. Zhong, S. L. Tighe, P. Hao, and D. Pickel, "Approaches for local calibration of mechanistic-empirical pavement design guide joint faulting model: a case study of Ontario," *International Journal of Pavement Engineering*, vol. 21, pp. 1347–1361, 2020.
9. Shakhan, M. R., A. Topal, and B. Şengöz, "A methodology for implementation of the mechanistic-empirical rigid pavement design in Turkey," *Turkish Journal of Science and Technology*, vol. 16, pp. 1–10, 2021.
10. Bustos, M., O. Cordo, P. Girardi, and M. Pereyra, "Calibration of distress models from the mechanistic–empirical pavement design guide for rigid pavement design in Argentina," *Transportation research record*, vol. 2226, pp. 3–12, 2011.
11. Fick, S. B., *Evaluation of the AASHTO empirical and mechanistic-empirical pavement design procedures using the AASHO road test*: University of Maryland, College Park, 2010.
12. AASHTO, *Guide for the Local Calibration of the Mechanistic-Empirical Pavement Design Guide*, 2010.
13. AASHTO, *Mechanistic-empirical pavement design guide: A manual of practice; 2nd Edition*: AASHTO, 2015.
14. Pierce, L. M. and G. McGovern, "Implementation of the AASHTO mechanistic-empirical pavement design guide and software," NCHRP Synthesis 457, 2014.
15. Haider, S. W., N. Buch, W. Brink, K. Chatti, and G. Baladi, "Preparation for implementation of the mechanistic-empirical pavement design guide in Michigan, part 3 : local calibration and validation of the pavement-ME performance models.," RC-1595, 2014.
16. Von Quintus, H. L., M. I. Darter, B. B. Bhattacharya, and L. Titus-Glover, "Calibration of the MEPDG transfer functions in Georgia: task order 2 report.," Georgia. Dept. of Transportation 2015.
17. Huang, B., H. Gong, and X. Shu, "Local Calibration of Mechanistic-Empirical Pavement Design Guide in Tennessee," Tennessee. Department of Transportation 2016 2016.
18. Kim, S., H. Ceylan, D. Ma, and K. Gopalakrishnan, "Calibration of pavement ME design and mechanistic-empirical pavement design guide performance prediction models for Iowa pavement systems," *Journal of Transportation Engineering*, vol. 140, pp. 04014052, 2014.
19. Bhattacharya, B. B., H. L. Von Quintus, and M. I. Darter, "Implementation and local calibration of the MEPDG transfer functions in Wyoming.," Wyoming Dept. of Transportation 2015.
20. Sun, X., J. Han, R. L. Parsons, A. Misra, and J. K. Thakur, "Calibrating the mechanistic-empirical pavement design guide for Kansas.," Kansas. Dept. of Transportation. Bureau of Materials & Research 2015.

21. Miner, M. A., "Cumulative damage in fatigue," 1945.
22. AASHTO, "Top-Down Cracking Enhancement https://me-design.com/MEDesign/Documents.," in *AASHTOWare*, 2020.
23. Ling, M., X. Luo, Y. Chen, F. Gu, and R. L. Lytton, "Mechanistic-empirical models for top-down cracking initiation of asphalt pavements," *International Journal of Pavement Engineering*, vol. 21, pp. 464–473, 2020.
24. Bayomy, F., A. Muftah, E. Kassem, C. Williams, and M. Hasnat, "Calibration of the AASHTOWare Pavement ME Design Software for PCC Pavements in Idaho," Idaho. Transportation Department 2019.
25. Mallela, J., L. Titus-Glover, B. Bhattacharya, M. Darter, and H. Von Quintus, "Idaho AASHTOWare pavement ME design user's guide, version 1.1.," Idaho Transportation Dept. 2014.
26. Titus-Glover, L., C. Rao, and S. Sadasivam, "Local Calibration of the Pavement ME for Missouri," Missouri. Department of Transportation. Construction and Materials Division 2020 2020.
27. Wu, Z., D. X. Xiao, Z. Zhang, and W. H. Temple, "Evaluation of AASHTO Mechanistic-Empirical Pavement Design Guide for designing rigid pavements in louisiana," *International Journal of Pavement Research and Technology*, vol. 7, pp. 405, 2014.
28. AASHTO, *Guide for Design of Pavement Structures*, vol. 1: AASHTO, 1993.
29. Buch, N., K. Chatti, S. W. Haider, and A. Manik, "Evaluation of the 1–37A Design Process for New and Rehabilitated JPCP and HMA Pavements," Michigan. Dept. of Transportation 2008.
30. Buch, N., K. Chatti, S. W. Haider, G. Baladi, W. Brink, and I. Harsini, "Preparation for implementation of the mechanistic-empirical pavement design guide in Michigan : part 2 - evaluation of rehabilitation fixes.," RC-1594, 2013.
31. Kutay, M. E., A. Jamrah, and M. S. U. D. o. C. a. E. Engineering, "Preparation for Implementation of the Mechanistic-Empirical Pavement Design Guide in Michigan: Part 1 – HMA Mixture Characterization.," RC-1593, 2013 2013.
32. Buch, N., S. W. Haider, J. Brown, and K. Chatti, "Characterization of truck traffic in Michigan for the new mechanistic empirical pavement design guide.," Michigan. Dept. of Transportation. Construction and Technology Division 2009.
33. Haider, S. W., G. Musunuru, N. Buch, O. I. Selezneva, P. Desaraju, and J. Q. Li, "Updated analysis of Michigan traffic inputs for pavement-ME design," Michigan State University. Dept. of Civil and Environmental Engineering 2018.
34. Baladi, G., T. Dawson, and C. Sessions, "Pavement subgrade MR design values for Michigan's seasonal changes: table E5.," 2010 2010.
35. Baladi, G. Y., K. A. Thottempudi, and T. Dawson, "Backcalculation of unbound granular layer moduli, final report," *Michigan Department of Transportation, Construction and Technology Division, PO Box*, vol. 30049, 2010.
36. Buch, N. and S. Jahangirnejad, "Quantifying coefficient of thermal expansion values of typical hydraulic cement concrete paving mixtures," Michigan. Dept. of Transportation. Construction and Technology Division 2008.
37. You, Z., X. Yang, J. Hiller, D. Watkins, and J. Dong, "Improvement of Michigan Climatic Files in Pavement ME Design–Final Report (RC-1626)," 2015.

38. Li, Q. J., K. C. Wang, G. Yang, J. Y. Zhan, and Y. Qiu, "Data needs and implementation of the Pavement ME Design," *Transportmetrica A: Transport Science*, vol. 15, pp. 135–164, 2019.
39. Schwartz, C., R. Li, H. Ceylan, S. Kim, and K. Gopalakrishnan, "Sensitivity evaluation of MEPDG performance prediction," NCHRP Report 1-47, 2011 2011.
40. Schwartz, C. W., R. Li, H. Ceylan, S. Kim, and K. Gopalakrishnan, "Global Sensitivity Analysis of Mechanistic–Empirical Performance Predictions for Flexible Pavements," *Transportation Research Record*, vol. 2368, pp. 12-23, 2013.
41. Yang, X., Z. You, J. Hiller, and D. Watkins, "Sensitivity of flexible pavement design to Michigan's climatic inputs using pavement ME design," *International Journal of Pavement Engineering*, vol. 18, pp. 622-632, 2017.
42. Li, X. Y., R. Zhang, X. Zhao, and H. N. Wang, "Sensitivity Analysis of Flexible Pavement Parameters by Mechanistic-Empirical Design Guide," *Applied Mechanics and Materials*, vol. 590, pp. 539-545, 2014.
43. Orobio, A., *Sensitivity analysis of flexible pavement performance parameters in the mechanistic-empirical design guide*: West Virginia University, 2010.
44. Orobio, A. and J. P. Zaniewski, "Part 2—Flexible Pavement Design: Sampling-Based Sensitivity Analysis of the Mechanistic-Empirical Pavement Design Guide Applied to Material Inputs," *Transportation Research Record*, pp. 85, 2011.
45. Orobio, A. and J. P. Zaniewski, "Sensitivity of the mechanistic-empirical pavement design guide to traffic inputs: a space-filling approach," *Road materials and pavement design*, vol. 14, pp. 735–746, 2013.
46. Graves, R. C. and K. C. Mahboub, "Pilot study in sampling-based sensitivity analysis of NCHRP design guide for flexible pavements," *Transportation Research Record*, vol. 1947, pp. 122–135, 2006.
47. Ceylan, H., K. Gopalakrishnan, S. Kim, C. W. Schwartz, and R. Li, "Global sensitivity analysis of jointed plain concrete pavement mechanistic–empirical performance predictions," *Transportation research record*, vol. 2367, pp. 113–122, 2013.
48. Ceylan, H., S. Kim, K. Gopalakrishnan, C. W. Schwartz, and R. Li, "Sensitivity quantification of jointed plain concrete pavement mechanistic-empirical performance predictions," *Construction and Building Materials*, vol. 43, pp. 545–556, 2013.
49. Hall, K. D. and S. Beam, "Estimating the sensitivity of design input variables for rigid pavement analysis with a mechanistic–empirical design guide," *Transportation Research Record*, vol. 1919, pp. 65–73, 2005.
50. Haider, S. W., N. Buch, and K. Chatti, "Simplified Approach for Quantifying Effect of Significant Input Variables and Designing Rigid Pavements using Mechanistic-Empirical Pavement Design Guide," 2009.
51. Darter, M. I., H. Von Quintus, B. B. Bhattacharya, and J. Mallela, "Calibration and implementation of the AASHTO mechanistic-empirical pavement design guide in Arizona.," Arizona. Dept. of Transportation. Research Center 2014.
52. Gassman, S. L. and M. M. Rahman, "Calibration of the AASHTO pavement design guide to South Carolina conditions-phase I," South Carolina. Dept. of Transportation 2016.
53. CDOT, "CDOT M-E Pavement Design Manual," in *Colorado Department of Transportation*, 2021.

54. VDOT, "AASHTOWare Pavement ME User Manual," 2017.
55. Rangelov, M., S. Nassiri, A. Ibrahim, F. Bayomy, A. Muftah, and B. Sigdel, "Portland Cement Concrete Material Characterization for Pavement ME Design Implementation in Idaho," Idaho. Transportation Department 2017.
56. Bayomy, F., A. Muftah, E. Kassem, F. Tousef, and H. Alkuime, "Calibration of the AASHTOWare pavement ME design performance models for flexible pavements in Idaho," Idaho. Transportation Department 2018.
57. Ceylan, H., S. Kim, K. Gopalakrishnan, and O. Smadi, "MEPDG work plan task no. 8: Validation of pavement performance curves for the mechanistic-Empirical pavement design guide," 2009.
58. Rao, C., "Guidelines for PCC inputs to AASHTOWare Pavement ME.," Mississippi. Dept. of Transportation 2014 2014.
59. Mallela, J., L. Titus-Glover, H. Von Quintus, M. I. Darter, M. Stanley, and C. Rao, "Implementing the AASHTO Mechanistic-Empirical Pavement Design Guide for Missouri. Vol. II, MEDPG Model Validation and Calibration," 2009.
60. Sebaaly, P. E., J. Thavathurairaja, and E. Hajj, "Characterization of Unbound Materials (Soils/Aggregates) Mechanistic-Empirical Pavement Design Guide (MEPDG)[2018]," Nevada Dept. of Transportation 2018.
61. Glover, L. T., J. Mallela, and I. Applied Research Associates, "Guidelines for Implementing NCHRP 1-37A M-E Design Procedures in Ohio : Volume 4 - MEPDG Models Validation & Recalibration," FHWA/OH-2009/9D, 2009.
62. Williams, R. C. and R. Shaidur, "Mechanistic-empirical pavement design guide calibration for pavement rehabilitation.," Oregon. Dept. of Transportation. Research Section 2013.
63. Zhou, C., "Investigation into key pavement materials and local calibration on MEPDG," 2013.
64. Darter, M., L. Titus-Glover, and H. Von Quintus, "Draft User's Guide for UDOT Mechanistic-Empirical Pavement Design Guide," Report No. UT-09.1 a, 2009.
65. Li, J., L. M. Pierce, and J. Uhlmeyer, "Calibration of flexible pavement in mechanistic–empirical pavement design guide for Washington state," *Transportation Research Record*, vol. 2095, pp. 73–83, 2009.
66. Ng, K. W., H. L. V. Quintus, K. Ksaibati, D. Hellrung, and Z. Hutson, "Characterization of Material Properties for Mechanistic-Empirical Pavement Design in Wyoming," Wyoming. Dept. of Transportation," 2016.

CHAPTER 3

1. Haider, S. W., N. Buch, W. Brink, K. Chatti, and G. Baladi, "Preparation for implementation of the mechanistic-empirical pavement design guide in Michigan, part 3: local calibration and validation of the pavement-ME performance models," Michigan. Dept. of Transportation. Office of Research Administration 2014.
2. You, Z., X. Yang, J. Hiller, D. Watkins, and J. Dong, "Improvement of Michigan climatic files in pavement ME design," Michigan. Dept. of Transportation 2015.
3. Miller, J. S. and W. Y. Bellinger, "Distress identification manual for the long-term pavement performance program," United States. Federal Highway Administration. Office of Infrastructure … 2003.

4. Kutay, M. E. and A. Jamrah, "Preparation for Implementation of the Mechanistic-Empirical Pavement Design Guide in Michigan: Part 1–HMA Mixture Characterization," 2013.
5. MDOT, "Michigan DOT User Guide for Mechanistic-Empirical Pavement Design," Michigan Department of Transportation Lansing, MI, USA, 2021.
6. Baladi, G. Y., A. Thottempudi, and T. Dawson, "Backcalculation of unbound granular layer moduli," 2011.
7. Baladi, G., T. Dawson, and C. Sessions, "Pavement subgrade MR design values for Michigan's seasonal changes, final report," *Michigan Department of Transportation, Construction and Technology Division, PO Box*, vol. 30049, 2009.
8. Singh, R. R., S. W. Haider, M. E. Kutay, B. Cetin, and N. Buch, "Impact of Climatic Data Sources on Pavement Performance Prediction in Michigan," *Journal of Transportation Engineering, Part B: Pavements*, vol. 148, pp. 04022048, 2022.

CHAPTER 4

1. NCHRP 1-37 A, "Guide for Mechanistic–Empirical Design of New and Rehabilitated Pavement Structures," *Final Rep., NCHRP Project 1-37A*, 2004.
2. AASHTO, "Guide for design of pavement structures," Aashto Washington, DC, 1993.
3. Li, Q., D. X. Xiao, K. C. Wang, K. D. Hall, and Y. Qiu, "Mechanistic-empirical pavement design guide (MEPDG): a bird's-eye view," *Journal of Modern Transportation*, vol. 19, pp. 114-133, 2011.
4. Officials, T., *Guide for the Local Calibration of the Mechanistic-Empirical Pavement Design Guide*: AASHTO, 2010.
5. Haider, S. W., N. Buch, W. Brink, K. Chatti, and G. Baladi, "Preparation for implementation of the mechanistic-empirical pavement design guide in Michigan, part 3: local calibration and validation of the pavement-ME performance models," Michigan. Dept. of Transportation. Office of Research Administration 2014.
6. Haider, S. W., N. Buch, W. Brink, K. Chatti, and G. Baladi, "Preparation for implementation of the mechanistic-empirical pavement design guide in Michigan, part 3: local calibration and validation of the pavement-ME performance models.," RC-1595, 2014.
7. Kim, S., H. Ceylan, D. Ma, and K. Gopalakrishnan, "Calibration of pavement ME design and mechanistic-empirical pavement design guide performance prediction models for Iowa pavement systems," *Journal of Transportation Engineering*, vol. 140, pp. 04014052, 2014.
8. Dong, S., J. Zhong, S. L. Tighe, P. Hao, and D. Pickel, "Approaches for local calibration of mechanistic-empirical pavement design guide joint faulting model: a case study of Ontario," *International Journal of Pavement Engineering*, vol. 21, pp. 1347-1361, 2020.
9. Officials, T., "Mechanistic-empirical pavement design guide: A manual of practice, 2nd Edition," *AASHTO: Washington, DC, USA*, 2015.

CHAPTER 6

1. Vennapusa, P. K. and D. J. White, "Comparison of light weight deflectometer measurements for pavement foundation materials," *Geotechnical Testing Journal*, vol. 32, pp. 1-13, 2009.
2. "Standard test method for measuring solar reflectance of horizontal and low-sloped surfaces in the field," vol. ASTM E1918-16.
3. "Corporation N Albedometer."
4. Zhou, F., "Development of an IDEAL Cracking Test for Asphalt Mix Design, Quality Control and Quality Assurance," NCHRP IDEA Project 195, 2019.
5. Zhou, F., S. Im, L. Sun, and T. Scullion, "Development of an IDEAL cracking test for asphalt mix design and QC/QA," *Road Materials and Pavement Design*, vol. 18, pp. 405-427, 2017.
6. Paris, P. E., F., "A critical analysis of crack propagation laws," *Journal of Basic Engineering, Transactions of the American Society of Mechanical Engineers*, vol. 85, pp. 528–534, 1963.
7. Zdenek, P. B. and C. P. Pere, "Effect of Temperature and Humidity on Fracture Energy of Concrete," *ACI Materials Journal*, vol. 85.
8. Al-Qadi, I. L., H. Ozer, J. Lambros, A. E. Khatib, P. Singhvi, T. Khan, J. Rivera-Perez, and B. Doll, "Testing protocols to ensure performance of high asphalt binder replacement mixes using RAP and RAS," 2015.
9. Kaseer, F., F. Yin, E. Arámbula-Mercado, A. E. Martin, J. S. Daniel, and S. Salari, "Development of an index to evaluate the cracking potential of asphalt mixtures using the semi-circular bending test," *Construction and Building Materials*, vol. 167, pp. 286-298, 2018.
10. Pérez-Jiménez, F., R. Botella, A. H. Martínez, and R. Miró, "Analysis of the mechanical behaviour of bituminous mixtures at low temperatures," *Construction and Building Materials*, vol. 46, pp. 193-202, 2013.
11. West, R., C. V. Winkle, S. Maghsoodloo, and S. Dixon, "Relationships between simple asphalt mixture cracking tests using Ndesign specimens and fatigue cracking at FHWA's accelerated loading facility," *Road Materials and Pavement Design*, vol. 18, pp. 428 - 446, 2017.
12. Rupnow, T. D. and P. Icenogle, "Evaluation of surface resistivity measurements as an alternative to the rapid chloride permeability test for quality assurance and acceptance," Louisiana Transportation Research Center 2011.
13. Park, S. W., and Y. R. Kim. "Interconversion between relaxation modulus and creep compliance for viscoelastic solids." Journal of materials in Civil Engineering 11, no. 1 (1999): 76-82.

CHAPTER 7

1. Haider, S. W., N. Buch, W. Brink, K. Chatti, and G. Baladi, "Preparation for implementation of the mechanistic-empirical pavement design guide in Michigan, part 3: local calibration and validation of the pavement-ME performance models.," RC-1595, 2014.

2. AASHTO, *Guide for* the *Local Calibration of the Mechanistic-Empirical Pavement Design Guide*, 2010.